Dissecting the events of the *Trichoderma*-plant interaction through proteomics and metabolomics approaches: *Trichoderma virens* and maize as model systems

_____

A thesis

submitted in partial fulfilment

of the requirements for the Degree of

Doctor of Philosophy

at

Lincoln University

by

Guillermo Nogueira López

Lincoln University

2019

Abstract of a thesis submitted in partial fulfilment of the requirements for the Degree of Doctor of Philosophy

Dissecting the events of the *Trichoderma*-plant interaction through proteomics and metabolomics approaches: *Trichoderma virens* and maize as model systems

by

Guillermo Nogueira López

In nature, almost every plant is colonised by fungi. *Trichoderma virens* is a biocontrol fungus which has the capacity to behave as an facutaltive plant endophyte. Even though many plants are colonised by this symbiont, the exact mechanisms by which it masks its entrance into its host plant remain unknown. They are likely to involve a) the secretion of different protein families into the apoplast and b) the modulation of the plant metabolome. Both mechanisms may play crucial roles in the suppression of plant immune responses to facilitate colonisation. The aim of this study was to investigate the molecular and cellular mechanisms of maize root colonisation by *T. virens.* To achieve this, the *T. virens*-maize interaction was investigated under hydroponic growth conditions using confocal microscopy, proteomics and metabolomics approaches, and functional characterisation of the 2-oxoglutarate/Fe (II)-dependent dioxygenase gene *tvox1*, from *T. virens*. This study demonstrated that upon host penetration, *T. virens* colonises inter- and intracellular spaces and modifies morphology and physiology of maize roots. Using a gel-free shotgun proteomics approach, secreted proteins from maize and *T. virens* were identified. A reduction in the maize secretome was induced by *T. virens*, including two major groups, glycosyl hydrolases and peroxidases. *T. virens* secreted proteins were mainly involved in cell wall hydrolysis, scavenging of reactive oxygen species and secondary metabolism, as well as putative effector proteins. Therefore, demonstrating that *T. virens* secretes an arsenal of proteins into the apoplast to facilitate colonisation of maize root tissues. In addition, the role of the *T. virens tvox1* up-regulated gene in secondary metabolism and iron regulation during the *T. virens*-maize interaction was explored by gene deletion. The functional analysis of TVOX1 suggested that it participates in the regulation of siderophore production and iron homeostasis in *T. virens*. To further explore the relevance of *tvox1* during the *T. virens*-maize interaction, an untargeted metabolic fingerprinting

approach by HPLC-DAD-ESI$^-$-QTOF-MS/MS of maize roots following *T. virens* (WT and Δ*tvox1*) colonisation revealed a modulation of the maize metabolome, showing general and specific metabolic responses of maize to both *T. virens* genotypes. Moreover, this work showed that the deletion of *tvox1* which is involved in fungal secondary metabolism shifted the metabolic flux in *T. virens.* Overall, three main mechanisms are proposed as the molecular interplay between *T. virens* and maize: a) glycosyl hydrolases and lignification, b) reactive oxygen species homeostasis, and c) iron and secondary metabolism.

Keywords: 2-oxoglutarate/Fe (II)-dependent dioxygenase, apoplast, endophyte, functional characterisation, iron, maize, metabolome, plant-microbe interactions, reactive oxygen species, root colonisation, secondary metabolism, secretome, *Trichoderma virens, tvox1*.

Acknowledgements

Firstly, I would like to express my gratitude to my supervisor team, Dr Artemio Mendoza Mendoza, Dr Johanna Steyaert, Prof David Greenwood, Prof John Hampton, Dr Michael Rostas, Dr Chris Winefield and Dr Carla Eaton. Your combined expertise and support have enabled me to finish this multidisciplinary work. I´ll be forever grateful, thank you for the opportunity.

I would like to extend my recognition to Prof Caroline Müller and Dr Rabea Schweiger for your genuine encouragement, positivity, support and feedback in relation with a very important part of my research. I would like to thank Martin Middleditch for your support and advice during the proteomic analysis. I would also like to extend my thanks to Dr Dave Saville for the statistical advice and assistance through all these years.

I would like to acknowledge the Consejo Nacional de Ciencia y Tecnología (CONACYT-Mexico) for funding my PhD and supporting this research project. Also, I want to extend my gratitude to the Marsden Fast Start, the Tertiary Education Commission and the Bio-Protection Research Centre for funding this research, and to Meadow Mushrooms Lincoln University Postgraduate Scholarships for supporting my research project.

I would also like to extend my thanks to all the staff at the Bio-Protection Research Centre who have offered their help and support and who in one way or another contributed to my project. Many thanks to the students who cross my path for making this journey a very enjoyable experience. Special thanks to Laura, Rob, Maria Eugenia, Anish, Francesco, Patricio, Federico, Jess, Hamish, Aimee, Claudia, Pavi, Abi and all the other members of Twisted Minds NZ. You are all amazing people, ¡MUCHAS GRACIAS! for all your help and friendship.

I would like to express my most sincere gratitude to my family for their support no matter the distance, for encouraging me to follow my dreams. I love you. I am very grateful for my friends. Thank you for making a real effort to keep in touch despite the distance.

Finally, I wish to express my love and gratitude to Fabi, who has been a special person in my life. Thank you so much for all your help, advice and patience, I wouldn't accomplish this without you. Thank you for being beside me in the good and bad moments. Thank you for your company in this amazing country and all the incredible memories. We have created a fantastic mutualistic symbiosis.

Contents

Abbreviations

A	Adenine
ABA	Abscisic acid
AF	Apoplastic fluid
AMF	Arbuscular mycorrhizal fungi
ANOVA	Analysis of variance
APs	Apoplastic proteins
Avr	Avirulence
BCA	Biocontrol agents
Blast	Basic local alignment search tool
BIC	Biotrophic interfacial complex
BRs	Brassinosteroids
bp	Base pair
BXs	Benzoxacinoids
Δ	Deletion
C	Cytosine
CKs	Cytokinins
cDNA	Complementary deoxyribonucleic acid
cm	Centimetre
CWDE	Cell wall degrading enzyme
D	Day
dATP	Deoxyadenosine triphosphate
DAMPs	Damage associated molecular patterns
DNA	Deoxyribonucleic acid
d.p.i	Days post inoculation
EIX	Ethylene-inducing xylanase
ER	Endoplasmic reticulum
ET	Ethylene
ETI	Effector triggered immunity
Fe	Iron
GA	Gibberellins
GHs	Glycosyl hydrolases
GO	Gene ontology
h	Hour
HSTs	Host-specific toxins
HR	Hypersensitive response
ISR	Induced systemic resistance
IAA	Indol acetic acid
JA	Jasmonic acid

JGI	Joint genome institute
Kb	Kilobases
LPS	Leaderless protein secretion
MAMPs	Microbial associated molecular patterns
MAPK	Mitogen-activated protein kinase
MDH	Malate dehydrogenase
mL	Millilitre
mM	Milimolar
MS	Mass spectrometry
mVOCs	Microbial volatile organic compounds
N	Nitrogen
NADPH	Nicotinamide adenine dinucleotide phosphate
NB-LRR	Nucleotide-binding site leucine-rich repeat
nt	Nucleotide
P	Phosphorus
PAMPs	Pathogen-associated molecular patterns
PHIs	Phospoinositides
PIs	Proteinase inhibitors
POX	Peroxidase
PR	Pathogenesis-related
PRR	Pattern recognition receptor
PTI	PAMP-triggered immunity
RLKs	Receptor-like kinases
RLPs	Receptor-like proteins
RNA	Ribonucleic acid
ROS	Reactive oxygen species
RT	Room temperature
SA	Salicylic acid
SMs	Secondary metabolites
SSPs	Small secreted proteins
SST2	Secretion system type 2
SD	Standard deviation

List of tables

List of figures

1 Introduction

1.1 Endophytic microorganisms

Plants and endophytic microbes have co-evolved over millions of years; as a consequence, they have created a mutualistic symbiosis where both organisms obtain benefits from this interaction. Plant tissues are micro-ecosystems where a variety of microorganism taxa interact with each other to create a biofunctional micro-environment. The endophytic microorganisms which inhabit diverse plant species are bacteria or fungi which colonise the internal tissues of roots, pseudostem and leaves of living plants in all or part of their life cycle (Rodriguez et al. 2009; Santoyo et al. 2016; Brader et al. 2017). Plant endophytes are characterised by conferring beneficial attributes during their mutualistic interactions with plants such as growth promotion, enhanced disease resistance, facilitation of nutrient acquisition, increased abiotic stress tolerance and improvements in plant fitness (Schulz and Boyle 2006; Tadych and White 2009; Busby et al. 2016). The main entry point of endophytic microorganisms is through the rhizosphere (Backman and Sikora 2008), followed by the phyllosphere (Hardoim et al. 2015). The rhizosphere is defined as the zone around the root where plants produce root-exudates with high amounts of carbohydrates, organic acids and amino acids attracting diverse microorganisms by quimiotaxis (Bais et al. 2006). Before attempting to penetrate the host plant, soil microbiome struggle and compete for nutrients within the rhizosphere, in order to establish a successful infection. This is when plant endophytes play their first main role, outcompeting other microorganisms (plant tissue colonising pathogen) in order to enter and colonise the plant (Brader et al. 2017), thus establishing a mutualistic symbiosis that directly influences plant health (Berendsen et al. 2012).

1.2 Secretome-mediated plant-fungal interactions

The plant-fungal secretome represents the set of proteins secreted by both the invader and the host on the plant surface and/or into the extracellular plant space, called the apoplast, under constitutive or induced conditions. Secreted proteins accomplish different biological functions in both organisms; for example, formation and maintenance of cell wall structure, cell-to-cell interaction, enabling nutrient uptake, sensing the external environment, regulating stress responses and mediating interactions with other organisms (Alexandersson et al. 2013; Yadav et al. 2015; McCotter et al. 2016). Protein families commonly found in the plant secretome are: proteases, peptidases, glycoside hydrolases (GHs), lipases, peroxidases (POX), cysteine-rich secretory proteins and pathogenesis-related (PR) proteins (Kwon et al. 2008; Alexandersson et al.

2013; Delaunois et al. 2014) that together mediate or control invasive microbial colonisation. The microbe involved, secrete principally hydrolytic enzymes and effector proteins to penetrate into plant tissue and overcome plant immune responses, respectively, and also secrete other families of proteins to influence adhesion and colonisation such as hydrophobins, which are deposited on the host surfaces (Kamoun 2009; Schmidt and Volker 2011; Gupta et al. 2015). Primary roots represent a favorable illustration of plant secretome function where mucilage production in *Zea mays* L. plays an important role in plant growth, creating a suitable environment and controlling the structure of the microbial community (Ma et al. 2010). For fungi, the arbuscular mycorrhizal *Rhizophagus irregularis* adjusts its secretome depending on the developmental stage inside the host plant, showing that fungal secreted proteins are necessary to create this symbiotic interaction with plants (Zeng et al. 2018). Overall, secreted protein families play essential roles during plant-fungal communication. However, it is still unknown how endophytes manipulate the molecular mechanisms to overcome and/or evade plant defences; therefore, the secretome is a key part to understanding this complex symbiosis.

1.3 Secretion systems

Protein secretion is an ability that all types of cells possess. It is an efficient and controlled mechanism that involves membrane transportation inside the cytoplasm and is fundamental for the proper functioning of the cell (Coulthurst 2013). The secretome is regulated by different environmental signals and regulatory factors in which organisms modify and optimise their secretory mechanisms to adapt to the changing environment (McCotter et al. 2016). Eukaryotic cells mainly transport and secrete proteins via conventional secretion system that involves the endoplasmic reticulum (ER)/Golgi apparatus-dependent pathway which is facilitated by vesicles (Vitale and Denecke 1999). These extracellular secreted proteins are characterised by a conserved N-terminal signal peptide and the absence of transmembrane domains or anchor membrane signals (Ma et al. 2010). This secretion system is common in fungi and plants. For example, *Trichoderma reesei* secretes cellulolytic enzymes through this mechanism (Saloheimo and Pakula 2012). Additionally, small secreted proteins, which follow the conventional pathway form part of the fungal secretome in different fungal phyla such as, Ascomycota, Basidiomycota, Glomeromycota, Microspora and Zygomycota (Kim et al. 2016). Furthermore, in response to environmental shifts, plants secrete proteins involved in cell wall metabolism, oxidation-reduction (redox) regulation, defence/stress and signaling via conventional secretion system (Yadav et al. 2015).

Alternatively, unconventional protein secretion systems that release proteins to the plasma membrane and the extracellular space without entering the ER-Golgi conventional pathway of secretion have also been demonstrated in prokaryotic and some eukaryotic organisms (Ding et al. 2012; Lloubes et al. 2013; Robinson et al. 2016; Rabouille 2017). In plants, non-vesicular and vesicular modes of transport are used to deliver leaderless secretory proteins into the apoplast

under stress conditions (Robinson et al. 2016; Wang et al. 2018). Moreover, bacterial pathogens have specialised mechanisms to secrete molecules which play special biological functions in their host. For example they can interact through direct cell contact with the host via type III, IV and VI secretion systems and indirectly via type I, II and outer membrane vesicles systems, depending on their lifestyle and niche (Jha et al. 2005; Coulthurst 2013; Lloubes et al. 2013; Costa et al. 2015). However, uncommon secretory pathways in fungi are still poorly understood. Recent studies have found that in the rice blast fungal disease agent, *Magnaporthe oryzae,* cytoplasmic effectors which are accumulated in the biotrophic interfacial complex are secreted by a non-ER system (Giraldo et al. 2013). Unconventional protein secretion has been also observed in other fungal pathogens including *Ustilago maydis, Phytophthora sojae* and *Verticillium dahlia* (Djamei et al. 2011; Stock et al. 2012; Liu et al. 2014). One suggested mechanism utilised by fungi and plants to unconventionally deliver proteins during plant-microbe interactions is through the formation of extracellular vesicles called exosomes (Lo Presti and Kahmann 2017; Rutter and Innes 2017). Therefore, this suggests that plants, plant-pathogenic and endophytic fungi have evolved distinct secretory mechanisms to deliver a collection of proteins in response to microbial infection or to manipulate host cell processes, respectively.

1.4 Molecular interplay during fungal-plant interactions

1.4.1 Role of hydrophobins in plant recognition and attachment

During their life cycle, filamentous fungi produce small cysteine-rich surface active amphipathic proteins called hydrophobins. The main roles of hydrophobins are as structural components for fungal growth and mediation of the cell with the environment (Linder et al. 2005; Wu et al. 2017; Appels et al. 2018). Hydrophobins are classified into two groups, class I and class II, based on the solubility of the aggregates they form, hydropathy patterns and solubility characteristics. During the fungal-plant interaction, fungal hydrophobins are produced in the first stages of root sensing. Their biological functions are the recognition and adhesion to host surfaces where they positively influence root colonisation ability (Viterbo and Chet 2006; Dubey et al. 2014; Moonjely et al. 2018). In addition, it has been hypothesised that hydrophobins might function as protection from detection by the plant (Viterbo and Chet 2006; Degani et al. 2013), and act as elicitors of the plant defence responses (Plett and Martin 2011; Ruocco et al. 2015). When the symbiotic ability in the ericoid mycorrhizal fungus *Oidiodendron maius* was tested, it was found that the hydrophobin-like effector OmSSP1 was necessary to colonise *Vaccinium myrtillus* roots (Casarrubia et al. 2018). The saprophytic *Trichoderma* spp. produce a much wider range of class II hydrophobins compared with other ascomycetes and some of these function during mycoparasitism to attach to the hyphae of other fungi (Kubicek et al. 2008). However, both classes of hydrophobins play an important role during the *Trichoderma*-plant interaction (Kubicek et al. 2008; Ruocco et al. 2015). For example, the hydrophobin-like TasHyd1 protein, isolated from *Trichoderma asperellum,* plays an important role in root attachment and colonisation (Viterbo and Chet 2006), while the knockout or

overexpression of class II hydrophobin TvHydII1 in *T. virens* resulted in reduction or enhancement of root colonisation, respectively (Guzmán-Guzmán et al. 2017). Furthermore, transcriptome analyses during the interaction of *T. virens* with maize roots revealed up-regulation of several hydrophobin-like genes (Lawry 2016).

1.4.2 Role of phytohormones in plant defence against microorganisms

Phytohormones play key roles in the plant immune signalling network that is activated upon microbe perception; particularly the involvement of primary defence hormones: jasmonates (JA), ethylene (ET) and salicylates (SA). Secondary defence hormones, such as auxins (IAA), abscisic acid (ABA), cytokinins (CKs), brassinosteroids (BRs) and gibberellins (GA), also have a significant role in plant defence, either alone or in conjunction with primary phytohormones (Kazan and Lyons 2014; Shigenaga and Argueso 2016; Berens et al. 2017). Inside plant tissues, plant symbionts can synthesise a wide range of phytohormones to stimulate plant growth, induce tolerance to abiotic stress and provide resistance to biotic factors (Egamberdieva et al. 2017). Additionally, plant pathogens have evolved mechanisms to manipulate hormone signalling pathways to spread into host tissues and cause disease; for example, production of signalling molecules, such as auxins; influencing the synthesis of secondary hormones that contributes to the suppression of primary hormonal signalling; or generating compounds that function as molecular mimics of the phytohormones (Kunkel and Brooks 2002; Spaepen and Vanderleyden 2011; Gimenez-Ibanez et al. 2014; Xu et al. 2015; Nobori et al. 2018). Beneficial microbes interact with the plant in a similar way as pathogens. *Laccaria bicolor*, a mutualistic symbiotic fungus, produces an effector-like protein MiSSp7 that acts as a negative regulator of JA, minimising the impact of JA during the interaction of *L. bicolor* with roots (Plett et al. 2014). The ability of *Trichoderma* to promote plant growth has been attributed to either the production or induction of different kinds of phytohormones (Sofo et al. 2011; Nieto-Jacobo et al. 2017). Plant hormones play other main roles in plant defence architecture during communication with fungi. Plants require phytohormones to control microbe colonisation; in the model *A. thaliana*-*Trichoderma*, it has been discovered that the host plant, without the support of SA, is unable to prevent the colonization of *T. harzianum* in the vascular system, leading to imminent plant death (Alonso-Ramirez et al. 2014). Moreover, GA signalling regulates the expression of arbuscular mycorrhizal induced genes that have a direct impact on hyphal entry and branching into the host root (Takeda et al. 2015). Therefore, it is important to study the mechanisms of how beneficial microorganisms interact with the plant via signalling pathways that involve the plant-microbe phytohormone network.

1.4.3 Role of secondary metabolites in plant-fungi interaction

Secondary metabolites (SMs) are low molecular weight compounds such as non-ribosomal peptides, polyketides, terpenoids and pyrones. Some of them are involved in growth (e.g.

siderophores) or biological interactions (e.g. toxins). The rhizosphere serves as a complex arena where plants and different microorganisms secrete SMs as major messengers to establish beneficial or detrimental relationships (Mhlongo et al. 2018). Species of the genus *Trichoderma* are known to produce a vast array of SMs which are mainly produced when the fungi interact with other microorganisms in the rhizosphere (Mukherjee et al. 2012; Schmoll et al. 2016). Moreover, *Trichoderma* SMs participate as defence molecules and serve as signal molecules to communicate with its environment (Zeilinger et al. 2016). The genes that are involved in the biosynthesis of SMs are predominantly in large biosynthetic gene clusters (Zeilinger et al. 2016).

Interestingly, SMs which are part of the chemical defence of plants such as alkaloids, coumarins, isoflavonoids, polyacetylenes, quinones, tannins and terpenes have antimicrobial activity (Reichling 2010). Another important role of secondary plant metabolites is that they act as mediators of plant-microbe interactions and they can shape the composition of microbial communities and their metabolic pathways (Musilova et al. 2016). Nonetheless, plant microbes have evolved to manipulate their host metabolism and induce favorable nutritional conditions. For instance, the fungal plant pathogen *Alternaria* secretes host-specific toxins (HSTs) that act as effectors to induce toxicity and pathogenicity (Friesen et al. 2008). In contrast, mutualistic-endophytic fungi secrete mycotoxins to protect the host plant against herbivores (Faeth 2002). Likewise, root endosymbionts can also modify the plant metabolome including secondary metabolite levels in leaves; for example, catalpol, which plays a role in direct plant defence (Schweiger et al. 2014). In summary, SMs are mainly studied in the context of economically significant plant pathogens. The function of SMs in beneficial microorganisms such as *T. virens*, which involve genes in the biosynthesis of SMs during its interaction with maize (Lawry 2016), is poorly understood.

1.4.4 **Role of effector proteins in plant immunity repression by microbes**

Plant pathogens, and most likely fungal endophytes, manipulate host cellular processes through the secretion of molecules named effectors which are microbe-produced molecules that have specific effects on the genotype of their host to establish a close relationship with the plant. Effectors are classified based on their localisation in the plant cell. Apoplastic effectors are secreted in the apoplast and act as counter-defence molecules by inhibiting host enzymes e.g. plant hydrolases and proteases (Morgan and Kamoun 2007; Clark et al. 2018), whereas cytoplasmic effectors are translocated into the cell cytoplasm where they interact with intracellular targets to suppress the plant immunity response (Kale 2012; Shi et al. 2018). Many cytoplasmic effectors delivered by oomycetes carry an N-terminal signal peptide for secretion; followed by the amino acid sequence RXLR that is in charge of the translocation process with the C-terminal domain having the biochemical activity associated with the effector (Schornack et al. 2009; Wang et al. 2017). Although this particular translocation motif has not yet been seen in the genome analysis of fungi, it is predicted that similar mechanisms are used by fungi to translocate their effectors (Lo Presti et al. 2015). Recently, the biotrophic interfacial complex (BIC) was discovered in *M. oryzea*. BIC is a

structure where the fungi accumulate effectors before delivery and translocation into the host cell (Zhang and Xu 2014). Apoplastic effectors are secreted mostly by the conserved endoplasmic reticulum (ER)-Golgi secretory pathway. Nevertheless, cytoplasmic effectors without a signal peptide which are secreted by non-conserved secretory mechanisms and accomplish diverse functions (Giraldo et al. 2013; Wang et al. 2017). For example, during the barley (*Hordeum vulgare)-Blumeria graminis* f. sp. *hordei* interaction, the avirulence (Avr) proteins AVRa10 and AVRk1 which are secreted and located in the cytoplasmic area, enhance infection in susceptible varieties yet do not carry the common signal peptide for secretion (Ridout et al. 2006). Also, the unconventionally secreted effector chorismate mutase Cmu1 from *U. maydis* which interferes in the salicylic acid pathway inside of the host plant (Djamei et al. 2011).

Both pathogenic and beneficial microorganism effectors have a great affinity with phosphoinositides (PHIs) which are important components of cell membranes and have crucial roles in various cellular processes (Kale et al. 2010; Rafiqi et al. 2012; Choy et al. 2017). Bacterial Type III effectors manipulate PHIs to alter membrane morphology facilitating their entry into host cells (Ham et al. 2011; Salomon et al. 2013). The eukaryotic effector MiSSP7 from the symbiotic fungus *L. bicolor* actively enters the cell via endocytosis mediated by the PHIs interaction (Plett et al. 2011). In addition, several biotrophic fungi and oomycetes create cell-cell feeding structures referred to as haustoria surrounded by an intact plant plasma membrane which plays a primordial role in delivering effectors (Koeck et al. 2011; Wang et al. 2017). All these mechanisms enhance the process of colonization of the cells to establish a close association with the host.

1.5 The plant immune system

Plants have evolved to respond to any infection using a conserved two-tier innate immune system. The first line provides basal defence and recognises self from non-self-structures, and responds to molecules known as microbe- or pathogen-associated molecular patterns (MAMPs or PAMPs) e.g. chitin and flagellin (Jones and Dangl 2006) (Figure 1.1), as well as endogenous elicitors which are described as damage-associated molecular patterns (DAMPs) e.g. cell wall fragments (Ibrahim et al. 2013). The second line leads to rapid and enhanced defence which results from recognition of pathogen effectors (virulence factors), either directly or indirectly by their effect on host targets (De Wit et al. 2009; Cook et al. 2015).

In the soil, biotrophic, hemibiotrophic and necrotrophic microbes are constantly fighting for nutrients and trying to colonise plant roots. After plant cells sense MAMPs/DAMPs via pattern recognition receptors (PRRs), they activate basal MAMPs/PAMPs-triggered immunity (MTI/PTI) (hereinafter referred as MTI) which prevents further penetration attempts of the host epidermal cells (Postel and Kemmerling 2009; Miller et al. 2017). Nevertheless, successful pathogens and beneficial microorganisms might overcome MTI by the release of effectors or effector-like proteins;

to this microbial-response, plants have co-evolved an adaptive effector-triggered immunity (ETI) which is activated based on the recognition of effectors via R proteins (Thomma et al. 2011). ETI is more specific than the MTI response and generally leads to a hypersensitive response (HR) at the infection site resulting in disease resistance (Boller and Felix 2009; Cui et al. 2015). Furthermore, receptor-like kinases (RLKs), receptor-like proteins (RLPs) and mitogen-activated protein kinase (MAPK) cascades are fundamental signalling modules downstream of PRR activation by MAMPs/DAMPs, triggering biochemical, biophysical and molecular changes in the plant; for example, reactive oxygen species (ROS) generation, stomatal closure and defence gene activation, respectively (Meng and Zhang 2013; Tang et al. 2017).

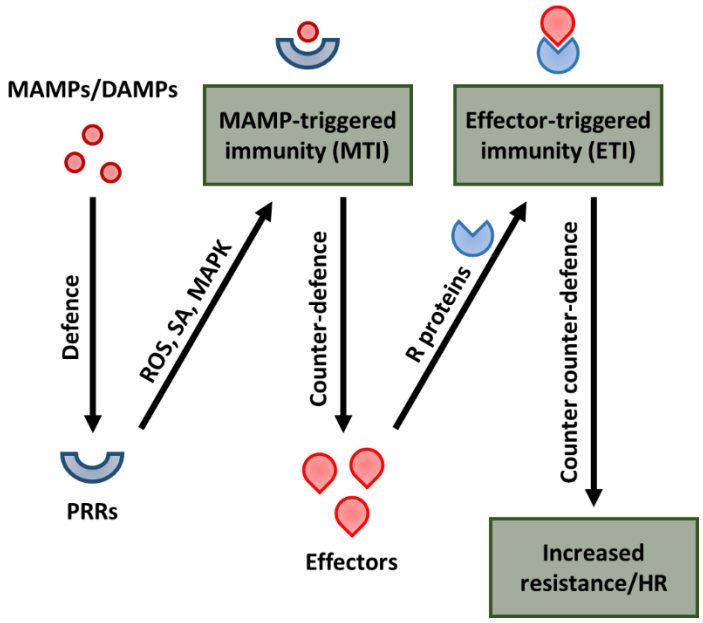

Figure 1.1 Schematic representation of zig zag model in plant immunity during plant-microbe interactions (Jones and Dangl 2006). In the first stage, microbe-/damage-associated molecular patterns (MAMPs/DAMPs) are detected via cognate pattern recognition receptors (PRRs) to initiate MAMPs-triggered immunity. In the second stage, microbes deliver effector-like proteins to overcome MTI and establish a successful infection, resulting in effector-triggered susceptibility (ETS). In the third stage, host recognition of one or more effector-like proteins by disease resistance (R) proteins, activates effector-triggered immunity (ETI), which is a robust and accelerated immune response. In the last stage, continuous cycles of MTI, ETS and ETI drive host-microbe co-evolution in effector functions and effector recognition, which might result in disease resistance and, usually, a hypertensive cell death response (HR) at the infection site. Abbreviations: ROS, reactive oxygen species; SA, salicylic acid; MAPK, mitogen-activated protein kinases. Image adapted from Incarbone and Dunoyer (2013).

1.6 Endophytic *Trichoderma*

Trichoderma spp. are ascomycetous fungi distributed in a large variety of ecosystems and are highly studied worldwide because of their properties as biocontrol agents (BCA). The major mechanisms that *Trichoderma* utilise for controlling plant pathogens are by direct competition for same niche-nutrients, mycoparasitism, production of cell wall degrading enzymes (CWDEs: cellulases, chitinases and glucanases) and secondary metabolites such as antibiotics which either induce

systemic resistance in plants (Brotman et al. 2010) or restrict the growth of potential microbial competitors. Another positive feature of *Trichoderma* spp. is their ability to promote plant growth, increase nutrient availability, improve crop production and enhance disease resistance (Vinale et al. 2008a; Mukherjee et al. 2013).

A large number of *Trichoderma* species behave as facultative-endophytic plant symbionts and have the capacity to penetrate plant tissues in order to create an endophyte-plant beneficial interaction. They act as free-living organisms and are found principally in plant root ecosystems (Harman et al. 2004; Vinale et al. 2008b). During this interaction *Trichoderma* produce compounds that cause substantial changes in the plant architecture, enabling successful colonisation. Endophytic *Trichoderma* penetrate the first or second layer of plant root systems, colonising first the root epidermis and then into the cortex; however, they do not reach the xylem or phloem systems (Chacon et al. 2007).

It has been proposed that before colonisation, *Trichoderma* establish a chemical dialogue with the plant. *Trichoderma* express and release a cocktail of MAMPs, DAMPs and protein-like effectors that can be recognised by plant receptors, inducing beneficial responses in the host and minimising the stimulation of the plant immune system (Hermosa et al. 2013; Schmoll et al. 2016; Mendoza-Mendoza et al. 2018). Once *Trichoderma* hyphae penetrate the roots, a series of cross-talk molecules likely come into play (Druzhinina et al. 2011; Nogueira-Lopez et al. 2018). In addition, many metabolites secreted by *Trichoderma* trigger the immune system of the plant. For example, secondary metabolites produced by two different species, *T. harzianum* and *T. atroviride* induce the up-regulation of gene expression of defence related-proteins such as chitinase class IV, endochitinase and PR-1 (Vinale et al. 2008a). In addition, the secondary metabolite 6-pentyl-alpha-pyrone produced by *T. atroviride* acts as an auxin-like compound inducing plant growth promotion and increasing leaf and root system volume (Vinale et al. 2008b). It is likely that each metabolite plays a particular role during the interaction. Furthermore, *Trichoderma* interaction with plant host roots increases sensitivity, allowing the plant to respond more successfully to later pathogen invasion, termed induced systemic resistance (ISR) (Shoresh and Harman 2008; Saravanakumar et al. 2016).

1.7 Summary

Symbiosis, including beneficial relationships that endophytic fungi establish with their host plant, is a complex interaction that occurs in nature (Figure 1.2). Although this interaction is technically a plant infection, endophytes do not cause perceptible disease symptoms compared with those caused by pathogenic microbes (Rodriguez et al. 2009). By contrast, endophytes promote plant growth, confer disease resistance, and increase tolerance to diverse abiotic stresses (Yedidia et al. 1999 ; Bakker et al. 2013). Meanwhile, endophytes obtain nutrients and protection from the host plant, creating a mutualistic symbiosis (Harman et al. 2004). Despite the direct benefits obtained

from this mutualistic interaction, plants react to endophyte colonisation via a basal immune response activation, which plants have evolved to recognise conserved microbial features referred to as MAMPs (Newman et al. 2013). Plants translate this signal into a defence response against any microorganism which tries to colonise them, including endophytes (Bittel and Robatzek 2007). Successful colonisation by endophytes suggest that these specialist microorganisms overcome the plant immune system or reprogramme and maintain the integrity of the host cells, therefore, eventually creating a long-term symbiosis (Vinale et al. 2008b). During this mutualistic symbiosis, beneficial microbes that are hosted in the root system are capable of triggering ISR in foliar tissues which, in turn, enhances host plant defences against a broad range of pathogens and insect herbivores (Pieterse et al. 2014). However, how the fungal-derived signals for ISR are transported into foliar tissues is not known.

Endophytes in many aspects function as biotrophic pathogens which require the presence of their host to complete their life cycle (Venkateshwaran et al. 2013). These pathogens manipulate and evade immune responses through releasing an arsenal of molecules known as effectors, as well as inducing cell surface changes (Plett et al. 2011). In response, plants contain extracellular immune receptors, such as, RLPs and RLKs (Toruño et al. 2016), also the nucleotide-binding, leucine rich repeat (NB-LRR) variety of intracellular receptors called R proteins to detect the activity of effectors, and as a consequence induce additional defence mechanisms which secure an extended protection against invaders (Jones and Dangl 2006; Tang et al. 2017). Coevolution between endophytes and plants has led both organisms to change. Endophytes have diversified or acquired additional effectors that suppress ETI; plants have developed novel R proteins to detect them. Communication between invading organisms and their host leads to a molecular re-programming of both organisms which includes activation and repression of genes (Bailey et al. 2006). Inside the host, activation of small RNAs plays a fundamental role in the transcriptional and post-transcriptional regulation of genes involved in the immune response (Reichling 2010; Deng et al. 2018). Interestingly, some effectors secreted by pathogens regulate the synthesis of plant-derived small RNAs or act directly as transcriptional factors in the host, resulting in the manipulation of gene expression involved in the immune system, minimising its stimulation (Katiyar-Agarwal et al. 2006; Huang et al. 2016). Therefore, the understanding of how endophytic *Trichoderma* modulate plant defence will provide new insights into the processes that are required for establishment of successful plant colonisation.

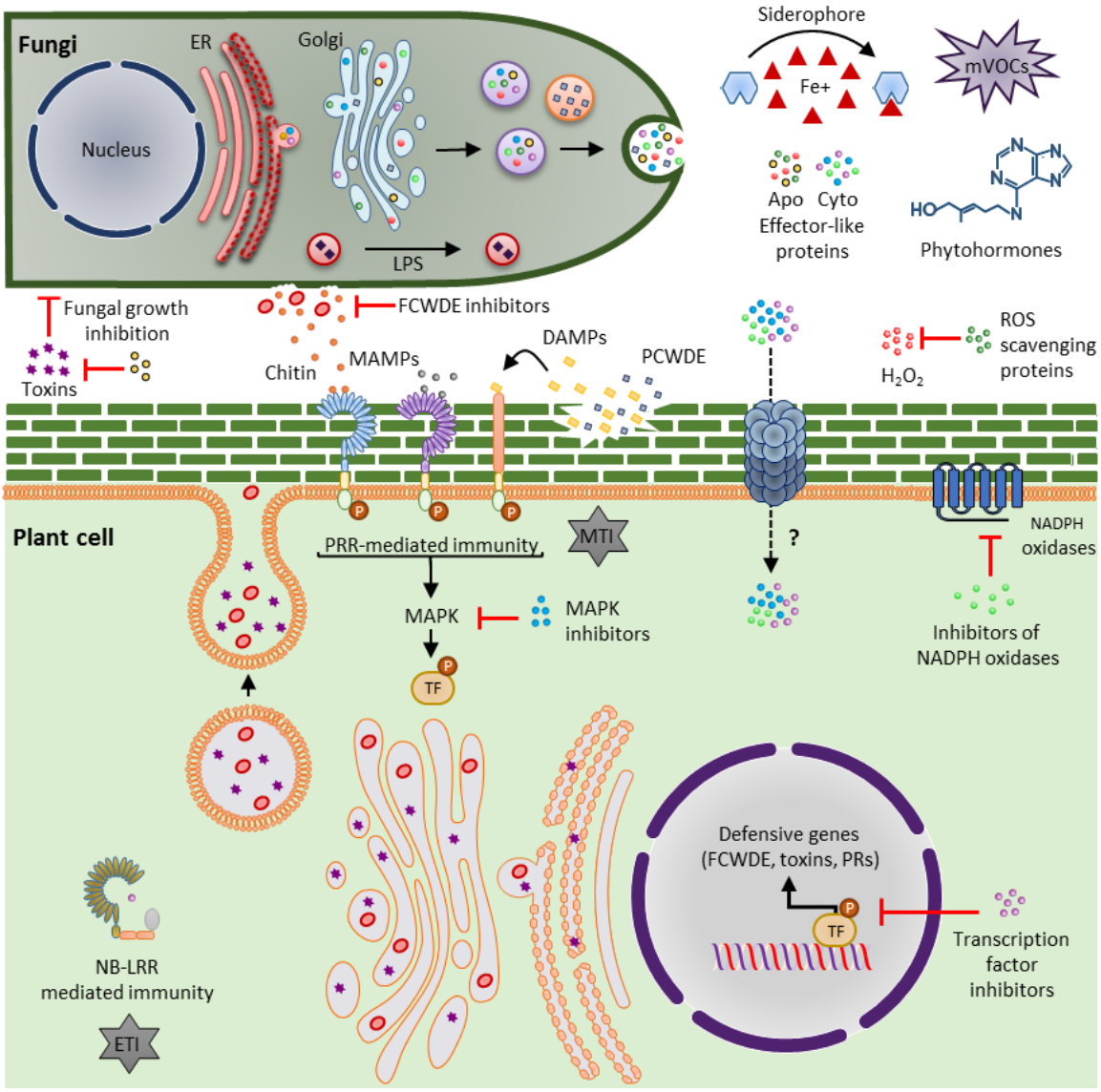

Figure 1.2 Molecular signalling microbe-plant interaction. Fungi continuously release proteins and secondary metabolites to interact with their host plant cell. Firstly, microbe-associated molecular patterns (MAMPs), e.g. chitin or damage-associated molecular patterns (DAMPs), e.g. plant cell wall oligosaccharides, are detected by pattern recognition receptors (PRR) activating MAMPS-triggered immunity (MTI). Secondly, fungi deliver apoplastic and cytoplasmic effector-like proteins to block at different levels the MTI response, but these proteins could be recognised by nucleotide binding and leucine rich repeat (NB-LRR) immune receptors that trigger the second layer of defence called effector-triggered immunity (ETI). Finally, secretion of fungal secondary metabolites, e.g. siderophores, phytohormones and microbial volatile organic compounds (mVOCs) that function as messengers between fungi and plants, and have a direct impact in plant nutrition, defence and signalling. Abbreviations: ER, endoplasmic reticulum; LPS, leaderless protein secretion; FCWDEs, fungal cell wall-degrading enzymes; PCWDEs, plant cell wall-degrading enzymes; PRs, pathogenesis-related proteins; ROS, reactive oxygen species; TF, transcription factor; MAPK, mitogen-activated protein kinase; NADPH, nicotinamide adenine dinucleotide phosphate; P, phosphorus; Fe, iron; H_2O_2, hydrogen peroxide. Image adapted from Schmoll et al. (2016) with modifications.

1.8 Aim of this study and hypotheses

Plant symbionts have an important role in plant performance and plant fitness. However, the way that these microorganisms interact with their host plant is far from being understood. The ability of *Trichoderma* spp. to behave as plant endophytes has led to their application as plant growth promoters and biocontrol agents. Even though the beneficial properties of *Trichoderma* as a plant symbiont are well known, the molecular mechanisms during fungal colonisation of the plant requires further elucidation.

The genus *Trichoderma* is an appropiate model to study plant-microbe interactions. A large number of *Trichoderma* species behave as facultative-endophytic plant symbionts and can penetrate plant tissues to create a beneficial interaction. Despite the fact that most plants are colonised by fungal endophytes, very few studies have focused on understanding the molecular mechanisms which determine these mutual interactions. Therefore, next generation ''omics'' technologies (e.g. proteomics and metabolomics) coupled with high-throughput tools for functional genomics (e.g. gene deletion, complementation and localisation) are desired for a better understanding of *Trichoderma's* biology.

The main purpose of this investigation is to understand the principal molecular mechanisms operating at the proteomic and metabolic levels, and responsible for the establishment of the beneficial relationship between endophytic *Trichoderma virens* Gv29.8 and its host plant, *Zea mays*. The findings will lay the foundation for future studies for a wider knowledge of plant-fungus interactions, particularly at the molecular level.

The following chapters describe the aims and hypotheses in this study:

Chapter 2

Aim: to unravel the endophytic behaviour of *T. virens* with maize under hydroponic growing conditions to establish a feasible methodology to study fungal endophytism, and subsequently perform the proteomic and metabolic analyses associated with the interaction.

Hypothesis: the interaction between *T. virens* and maize, including the ability of *Trichoderma* to colonise root tissues endophytically can be demostrated using a hydroponic growing system.

Chapter 3

Aim: to uncover the proteomic dialogue of *T. virens* in the apoplast of maize plants during fungal-root colonisation.

Hypothesis: By comparing un-inoculated to inoculated maize roots with *Trichoderma*, differences in the apoplastic secretome could be expected, including the expression of protein families that constitute the molecular dialogue between *T. virens*-maize and may play major roles in root colonisation and plant defence.

Chapter 4

Aim: to characterise the role of an up-regulated gene involved in secondary metabolism during the *Trichoderma*-maize interaction.

Hypothesis: knocking out an encoding protein gene that is up-regulated during the *Trichoderma*-maize interaction, will create a mutant less effective in colonising the plant, and likely induce higher plant immune response changes during the fungal-plant interaction.

Chapter 5

Aim: to assess differences in maize root metabolic responses to fungal colonisation using two *T. virens* genotypes (WT and the deletion mutant created in chapter 4).

Hypothesis: During the *Trichoderma*-maize interaction, shifts in the metabolic profile from maize roots could be triggered by *T. virens* (WT and *Δtvox1*), including general and genotype-specific metabolic responses.

The conclusion, **chapter 6,** the main outcomes of this study are discussed, evaluating the successes and setbacks of the research, and its future applications.

2 Endophytic *Trichoderma*: unravelling the interaction between *T. virens* and maize using an hydroponic growing system

2.1 Introduction

Trichoderma spp. are cosmopolitan soil fungi with the capacity to establish symbiotic relationships within the roots of most plant species (Harman et al. 2004). *Trichoderma* spp. can promote plant growth, increase nutrient availability and improve crop production, they can also increase the plant ability to respond successfully to later pathogen invasion, through a process termed ISR (Shoresh and Harman 2008; Vinale et al. 2008a; Shoresh et al. 2010). The plants react to endophyte colonisation via a basal immune response activation, whereby plants have evolved different strategies to recognise conserved microbial features referred to as MAMPs (Lorito et al. 2010; Zamioudis and Pieterse 2012; Schmoll et al. 2016; Mendoza-Mendoza et al. 2018). Diverse MAMPs synthesized by *Trichoderma* have been identified (Hermosa et al. 2013), including the cerato-platanin protein Sm1 (Djonovic et al. 2006), and the ethylene-inducing xylanase (EIX) (Ron and Avni 2004). The proteinaceous elicitor Sm1 is induced during the *Trichoderma virens*-plant interaction, and promotes the expression of pathogenesis-related genes (Djonović et al. 2007). EIX has a dual role during plant colonisation, involving both lytic enzyme activity and induction of systemic resistance in specific cultivars of tobacco and tomato (Rotblat et al. 2002; Ron and Avni 2004). Moreover, MAMPs secreted by different *Trichoderma* species such as swollenins, cellulases and polygalacturonases function to induce plant defence and systemic resistance (Hermosa et al. 2013; Saravanakumar et al. 2016). Secondary metabolites produced by two *Trichoderma* strains: *T. harzianum* and *T. atroviride* can also elicit the plant immune system, by the induction of gene expression of defence related-proteins such as chitinase class IV, endochitinase and pathogenesis-related protein 1 (Vinale et al. 2008a).

Endophytic *Trichoderma* penetrate the first and second layers of plant root systems, first colonising the root epidermis and then into the cortex area, without reaching the vascular system (Chacon et al. 2007). The initial step of root colonisation by *Trichoderma* start with attachment on the root surface followed by the formation of appressoria-like structures that may help for penetration into the internal tissues (Lawry, 2016; Nogueira-Lopez et al. 2018). After recognition by *Trichoderma* MAMPs, the plant roots respond by depositing callose in the neighbouring non-colonised cells, allowing only superficial cell-colonisation. Microscopic observations of early colonisation of tomato roots by *T. harzianum* showed the capacity of the fungus to colonise inter- and intracellular spaces without disrupting cell integrity (Chacon et al. 2007). However, *T. asperellum* (formally called *T. harzianum*) induces morphological and physiological changes in cucumber plant roots, which include necrosis of the penetration peg, high chitinase activity and formation of fluorescent

products in intercellular spaces of the colonised roots (Yedidia et al. 2000). Additionally, enhanced protection against ROS, and repression of the ET synthesis pathway is proposed to enable root colonisation by *Trichoderma* as has been shown for other endophytes (Shoresh et al. 2010). Recently, it was observed that the cerato-platanin elicitor Sm2 from *T. virens* is required for root colonisation (Crutcher et al. 2015), although the mode of action is currently unknown.

The aim of this study was to investigate the endophytic behaviour of *T. virens* under hydroponic growing conditions using maize as a host plant, and to compare phenotypic changes in the root system between un-inoculated and inoculated plants. The findings provide sufficient evidence to demonstrate that the hydroponic methodology is suitable to allow proteomic and metabolic analysis during the interaction.

2.2 Materials and methods

2.2.1 Maize germination

Maize seeds from hybrid line 34H31 (Pioneer® Brand Products, New Zealand) were surface sterilised by soaking in 2% (w/v) sodium hypochlorite (NaOCl) (active ingredient) for 7 min, followed by 70% ethanol for 7 min, then washed three times with sterile nanopure water. Seeds were germinated on sterile seed germination papers (30 cm x 45 cm; Anchor Paper Company, USA) previously soaked in sterile Hoagland's No.2 basal salt solution (Sigma-Aldrich, USA) (Hoagland and Arnon 1950), for 60 h in a humidity controlled plant growth chamber (Humidity Control Versatile Environmental Test Chamber, SANYO, Japan) at 25°C under a 16 h light/8 h dark cycle and a relative humidity of 80%.

2.2.2 Inoculum preparation

Trichoderma virens Gv 29.8 conidia kindly provided by Dr. Charles M. Kenerley (Texas A&M, USA), were grown on potato dextrose agar (PDA) (Difco, Fisher Scientific, USA) at 25°C under a cycle of 12 h light and 12 h dark for 7 d to induce conidiation. Conidia were collected using sterile nanopure water and filtered through a double layer of sterile Miracloth (Merck Millipore, USA). The conidial concentration was determined using a Neubauer chamber and adjusted to $1x10^8$ conidia/mL in sterile nanopure water.

2.2.3 Colonisation of maize by *Trichoderma virens*

Sterilised maize seeds were surface inoculated with *T. virens* conidia as follows: Pre-sterilised seeds were placed in a sterile petri dish to let them dry, then 10 µL of conidial solution ($1x10^8$ conidia/mL), containing $1x10^6$ *Trichoderma* conidia was applied on the seed surface. The seeds were left in the petri dish until all the water was evaporated from the seed surface and then were germinated on sterile seed germination paper (see section 2.2.1). After germination, seedlings were grown under

hydroponic conditions without aeration in 50 mL centrifuge tubes containing 45 mL of sterile Hoagland's solution with a piece of sterile cotton to support the seedling (Figure 2.1 A). Seedlings were incubated for an additional 60 h as described in section 2.2.1. For sampling, fresh root tissues were washed gently with sterile nanopure water, and then 2 cm sections nearest to the seed were cut from the primary root, known to be the primary colonisation area for *T. virens* (Lawry 2016). Un-inoculated roots samples were taken as the control.

2.2.4 Confocal visualisation of maize roots colonisation by *Trichoderma virens*

T. virens-maize root colonisation was examined using confocal microscopy (Fluoview FV 10i, Olympus, Tokyo, Japan). For this analysis, transverse free-hand sections of maize roots were prepared using the following procedure: After 5 days post inoculation (d.p.i) maize roots were collected and either washed in phosphate-buffered saline (PBS) pH 7.4 or fixed in fresh ethanol: acetic acid (3:1, v/v) solution. Two staining methods were used: for fresh tissues 10 µg/mL of wheat germ agglutinin (WGA)-Alexa Fluor™488 (Thermo Fisher Scientific, USA)/5 µg/mL of FM4-64 dye/20 µg/mL propidium iodide (PI) (Thermo Fisher Scientific, USA) mixture was used, while fixed tissues were stained with 10 µg/mL of WGA-Alexa Fluor™ 488/20 µg/mL PI (Sigma-Aldrich, USA) mixture. Fungal material was stained with WGA-Alexa Fluor™ 488 (Mochizuki et al. 2011). Plant cell walls were stained with PI, while the plasma membranes were stained with FM4-64 (Bolte et al. 2004). For fixed tissues, roots were treated with 10% KOH for 4 h at 95°C and then transferred to PBS pH 7.4 for 1 h. Samples were infiltrated with the staining solution (20 µg/mL PI; 10 µg/mL WGA-Alexa Fluor™ 488, 0.02% Tween 20 made up in 1X PBS pH 7.4) for 15 min twice. Samples were stored in PBS-tween (0.02%) in the dark at 4°C until they were examined. For fresh tissues, samples were washed in PBS solution and infiltrated with the same staining solution mentioned above, except that PI was substituted for FM4-64.

2.2.5 Transmission electron microscopy visualisation of maize roots colonisation by *Trichoderma virens*

T. virens root colonisation was followed by using transmission electron microscopy (TEM). Maize plants were grown under hydroponic conditions and inoculated with *T. virens* conidial suspension as described in section 2.2.3. After 5 and 7 d.p.i maize roots were collected and fixed in modified Karnovsky's fixative solution (3% glutaraldehyde, 2% formaldehyde in 0.1 M PO_4 buffer pH 7.2) (Karnovsky 1965). The first centimetre of the primary root of each plant was cut in 1 mm sections with a razor blade and immersed into Karnovsky's fixative solution. Root sections were vacuum infiltrated reducing the pressure to -45 kPa for 1 hr and then incubated overnight at 4°C. Fixed tissues, were transferred to 100 mM PBS solution pH 6.5. Root sections were processed and stained using standard TEM methods. TEM analyses were conducted at The Manawatu Microscopy and Imaging Centre at Massey University, under the supervision of Dr. Carla Eaton.

2.3 Results

2.3.1 *Trichoderma virens*-maize root interaction

A hydroponic system was used to assess communication between *T. virens* and maize plant roots (Figure 2.1 A). When maize seeds were inoculated with the fungal conidia and then germinated on germination paper soaked with Hoagland's solution, germination was not inhibited by the fungus (data not shown).

The presence of *T. virens* altered seedling root morphology when compared with un-inoculated seedlings (Figure 2.1 B and C); a reduction in the length of secondary roots and the presence of a brownish pigment on the surface were evident in the inoculated seedlings (Figure 2.1 C and E). The brownish pigment was independent of the original *T. virens* spore inoculum (seedlings inoculated from 10^4 to 10^7 conidia per seed, Supplementary Figure 1). This pigmentation, which extended from the epidermal to cortical cell layers (Figure 2.1 E and G), was not present in un-inoculated roots (Figure 2.1 D and F), but was not observed in the vascular system (see Figure 2.1 E and G).

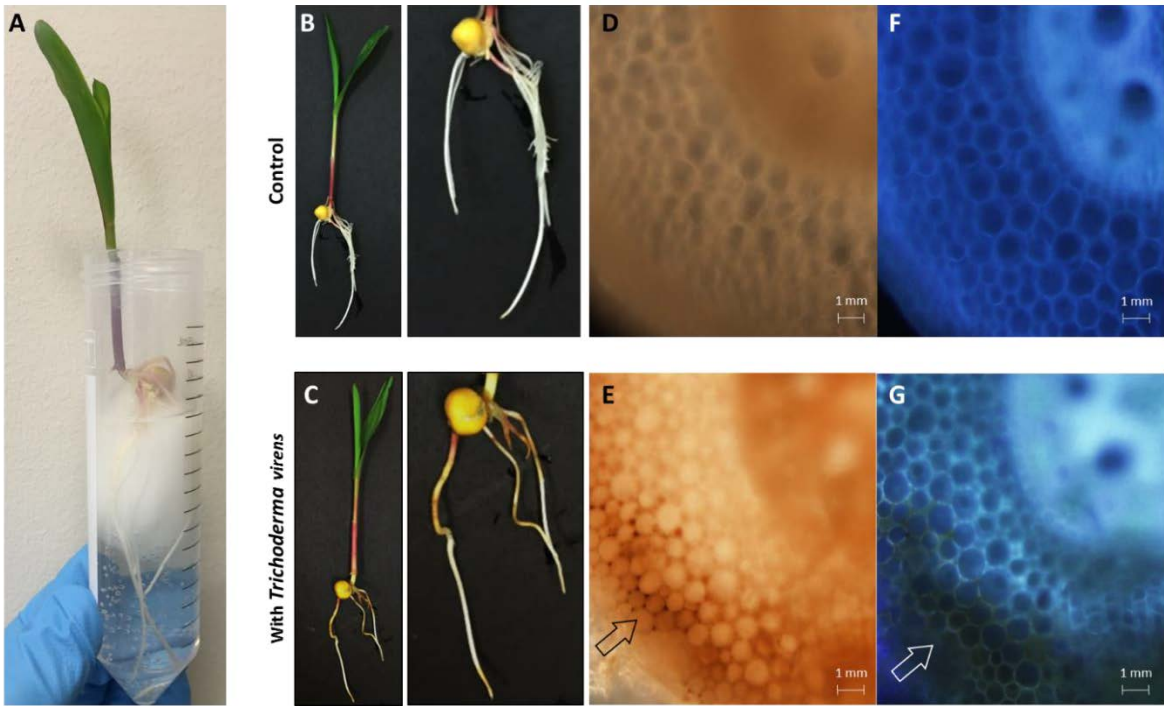

Figure 2.1 Overview of *T. virens*-maize interaction under a hydroponic system. (A) Five days old maize seedling growing aseptically under hydroponic conditions. **(B)** Un-inoculated and **(C)** plants inoculated with *T. virens*. Inoculated plants show phenotypical changes in their root system compared to the control. Cross section of un-inoculated primary root **(D)** bright-field and **(F)** DAPI. Cross section of inoculated primary root **(E)** showing accumulation of brown pigmentation in epidermal and cortical cells, bright-field and **(G)** DAPI. Images were obtained with a fluorescent microscope.

2.3.2 Confocal visualisation

To examine the colonisation of *T. virens* in the root system, staining of the fungal cell wall (WGA-Alexa Fluor™ 488) and the plant cell wall (PI) and/or plant membrane (FM4-64) was performed. Superficial fungal root colonisation was predominantly found in the first two centimetres of the primary root (closer to the seed) compared with other sections of the primary root (Figure 2.2 A and C). In addition, *T. virens* colonised secondary roots and new root tips (Figure 2.2 B and D), showing hyphal affinity to secondary roots when they are emerging (Figure 2.2 D). The formation of appresorium-like and haustorium-like structures was also observed, suggesting that *T. virens* uses specialised structures to interact and penetrate host cells (Figure 2.2 E and F). Interestingly, these structures were multinucleated (Figure 2.2 E and F). A transverse cut of the primary maize root enabled visualisation of the internal colonisation by *T. virens*. The fungus colonised the cortex layer adjacent to the vascular system of the primary root (Figure 2.2 G). *T. virens* colonised intercellular spaces (apoplast) (Figure 2.2 H). To visualise if *T. virens* colonised intracellular spaces, the plasma membrane dye (FM4-64) in combination with WGA-Alexa Fluor™ 488 was used to follow the fungus. As observed in Figure 2.2 I, *T. virens* colonised intracellular spaces and grew between the plasma membrane and the plant cell wall.

2.3.3 Transmission electron microscopic visualisation

To follow the endophytic colonisation pattern of *T. virens* in the root system, fresh maize tissue 5 and 7 d.p.i were analysed using TEM. Transverse sections of root samples taken from maize seedlings revealed the presence of fungal hyphae-like structures growing inter- and intracellularly in the epidermal and cortical area of the host (Figure 2.3). As previously observed by confocal microscopy, these findings confirm that *T. virens* has the ability to colonise different sections of the root system. However, the formation of appresorium-like and haustorium-like structures that the fungus may utilise to penetrate or interconnect between cells was not observed.

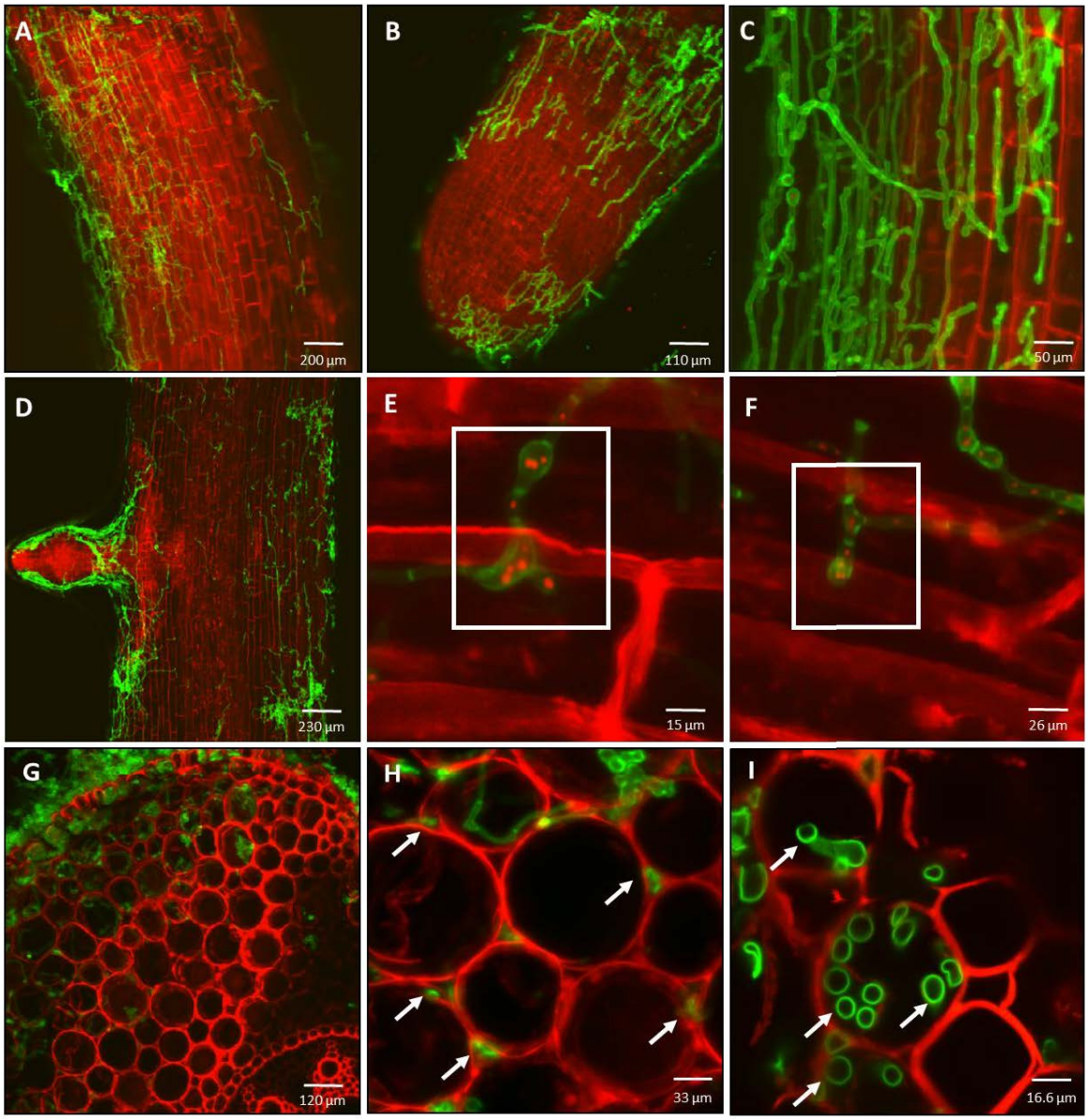

Figure 2.2 Colonisation pattern of *T. virens* in maize roots. (A) After 5 d.p.i, *T. virens* hyphae inhabit epidemical cells of maize primary root and **(B)** root tip of secondary root. **(C)** Close up of the hyphae occupying epidemical cells of the differentiation zone of primary root. **(D)** *T. virens* hyphae surrounding secondary root in development. **(E)** Formation of haustorium-like and **(F)** appresorium-like structures in epidermal cells. **(G)** Cross section of primary root showing internal colonisation of epidermal and cortical layers near to the vascular system. **(H)** Intercellular and **(I)** intracellular colonisation of cortex cells by *T. virens* hyphae (arrows). Fungal and plant cells were detected using WGA-Alexa Fluor 488 (green channel), propidium iodide (PI) and FM 4-64 Dye (red channel). Plant cell walls were detected with PI **(A-F)** and plant plasma membrane with FM 4-64 **(G-I)**. Fungal cells were detected with WGA-Alexa Fluor 488 **(A-I)**. Images were obtained with a confocal microscope.

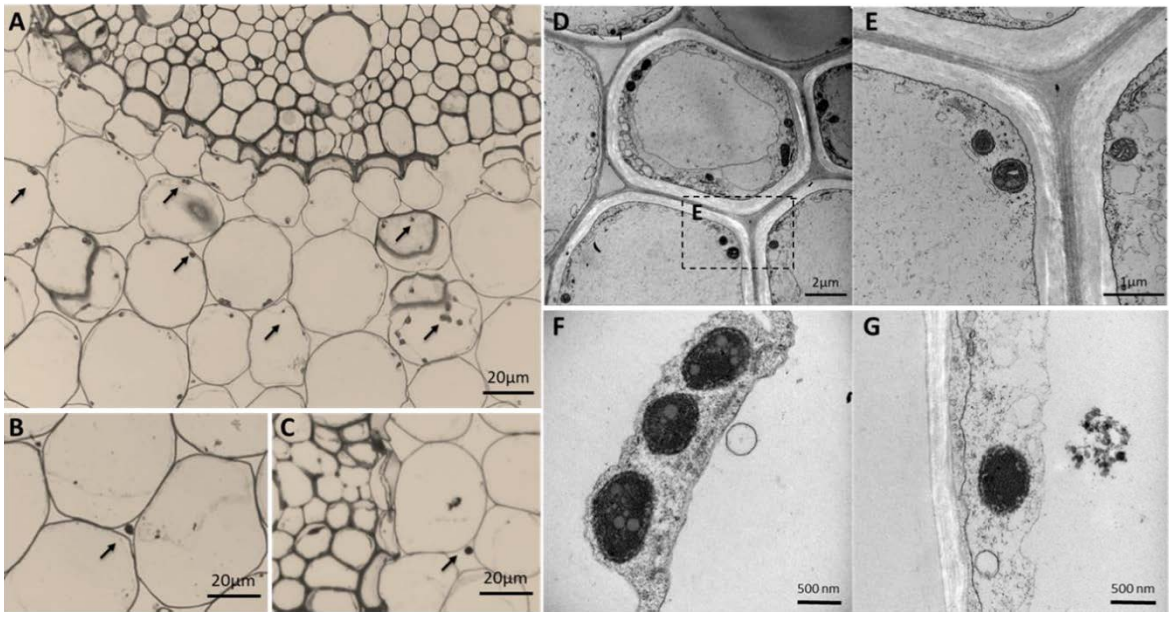

Figure 2.3 Transmission electron micrographs during *T. virens*-maize interaction. Light micrographs of ultra-thin cross-sections of maize primary root inoculated with *T. virens*. **(A)** Hyphae-like structures (black arrows) colonising intracellular spaces of cortex cells and **(B)** hyphae-like (black arrows) structure colonising intercellular spaces in the cortex area. TEM micrographs magnified **(D)** X1,000, **(E)** X2,000, **(F)** and **(G)** X4,000 showing hyphae-like structures colonising in the intracellular spaces of the cortical cells.

2.4 Discussion

2.4.1 Root interaction with *Trichoderma virens*

Previous reports describe *T. virens* as being endophytic in different host plants (Vargas et al. 2009; Moran-Diez et al. 2015; Lawry 2016; Romão-Dumaresq et al. 2016). Our findings showed that *T. virens* colonised different sections of the root system, including primary and secondary roots (Figure 2.2). Both appresorium and haustorium-like structures were visualised when *T. virens* was colonising epidermal maize cells, suggesting that *T. virens* utilises these structures to directly penetrate and uptake nutrients from the host roots. The formation of specialised structures during plant-microbe interactions has been widely studied in other fungal models including *Trichoderma* (Mendgen and Deising 1993; Bailey et al. 2009; Lawry 2016). The presence of multinucleated hyphal structures in a plant-microbe interactions is an interesting event which has been previously reported in oomycete haustoria formation (Fraymouth 1956). However, its functionality has not been characterised. Recent studies in filamentous fungi have examined nuclear movements in multinucleated cells (Gibeaux et al. 2017), and nuclear division and displacement during appresorium formation, implying a continuous gene expression *in planta* that facilitates fungal proliferation after penetration; for example, effectors and virulence factors (Jenkinson et al. 2017). The presence of multinucleated hyphae in *Trichoderma* suggests that these specialised structures may contribute to fungal proliferation and as a vehicle to deliver molecules inside the plant. Interestingly, *T. virens* is able to endophytically colonise inter- and intracellular spaces of maize

roots (Figure 2.2 and Figure 2.3), suggesting that the fungus utilises both pathways to establish itself in the host root system. This colonisation pattern was similar to that previously seen in the *T. harzianum*-cucumber model, where *T. harzianum* had the capacity to colonise both cell spaces in the root system (Yedidia et al. 1999).

During the interaction, phenotypic responses of maize roots were detected when colonised by *T. virens*; for example, the appearance of a brownish pigment and reduction of secondary root growth (Figure 2.1). Accumulation of browning of inoculated roots has been observed previously in *T. virens* (Moran-Diez et al. 2015) and *Trichoderma harzianum* (Palaniyandi et al. 2017). In other fungal systems, Allen et al. (1989) demonstrated that in incompatible interactions between vesicular-arbuscular mycorrhizal fungi and the non-mycotrophic weed *Salsola kali*, invaded roots segments turned brown in response to fungal invasion; however, during a compatible interaction with the mycotrophic grass *Agropyron dasystachmyum*, browning wasn't observed. In addition, susceptible reactions such as root tip browning and expansive browning on root surfaces were reported by Sutton et al. (2006) and Ye et al. (2013) during adverse interactions between their host plant and the pathogens *Pythium aphanidermatum* and *Fusarium graminearum*, respectively. Therefore, it could be argued that maize cells may be responding to *T. virens* colonisation by triggering accumulation of phenolic compounds involved in initial responses to stress to reinforce plant cell walls and inhibit fungal growth (Beckman 2000). Nevertheless, it cannot be discounted that the physiological changes in maize roots were due to the deposition of *T. virens* secondary metabolites such as melanin onto the root surface or into the media, or that *T. virens* mycelia were blocking the aeration of the media creating anoxic conditions and inducing this physiological change (browning). This phenotype was also observed in maize seedlings inoculated with *T. virens* using vermiculite as substrate (Dr Artemio Mendoza, personal communication).

Endophytic colonisation (both inter- and intracellular) by *T. virens* showed different mechanisms that the fungus undertakes to develop an interaction with its host plant and to promote fungal growth on plant tissue. A similar pattern of colonisation was observed in the interaction of the endophytic fungus *Piriformospora indica* with barley plants (Deshmukh et al. 2006). This symbiotic fungus requires host cell death in differentiated barley roots, in order to proliferate and become endophytic and form a mutualistic interaction. This implies that the fungus biotrophically colonises by digesting plant cell walls and subsequently either interferes with the host cell death program or actively kills host cells (Deshmukh et al. 2006). It is likely that under hydroponic conditions, *T. virens* may employ similar mechanisms to colonise maize roots.

2.5 Conclusion

Overall, this study has confirmed that *T. virens* behaves as an endophyte of maize plants under hydroponic growing conditions. During the interaction, the physiological changes present in the root system suggested that maize roots are responding to the presence of *Trichoderma*. Microscopic observations revealed that *T. virens* colonises only epidermal and cortical cell layers of primary and secondary roots. Moreover, specialised hyphae such as appressorium- and haustorium-like structures were present, and are possible mechanisms used by *T. virens* to penetrate and extract nutrients from the root tissues. Following the endophytic behaviour of *T. virens*, inter- and intracellular colonisation were confirmed as routes to develop an interaction with the host plant. Therefore, the following experiments were designed to elucidate the molecular mechanisms of *Trichoderma* that occur in the root system for developing an endophytic relationship by manipulating host defence responses.

3 Proteomic analysis of the apoplast during the *Trichoderma*-plant interaction

3.1 Introduction

Higher plants establish close relationships with beneficial and detrimental microbes such as bacteria, oomycetes and fungi. To achieve successful infection of host roots and progressively colonise the internal tissues, plant microbes have evolved several strategies to manipulate and overcome plant immune responses. Accordingly, plants have developed specific structural and chemical pathways to counter microbial invasions. The plant cell wall and cuticle represent the first layers of plant defence (Pusztahelyi et al. 2015; Houston et al. 2016). The initial steps of infection during plant-microbe interactions start with the recognition of plant surface cues that induce the secretion of proteins and formation of infection structures, e.g. appressorium-like structures, to facilitate penetration (Lanver et al. 2014). After penetration, a second layer of defence takes place in the apoplast (Gupta et al. 2015). The apoplast is the space outside the plasma membrane, and includes the plant cell wall and the surrounding intercellular space (Figure 3.1), where several physiological processes take place; for example, water transport, nutrient uptake, growth regulation, and gas exchange (Hoson 1998; Sattelmacher 2001; Fatima and Senthil-Kumar 2015). The apoplast is also considered an interface which mediates the molecular crosstalk between microbes and plants (Doehlemann and Hemetsberger 2013). Apoplastic proteins which are secreted by both organisms have major roles in physiological and biological processes associated with the maintenance of cell wall structure, stress responses, primary and secondary metabolism, and signalling (Alexandersson et al. 2013; Kim et al. 2013). For example, secreted plant cell wall degrading enzymes induce remodelling of plant cell walls and are highly expressed in the presence of plant root intruders (Mitsumasu et al. 2015).

Plant microbes and their host plants continuously secrete an arsenal of proteins into the apoplast (Figure 3.2), either by conventional or unconventional secretion systems (Giraldo et al. 2013; Liu et al. 2014). The conventional secretion system involves the Golgi-endoplasmic reticulum pathway for those proteins that carry a defined N-terminal signal peptide. This signal is usually 20-30 amino acids in length and an overall positive charge (Sonah et al. 2016). Originally, this conventional secretion system was considered the only mechanism for the secretion of apoplastic proteins; but there is evidence which suggests that apoplastic proteins are also delivered into the apoplast by leaderless secretory pathways that constitute, on average, 50% of the plant and fungal secretome (Agrawal et al. 2010; Ding et al. 2012; Girard et al. 2013; Delaunois et al. 2014).

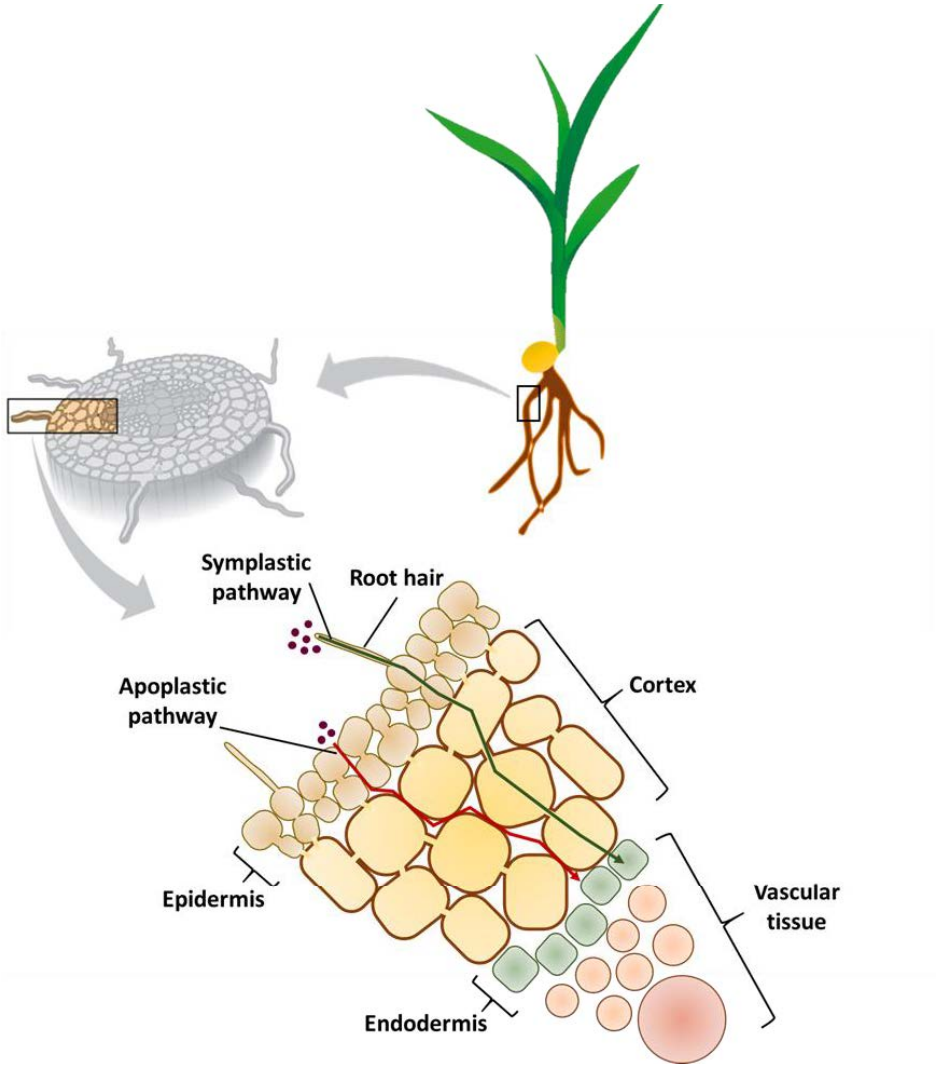

Figure 3.1 Overview of the apoplast route in the root system. The apoplast is considered the intercellular space that communicates with neighbourhood cells, where different biological processes take place, for example, transport of water and minerals that are essential for plants.

Apoplastic proteins that are typically secreted by plant microbes during successful interactions include plant CWDEs, such as endoglucanases, xylanases, cellulases and pectinases. These enzymes degrade the host plant cell walls which function as a physical barrier against abiotic and biotic factors (Kubicek et al. 2014). Plants counter-attack by secreting proteases and hydrophobic proteins into the apoplast to disrupt the function of microbe-associated proteins and effectively perceive MAMPs to enable a quick response against intruders and maintenance of cell wall integrity (Fernandez et al. 2012; Jashni et al. 2015). Moreover, during plant basal defence responses upon infection into the apoplast, several defence-related proteins are induced, including pathogenesis-related (PR) proteins which exhibit direct antimicrobial activities. Among the most recognised families of PR proteins are ß-1,3-glucanases, chitinases, thaumatin-like proteins, proteinase inhibitors (PIs), peroxidases and ribonuclease-like proteins. For example, chitinases degrade chitin present in fungal cell walls, which consequently results in the generation of chitin oligosaccharides (N-acetylchitooligosaccharides) that act as fungal elicitors perceived by plant cells to trigger further defensive mechanisms (van Loon et al. 2006).

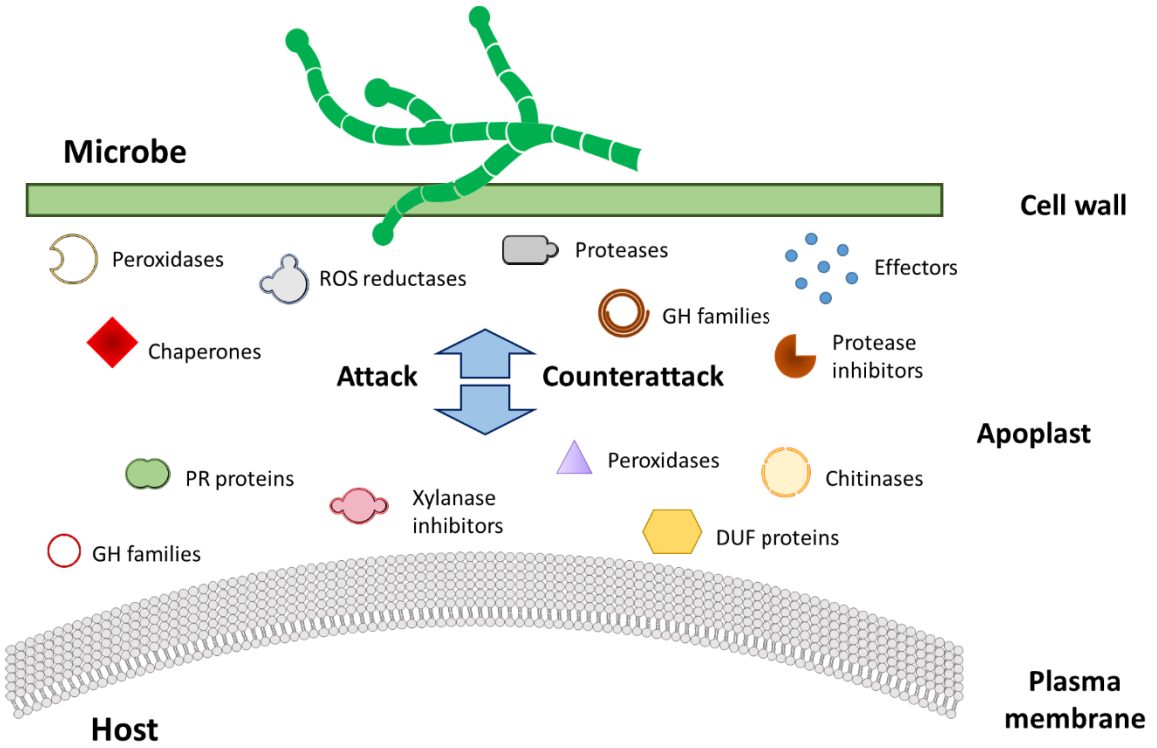

Figure 3.2 Overview of secreted proteins delivered into the apoplast during plant-microbe interactions. Secreted proteins from microbes are listed above the midpoint while proteins from plant are listed below. Figure adapted from Gupta et al. (2015).

Plant symbionts have developed specific strategies to promote colonisation by evading the first layer of plant defence called MTI. Plant microbes secrete molecules including effector proteins into the apoplast where they can interact with their molecular targets or are translocated into plant cell cytoplasm blocking downstream signals, thereby suppressing MTI. Effectors have been defined as small secreted proteins with an arbitrary length of 300 amino acid residues, and maintain their conformational stability due to their rich cysteine residues content that allows them to survive in an unsuitable environment created by plants in the apoplast (Gohre and Robatzek 2008; Lo Presti et al. 2015; Sperschneider et al. 2016). Conventional effectors have been reported in both symbiotic and pathogenic microorganisms; for example, the effector PIIN_08944 contributes to root colonisation in *Piriformospora indica* (Akum et al. 2015), Ecp6 prevents elicitation of host immunity during infection by sequestering chitin oligosaccharides of *Cladosporium fulvum* (de Jonge et al. 2010), and toxin-like protein ToxB which is secreted into the apoplast by the necrotrophic fungus *Pyrenophora tritici-repentis* and is necessary for complete disease development in wheat (Figueroa et al. 2015). The biotrophic fungal plant pathogen *U. maydis* secretes 467 potential effector proteins via conventional secretion pathway (Lanver et al. 2017).

Furthermore, unconventionally secreted effector proteins also play important roles in the manipulation of plant defence processes. The protein chorismate mutase Cmu1, secreted by *U. maydis*, manipulates the metabolome of neighbouring cells to favour parasite infection (Djamei et al. 2011). Other examples of unconventionally secreted effectors are Pslsc1 and Vdlsc1 from *P.*

sojae and *V. dahlia*, respectively; both effectors participate in the suppression of the SA pathway to alter plant immune responses (Liu et al. 2014). The direct or indirect recognition of effectors by plant receptors activates the third layer of plant defence called ETI which is stronger than MTI. Both MTI and ETI are recognised as the principal plant immune responses against microbes (Stotz et al. 2014).

Endophytic *Trichoderma* species have the capacity to penetrate root tissues and subsequently colonise the host plant. Recent studies have focused on the secretome of *T. virens* in the presence of maize roots (Lamdan et al. 2015). However, the proteins secreted in the apoplastic region where *T. virens* closely interacts with the host cells are not known. Proteomic tools such as mass spectrometry (MS) enable identification of proteins of the secretome during complex physiological cell processes such as microbe-host interactions (Schmidt and Volker 2011; Delaunois et al. 2014; Gupta et al. 2015). For example, in the study of the apoplastic secretome of rice plants colonised by *Magnaporthe oryzea* more than 200 proteins secreted into the apoplast of which several may act as effector proteins (Kim et al. 2013).

Therefore, the aim of this study was to analyse the apoplastic secretome during the interaction between *T. virens* and maize roots. Two proteomic strategies were used: (1) gel-based, sodium dodecyl sulphate polyacrylamide gel electrophoresis (SDS-PAGE) coupled with LC-MS/MS which allows separation and identification of large numbers of proteins; and (2) gel-free shotgun proteomics, which is a more powerful technology for large-scale separation and identification of complex mixture of proteins (advantages and disadvantages of these methods are described in Table 3.1) (González-Fernández et al. 2010; Jayaraman et al. 2012; Delaunois et al. 2014). The results should provide better understanding of how *T. virens* modulates host plant defensive processes and how the plants respond to the presence of the fungus, and will provide an insight into the crosstalk in the apoplast which is essential to maintain the *T. virens*-maize interaction.

Table 3.1 Advantages and disadvantages of gel-based and gel-free proteomics technologies.

Gel-based proteomics	
Advantages	Disadvantages
● High-throughput and quality method ● Identification of protein expression ● Identification of protein isoforms ● Identification of protein isoelectric point ● Identification of protein molecular mass ● Identification of protein post-translational modifications ● Separation and visualisation of complex proteins	● Gel variation and reproducibility limitations ● Proteins losses during process ● Time-consuming ● Incapable of separating all proteins present in complex samples (e.g. cell) ● Unable of detecting all proteins present in complex samples ● Insensitive to low abundance proteins
Gel-free proteomics	
Advantages	Disadvantages
● Analysis of low abundance proteins in complex samples ● High-throughput, quality and reproducible method ● Higher identification of peptides for protein identification ● Higher separation of peptides for protein identification ● Identification of protein post-translational modifications ● Separation of proteins present in complex samples ● Time-saving	● No identification of protein isoelectric point ● No identification of protein isoforms ● No identification of protein molecular mass

(González-Fernández et al. 2010; Jayaraman et al. 2012; Delaunois et al. 2014).

3.2 Materials and methods

3.2.1 Colonisation of maize roots by *Trichoderma*

For the proteomics study, maize germination and inoculation were performed as described in sections 2.2.1 and 2.2.3.

3.2.2 Isolation of total protein from maize primary root

For total protein extraction and precipitation from maize roots the methodology described by Wu et al. (2014) was used with modifications as follows. Root tissue (0.25 g) was ground into a fine powder in liquid nitrogen, then homogenised in 2.5 mL of ice cold Tris/ethylenediaminetetraacetic acid (EDTA) extraction buffer, containing 1 mM EDTA, 10 mM Tris-HCL pH 8, 2% w/v polyvinylpolypyrrolidone (PVPP) and with 0.3% (v/v) Pefabloc (Sigma-Aldrich, USA). Samples were centrifuged at 5,000 x g for 30 min at 4°C, then supernatant proteins were precipitated with 10 mL

of cold trichloroacetic acid (TCA)/acetone (-20°C). After centrifugation at 3,000 x g for 10 min, the pellet was washed three times with ice cold acetone containing 0.007% w/v dithiothreitol (DTT). Protein pellets were dried to evaporate any remaining acetone and stored at -80°C.

3.2.3 Isolation of apoplastic proteins

3.2.3.1 Isolation of apoplastic fluid for gel-based proteomics

Three different methods were used to harvest the apoplastic fluid (AF) from maize primary roots. For isolation of the apoplastic fluid, the primary root on the proximal side near to the seed (2 cm section) was cut from one side and collected using: (a) infiltration-centrifugation, (b) sorption and (c) pressure chamber methodologies. Individual primary roots from 20 plants were combined for each replicate. Three replicates were used for each condition: a) inoculated and b) un-inoculated plants. Roots were sampled after 5 d.p.i.

3.2.3.1.1 Infiltration-centrifugation method

Visible fungal material was removed from the root surface to avoid contamination of the sample. This was carried out by submerging the root sample in 4°C sterile nanopure water and then with an artist's round paint brush the root surface was gently brushed until excess visible fungal mycelium was removed. Primary root sections (2 cm) were placed immediately into a 2 mL microcentrifuge tube containing 1.5 mL of a solution of 100 mM sodium phosphate buffer (SPB) pH 6.5 (Witzel et al. 2011) supplemented with 0.3% (v/v) Pefabloc and 10 mM EDTA. The chilled samples were vacuum infiltrated with the SPB buffer solution in a vacuum desiccator by reducing the pressure at -45 kPa for 15 min using a diaphragm vacuum pump (Rocker 400, Rocker Scientific, Taiwan), followed by a slow return to atmospheric pressure to avoid cell damage (Dragisic Maksimovic et al. 2008). Roots were then placed in a 5 mL syringe without the plunger and placed inside a 15 mL centrifuge tube then centrifuged at 2,000 x g for 15 min at 4°C (Model 5810R, Eppendorf, Germany). The harvested AF was filtered through cellulose acetate membrane filters (0.2 µm porosity; Axiva Sichem Biotech, India) and immediately snap frozen in liquid nitrogen and stored at -80°C.

3.2.3.1.2 Sorption method

Fungal material was removed from the root surface as mentioned in the infiltration-centrifugation method. The plants were placed immediately on germination paper (30 cm x 45 cm) soaked with sterile Hoagland´s solution. For collection of root AF, filter paper strips (10 mm x 5 mm; GE Healthcare, USA) were used as sorption media. The strips were washed in methanol and sterile nanopure water and dried before being applied to the root surface (Dragisic Maksimovic et al. 2014). Two filters per plant were positioned onto the first 2 cm root surface and kept in place for 1 h. To prevent root drying, the remaining root system was covered with filter paper moistened with Hoagland´s solution. After 1 h, forty filter paper strips (equivalent to 20 plants) with absorbed AF were removed and placed into a microcentrifuge tube containing 1 mL SPB buffer solution

supplemented with 0.3% (v/v) Pefabloc and 10 mM EDTA. Apoplastic proteins (APs) were extracted from the filter paper strips by vigorously vortexing the tubes for 5 min. The filters were then transferred to a new microcentrifuge tube. Both tubes, one containing filters and the other containing the buffer were immediately snap frozen in liquid nitrogen and stored at -80°C.

3.2.3.1.3 Pressure chamber method

The root system was separated from the above ground parts (stem and leaves) and placed into a rubber tube of an appropriate diameter to the primary root size and then inserted into the pressure vessel of a Plant Water Status Console (model 3005F01, Soilmoisture Equipment Corp, U.S.A). AF was obtained after 1-2 min at 250 psi pressure (Adele Scott and Hoda Ghazalibiglar, personal communication) and collected into 1.7 mL centrifuge tubes. The harvested AF was snap frozen in liquid nitrogen and then stored at -80°C.

3.2.3.2 Precipitation of apoplastic proteins

AP samples were concentrated using the TCA-sodium deoxycholate (Na-DOC)/acetone method described by Bensadoun and Weinstein (1976) with modifications. Briefly, for every volume of AF solution, 0.1 vol. of a solution of 2% of Na-DOC (0.02% final concentration) and 0.1 vol. of 100% TCA (10% final concentration) were added and the samples were mixed and kept at room temperature (RT) for 1 h. Samples were then centrifuged at 14,000 x g for 10 min at 4°C, the supernatant removed, and the pellet dried by inversion on tissue paper. The pellet was then washed in 200 µL of ice-cold acetone, placed on ice for 15 min, then centrifuged at 14,000 x g for 10 min at 4°C. The pellet was air dried to eliminate any acetone residue before being re-suspended in 10 µL of PBS, buffer pH 7.0.

3.2.3.3 Isolation of apoplastic fluid for gel-free proteomics

For gel-free shotgun proteomics, modifications were carried out to improve the infiltration-centrifugation methodology described above. After removing fungal material from root surfaces, root sections were weighed, then placed immediately into 50 mM potassium phosphate buffer (PPB), pH 5.5, supplemented with 0.3% (v/v) Pefabloc and 10 mM EDTA (Dragisic Maksimovic et al. 2008). In ice conditions, roots were vacuum infiltrated with PPB. The roots samples were then centrifuged at 2,000 x g for 15 min at 4°C (Dragisic Maksimovic et al. 2008), and harvested AF was measured and immediately snap frozen in liquid nitrogen. APs samples from un-inoculated and inoculated roots were concentrated by freeze drying (Thermo Savant Micro Modulyo-115, Thermo Fisher Scientific, USA). Samples were rehydrated in 30 µL of 50 mM ammonium acetate buffer pH 5.5 for quantification and then stored at -80°C until use.

3.2.3.4 Quantification of apoplastic proteins

AF samples stored at -80°C were recovered and kept on ice before determining protein concentration. Quantification of APs was measured by fluorimetry (Qubit protein assay kit, Invitrogen, USA) using 2 µL of each concentrated sample, and AP concentrations calculated according to the manufacturer's instructions.

3.2.4 Malate dehydrogenase activity

Malate dehydrogenase (MDH) activity was assayed to determine cytoplasmic contamination in AF. MDH was determined as described by Husted and Schjoerring (1995) with modifications. A total of 5 µg of protein extract (total or apoplastic) were added into 3 mL reaction mixtures containing 0.094 mM β-NADH (Sigma-Aldrich, USA), 0.17 mM oxaloacetic acid (Sigma-Aldrich, USA), and 0.1 M phosphate buffer, pH 7.5. Oxidation of NADH was measured at 340 nm using a UV-Vis spectrophotometer (Genesys 10S, Thermo Fisher Scientific, USA), monitoring for 5 min at 25°C. A non-enzyme reaction mix was used as a blank. Enzymatic activity in AF was expressed as a percentage of the total root protein activity.

3.2.5 Identification of apoplastic proteins by gel-LC-MS/MS

3.2.5.1 Separation and visualisation of apoplastic proteins by 1-D SDS-PAGE

APs were separated by 1-D SDS-PAGE on a 4-12% pre-cast NuPAGE bis-tris gel (Novex, Life Technologies, USA). Prior to loading, 10 µL samples were mixed with 2 µL 6X Tris-Glycine SDS sample buffer (0.378 M Tris-HCl pH 6.8, 0.6 M dithiothreitol (DDT), 12% SDS, 60% Glycerol, 0.06% Bromophenol Blue). The mixtures were incubated at 95°C for 5 min and then placed on ice for 1 min, followed by 30 s centrifugation. The protein gel was run using a 1X MOPS-SDS running buffer (2.5 mM MOPS, 50 mM Tris, 0.1% SDS, 1 mM EDTA, pH 7.7) on a Novex Mini-Cell electrophoresis chamber (Novex, Life Technologies, USA) at a constant voltage of 100 V for 1 h until the dye front reached the anode end of the gel. To visualise the proteins, the acrylamide gel was stained with a solution of Coomassie Brilliant Blue (10% acetic acid, 50% methanol, 0.25% (w/v) Coomassie Brilliant Blue R-250) and incubated overnight at RT at 100 rpm on a shaker. The gel was destained using the same conditions (100 rpm at RT) with a destaining solution (7.5% acetic acid, 25% methanol) replacing the solution several times with fresh rinse solution until the excess dye was removed. Molecular weights were determined using from the SDS-PAGE PageRuler Plus prestained protein ladder (Fermentas, USA).

3.2.5.2 Identification by gel-LC-MS/MS

For identification, appropriate protein zones were excised and subjected to trypsin digestion. Briefly, excised gel plugs were washed three times with 200 µL of 1:1 acetonitrile (ACN): 50 mM

ammonium bicarbonate (ABC) solution, pH 8.3, and dried in a vacuum centrifuge. The plugs were then incubated with 10 mM DTT in 50 mM ABC solution, pH 8.3, for 1 h at 56 °C. Each plug was diced into small cubes with dimensions of 0.5-1.0 mm. For destaining, 200 µL of 50% ACN/ 50 mM ABC was added and the tubes were vortexed for 30 s. Plugs were then incubated at 45°C for 15 min in a Discoverer II System microwave (CEM Corporation, USA). For gel dehydration and reduction, 200 µL of 100% ACN was added and the tubes vortexed for 30 s and placed in a heating block (Thermomixer, Eppendorf, USA) at 56°C with the lids open to allow ACN evaporation. Once the plugs were dried, 50 µL of 10 mM DTT was added and tubes were incubated at 56°C for 15 min, for protein reduction. For alkylation, the remaining liquid was removed and 50 µL of 50 mM iodoacetamide (IAM) was added and the plugs were incubated in darkness for 60 min at RT. The digestion was carried out by adding 50 µL of freshly prepared 12.5 ng/µL trypsin (Roche, Switzerland) suspended in 50 mM ABC solution supplemented with 10% ACN and incubated at 37°C for 18 h. The resulting peptides were extracted first with water and twice with water–ACN–formic acid solution (45/50/5) then concentrated to a minimal volume (~10 µL), and mixed with 30 µL of 5% ACN in nanopure water containing 1% formic acid.

Peptide samples were then subjected to electrospray LC-MS/MS using a Finnigan™ LTQ-FT™ tandem mass spectrometer (Thermo Fisher Scientific, USA). The peptides were separated by reversed-phase chromatography on a Zorbax SB-300 C-18 column (150 mm × 300 µm, 5 µm particle size 300 Å pore size) (Agilent Technologies, USA) eluting with an ACN gradient in water containing 0.1% formic acid from 5 to 60% over 40 min using a Surveyor MS pump (Thermo Fisher Scientific, USA). The eluent entered the electrospray source at a flow rate of 5-6 $\mu L.min^{-1}$ produced by splitting the Surveyor flow of 100 $\mu L.min^{-1}$ with an UpChurch variable flow splitter. The mass spectrometer was operated in the positive ion mode with helium as the collision gas; the mass/charge range selected was 300–2,000 *m/z*. The capillary temperature was set at 210°C and the source voltage set at 3.8 kV. Data were acquired using a Top 5 experiment (one full scan in both the ion trap and ICR cell (parallel mode) followed by two averaged MS/MS microscans of each of the top five ions recorded in the ion trap) in data-dependent mode with dynamic exclusion enabled. Full scan Fourier transform data were obtained at a resolution of 100,000 at *m/z* 400 and used to refine the database search parameters.

Identification of the peptides was undertaken using Proteome Discoverer 1.4 (Thermo Fisher Scientific, USA), which was used to search fragment ion spectra matching peptides previously digested in silico using the proteome from maize (*Z. mays*) (http://www.plantgdb.org) and *T. virens* Gv29.8 (http://genome.jgi-psf.org/TriviGv29_8_2) databases.

3.2.6 Identification of apoplastic protein by gel-free shotgun proteomics

3.2.6.1 Identification by gel-free LC-MS/MS

For this analysis, APs (15 µg) for each biological replicate were digested separately. For each sample, 15 µL of 1 M of ABC were added, and adjusted to 100 µL with 50 mM ABC. Samples were reduced as follows: 1 M DTT was added to the samples to a final concentration of 10 mM, and then incubated at 56°C using 50 W for 15 min in a Discoverer II System microwave. The pH of the samples was adjusted to pH 8 with 1 M ABC. For alkylation, 1 M IAM was added to the samples to reach a final concentration of 50 mM. APs samples were kept in total darkness at RT for 30 min. After incubation, 1 M DTT was added to the samples to a final concentration of 20 mM. For protein digestion, 1 µg of trypsin (Promega, USA) was added to 15 µg of total protein. Digestion was conducted for 60 min using microwave digestion at 45°C and 15 W power. After digestion, the reaction was quenched by addition of 2 µL of 50% formic acid. The tryptic peptides were desalted using a sensitive solid phase extraction (SPE) method with 1 mL Oasis HLB 10 mg extraction cartridges (Waters, USA). Samples were diluted to 0.5 mL in 0.1% formic acid and pH was verified to a pH between 2 and 3 using pH indicator strips (Merck Millipore, USA). A second SPE extraction was performed using 1 mL Oasis MCX 30 mg extraction cartridges (Waters, USA). APs samples were eluted with 0.3 mL of freshly prepared 50% ACN in water, then concentrated in a Speedvac concentrator (Thermo Scientific, USA) to a volume between 10-15 µL, vortexed vigorously, then centrifuged at 16,000 xg for 30 s and finally diluted in 0.1% formic acid for mass spectrometry analysis.

APs digests were separated on a 0.075 x 200 mm picofrit column (New Objective, Scientific Instrument Service, USA) packed with Reprosil C18 media (Dr Maisch GmbH HPLC, Germany) using the following gradient: 0 min 5% B, 72 min 35% B, 76 min 95% B, 82 min 95% B, 83 min 5% B, 90 min 5% B, where A was 0.1% formic acid in water and B was 0.1% formic acid in ACN. The gradient was formed at 250 nL/min using a NanoLC 400 UPLC system (Eksigent Technologies, USA). The picofrit spray was directed into a TripleTOF 6600 Quadrupole-Time-of-Flight mass spectrometer (Sciex, USA) scanning from 350-1600 *m/z* for 150 ms, followed by 40 ms. MS/MS scans were conducted on the 40 most abundant multiply-charged peptides (*m/z* 80-1600) for a total cycle time of 1.8 s. The mass spectrometer and HPLC system were under the control of Analyst TF 1.7 software (Sciex, USA).

The mass spectrometry data were searched against a database which combined the Uniprot proteomes from *Z. mays* (http://www.uniprot.org/proteomes/UP000007305) and *T. virens* (http://www.uniprot.org/proteomes/UP000007115) along with common contaminant entries (141,930 entries in total), using ProteinPilot version 5.0 (Sciex, USA) for peak picking identification selecting the following parameters: Cys-alkylation, iodoacetamide; digestion, full-trypsin digestion; and ID focus, biological modifications. Protein and peptide level false discovery rates (FDRs) were

filtered to 1% and proteins with a threshold ProtScore ≤ 0.99 were discarded. The tandem MS/MS data were also analysed using PEAKS Studio version 8 (BSI, Canada). All resulting matched peptides were then confirmed by visual examination of the individual spectra. The proteomic analysis was conducted at The Centre of Genomics, Proteomics and Metabolomics at the University of Auckland, under the supervision of Assoc. Prof. David Greenwood and Martin J Middleditch.

3.2.7 Label-free quantification analysis

The mass data were quantified by label free analysis using PEAKS software version 8 (BSI, Canada). Quantification was performed versus full tryptic digestion with a mass error tolerance of 20 ppm and 5.0 min for retention time shift tolerance. The quantification ratios were normalised using total ion current (TIC). Protein and peptide level FDRs were filtered to 1%. In addition, proteins with significance ≥ 10, fold change ≥ 1.5 and unique peptide ≥ 1 scores were selected.

3.2.8 Identification of potential functional analysis domains and gene ontology

A comprehensive pipeline was designed to identify secreted proteins and predict their characteristic features such as: a) presence of a signal peptide (SignalP 3.0 and 4.0) (Bendtsen et al. 2004b; Petersen et al. 2011); presence of transmembrane domains (TMHMM 2.0) (Emanuelsson et al. 2007), subcellular localisation (WoLF PSORT and TargetP 1.1) (Emanuelsson et al. 2000; Horton et al. 2007), and d) non-classical protein secretion (SecretomeP 2.0) (Bendtsen et al. 2004a). Prediction of secretory proteins was based on bioinformatics tools and parameters reported by two different fungal secretome databases: Fungal Secretome Database (FSD) (Choi et al. 2010) and FunSeckB2 (Meinken et al. 2014), and one plant secretome database: PlanSeckB (Min et al. 2014). Additionally, the prediction tool EffectorP was used to identify putative effector-like proteins from *T. virens* (Sperschneider et al. 2016). Predicted functional analysis of the APs was performed using Blast2GO (Conesa et al. 2005) that combines GO, BLAST, and Interpro databases and searches for protein annotation (Table 3.2). Overall, the workflow used in the proteomic study during the *Trichoderma*-maize interaction is presented in Figure 3.3.

Table 3.2 Software used to predict protein secretion, subcellular localisation, non-classical secretion, effector-like protein and functional analysis of apoplastic proteins.

Software	Web address
SignalP 3.0	http://www.cbs.dtu.dk/services/SignalP-3.0/
SignalP 4.0	http://www.cbs.dtu.dk/services/SignalP-4.0/
TMHMM 2.0	http://www.cbs.dtu.dk/services/TMHMM/
WoLF PSORT	http://www.genscript.com/wolf-psort.html
TargetP 1.1	http://www.cbs.dtu.dk/services/TargetP/
SecretomeP 2.0	http://www.cbs.dtu.dk/services/SecretomeP/
Effector P	http://effectorp.csiro.au/
GO	http://geneontology.org/
BLAST	http://blast.ncbi.nlm.nih.gov/Blast.cgi
Interpro	https://www.ebi.ac.uk/interpro
Uniprot	http://www.uniprot.org/

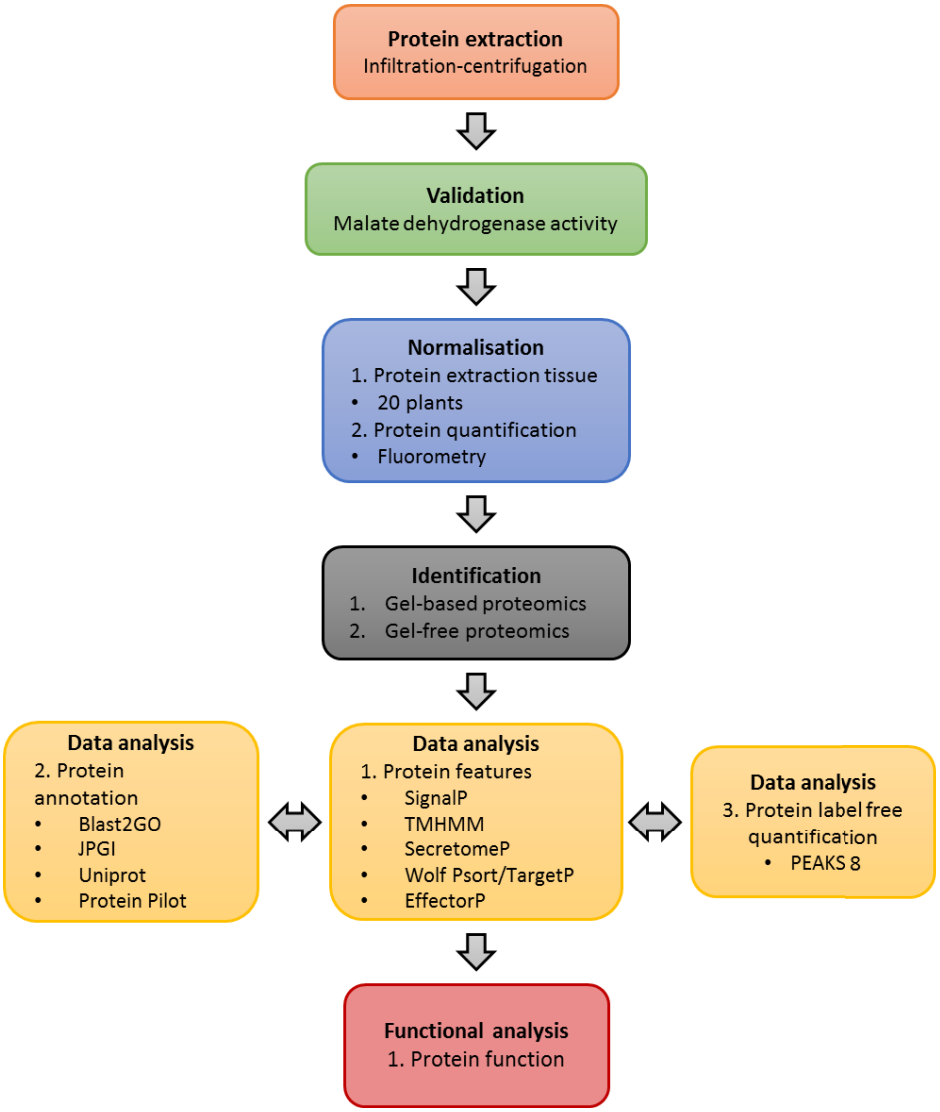

Figure 3.3 Diagram of the workflow used in proteome analysis. Isolation of apoplastic proteins used the infiltration-centrifugation method. Validation used malate dehydrogenase activity. Normalisation used the same amount of tissue and extracted proteins. Data and functional analysis used a variety of software including ProteinPilot, Blast2GO and PEAKS packages.

3.2.9 Peroxidase activity

To determine peroxidase (POX) activity in the AF, methodology described by Urbanek et al. (1991) was followed with modifications, using guaiacol as a hydrogen donor. The reaction mixture comprised 2 mL of a mixture containing 50 mM PPB pH 6.8, 20 mM guaiacol (Sigma-Aldrich, USA) and 20 mM hydrogen peroxide (H_2O_2) (Merck Millipore, USA). The enzyme reaction was started by adding 10 µL containing 1 µg of APs and incubating for 10 min at 30°C. The reaction was stopped by adding 0.5 mL of 5% (v/v) TCA and the absorbance was read at 480 nm. One unit of peroxidase activity was defined as the amount of enzyme that increased the absorbance by 0.01, expressed as units of POX/µg protein. The enzyme activity experiment had three replicates for treatment.

3.2.10 Statistical analyses

Statistical analyses were performed using general analysis of variance (ANOVA) in the GenStat 18th package (VSN International, UK). Each value is the mean ± standard desviation (SD) for three replicates in each group, and $P<0.05$ was considered as significant. The least significant differences of means (l.s.d.) at a significance level of 5% ($P<0.05$) were determined for each experiment and Multiple Comparisons of the treatments of each experiment were carried out using Fisher's Unprotected LSD algorithm (at $P<0.05$).

3.2.11 Localisation of *Trichoderma virens* apoplastic proteins

For localisation of *T. virens* proteins that were expressed during colonisation of maize roots, two different apoplastic proteins candidates were selected. The small protein 1 (Sm1) (TV_110852) which contains a signal peptide for conventional secretion; and the aminotransferase (GliI) (TV_53497) which lacks a signal peptide and was identified in the apoplast as an unconventionally secreted protein.

3.2.11.1 Golden Gate vector construct strategy

Using the Golden Gate strategy based on the use of type II restriction enzymes which cleave outside of their recognition sequence, resulting in 5' or 3' DNA overhangs (Engler et al. 2008; Engler et al. 2009; Weber et al. 2011), entry vectors and final vectors were created to study localisation of proteins that were expressed during the *Trichoderma*-maize interaction (Supplementary Figure 3).

3.2.11.1.1 Construction of entry vectors and PCR products for localisation

Entry vectors and PCR products for localisation of *T. virens* Sm1 and GliI were created as follows: primers were designed to amplify open reading frames (ORFs) of selected genes using the published *T. virens* genome (https://genome.jgi.doe.gov/TriviGv29_8_2/TriviGv29_8_2.home.html); and synthetic molecules including, the glyceraldehyde 3-phosphate dehydrogenase (*gpdh*) promoter; fluorescent marker (mCherry) which was codon optimised for *Trichoderma* (A. Mendoza-Mendoza,

unpublished) and designed to contain a glycine and serine rich flexible linker (GSAGSAAGSGEF) located at the N-terminus of the mCherry (Waldo et al. 1999; Chen et al. 2013b); a resistance cassette (hygromycin B phosphotranferase gene (*hph*)); and a nopaline synthase terminator (T-nos) (Supplementary Table 5). All these molecules were previously subcloned into independent vectors and kindly provided by Dr. Artemio Mendoza. These molecules were used as DNA templates to amplify the coding region with primers containing *Bsa*I restriction sites flanking the PCR product. This created specific four nucleotide overhangs regions to each molecule which are complementary to the next overhang in the next molecule (Supplementary Figure 3 A).

PCR products were amplified using the following cycling conditions in an iCycler PCR machine (Biorad, USA): 98°C for 1 min: followed by 35 cycles of 98°C for 10s; 60°C for 15s; 72°C for 2 min, and a final extension at 72°C for 10 min. For each PCR reaction, 100 ng of genomic DNA (gDNA) from *T. virens* Gv 29.8 or purified plasmids containing the desire molecule (e.g. *gpdh1* promoter, mCherry, *hph*, T-nos, etc) were used as template. Reactions were carried out in a total volume of 50 µL containing: 25 µL CloneAmp HiFi PCR Premix (Clontech, Takara, Japan) and 1 µL (0.2 µM) of each primer. Visualisation of PCR products was conducted by using 0.8% agarose TAE gel-electrophoresis. All PCR products were purified using Wizard SV Gel and PCR Clean-Up System (Promega, USA) using manufacturer's instructions. Purified molecules were quantified using a NanoDrop (NanoDrop Technologies Inc, USA), and subcloned into pUC19b containing the *lacZ* ß-galactosidase gene (kindly provided by Dr Kee Sohn). The restriction site *Bsa*I in the ampicillin resistance gene from pUC19b was removed by a point mutation (Supplementary Figure 3 B). For ORFs that were specific for target genes (*sm1* and *gliI*), the purified PCR products were used instead of being subcloned for the construction of the final vectors.

The ligation reaction was carried out in a total volume of 20 µL containing: 1 µL (5U) of T4 DNA ligase (Thermo Fisher Scientific, USA), 2 µL of 10X T4 DNA ligase buffer, 100 ng of linear vector (pUC19b) (previously linearised with *Sma*I), and 200 ng of purified molecule (1:2 ratio of vector:insert). The ligation was incubated for 20 min at RT and then overnight at 4°C. The recombinant plasmids were transformed into *Escherichia coli* TOPO10F' using chemically competent cells. A total of 10 µL of ligation product were mixed with 40 µL of *E. coli* competent cells and then incubated on ice for 10 min. The *E. coli* cells were heat shocked at 42°C for 1:30 min using a Thermocycler (Eppendorf, USA) and placed immediately on ice. The cells were grown in 500 µL of S.O.C. medium and incubated for 1 h at 650 rpm/37°C. One aliquot of 100 µL cells was plated on Luria Broth (LB) agar plates supplemented with 100 µg/mL ampicillin (PanReac AppliChem, Germany), IPTG (Zymo Research, USA) and X-gal (PanReac AppliChem, Germany). The plates were incubated at 37°C overnight. Single white colonies were inoculated into 4 mL LB medium supplemented with 100 µg/mL ampicillin and incubated at 37°C for 18 h with continuous shaking at 260 rpm. The plasmids were isolated, quantified and digested to determine construct insertion. To digest isolated plasmids the following conditions were used. Each restriction reaction contained a total volume of 20 µL containing 1 U *Bsa*I (New England Biolabs, USA), 10 X NEB CutSmart Buffer

and 500 ng of purified plasmid. Each reaction was incubated at 37°C for 1.5 h. After digestion, the reactions were visualised by 0.8% agarose TAE gel-electrophoresis to verify plasmid fragment sizes. The plasmids were then sequenced to confirm the nature of the construct at the Bio-Protection Sequencing Facility, Lincoln University. The sequence integrity was analysed using Clone Manager Professional v. 8 (Sci-Ed Software, USA).

3.2.11.1.2 Construction of final vectors for localisation

For the construction of the final vectors the receptor vector pAGM1311 (Addgene, USA) was used to insert the desired construct. This vector contained the *lacZ* ß-galactosidase gene bordered by *Bsa*I restriction sites, and the kanamycin resistance gene for selection in *E. coli* (Supplementary Figure 3 C). One tube restriction-ligation reactions were set up independently for each construct as follows: in a total volume of 10 µL containing 10 U of restriction enzyme (*Bsa*I) (New England Biolabs, USA), 10 U T4 DNA ligase, 1 µL of 10X T4 DNA ligase buffer, (~80 ng) PCR products (in the case of *sm1* and *glil*) and entry vectors (~75 ng) containing DNA fragments and receptor vector (~50 ng) were cut and ligated in the same reaction. The reaction was incubated for 2 min at 37°C and 5 min at 16 °C, both steps were repeated 40 times, followed by final digestion for 5 min at 50°C and then heat inactivation for 5 min at 80°C. Transformation into *E. coli,* selection of positive colonies, isolation of plasmid, validation by restriction and confirmation by sequencing was performed as described in section 3.2.11.1.1 with modifications. The recombinant plasmid was transformed into *E. coli* competent cells using 10 µL of restriction-ligation product. Selection of positive colonies was performed on LBA plates supplemented with 50 µg/mL kanamycin (Sigma Aldrich, USA). To digest isolated plasmids the following conditions were used. Each restriction reaction contained a total volume of 20 µL containing 1 U *Hind*III (New England Biolabs, USA), 10 X NEB CutSmart Buffer and 500 ng of purified plasmid. Each reaction was incubated at 37°C for 1.5 h. Reactions were visualised by 0.8% agarose TAE gel-electrophoresis. The plasmids were then sequenced to confirm the nature of the construct.

3.2.11.1.3 Transformation of Trichoderma virens

Transformation of *T. virens* protoplasts with the localisation vectors was performed according to the method reported by Baek and Kenerley (1998) with modifications for the protoplast isolation described by Lawry (2016). *T. virens* conidia ($1x10^5$ conidia/mL) contained in 100 µL of nanopure water were spread with a triangular spreader onto a large PDA petri dish (150 mm x 150 mm) (NEST Scientific, USA) which was previously covered with sterile cellophane sheet. Plates were incubated for 16 h at 25°C in darkness. For digestion of *T. virens* mycelia a digestion solution was prepared containing 0.5 g Glucanex (Novozyme, Denmark) and 0.24 g cellulase (Sigma-Aldrich, USA) dissolved in 50 mL of 0.7 M sterile mannitol osmoticum solution, pH 5.5, containing 50 mM $CaCl_2$, 0.7 M mannitol and 50 mM MES hydrate. The enzymatic solution was sterilised using 0.45 µm cellulose acetate membrane syringe filters (GVS Filter Technology, UK). The cellophane covered with *T. virens* mycelia was moved into a new large petri dish and then 15 mL of digestion solution were placed on the cellophane until it was totally immersed in the solution. The plate containing the

digestion mix was incubated for 4 h at 25°C and continuous shaking at 150 rpm. Digested mycelia were filtered twice to recover *T. virens* protoplasts, firstly through two layers of sterile Miracloth and secondly through a Swinnex filter holder (Merck Millipore, USA) using 40 µm nylon mesh. The protoplast solution was centrifuged at 4,000 x g for 10 min at 4°C and the supernatant was removed by inversion. The protoplast pellet was washed with 20 mL of 0.7 M mannitol osmoticum solution and centrifuged at 7,000 x g for 7 min and then resuspended in 500 µL of 0.7 M mannitol osmoticum solution. Protoplast concentration was determined using a haemocytometer.

For protoplast transformation, ten micrograms of each DNA construct (Sm1-Loc and GliI-Loc) were linearised using the following conditions. The restriction reactions were performed in a total volume of 20 µL containing 5 U *EcoR*V (New England Biolabs, USA), 10 X NEB CutSmart Buffer. Each reaction was incubated at 37°C for 2 h. The digested plasmids were purified and visualised as previous described to verify their integrity. The linearised constructs (10 µg) were added to 240 µL containing 10^8 protoplasts in mannitol osmoticum solution and mixed gently. The mix protoplast + DNA construct was incubated on ice for 20 min. After incubation, 130 µL of 40% polyethylene glycol (PEG) solution (40 g PEG 4,000, dissolved in 100 mL of 0.7 mannitol osmoticum) were added and mixed by inversion, this step was repeated 2 times and then incubated for 20 min at RT. For regeneration of transformants, the protoplast solution was mixed with 10 mL recovery media (RM) (PDB; 1% bacteriological agar; 0.5 M sucrose) + 100 µg/mL hygromycin B (AG Scientific, USA). The mixture was then poured onto prepared plates containing 10 mL RM + 100 µg/mL hygromycin B. A negative control containing RM + hygromycin B and protoplast solution without DNA construct was used, together with a positive control consisting of RM and protoplast solution. Plates were incubated for 7 d at 25°C.

Transformants (Sm1-Loc and GliI-Loc) that were able to grow on PDA supplemented with 100 µg/mL of hygromycin B were selected. Ten rounds of selection from colonies derived from single-spores were undertaken before their confirmation by PCR using primers mCherry ORF-f and mCherry ORF-r, which amplify the mCherry encoding gene. PCR products were amplified using the following cycling conditions in an iCycler PCR machine (Biorad, USA): 95°C for 5 min: followed by 35 cycles of 95°C for 30 s; 60°C for 30 s; 72°C for 45 s, and a final extension at 72°C for 10 min. For each PCR reaction, 1 µL gDNA (100 ng of total DNA) was used as the template. Reactions were carried out in a total volume of 25 µL containing: 0.5 µL (2.5 U) FastStart Taq DNA Polymerase (Roche, Switzerland), 2.5 µL Buffer with 20 mM $MgCl_2$, 1 µL dNTPs (2.5mM each), 1 µL (0.2 µM) of each primer (mCherry ORF-f and mCherry ORF-r). The PCR products were size fractionated and visualised as mentioned in section 3.2.11.1.1. Once integration was confirmed, conidia were stored in 25% glycerol solution at -80°C.

3.2.11.2 Protein extraction

3.2.11.2.1 Culture conditions

T. virens (WT, Sm1-Loc and GliI-Loc) conidia, obtained from the glycerol stock from -80°C freezer, were inoculated on PDA plates, and incubated at 25°C with a 12 h day/night cycles for 7 d. Conidia were harvested as described in section 2.2.2. Conidial suspension ($1x10^6$ conidia) was inoculated in 100 mL flasks containing 50 mL of potato dextrose broth (PDB) (Difco, Fisher Scientific, USA) and incubated for 72 h at 25°C with shaking (160 rpm). The mycelia from the culture media was harvested by filtration and washed three times using sterile nanopure water, and then frozen in liquid nitrogen and stored at -80°C until protein extraction. The supernatant (50 mL) from the culture media was filtered through a double layer of sterile Miracloth, and then filtered again through a 0.45 µm nylon filter (ReliaPrep, Ahlstrom-Mujnksjö, Finland) to remove any mycelia particles. The collected supernatant was stored at -80°C until protein extraction.

3.2.11.2.2 Mycelia protein extraction

For total protein extraction from *T. virens* mycelia the methodology described by Bhadauria and Peng (2010) was implemented with modifications. Frozen mycelia (0.5 g) was ground into a fine powder using liquid nitrogen in precooled conditions. The powder was homogenised in 5 mL of ice cold Tris/EDTA extraction buffer, containing 10 mM Tris-HCL pH 8, 1 mM EDTA, 2 % w/v polyvinylpolypyrrolidone (PVPP) and with 0.3% (v/v) Pefabloc, and then samples were centrifuged at 5,000 x g for 30 min at 4°C. The supernatant was collected and proteins were precipitated with four volumes of cold (-20°C) 10% w/v TCA/acetone with 0.007% w/v DTT. Samples were centrifuged at 3,000 x g for 10 min, the pellet was washed three times with ice cold acetone containing 0.007% w/v DTT. Protein pellets were dried to evaporate any remaining acetone and resuspended in rehydration buffer containing 7 M Urea, 2 M thiourea, 20 mM DTT and 2% w/v Triton X-100. Resuspended pellets were stored at -80°C.

3.2.11.2.3 Supernatant protein extraction

For protein extraction of the *T. virens* secreted fraction the methodology described by Medina and Francisco (2008) was implemented with modifications. For protein precipitation, 20 mL of broth supernatant was mixed with an equal volume of cold 20% (w/v) TCA solution. The mixture was incubated for 2 h at -20°C to allow protein precipitation, and then centrifuged for 10 min at 14,000 x g. The supernatant was decanted, and the pellet was washed with 1 mL of cold 70% ethanol. The samples were vortexed and centrifuged for 3 min, this step was repeated three times. The final pellet was dried with the addition of 1 mL of acetone, the samples were vortexed and centrifuged for 1 min. The acetone was decanted, and the pellet air dried for 30 min, and resuspended in the rehydration buffer mentioned above, and stored at -80°C.

3.2.11.3 Western blot

For western blot analysis, quantification, separation and visualisation of mycelial and supernatant proteins were performed as described in sections 3.2.3.4 and 3.2.5.1. Equal amounts (20 µg) were loaded into the wells of a SDS-PAGE gel, along with a molecular weight marker, and run at 100 V for 1 hr. Transfer of proteins to a PVDF blotting membrane (Amersham Hybond P; GE Healthcare Life Sciences, UK) was achieved as follows: a) the gel was placed in 1X transfer buffer pH 8.3 (25 mM Tris, 190 mM glycine and 20% methanol) for 15 min; b) the transfer sandwich was assembled as described in a general protocol for western blotting (Biorad, USA); and c) the transfer tank was placed on ice and run at a constant current of 50 mA for 2 hr. For antibody incubation, the membrane was blocked in 5% skim milk in Tris-buffered saline Tween 20 buffer (TBST) (20 mM Tris pH 7.5, 150 mM NaCl and 0.1% Tween 20) at RT for 1 hr. The membrane was then incubated overnight with the addition of 1:10,000 (v/v) anti-mCherry antibody (BioVision, USA) dilution. The blot was rinsed three times for 5 min in TBST and incubated with 1:10,000 (v/v) HRP-linked secondary antibody (Cell Signaling Technology, USA) solution for 1 hr at RT. The blot was rinsed again for the previous step. A chemiluminescent substrate (500 µL luminol enhancer + 500 µL peroxide solution) was applied to the blot according to the manufacturer's recommendations (Amersham ECL Prime Western Blotting Detection Reagent; GE Healthcare Life Sciences, UK), and the membrane placed between transparent plastic sheets for imaging. The chemiluminescent substrate signal from the membrane was captured on CL-Exposure film (Thermo Scientific, USA) exposed for 5 min in a X-ray film cassette (Advansta, USA) in darkness. The film was developed by submerging for 1 min in developer solution (Kodak, USA) washing in tap water and fixing for 1 min in fixer solution (Kodak, USA) and washed again in tap water. The film was air dried and the results were analysed visually.

3.2.11.4 Microscopic visualisation of *Trichoderma virens* transformants

T. virens positive transformants (Sm1-Loc and GliI-Loc) were examined using fluorescent microscopy (Olympus BX51, Olympus, Japan). For visualisation, 3 d old colonies were incubated as described in section 3.2.11.2.1. Fresh mycelia was analysed under fluorescent microscopy to localise fluorescent protein mCherry fusions within cells. Fluorescent protein detection was observed by exciting at 561 nm and detecting at 580-630 nm and analysed using cellSens software (Olympus, Japan).

3.3 Results

3.3.1 Isolation and identification of apoplastic proteins from maize root seedlings confronted or not with *Trichoderma virens*

To determine the efficiency of different methodologies used for the extraction of AF from maize roots, three methods were tested. AF was successfully harvested by the infiltration-centrifugation and sorption methods; however, the pressure chamber method was unsuccessful due to the complexity of manipulating the equipment and the small diameter of the roots (up to 0.3 cm), which made it extremely difficult to fit into the pressure chamber for the extraction of AF. APs were more efficiently obtained by the infiltration-centrifugation system compared to sorption when observed on the 1-D SDS-PAGE gel (Figure 3.4 and Supplementary Figure 4).

To evaluate the infiltration-centrifugation methodology competence, protein concentration, fresh weight and AF volume between un-inoculated and inoculated roots after 5 d.p.i were all analysed. Fresh weight and AF volumes were measured from primary root sections in relation to the amount of protein obtained from each sample. The protein concentration in relation to the volume of isolated AF, demonstrated differences between un-inoculated and inoculated root samples. Principally, a higher protein concentration and volume of AF was obtained from un-inoculated compared to inoculated roots (Supplementary Table 1).

To evaluate levels of cytoplasmic contamination the activity of malate dehydrogenase (MDH) was used as a biomarker, which is commonly tested during extraction of AF (Gupta et al. 2015). The activity of MDH detected in AF extracted from un-inoculated and inoculated roots was up to 1.5% compared to the total soluble protein extracted from roots (Supplementary Table 2). MDH levels below 2% are considered suitable for plant apoplast studies (Dannel et al. 1995; Dragisic Maksimovic et al. 2008; Dragisic Maksimovic et al. 2014; Yang et al. 2015).

Multiple methods were used to obtain proteome coverage in this study: a) gel-LC-MS/MS and b) gel-free shotgun proteomics.

3.3.1.1 Identification of apoplastic proteins by gel-LC-MS/MS

APs were separated by 1-D SDS-PAGE, with three biological replicates for each condition (Figure 3.4). The APs showed differences in their protein complement with distinctly different protein bands visible in inoculated plants (M+Tv) compared with un-inoculated plants (M). The patterns of protein fractions from 15 to 75 kDa and 130 to 250 kDa were largely similar in their intensity and mass separation. Substantial differences were observed in the protein fractions between 75-130 kDa sections in inoculated samples compared with the un-inoculated (Figure 3.4). Specifically, two treatment-specific bands were observed; one was located above the 100 kDa fraction and the other

below (Figure 3.3). Based on their mass, the protein bands were cut from the gels in five sections (Figure 3.3), and then analysed by LC-MS/MS.

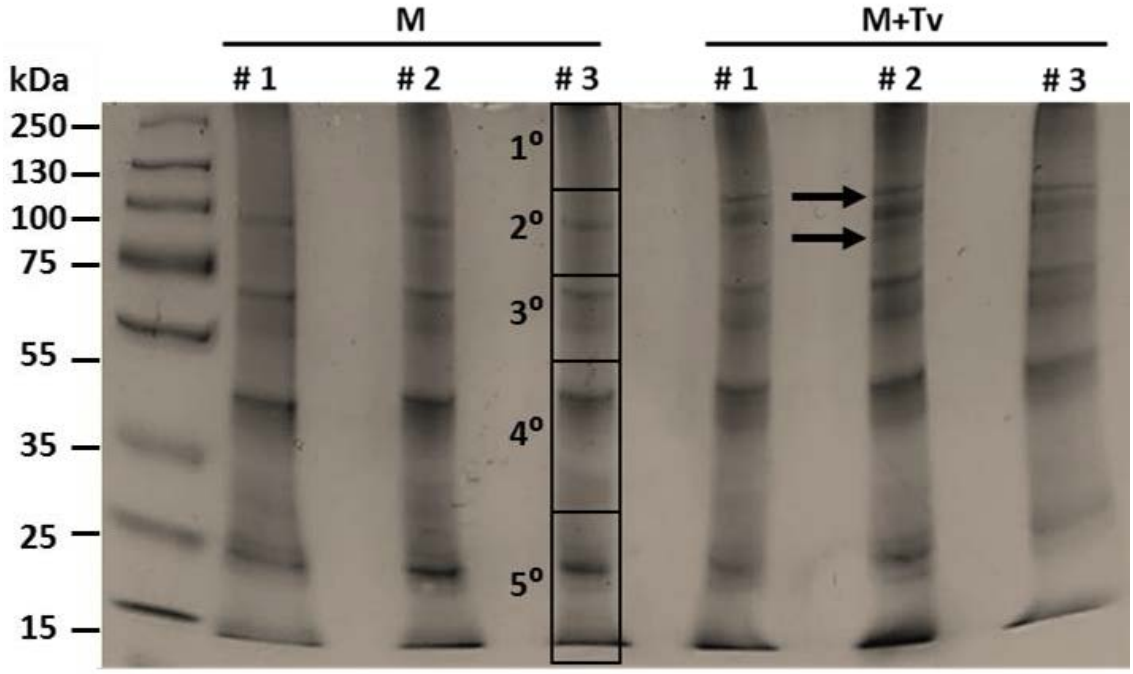

Figure 3.4 Electrophoretic profile (SDS-PAGE) of protein extract of apoplastic fluid from maize primary roots (first 2 cm below the coleoptile). Apoplastic proteins isolated by the infiltration-centrifugation method. Three biological replicates of apoplastic proteins fractions from maize roots un-inoculated (M) and inoculated (M+Tv) with *T. virens* were separated by 1D-SDS-PAGE. Black squares represent the five sections that protein fractions were divided into for MS identification; section 1 represents (250-120 kDa), section 2 (120-75 kDa), section 3 (75-50 kDa), section 4 (50-30 kDa), and section 5 (30-15 kDa). Black arrows indicate visible differences in protein fractions located in section 2 in inoculated compared with un-inoculated protein profiles.

Using this gel-based proteomic approach coupled with LC-MS/MS, 13 proteins were identified, of which 12 corresponded to maize and one to *T. virens* (Supplementary Table 3). Five of these maize proteins: LRR receptor-like serine/threonine-protein kinase (A0A1D6ERY2_MAIZE), aspartic-type endopeptidase (A0A1D6F8J3_MAIZE), germin-like protein (B4FRS8_MAIZE), barwin-like protein (Win1) (B6SH12_MAIZE), and peroxidase (Per66) (PER66_MAIZE) were common to both conditions un-inoculated and inoculated maize samples and were located in the 75-15 kDa fractions. Proteins that were only present in the un-inoculated samples included two peroxidases (A0A1D6LS36_MAIZE; A0A1D6PD14_MAIZE) and a pathogenesis-related protein 1 (PR-1) (A0A1D6K5Y8_MAIZE) which were identified in the 50-15 kDa fractions. Four maize proteins identified from the inoculated samples exclusively were in the 120-30 kDa fractions: methionine synthase (C0P5Y3_MAIZE), heat shock protein 70 (Hsp70) (A0A1D6MWU7_MAIZE), adenosylhomocysteinase (C0PHR4_MAIZE), and pectinesterase (B6SSX0_MAIZE). In contrast, the protein TV_29366, which encodes for a β-xylosidase, was the only protein detected from T. virens and this was present in the 120-75 kDa fraction.

3.3.1.2 Identification of proteins by gel-free shotgun proteomics

The low number of proteins identified by gel-LC-MS/MS based technology required the use of a more powerful proteomic tool (gel-free shotgun proteomics) to increase the identification number of proteins present in the apoplast which has a complex protein mixture. Using the gel-free shotgun proteomics approach, 148 maize proteins were identified in the un-inoculated control roots that were present in all three biological replicates. In the inoculated roots, a total of 177 were identified, where 85 and 92 proteins corresponded to the maize and *T. virens* proteomes, respectively.

Interestingly, in comparison with the un-inoculated roots, the inoculated roots showed a 43% (63 proteins) reduction in the number of total maize proteins identified. These results suggest that an alteration in the maize proteome is triggered by the presence of *T. virens*. In contrast to gel-LC-MS/MS, gel-free shotgun proteomics showed an increase of identified proteins from 13 to 272 proteins, showing that gel-free shotgun proteomics coupled with next generation LC-MS/MS instruments, is a useful technology to identify larger numbers of proteins in complex samples, such as in AF during plant-microbe interactions.

3.3.2 Prediction and annotation of secreted apoplastic proteins through bioinformatic tools

Putative secreted proteins were classified into two classes: a) classical secreted proteins and b) non-classical secreted proteins. In addition, the literature was used as a point of reference for those proteins that were not predicted as being derived from classical and non-classical secretion systems by bioinformatics analysis but have been reported as secreted proteins in other fungal and plant models. Based on the above criteria, in the un-inoculated maize roots 76 (51%) of the proteins were predicted to be secreted. Of these 56 (74%) followed the classical secretion system, while 20 (26%) were seemingly secreted by a non-classical mechanism and consequently were classified as leaderless secretory proteins (LSPs) (Figure 3.5 A). From the 85 maize proteins identified from the inoculated maize roots, 49 were predicted to be secreted and of these, 22 (45%) followed the classical and 27 (55%) the non-classical secretion system (Figure 3.5 A). In addition, un-inoculated roots showed 46 unique secreted proteins, while 18 unique secreted proteins were present in inoculated roots (Figure 3.5 A). Of 92 conserved *T. virens* proteins, 43 (46%) were predicted to be secreted, where 20 (46%) followed the Golgi-ER secretion system and 23 (54%) were secreted by non-conventional secretion systems (Figure 3.5 B). These results indicate that both organisms use both classical and non-classical secretion systems to deliver proteins into the apoplast.

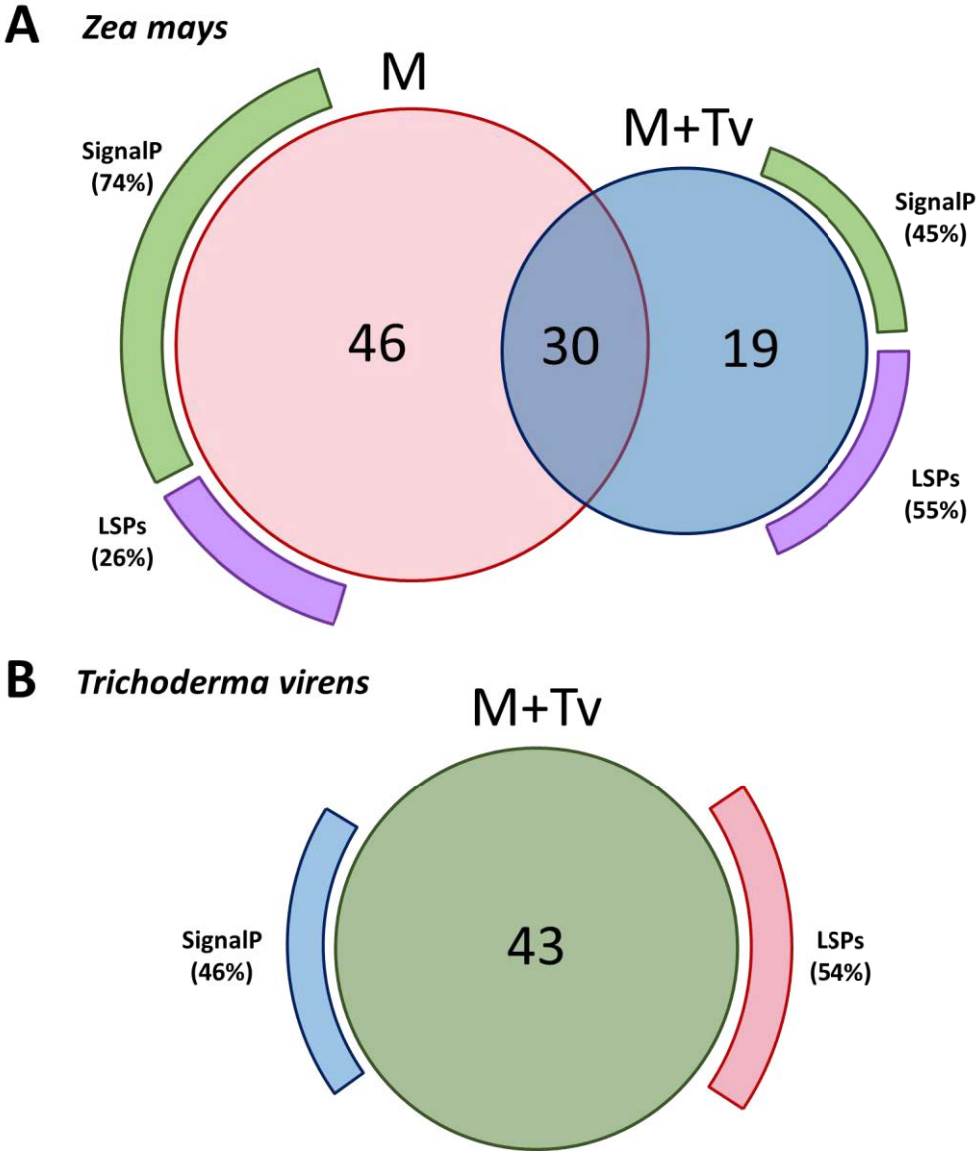

Figure 3.5 Apoplastic proteins secreted by *T. virens* and maize roots. Delineation of apoplastic proteins that are secreted by classical and non-classical secretion systems. **(A)** Relationship of apoplastic proteins identified from maize in un-inoculated (M) and inoculated (M+Tv) roots and their secretion system prediction. **(B)** Apoplastic proteins identified from *T. virens* in inoculated roots and their secretion system prediction. Abbreviation: LSPs, leaderless secretory proteins.

3.3.3 Functional annotation of maize secreted apoplastic proteins a 5 days post inoculation

Secreted proteins were organised into functional categories for biological processes and molecular function based on their gene ontologies (GO) (Figure 3.6 A,B). In un-inoculated maize roots, the four major biological process groups of proteins were: catabolic processes (22%), response to stress (19%), carbohydrate metabolic processes (11%), and cellular nitrogen compound metabolic processes (11%) (Figure 3.6 A). The three main molecular functions were: ion binding (47%), oxidoreductase activity (35%) and glycosyl hydrolase activity (18%) (Figure 3.6 B). In inoculated

samples, the four major biological function groups were: response to stress (27%), catabolic processes (17%), carbohydrate metabolic processes (10%), or sulphur compound biosynthetic processes (10%) (Figure 3.6 A). The three main molecular functions were: ion binding (33%), oxidoreductase activity (20%) and enzyme regulator process (15%) (Figure 3.6 B).

Multiple changes were identified in the predicted suite of functions of the proteins secreted from un-inoculated compared with inoculated roots. Response to stress was increased during the interaction with *T. virens* from 19 to 27%; in contrast, catabolic processes were reduced from 22 to 17%. No differences were observed in proteins belonging to carbohydrate metabolic processes; however, some differences were present in secondary metabolism, changing from nitrogen to sulphur metabolic processes (Figure 3.6 A). Major changes in molecular functions were observed; a reduction of ion binding from 47 to 33%, oxidoreductases from 35 to 20%, and glycosyl hydrolases from 18 to 7% activity. Conversely, lipid binding, protease and transferase activities were present only in inoculated roots (Figure 3.6 B).

Putative identification based on conserved domains and function was performed on the identified protein family members from maize roots that were secreted into the apoplast in un-inoculated and inoculated plants after a 5 d.p.i with *Trichoderma*. The major protein groups from maize were: a) 11 GHs that are involved in the degradation of carbohydrate complexes; b) 9 antioxidant proteins that catalyse reactions to neutralize free radicals and ROS; c) 15 peroxidases, that participate in the biosynthesis of the cell wall and defence responses and have multiple tissue-specific functions; d) PR proteins that are activated under biotic stresses; e) proteases/peptidases that are responsible for the hydrolysis of peptide bonds, and f) PIs that participate in the inactivation of proteases. Additionally, other family groups that were identified belonged to the domain of unknown function (DUF) proteins, oxidoreductases, lipases, ribonucleases, chaperones, calmodulin, ribosomal proteins and cyclophilin (Table 3.3 and Supplementary Table 4).

Interestingly, protein family groups were found in higher abundance in un-inoculated than inoculated roots; for example, maize GHs were reduced from 15 to 6%, respectively. Similar results were identified in the peroxidase group where their reduction was from 19 to 13%. In contrast, pathogen-related proteins increased from 3 to 10% and protease/peptidase and PIs from 8 to 16%. These results indicate that the maize proteome is altered by the presence of *T. virens* affecting the expression and suppression of different protein families, suggesting that the fungus is re-shaping the plant secretome.

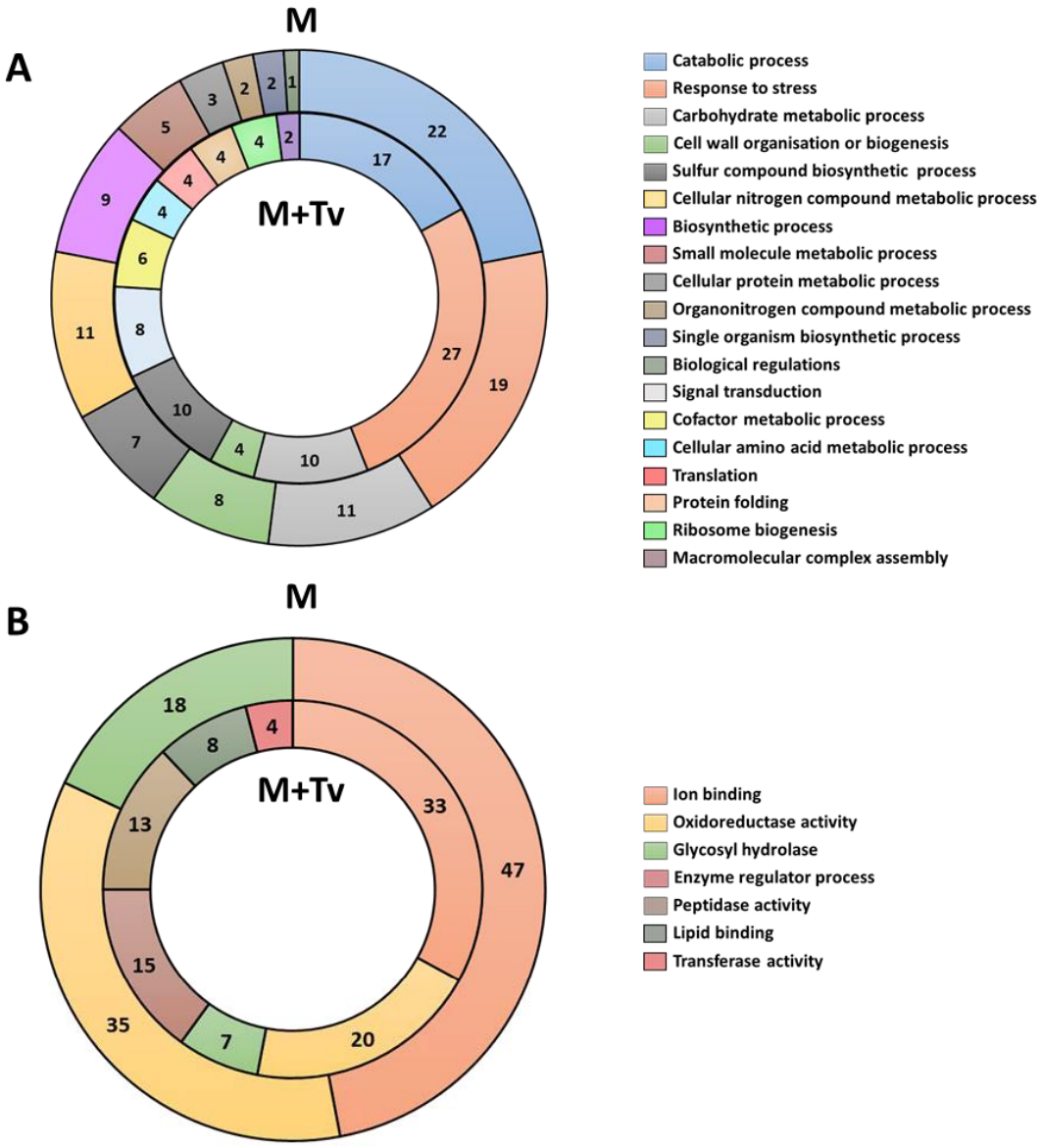

Figure 3.6 Functional classification of all secreted proteins from un-inoculated and inoculated maize roots at 5 d.p.i. (A) Blast2GO multilevel chart for biological process of un-inoculated (M) and inoculated (M+Tv) maize roots. **(B)** Multilevel chart for molecular function of un-inoculated and inoculated maize roots. Score distribution represented as a percentage of each group is indicated inside the pie slices.

3.3.4 Functional annotation of *Trichoderma virens* secreted apoplastic proteins at 5 days post inoculation

A total of 43 secreted proteins from *T. virens* were identified during the interaction with maize roots (Table 3.4). Secreted proteins were organised into functional categories for biological processes and molecular function based on their GO assignments (Figure 3.7 A-B). The four major biological process groups of proteins identified were: carbohydrate metabolic (12%), oxidation-reduction (12%), catabolic (11%), and response to stress (11%) (Figure 3.7 A). The three main molecular functions were oxidoreductase activity (41%), glycosyl hydrolase (13%) and lyase activity (10%) (Figure 3.7 B).

Table 3.3 Summary of the apoplastic proteins secreted by *Zea mays* after 5 d.p.i (inoculated)

Uniprot ID [a]	Protein annotation [b]	SignalP [c]	TMHMM [d]	SecretomeP [e]	WoLF PSORT [f] / TargetP [g]	Protein group
GSTF4_MAIZE	**Glutathione S-transferase (Gst4)*[3]**	N	N	N	Extracellular	
B6TL20_MAIZE	**Glutathione S-transferase (Gstu6)**	Y	N	N	Extracellular	
C0PK05_MAIZE	Lactoylglutathione lyase*[4]	N	N	N	Cytoplasm	
A0A1D6QGI0_MAIZE	**Peroxidase (Per67)**	Y	Y	N	Extracellular	
A0A1D6N0K3_MAIZE	Peroxidase (Per12)	Y	Y	N	Extracellular	Detoxifying and ROS related enzymes
K7VH58_MAIZE	Peroxidase (Per52)	Y	N	N	Extracellular	
A0A1D6F4C8_MAIZE	**Peroxidase (Per66)**	Y	N	N	Extracellular	
A0A1D6KAW3_MAIZE	**Peroxidase (Per54)**	Y	Y	N	Extracellular	
A0A1D6E530_MAIZE	Peroxidase (Per12)	Y	Y	N	Extracellular	
SODC5_MAIZE	**Superoxide dismutase [Cu-Zn]**	N	N	Y	Cytoplasm	

B6SH12_MAIZE	Barwin superfamily protein (Win1)	N	Y	Y	Plasma membrane	
Q9SYS1_MAIZE	**Beta-amylase (Amy2)**	N	N	Y	Extracellular	
B4FTS6_MAIZE	**Endochitinase A**	Y	N	N	Extracellular	
C0P451_MAIZE	**Endochitinase B1**	Y	N	N	Extracellular	
B4FWD0_MAIZE	**Minor allergen Alt a 7**	N	N	N	Extracellular	Microbe related proteins
B6TFN1_MAIZE	Minor allergen Alt a7	N	N	N	Cytoplasm/ Extracellular	
A0A096RTN1_MAIZE	Pathogenesis-related protein 10 (PR-10)*[5]	N	N	N	Cytoplasm	
Q29SB6_MAIZE	**Pathogenesis-related protein 10 (PR10)*[5]**	N	N	N	Cytoplasm	
A0A1D6N932_MAIZE	**Osmotin-like protein**	Y	N	N	Extracellular	
A0A1D6GKZ3_MAIZE	Osmotin-like protein	Y	Y	N	Extracellular	
A0A0B4J327_MAIZE	**Aspartic-type endopeptidase**	Y	N	N	Extracellular	Proteases
A0A096RR58_MAIZE	Cysteine-type endopeptidase	Y	N	N	Extracellular	

C0PBS1_MAIZE	**Lipase**	Y	Y	N	Vacuole	Protein involved in lipid metabolism
B6SHR9_MAIZE	PVR3-like protein	Y	Y	N	Extracellular	
Q7FU57_MAIZE	**Bowman-Birk type wound-induced proteinase inhibitor (Wip1)**	Y	Y	N	Extracellular	Proteinase inhibitors
Q42420_MAIZE	Proteinase inhibitor (Pis7)	N	N	Y	Cytoplasm	
C0HII8_MAIZE	**Bowman-Birk type trypsin inhibitor**	N	N	Y	Extracellular	
K7U234_MAIZE	Serine-type endopeptidase inhibitor	Y	N	N	Extracellular	
B6SNA6_MAIZE	**Subtilisin-chymotrypsin inhibitor CI-1B**	N	N	Y	Cytoplasm	
B4FBW7_MAIZE	**Calmodulin**	N	N	Y	Cytoplasm	Proteins involved in signaling
B6SIF5_MAIZE	Translationally-controlled tumor 1 protein	N	N	Y	Extracellular	
C0P4M0_MAIZE	Monodehydroascorbate reductase 1 peroxisomal	N	N	Y	Cytoplasm	Proteins involved in cell redox homeostasis
Q5EUE1_MAIZE	**Protein disulfide-isomerase (Pdil1)**	Y	N	N	Extracellular	

C0HGV5_MAIZE	Enolase 2 (Eno2)*[1,3,6,7]	N	N	N	Cytoplasm	
SCRK1_MAIZE	Fructokinase-1 (Frk1)*[2]	N	N	N	Cytoplasm/ Extracellular	Proteins involved in energy production pathways
B4FAG0_MAIZE	**GDP-mannose 4,6 dehydratase*[9]**	N	N	N	Cytoplasm	
A0A1D6HV20_MAIZE	**Glucose/Sorbosone dehydrogenase**	Y	N	N	Extracellular	
Q8S4W9_MAIZE	Pyruvate decarboxylase (Pdc3)	N	N	Y	Cytoplasm	
B6T1H5_MAIZE	60S ribosomal protein L12	N	N	Y	Cytoplasm	
B7ZZ42_MAIZE	**Hsp70*[3]**	N	N	N	Cytoplasm	Proteins involved in protein synthesis, folding and stabilisation
B4FZZ2_MAIZE	**Peptidyl-prolyl cis-trans isomerase (Cyclophilin)*[1,7]**	N	N	N	Cytoplasm	
K7UR51_MAIZE	**40S ribosomal protein S8**	Y	N	N	Extracellular	

A0A1D6N1Z8_MAIZE	**6-phosphogluconate dehydrogenase**	Y	N	N	Extracellular	
C0PHR4_MAIZE	**Adenosylhomocysteinase*[1,3]**	N	N	N	Cytoplasm	Proteins involved in secondary metabolism
C0P5Y3_MAIZE	**Methionine synthase*[3,6]**	N	N	N	Cytoplasm	
BX9_MAIZE	**DIMBOA UDP-glucosyltranferase (BX9)*[8]**	N	N	N	Cytoplasm	
C0PEP2_MAIZE	ACC oxidase 1*[6]	N	N	N	Cytoplasm	
PROF5_MAIZE	**Profilin-5**	N	N	Y	Cytoplasm	Structural protein
A0A1D6E7A7_MAIZE	DUF642 protein	Y	N	N	Extracellular	Unknown

Abbreviations: a www.uniprot.org/uniprot/; b Blast2GO https://www.blast2go.com/; c http://www.cbs.dtu.dk/services/SignalP; d http://www.cbs.dtu.dk/services/TMHMM; e http://www.cbs.dtu.dk/services/SecretomeP; http://www.genscript.com/wolf-psort.html h hhttp://www.cbs.dtu.dk/services/TargetP; * Hypothetical secreted proteins identified by literature review: [1](Tanveer et al. 2014); [2](Hajirezaei et al. 2000); [3](Agrawal et al. 2010); [4](Zhang et al. 2016b); [5](Choi et al. 2012); [6](Ding et al. 2012); [7](Fernandez et al. 2012); [8](Schulz et al. 2016); [9](Liao et al. 2012); Y, yes; N, no. Bold names represent proteins that were present in both conditions (un-inoculated and inoculated).

Identification of putative proteins based on their conserved domains and function was performed on the proteins from *T. virens* that were secreted into the apoplast in plants 5 d.p.i. The GHs family was the most represented in the *T. virens* secretome (Table 3.4). Proteins that participate in antioxidant processes and oxidative stress resistance, in addition to secondary metabolism related proteins were also identified (Table 3.4). Furthermore, in the presence of maize roots, groups of proteins corresponding to putative effector-like proteins, chaperones, 14-3-3 like proteins and ribosomal proteins were identified as part of the *T. virens* secretome (Table 3.4). Overall, these results suggest that *T. virens* activates different mechanisms during host root colonisation.

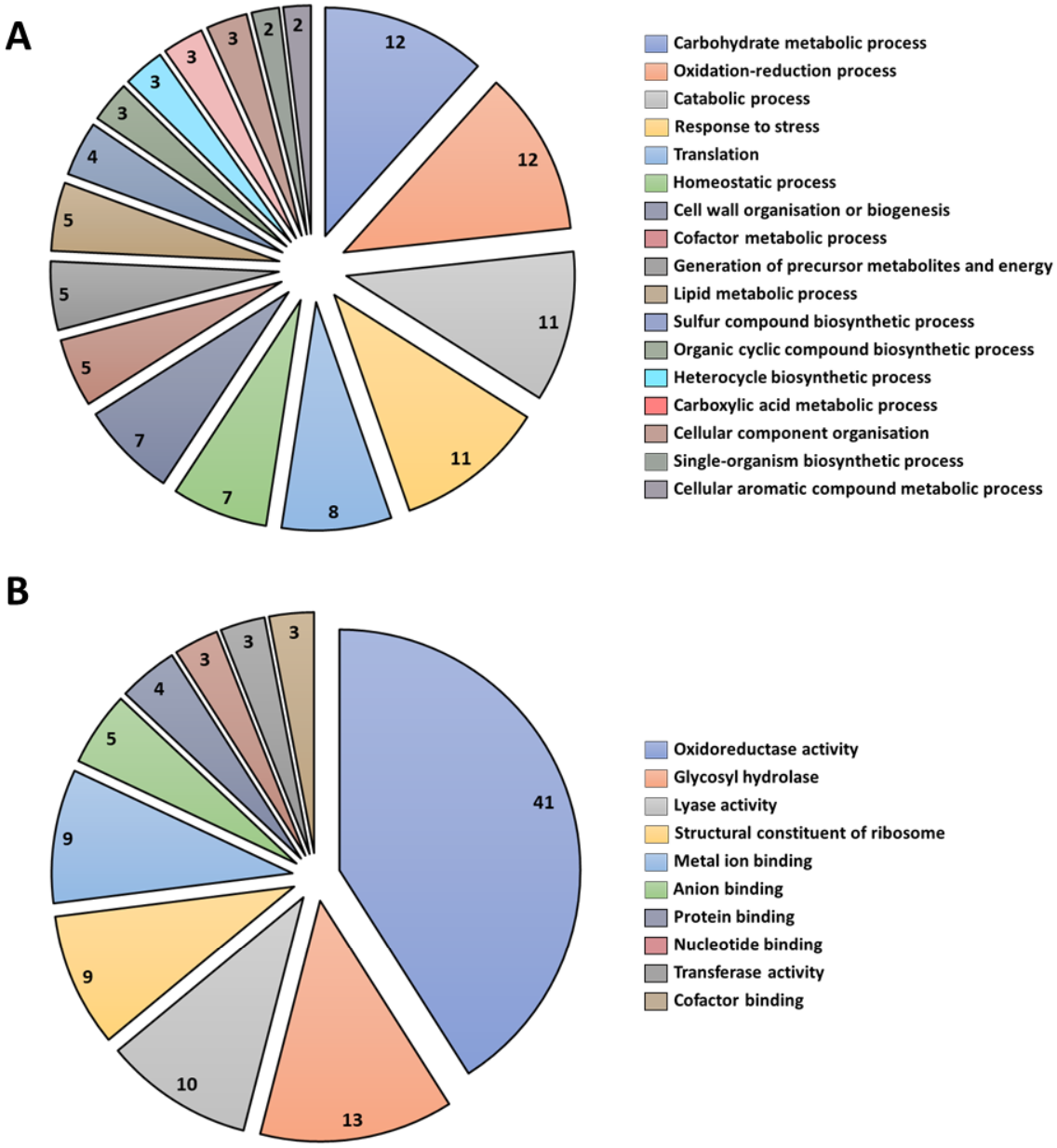

Figure 3.7 Functional classification of all secreted proteins from *T. virens* at 5 d.p.i. Blast2GO multilevel chart for **(A)** biological process and **(B)** molecular function. Score distribution represented as a percentage of each group is indicated inside the pie slices.

Table 3.4 Summary of the apoplastic proteins secreted by *Trichoderma virens* 5 d.p.i

Protein Identifier JPGI [a]	Uniprot ID [b]	Protein annotation [c]	SignalP [d]	TMHMM [e]	SecretomeP [f]	EffectorP [g]	WoLF PSORT [h]/ TargetP [i]	Protein group
TV_75509	G9N8W5_HYPVG	Enolase*[5,7]	N	N	N	Non-effector	Cytoplasm	Proteins involved in energy producing pathways
TV_87809	G9N9Z6_HYPVG	Galactose mutarotase-like protein	Y	N	N	Non-effector	Extracellular	
TV_92614	G9N6G5_HYPVG	Malate dehydrogenase*[8,9,10]	N	N	Y	Non-effector	Extracellular	
TV_42143	G9N7I4_HYPVG	Beta-galactosidase	Y	N	N	Non-effector	Extracellular	Glycoside hydrolases
TV_90504	G9MY26_HYPVG	Cellobiohydrolase	Y	N	N	Non-effector	Extracellular	
TV_110754	G9ML80_HYPVG	ß-glycosidase	Y	N	N	Non-effector	Extracellular	
TV_29366	G9MSH9_HYPVG	ß-xylosidase	Y	N	N	Non-effector	Extracellular	
TV_71600	G9MLE1_HYPVG	α-glycosidase	Y	N	N	Non-effector	Extracellular	
TV_78372	G9MWK2_HYPVG	Peptidase M24B family	Y	N	N	Non-effector	Cytoplasm	Peptidase
TV_50666	G9N1W4_HYPVG	Cupin 1/Bicupin	Y	N	N	Non-effector	Extracellular	Microbial elicitor

TV_110852	G9MJD8_HYPVG	Small protein 1 (Sm1)	Y	N	N	Non-effector	Extracellular	
TV_111995	G9MUU9_HYPVG	SSCP	Y	N	N	Effector	Extracellular	Small secreted protein
TV_92810	G9N192_HYPVG	SSCP/CFEM	Y	N	N	Non-effector	Extracellular	
TV_111061	G9MI10_HYPVG	Protein disulfide-isomerase (pdi1)	Y	N	N	Non-effector	Extracellular	
TV_138628	G9MTV5_HYPVG	Pyridine nucleotide-disulphide oxidoreductase	Y	N	N	Non-effector	Cytoplasm	
TV_139551	G9N846_HYPVG	Ribosomal protein 60S	Y	N	N	Non-effector	Cytoplasm	Proteins involved in protein synthesis, folding and stabilisation
TV_78230	G9NDN5_HYPVG	Ribosomal protein L11C	N	N	Y	Effector	Cytoplasm	
TV_88756	G9N6G6_HYPVG	Ribosomal protein L28e	Y	N	N	Effector	Cytoplasm	
TV_74544	G9NCR5_HYPVG	Ribosomal protein S7	N	N	Y	Effector	Cytoplasm	
TV_216375	G9MYT5_HYPVG	Proteinase inhibitor	N	N	Y	Effector	Cytoplasm	Proteinase inhibitor
TV_58449	G9N458_HYPVG	Glucose-methanol-choline oxidoreductase	N	N	Y	Non-effector	Extracellular	Protein involved in cell redox

TV_53497	G9MU78_HYPVG	Aminotransferase (GliI)*[11]	N	N	N	Non-effector	Cytoplasm	
TV_82877	G9N875_HYPVG	S-adenosylhomocystein hydrolase*[3,4]	N	N	N	Non-effector	Cytoplasm	
TV_215323	G9MGG3_HYPVG	Alcohol dehydrogenase	N	N	Y	Non-effector	Cytoplasm	
TV_74949	G9NAQ0_HYPVG	Cytochrome P450	Y	N	N	Non-effector	Cytoplasm	
TV_186579	G9MVE5_HYPVG	Cytochrome P450*[12]	N	N	N	Non-effector	Cytoplasm	Proteins involved in secondary metabolism
TV_87758	G9NA55_HYPVG	S-adenosylmethionine synthase*[4]	N	N	N	Non-effector	Cytoplasm	
TV_72386	G9MID9_HYPVG	Short-chain dehydrogenase/reductase (SDR)	Y	N	N	Effector	Cytoplasm	
TV_91355	G9MU80_HYPVG	S-adenosyl-L-methionine methyl transferase (GliN)*[11]	N	N	N	Non-effector	Cytoplasm	
TV_215037	G9MF42_HYPVG	Thiamine biosynthesis (Thi4) protein	N	N	Y	Non-effector	Cytoplasm	
TV_88738	G9N6E1_HYPVG	Translation controlled tumour-associated (TCTP)	N	N	Y	Non-effector	Cytoplasm	Proteins involved in signalling processes
TV_217216	G9NCG7_HYPVG	14-3-3 protein*[6]	N	N	N	Non-effector	Cytoplasm	

TV_215514	G9MJV5_HYPVG	Catalase-peroxidase haem*[1,6,10]	N	N	N	Non-effector	Cytoplasm	
TV_72131	G9ML11_HYPVG	Hsp70 (bip1)	Y	Y	N	Non-effector	Extracellular	
TV_54541	G9MKH2_HYPVG	Glutathione reductase*[4]	N	N	N	Non-effector	Cytoplasm	
TV_72615	G9MJ35_HYPVG	L-domain-like protein (Ecm33)	Y	N	N	Non-effector	Extracellular	Proteins involved in stress/defence mechanisms
TV_183329	G9N7N4_HYPVG	Superoxide dismutase [Cu-Zn]	Y	N	N	Effector	Cytoplasm	
TV_81963	G9MIH3_HYPVG	Thioredoxin reductase*[2]	N	N	N	Non-effector	Cytoplasm	
TV_216458	G9N026_HYPVG	Thioredoxin-related protein	N	N	Y	Effector	Cytoplasm	
TV_40034	G9NAK1_HYPVG	Hypothetical protein	N	N	Y	Non-effector	Cytoplasm	
TV_76398	G9N4X8_HYPVG	Hypothetical protein (HGD-D superfamily)	N	N	Y	Effector	Cytoplasm	Unknown
TV_141673	G9MH43_HYPVG	Hypothetical protein DUF3759 (CipC1)	N	N	Y	Non-effector	Cytoplasm	
TV_216138	G9MTV6_HYPVG	Hypothetical protein DUF1857*[6]	N	N	N	Effector	Cytoplasm	

Abbreviations: a http://genome.jgi.doe.gov/TriviGv29_8_2/TriviGv29_8_2.home.html; b www.uniprot.org/uniprot/; c Blast2Go https://www.blast2go.com/; d http://www.cbs.dtu.dk/services/SignalP/; e http://www.cbs.dtu.dk/services/TMHMM/; f http://www.cbs.dtu.dk/services/SecretomeP/Protein; g http://effectorp.csiro.au/; h http://www.genscript.com/wolf-psort.html i hhttp://www.cbs.dtu.dk/services/TargetP/ *Hypothetical secreted proteins identified by literature review [1](Tanabe et al. 2011), [2] (Shi et al. 2012), [3] (Luo et al. 2008), [4](Lamdan et al. 2015), [5] (Lopez-Villar et al. 2006), [6] (Yang et al. 2015), [7](Sundstrom and Aliaga 1994), [8](Giardina and Chiang 2013), [9] (Weber et al. 2012), [10] (Chu et al. 2015), [11] (Kim et al. 2014), [12] (Druzhinina et al. 2012); Y, yes; N, no.

3.3.5 Label-free quantification of apoplastic proteins during the *Trichoderma virens*-maize interaction

3.3.5.1 Label-free quantification

By using the label-free quantification approach 10 proteins were identified from maize that were significantly (significance ≥ 10; fold change ≥ 1.5) different in their intensities between un-inoculated and inoculated roots (Figure 3.8). Analysis of the correlation of the signal intensities showed that the biological repeats of each treatment were clustered together, with an average correlation of 0.87 for un-inoculated roots (M) and 0.90 for inoculated roots (M+Tv). Correlation between all biological repeats showed an average relationship of ≥ 0.70. Proteins that showed a decreased abundance during the interaction with *T. virens* were 40S ribosomal protein (B4FSW0_MAIZE), pathogenesis-related protein (PR-10) (Q29SB6_MAIZE), peroxidase (Per12) (B4FG39_MAIZE), cytosolic ascorbate peroxidase (Apx1) (B6TM55_MAIZE), cysteine endopeptidase (K7W288), blue copper protein (B6UHQ8_MAIZE), adenosylhomocysteinase (C0PHR4_MAIZE), protein disulphide-isomerase (Pdil1-1) (Q5EUE1_MAIZE), and ribonuclease 1 (B4FBD6_MAIZE). In contrast, the protein serine-type endopeptidase inhibitor (K7U234_MAIZE) showed an increased abundance. Overall, these results suggest that the abundance of proteins involved in different plant biological processes, including plant defence, are manipulated by the presence of *T. virens*.

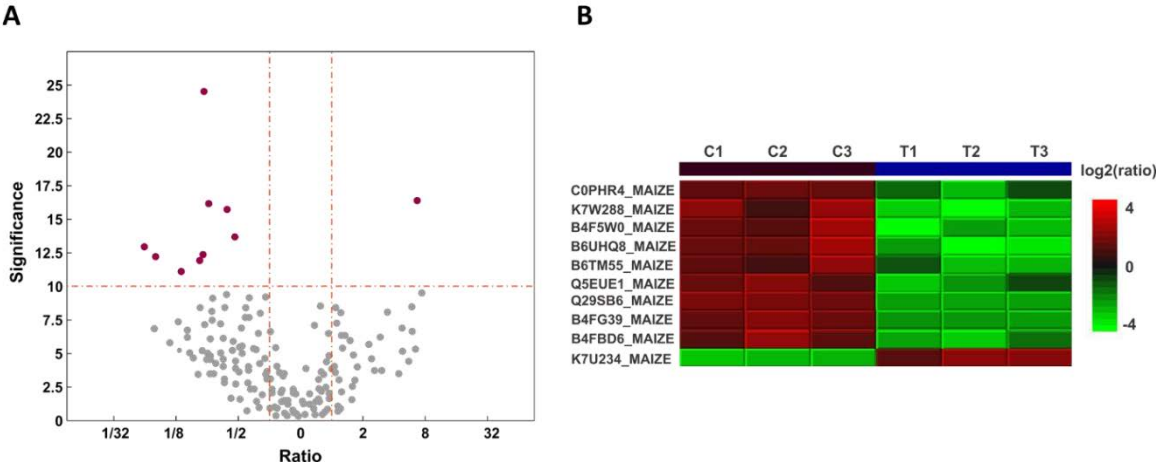

Figure 3.8 Label-free quantification of apoplastic proteins during the *T. virens*-maize interaction at 5 d.p.i. (A) Volcano plot for maize proteins statistically significant (significance ≥ 10; fold change ≥ 1.5) during interaction. **(B)** Protein profile heat map of the most significantly different maize proteins comparing un-inoculated (C) and inoculated (T) plants. Cell colour represents the log2 (ratio) to the average are across different samples (C1, C2, C3, T1, T2 and T3).

3.3.6 Peroxidase levels influenced by *Trichoderma virens*

The peroxidase activity in the AF after 5 d.p.i was measured in maize root tissues un-inoculated and inoculated with *T. virens*. Shifts in the enzyme activity were observed, where roots inoculated with *T. virens* showed a significant reduction in peroxidase activity compared with un-inoculated roots

(*P*<0.05) (Figure 3.9). These results indicated that the peroxidase activity was higher in un-inoculated roots compared to inoculated, showing that the peroxidase activity was directly influenced by the presence of *T. virens* in the root system.

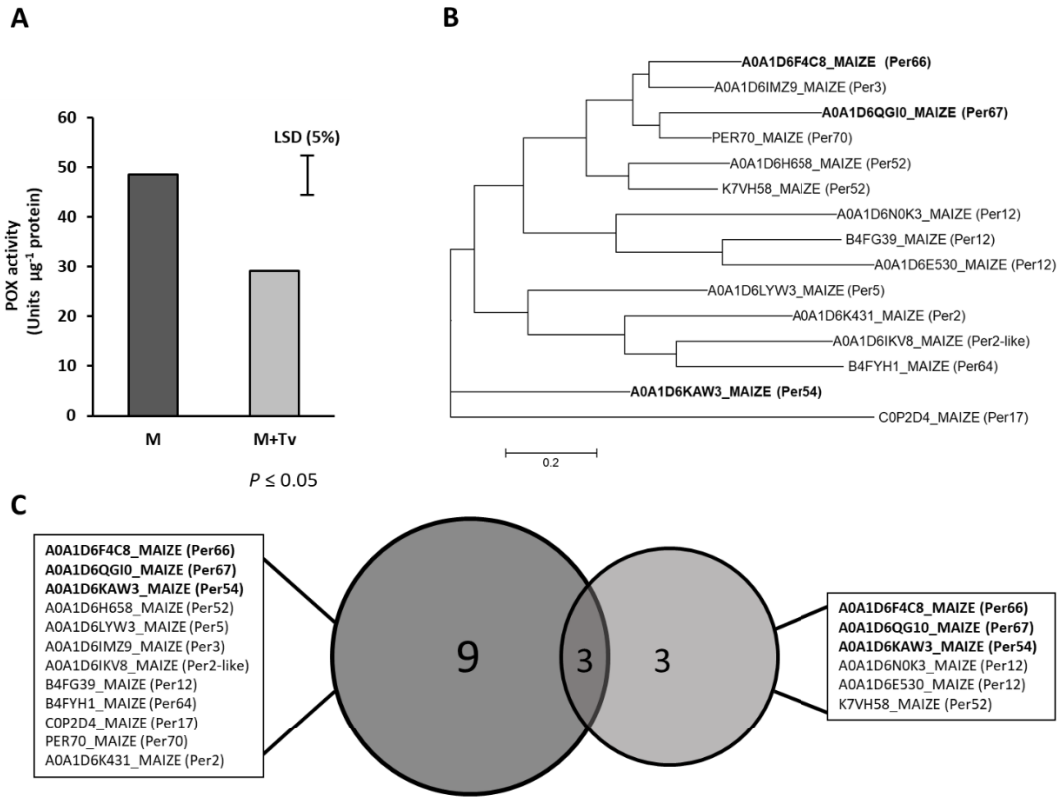

Figure 3.9 Peroxidase study during *T. virens*-maize interaction. (A) Peroxidase activity in un-inoculated (M) and inoculated (M+Tv) maize roots after 5 d.p.i (*P*<0.05). **(B)** Phylogenetic tree of peroxidases identified in the maize apoplast zone. Using Muscle, the composite proteins were aligned, and the Maximum likelihood tree, was generated in MEGA6. **(C)** Comparison between peroxidases expressed in maize roots with or without *T. virens*. Bold names represent peroxidases that were present in both conditions.

3.3.7 Localisation of *Trichoderma virens* apoplastic proteins

Localisation vectors were created successfully using the Golden Gate cloning strategy (Figure 3.10 and Supplementary Figure 3). gDNA was extracted from *T. virens* positive transformants containing Sm1-linker-mCherry and GliI-linker-mCherry constructs, respectively. Amplification of mCherry ORF (730 bp) was used to confirm integration of the vector in the *T. virens* positive transformants genome (Figure 3.11 A). Protein extractions of mycelia and the supernatant fraction were performed to verify protein localisation and secretion. Western blot results showed that both fusion tagged proteins were present in the total protein extracts (Sm1-linker-mCherry fusion (~41 kDa); GliI-linker-mCherry fusion (~78 kDa)) from *T. virens* mycelia, but only the Sm1 protein was identified in the secreted fraction (Figure 3.11 B). Additional bands (< 30 kDa) observed in the blot, suggest possible cleavage between target protein and mCherry (~28 kDa) or proteolytic degradation of mCherry (shorter version). Multiple bands observed in secreted fraction in Sm1

could suggest formation of dimers that has been reported by Vargas et al. (2008). To visualise protein localisation during fungal development, Sm1-mCherry and GliI-linker-mCherry fusion proteins were expressed in *T. virens* independently, under the constitutive *gpdh* promoter. Fluorescence observations revealed that both proteins are expressed and localised in the cytosol or are attached to the fungal membrane (Figure 3.11 C).

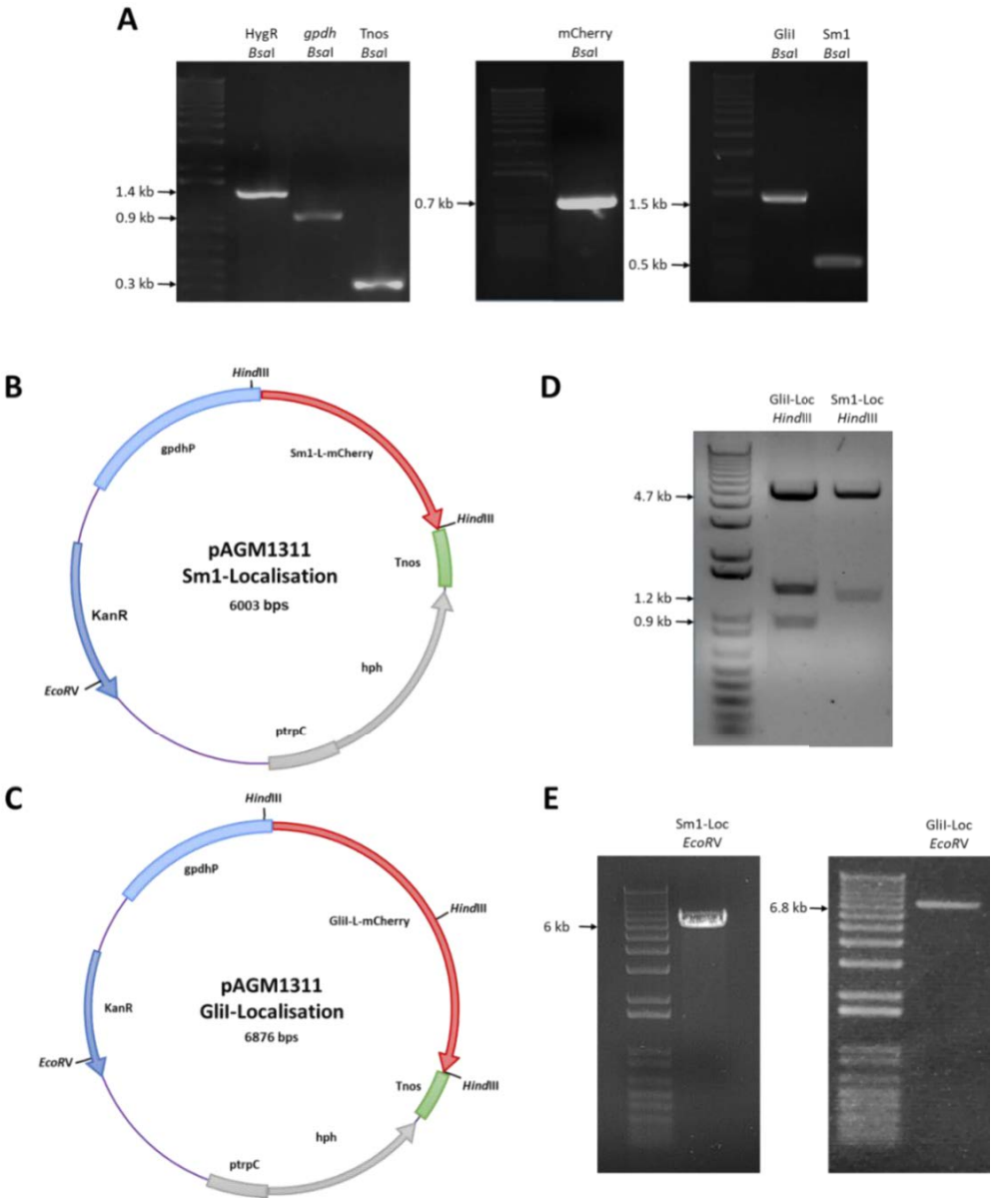

Figure 3.10 Vectors to localise *T. virens* apoplastic proteins. (A) Purified PCR products containing *Bsa*I sites. Vectors containing **(B)** Sm1 (TV_ 110852) and **(C)** GliI (TV_53497) localisation constructs. **(D)** Final vectors for localisation (pAGM1311 Sm1-Localisation and pAGM1311 GliI-Localisation) were verified by restriction enzyme digestion (cut with *Hind*III restriction enzyme; fragment sizes: 1.2 kb and 4.7 kb for Sm1-linker-mCherry, and 0.9 Kb, 4.7 kb and 1.2 kb for GliI-linker-mCherry). **(E)** Linearisation of final vectors for localisation (cut with *EcoR*V) to transform *T. virens* protoplasts. Abbreviations: KanR, kanamycin resistance cassette; ptrpC, tryptophan gene promoter; hph, hygromycin B phosphotransferase gene; gpdhP, glyceraldehyde 3-phosphate dehydrogenase promoter; T-nos, nopaline synthase terminator; Sm1-L-mCherry, Sm1-Linker-mCherry; GliI-L-mCherry, GliI-Linker-mCherry.

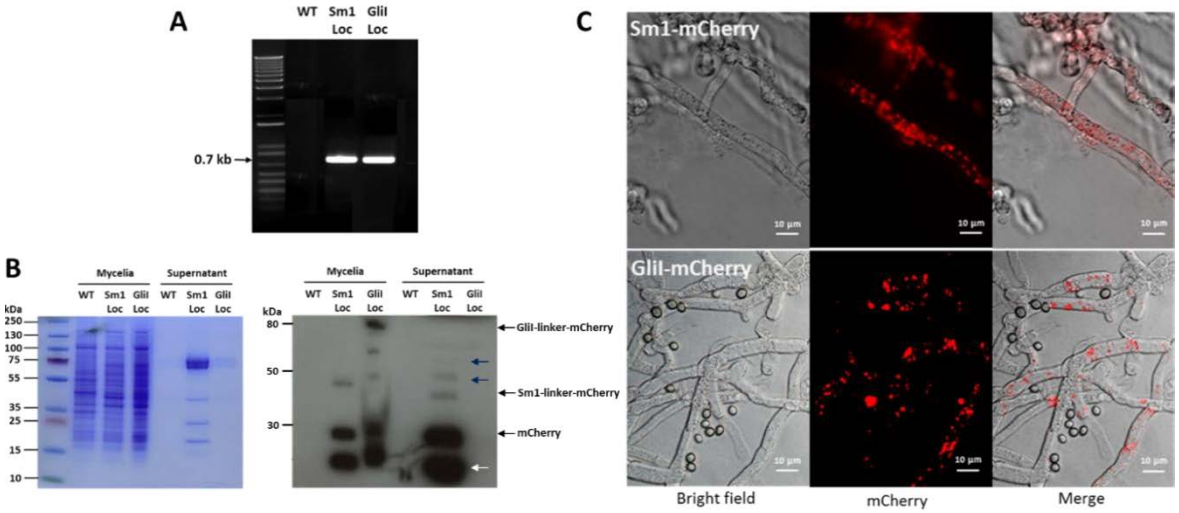

Figure 3.11 Analysis of *T. virens* apoplastic proteins. (A) Confirmation by PCR of integration of marker ORF (mCherry) in *T. virens* positive transformants (Sm1-linker-mCherry-localisation and GliI-linker-localisation), WT DNA was used as negative control. **(B)** Detection of Sm1-mCherry and GliI-mCherry proteins in mycelia and culture supernatants. Separation by 1D-SDS-PAGE of total and secreted protein fractions, and western blot analysis (blue arrows indicate probable dimerisation of Sm1; white arrow indicates possible degradation product of mCherry). **(C)** Fluorescent microscopy of Sm1-linker-mCherry and GliI-liker-mCherry expressed in *T. virens* mycelia.

3.4 Discussion

In this study, the repertoire of *T. virens* secreted proteins expressed during the interaction with maize was analysed by tandem mass spectrometry. Furthermore, the extraction, identification and function of these proteins were analysed to understand the molecular dialogue that exists in the apoplast between *T. virens* and maize, and to unravel the role that these proteins may play during the symbiotic interaction.

3.4.1 Identification of apoplastic proteins by gel-based proteomic technology

The infiltration-centrifugation method was the most efficient approach for the extraction of AF and APs, which has been previously reported in other studies for the identification of microbe-secreted proteins *in planta* (Floerl et al. 2012; Shenton et al. 2012). Using the gel-based LC-MS/MS approach, maize proteins such as methionine synthase, Hsp70, adenosyl homocysteine hydrolase and pectin esterase were expressed and identified in the AF during the interaction with *T. virens*. These proteins have been previously reported as part of the plant immune response pathways by activation of microbe elicitors (Kawalleck et al. 1992; Lionetti et al. 2007; Maimbo et al. 2007; Balmer et al. 2013); suggesting that maize roots are sensing *T. virens* elicitors; for example, chitin, and are responding to *T. virens* colonisation.

The protein β-xylosidase (TV_29366) from *T. virens* was confirmed in this analysis, suggesting the secretion of hydrolytic enzymes in to the apoplast by *T. virens*. The precursor of β-xylosidase has been reported as a virulence factor of *Sclerotinia sclerotiorum* (Yajima et al. 2009), and has been observed previously in the secretome of *T. virens* interacting with maize roots under hydroponic growth conditions (Lamdan et al. 2015). β-xylosidase participates in the hydrolysis of xylan, one of the major polysaccharides present in plant cell walls.

The fact that few secreted proteins were identified from both organisms in this first study may suggest that both the quantity of secreted proteins is limited in the apoplastic area of maize roots, and their stability or modifications made it difficult to identify them by the first methodology used. Additionally, it is also possible proteins were lost during the processes of extraction and concentration. Therefore, improvements in the methodology using shotgun proteomics were performed to overcome protein losses and to increase their yield. In addition, quantification of the APs present in the AF was performed to have a more accurate measurement before samples were analysed by LC-MS/MS. Additionally, the mass spectrometer utilised in the second study is > 50X more sensitive as well and can cope with higher data collection rates.

3.4.2 **Identification of apoplastic proteins by gel-free proteomic technology**

Using the gel-free shotgun proteomics approach, a total of 148 and 177 proteins were identified in un-inoculated and inoculated roots, respectively.

A number of cytosolic proteins were identified in this study which may suggest levels of contamination by cytoplasm from both organisms despite a low level of cytoplasm biomarker being detected (< 1.5% of total MDH activity). Similar results were observed by Dragisic Maksimovic et al. (2008), using the vacuum-infiltration technique to extract AF from maize roots. Other studies have identified classical cytoplasmic proteins as part of the secretome of different organisms; for example, plants and fungi (Agrawal et al. 2010; Kim et al. 2013). Techniques used for the isolation of APs may induce mechanical damage to host cells leading to cell breakdown and possible contamination by cytoplasmic proteins, which is a constraint in plant-microbe secretomics.

A comprehensive filter-pipeline was used in this study to identify and select putative secreted proteins from both organisms using available prediction software and literature (Supplementary Figure 2). Nevertheless, proteins that were discarded as being secreted proteins in this study may have an important function during *T. virens*-maize interaction.

3.4.3 Secretion systems of apoplastic proteins during the *Trichoderma virens*-maize interaction

Identification of potential secreted-APs from maize under both conditions, suggests that maize roots secrete APs by using both conventional (with proteins containing signal peptide) and unconventional secretion systems which include the LSPs. These findings have been previously reviewed in plant models by Yadav et al. (2015). Interestingly, *T. virens* seems to induce the secretion of LSPs; the plant apoplastic LSPs increased from 25% to 57% when the fungus was present. These changes in the population of host secreted proteins during fungal colonisation have been reviewed by Agrawal et al. (2010), suggesting that plant LSPs are involved in the defence/stress responses against microbial invasions. This may suggest that maize roots are responding to *T. virens* colonisation by secreting proteins related to defence pathways through conventional and unconventional secretion systems.

Remarkably, 54% of the 92 identified *T. virens* secreted-apoplastic proteins lacked a signal peptide (Figure 3.5). In fungi under biotic conditions the secretome population includes LSPs and reveals unknown mechanisms of secretion that are active during the microbe-plant interaction (Girard et al. 2013). It was expected that different mechanisms of secretion would be found in *T. virens* during the interaction. This secretion pattern has previously been reported during the detrimental interaction between *M. oryzea* and rice (Kim et al. 2013), where 48% of the total secretome identified corresponded to LSPs. Similar results were observed by Weber et al. (2012) during the secretome analysis of the fungus *Paracoccidioides*; where they predicted that 52% of identified secreted proteins are released by non-classical secretion systems. However, the exact mechanisms of secretion for leaderless secretion pathways remain largely unknown for plant-microbe interactions.

3.4.4 Maize secretome: the influence of *Trichoderma virens* colonisation

Functional analysis of the maize secretome present in the apoplast during colonisation by *T. virens* showed that *T. virens* is inducing several changes in plant metabolism and activating pathways of stress responses against biotic factors. Interestingly, oxidoreduction activity seems to be reduced in the presence of *T. virens* in the apoplast (Figure 3.6). Similar results were observed in the transcriptome analysis at 5 d.p.i performed by Lawry (2016), where genes involved in plant defence responses were identified, implying that maize roots are responding to fungal colonisation and vice versa.

3.4.4.1 Detoxifying and reactive oxygen species related proteins influence by *Trichoderma virens*

A larger number of proteins were observed during non-interaction conditions compared with inoculated roots, where a reduction of secreted proteins was observed in roots interacting with *T. virens*; for example, proteins belonging to the peroxidase family. Peroxidases are principal components in plant defence responses against pathogens either by cell wall reinforcement and/or for inducing plant oxidative bursts in the apoplast (Mehdy 1994), creating unsuitable conditions for microbe interactions.

Differences were found in the secretion of peroxidases in this study; where 12 were secreted in the control roots; this number reduced to six during the *Trichoderma*-plant interaction, three of which were unique to the inoculated roots (A0A1D6N0K3_MAIZE; A0A1D6E530_MAIZE; K7VH58_MAIZE) (Table 3.3). This suggest that these latter peroxidases are part of the immune respond of maize to *T. virens* colonisation. Remarkably, two other peroxidases (B4FG39_MAIZE and B6TM55_MAIZE) were significantly reduced in their abundance when *T. virens* was present (Figure 3.8). These results demonstrate that recognition of the endophyte *T. virens* by resistance proteins involves plant defence mechanisms and that this reduction in plant defence molecules such as peroxidases suggests that *T. virens* may be re-shaping plant secretome responses as a mechanism to supress plant immunity. In the symbiotic interaction between *Glomus mossea* and tobacco roots, oxidative reduction activity plays an important role; activity of ascorbate peroxidases was increased in mycorrhizal roots at earlier stages, but after the interaction is established the fungus is able to diminish the plant immune responses (Blilou et al. 2000).

Additionally, we identified proteins in un-inoculated maize such as superoxide dismutase [Cu-Zn] (SODC5_MAIZE), peoxiredoxin-2B (B4FN24_MAIZE), thioredoxin (Trxh1) (B6SHW5_MAIZE), and glutathione S-transferase (B4FSR6_MAIZE; GSTF4_MAIZE; B6TL20_MAIZE) that are involved in detoxification of apoplast ROS, but in inoculated roots the peroxiredoxin, thioredoxin and one gluthatione S-transferase weren't present. ROS play a major role in plant defence; hence in order to maintain a balance during the plant-microbe interaction, all these enzymes are necessary to confer resistance to oxidative stresses. Interestingly, antioxidant activity is reduced in maize roots during the interaction with *T. virens,* suggesting that alterations in redox activity are influenced by fungal colonisation.

3.4.4.2 Pathogenesis related proteins secreted in presence of *Trichoderma virens*

Plant defence-related proteins, called PR proteins were also identified in the secretome in both the presence and absence of *T. virens*. PR proteins are produced in plants in the event of microbial recognition, and involve antimicrobial activity. Most PR proteins are induced through JA, SA and ET defence signalling (van Loon et al. 2006). Extracellular defence-related proteins are considered the

first line of defence against invading attackers before tissue penetration takes place. Several PR-like proteins were detected in the apoplast from un-inoculated and inoculated plants including chitinase, endochitinase B, nine peroxidases (PR-9), two ribonucleases (PR-10), two proteinase inhibitors (PR-6), and an osmotin-like protein (PR-5) (Table 3.3 and Supplementary Table 4). These proteins may be considered as part of basal defence mechanisms in maize, because they were present in both conditions. Additionally, other defence-related proteins were identified; for example, a Bowman-Birk type wound-induced proteinase inhibitor that were probably induced by mechanical wounding provoked by the manipulation of the samples. Hence the possibility that that some of the previous proteins described were activated through this process cannot be discarded, given that several-defence proteins are induced during wounding or cold stress (van Loon et al. 2006).

In the presence of *T. virens*, the expression of different PR-like proteins from maize was increased. APs such as Barwin superfamily protein (B6SH12_MAIZE), cysteine-type endopeptidase (A0A1D6ICV7_MAIZE), PR-10 (A0A1D6JZU3_MAIZE), three peroxidases (A0A1D6N0K3_MAIZE; A0A1D6E530_MAIZE; K7VH58_MAIZE), proteinase inhibitor (Pis7) (Q42420_MAIZE), serine-type endopeptidase inhibitor (K7U234_MAIZE), and osmotin-like protein (A0A096PW84_MAIZE) were activated during fungal colonisation. This suggests that these proteins are specifically activated during *T. virens* recognition. Comparable findings during the three-way interaction between *Trichoderma atroviride*, a host plant and a fungal pathogen were identified, where PR proteins were up-regulated when *T. atroviride* was interacting with the plant (Marra et al. 2006). Although maize responded by constitutive expression of various PR proteins, they did not affect colonisation by the beneficial *T. virens.* Similar findings were observed during the beneficial relationship between the mycorrhizal fungus *G. mosseae* and its host plant (Vierheilig et al. 1995). Remarkably, *T. virens* may directly affect the secretion of specific PR proteins such as ribonuclease (B4FBD6_MAIZE) and PR-10 (Q29SB6_MAIZE) as their abundance in the apoplast was reduced; however, the plant may counter attack by activating other PR proteins; for example, serine-type endopeptidase inhibitor (K7U234_MAIZE) to target proteins secreted by *T. virens* in the apoplast (Figure 3.8). The serine-type endopeptidase inhibitor was identified as the only protein whose abundance was higher in the presence of *T. virens* (Figure 3.8).

3.4.4.3 Secreted proteins involved in hormone signalling, cell wall modification, nutrient acquisition, protein modification and metabolism

Proteins involved in phytohormones signalling were identified. These were predominantly from the ET biosynthesis pathway and included proteins responsible for the biosynthesis of precursor components such as methionine synthase (C0P5Y3_MAIZE), adenosylhomocysteinase (C0PHR4_MAIZE) and the enzyme 1-aminocyclopropane-1-carboxylate (ACC) oxidase (COPEP2_MAIZE) which catalyses the final stage of ET biosynthesis. Levels of adenosylhomocysteinase were influenced by the presence of *T. virens* and ACC oxidase was only

expressed in inoculated plants, suggesting that one strategy of the fungus is the manipulation of plant immunity responses via the ET pathway. In the pathosytem *Arabidopsis-Pseudomonas syringae,* Kaffarnik et al. (2009) observed that the protein abundance of methionine synthase was dramatically influenced in the apoplast and not intracellularly by bacterial effector-like proteins. Other proteins with relevance in the AF that were identified are involved in cell wall modification and nutrient acquisition (GHs); signal transduction and secondary messengers (14-3-3 protein and calmodulin) (Cui et al. 2005; Lozano-Duran and Robatzek 2015); protein modification and folding (Hsp70 and disulphide-isomerase) which are essential for protein functionality (Park and Seo 2015; Porter et al. 2015). Ribosomal proteins, cyclophilin and proteins involved in lipid transport and secondary metabolism that have potential roles in defence/stress responses (Agrawal et al. 2010) were also observed in the AF.

Overall the identified proteins play major roles in basal and induced defence/stress responses, metabolism, signalling and protein modifications in plants as observed in other plant-microbe studies (Agrawal et al. 2010) and have been previously reported as part of the apoplastic secretome *in planta* (Gupta et al. 2015), where several plant response pathways were activated or inactivated by the presence of *T. virens.*

3.4.5 *Trichoderma virens* secretome during interaction with maize roots

Diverse mechanisms are involved in the *Trichoderma*-plant interactions during the process of root colonisation (Harman 2006). In this study several protein families were identified that may have a direct influence on *T. virens* colonisation and plant defence manipulation, which correlates with the findings previously reported by Lamdan et al. (2015), where protein families such as GHs, antioxidant proteins, SSCPs and secondary metabolism proteins were secreted in the presence of maize roots.

3.4.5.1 Glycosyl hydrolase protein family (Cell wall modification)

Both the endophyte and host glycosyl hydrolases secreted have an important role during the interaction, either promoting successful colonisation via the degradation of the host cell wall or resisting the microbe invasion through the reinforcement of host defence via cell wall maintenance during early stages of interaction. Five GHs were identified including ß-galactosidases (TV_42143) that hydrolyses galactose-rich polysaccharides in plant cell walls (Ranwala et al. 1992), α-glycosidase (TV_71600) involved in catabolism and turnover of plant N-glycans (Minic 2008), ß-glucosidase (TV_110754) involved in cellulose degradation (Tiwari et al. 2013), ß-xylosidase (TV_29366), and cellobiohydrolase (TV_90504) for degradation of xylan and cellulose, respectively (Nummi et al. 1983; Biely 1985). Interestingly, the secretion of the glycosyl hydrolases including CWDEs identified in this study are mediated through the Golgi-ER secretion pathway. In addition, all identified enzymes were transcriptionally up-regulated after 5 d.p.i with maize roots compared

with axenic conditions (Lawry 2016). CWDEs have also been proposed to act as virulence factors (effectors) in *U. maydis* and *M. oryzea*; however, the exact role they play in plant immunity is not known (Kubicek et al. 2014). The results suggest when *T. virens* encounters its host plant root system, to overcome the barrier of the plant cell wall and successfully penetrate and colonise internally, *T. virens* may secrete enzymes into the apoplast such as GHs which focus on the degradation of cell wall polymers necessary for colonising host tissues.

3.4.5.2 Antioxidant secreted proteins

The oxidative burst is one of the most critical events upon plant recognition of plant pathogens (Heller and Tudzynski 2011). This reaction is activated by a rapid production of ROS in the apoplast such as superoxide, hydroxyl radical and hydrogen peroxide which are also involved in plant response signalling. In addition, ROS activate physiological changes in the plant such as cell wall strengthening. Although ROS induction is transient *in planta,* the compounds are highly reactive and can cause detrimental oxidation of essential macromolecules causing host cell damage and triggering the HR, if they are not controlled (Nanda et al. 2010). ROS are not only toxic, but are also signalling molecules involved in growth and environmental adaptation (Marschall and Tudzynski 2016). Antioxidants can protect the cell from oxidative damage by scavenging the ROS. Therefore, cellular redox homeostasis is important to maintain plant-microbe symbiotic interactions (Marschall and Tudzynski 2016). In this study, *T. virens* secreted proteins were identified that work as detoxification enzymes. The enzyme superoxide dismutase [Cu-Zn] (TV_183329) was present in the apoplast and is involved in the breakdown of ROS molecules protecting fungal integrity. Superoxide dismutase is an essential molecule during plant microbe interactions. During the beneficial relationship between the fungal endosymbiont *Epichloë lolii* and ryegrass, superoxide dismutase is necessary for limited host defence and normal endophytic growth (Zhang et al. 2011). The protein catalase-peroxidase haem (TV_215514) was also identified. This enzyme exhibits both catalase and peroxidase activity, and provides protection against oxidative stress dismutating H_2O_2 to $O_2 + H_2O$. In the fungus *M. oryzea*, the secreted catalase-peroxidase confers resistance to H_2O_2 accumulated in epidermal cells of rice, but is not essential for pathogenicity (Tanabe et al. 2011). As part of the antioxidant protein arsenal, the enzyme glutathione reductase was found, which is required for protection against oxidative stress. Glutathione reductase (TV_54541) plays an essential role in rice blast disease, facilitating biotrophic colonisation of host cells and by suppression of host ROS accumulation (Fernandez and Wilson 2014). In the *Gluconacetobacter diazotrophicus*-rice system glutathione reductase was determined to be crucial for endophytic colonisation (Alqueres et al. 2013). Also identified was the protein pyridine nucleotide-disulphide oxidoreductase (TV_138628) that is associated with antioxidant activity. All these antioxidant proteins secreted by *T. virens* have been related to inactivation of ROS during plant-microbe interactions. Moreover, the GPI-anchored protein Ecm33-like (TV_72615) from *T.* virens was identified in the secretome. Ecm33 protein has been reported as a GPI-anchored protein that attaches into the plasma membrane in *Beauveria bassiana* and *Metarhizium robertsii*, where it

contributes to multi-stress tolerance against oxidant molecules, fungicides and osmotic stress (Chen et al. 2014). In *T. virens*, Ecm33 was found by Lamdan et al. (2015) as part of the secretome in the presence of maize roots. This may suggest that during colonisation Ecm33-like protein may play an important role due to its properties as a multi-stress tolerance molecule, protecting *T. virens* hyphae against the oxidative burst created by host cells. Overall, the results presented here suggest that antioxidant secreted proteins collaborate in the suppression of basal resistance through the regulation of the cellular redox state, and by modifying gene expression in the host plant to maintain symbiosis between *T. virens* and maize.

3.4.5.3 Secreted proteins involved in secondary metabolism biosynthesis

Fungal SMs are classified into four classes: polyketides, terpenoids, shikimic acid derived compounds, and non-ribosomal peptides. During plant-microbe interactions, secondary metabolites such as phytohormones and toxins play major roles in the regulation of plant metabolic and defence response processes (Pusztahelyi et al. 2015). In addition, fungal secondary metabolites can shape the fungal-plant interactions in similar way as do effector proteins (Pusztahelyi et al. 2015). The protein S-adenosylmethionine (SAM) synthase (TV_87758), involved in the biosynthesis of the precursor of ET was identified, ET being one of the phytohormones involved in plant defence responses (Broekgaarden et al. 2015). Interestingly, SAM synthase is predicted to be secreted into the apoplast through a non-classical secretion system, and was identified as part of the secretome of *T. virens* in presence of maize roots (Lamdan et al. 2015). ET is a crucial phytohormone for plant defence responses during plant-microbe interactions, where successful plant symbionts have evolved different strategies to manipulate plant responses by affecting the ethylene pathway. For example, the small secreted protein SP7 from the arbuscular mycorrhizal *Glomus intraradices* is translocated into the cell nucleus and interacts with host ethylene-responsive transcription factor (ERF19) interfering with the defence cascade, thereby promoting mycorrhizal colonisation (Kloppholz et al. 2011). In *T. harzianum*, activation of the enzyme ACC deaminase promotes root elongation of canola seedlings by modulating ET levels in the host plant (Viterbo et al. 2010). Results suggest that *T. virens* may influence ET levels in the apoplast allowing *T. virens* to colonise the intercellular spaces without triggering a major immune response.

Additionally, the proteins S-adenosyl-L-methionine methyltransferase (GliN) (TV_91355) and aminotransferase (GliI) (TV_53497) which are involved in gliotoxin biosynthesis and belong to the gliotoxin cluster in *T. virens* (Mukherjee et al. 2012) were identified. Gliotoxin is a fungistatic mycotoxin that confers protection to oxidative stress and participates in mycoparasitism but does not have an influence in *T. virens* root colonisation (Vargas et al. 2014). The role of mycotoxins in plant microbe interactions are mainly ascribed as virulence or pathogenicity factors. It will be necessary to elucidate the function of *Trichoderma* toxins during host colonisation, which may act as neutralisers of plant defence mechanisms (Pedras and Ahiahonu 2005).

3.4.5.4 Putative effector-like proteins

To establish a beneficial or detrimental interaction plant microbes deliver effector-like proteins into host tissues, where they play a central role in the suppression of plant defence responses and modulate plant physiology by reprogramming metabolic processes of colonised tissues (Doehlemann et al. 2014; Mendoza-Mendoza et al. 2018). Effector-like proteins are defined as stable small secreted proteins ≤ 300 amino acids, although larger proteins have been identified that play similar roles (Lo Presti et al. 2015). Effector-like proteins are secreted either into the apoplast or translocated into plant cells (Lo Presti et al. 2015). Putative effector-like proteins were identified in the secretome of *T. virens* during the interaction with maize roots. The effector-like proteins were divided into subgroups according to their predicted functions.

3.4.5.4.1 Thioredoxin-like proteins

As mentioned above, oxidative burst and the progressive induction of ROS have a major impact during plant microbe interactions; hence their homoeostasis in the apoplast is necessary for a long-term relationship. Two thioredoxins (TV_81963 and TV_216458) and one disulphide-isomerase (TV_11061) were identified which participate in the rearrangement of disulphide (-S-S-) bonds in proteins. Several studies have summarised the importance of thioredoxins in plant-microbe interactions. The thioredoxin GBNRx1 from *V. dahlia* plays a crucial role in the apoplastic immune response functioning in apoplastic ROS scavenging in cotton (Li et al. 2016b). The thioredoxin system has a major influence in *Botrytis cinerea* pathogenicity protecting it from oxidative stress (Viefhues et al. 2014). The thioredoxin complex influences several cellular processes by affecting protein folding or their activity by thiol-disulphide redox control (Arner and Holmgren 2000). In *Ralstonia solani*, the thioredoxin TRX2 is necessary for the activation of the effector RipAy that degrades glutathione which is involved in the plant immune response (Mukaihara et al. 2016). Thioredoxins are also involved in the bacterial-plant interactions where they play a role in melanin synthesis and contribute to signal transduction during symbiotic nitrogen fixation, giving resistance to oxidative stress (Castro-Sowinski et al. 2007). Results suggest that *T. virens* may use antioxidant-secreted proteins that can act as effector-like proteins to control ROS levels in the apoplast which diminishes the plant immune response thus enabling fungal colonisation.

3.4.5.4.2 Small secreted cysteine proteins

SSCPs are widely distributed in plant symbionts. *Trichoderma* spp. (*T. virens, T. atroviride* and *T. reesei*) contain around 173 SSCPs. Of these, 129 are specific to *Trichoderma* species and around 25 are unique having no BLAST matches (Lawry 2016). Three SSCPs were identified, including Sm1 (TV_110852), SSCP1 (TV_92810), and SSCP2 (TV_111995) in the secretome from *T. virens* in the apoplast. Sm1 belongs to the cerato-platanin family and was reported as an elicitor that induces systemic disease resistance through activating the JA pathway in the host plant (Djonović et al. 2007). However, the specific role Sm1 has during *T. virens* colonisation is not known. Several

paralogs of Sm1 have been identified: Sm2, Sm3 and Sm4 (Crutcher et al. 2015). Sm2, was highly expressed in the presence of maize roots compared with the other homologs, is involved in colonisation process and is more important than Sm1 in the promotion of plant protection (Gaderer et al. 2015); however, we did not identify Sm2 in the *T. virens* secretome. The protein SSCP1 exhibits an 8 cysteine-containing CFEM domain and was reported in the secretome of *T. virens* in the presence of maize roots (Lamdan et al. 2015). SSCP1 was predicted to act as a negative effector, directly affecting the defence level in the plant. The SSCPs in *T. virens* may play essential roles additional to elicitor and effector functions such as cell surface receptors, signal transducers, or adhesion molecules during colonisation. Few of the SSCPs have been characterised so far in *Trichoderma* (Djonović et al. 2007; Crutcher et al. 2015; Gaderer et al. 2015; Lamdan et al. 2015). Further research is required to understand the redundancy and abundance of SSCPs in *T. virens* during the symbiotic relationship with it host plant.

3.4.5.4.3 Proteinase inhibitors

The proteinase inhibitor I9 (TV_216375) was identified in the *T. virens* secretome. This protein belongs to the protease inhibitor superfamily, which are responsible for the modulation of folding and activity of the peptidase pro-enzyme. PIs may be indispensable for the inactivation of plant defences. Several apoplastic effectors in fungal plant pathogens with protease inhibitor activity have been described during successful infection; for example, the effector Pit2 in *U. maydis* functions as an inhibitor of maize cysteine proteases, and is required for fungal virulence and suppression of host immunity (Mueller et al. 2013). Other examples are the protease inhibitor Avr2 secreted by the fungal plant pathogen *C. fulvum* that targets the tomato defence protease Rcr3 (Song et al. 2009), and recently, a candidate effector predicted in *S. sclerotiorium* with a conserved serine protease I9 domain, which may be necessary to suppress host resistance (Guyon et al. 2014). In the *T. virens*-maize interaction different proteases such as aspartic-type endopeptidase (A0A0B4J327_MAIZE) and cysteine-type endopeptidase (A0A096RR58_MAIZE) were expressed by maize during fungal colonisation. For that reason, PIs may be essential to inactivate or block the plant immune proteases.

3.4.5.5 Peroxidase levels influenced by *Trichoderma virens*

Peroxidases are defence-related enzymes that are induced in the presence of plant associated microbes that is triggered by elicitor-induced signal transduction pathways (Almagro et al. 2009). The fact that peroxidase activity levels were significantly reduced in the presence of *T. virens* at 5 d.p.i (Figure 3.9) may suggest that fungal colonisation does not activate stronger immune responses in maize roots at this development stage of the interaction. Moreover, any reduction in peroxidase activity may directly influence lignification and suberisation of cell walls and crosslinking of cell wall structural (Tanaka et al. 2006) and defence reactions such as cell wall reinforcement (Hiraga et al. 2001; Almagro et al. 2009). In poplar plants, peroxidase activity was influenced by the ectomycorrhizal *Paxillus involutus* and dependent on the compatibility of the isolate, showing that

during compatible interaction, changes in the level of peroxidases were not observed, but under incompatible interaction the levels were significantly higher compared to the control plants (Gafur et al. 2007).

ROS scavenging enzymes secreted by *T. virens* into the apoplast, such as glutathione reductase (TV_54541), catalase-peroxidase haem (TV_215514), superoxide dismutase [Cu-Zn] (TV_183329), thioredoxin reductase (TV_81963) and thioredoxin-related protein (TV_216458) help overcome the oxidative burst, which may have an effect on the activation of robust plant defence reactions including plant peroxidases. It has been demonstrated that production of fungal ROS can result in the suppression of endophyte growth in the host plant, which is critical in the mutualistic *Epichloë festucae* and grass interaction (Tanaka et al. 2006). Therefore, we suggest that *T. virens* secretes detoxifying enzymes into the apoplastic as a strategy to maintain ROS stability to mitigate the impact of stress and to manipulate further plant immune responses diminishing the effect of peroxidases in the apoplast.

3.4.6 **Localisation of *Trichoderma virens* apoplastic proteins**

The development of novel genomic tools such as Golden Gate are necessary to effectively study *Trichoderma´s* biology as a plant endophyte and try to understand complex interactions between fungi and plants; for example, *T. virens*-maize. In another fungal model, a similar strategy (Gateway technology) has been used to investigate *M. oryzae* effector localisation during colonisation of host cells (Gong et al. 2014), revealing the mechanisms used by the fungus to deliver effector proteins.

Localisation of *T. virens* apoplastic proteins confirmed that the Sm1 protein was secreted by *T. virens,* which has been previously reported by Djonovic et al. (2006). In the case of GliI protein, no evidence was obtained to suggest that this protein can be secreted under culture media conditions; however, it was identified in the apoplast study. Therefore, it may suggest that specific signals from the host plant are necessary for the secretion of this protein. For example, analysis of the secretome of rice suspension-cultured cells treated with rice blast fungus *Magnaporthe grisea* and its elicitors showed an induction of genes and proteins such as chitinases, expansins, oxalate oxidases and DUF26 which are associated with defence mechanisms (Kim et al. 2009). Also, the plant induces the secretion of fungal proteins involved in the breakdown of host plant cell walls and oxidation-reduction processes during infection (Xu et al. 2016). New experiments *in planta* need to be performed to localise both proteins during the interaction and to validate the data obtained in this study.

3.5 Conclusion

In closing, this study reveals possible mechanisms necessary for *T. virens* endophytism (Figure 3.12). Host cell wall degradation and modification are essential during internal colonisation. Several pathways are activated during the interaction. In particular, redox homeostasis is crucial to maintain a controlled environment in the apoplast. Both organisms secreted proteins into the apoplast via conventional and unconventional secretory mechanisms. Putative effector-like proteins secreted by *T. virens* that may lead the symbiotic relationship by the suppression of plant immune pathways were identified; for example, peroxidase activity. This study lays the foundation for future studies for a better understanding of plant-fungus mutualism, particularly at the proteomic level.

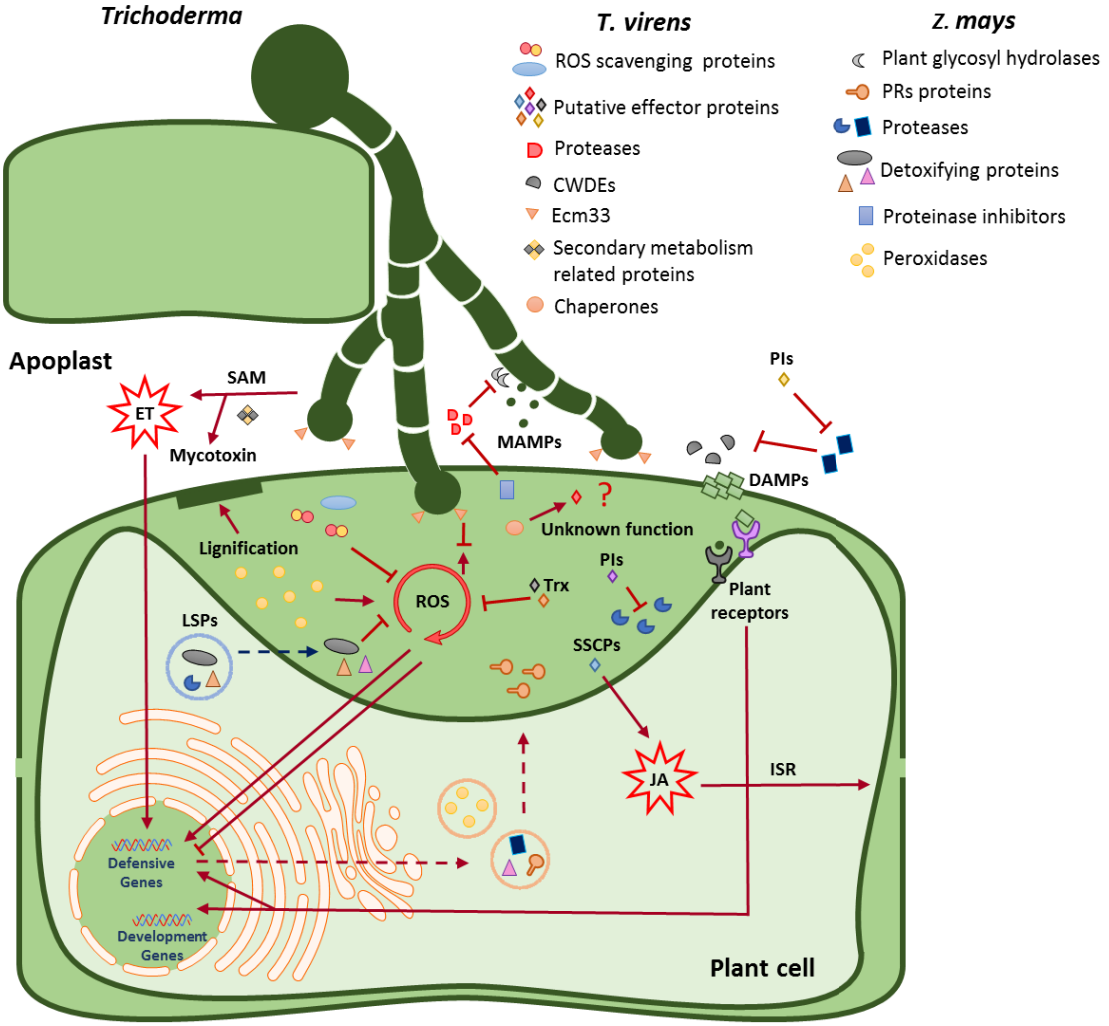

Figure 3.12 Model of apoplastic proteins identified in the *T. virens*-maize interaction. Location and putative function of apoplastic proteins secreted by *T. virens* and maize. Abbreviations: ET, ethylene; JA, jasmonic acid; ISR, induced systemic resistance; ROS, reactive oxygen species; MAMPs, microbial-associated molecular patterns; DAMPS, damage-associated molecular patterns; CWDEs, Cell wall degradative enzymes; PRs, pathogenesis-related proteins; PIs, proteinase inhibitors; Trx, thioredoxin; LSPs, leaderless secretory proteins; SAM, S-adenosyl-l-methionine; SSCPs, small secreted cysteine-rich proteins.

4 Role of up-regulated 2-oxoglutarate/Fe (II) dioxygenase (*tvox1*) during the *Trichoderma virens*-plant interaction

4.1 Introduction

Iron (Fe) is an essential microelement which is vital for animals, plants and microorganisms. Iron participates as a cofactor in multiple metabolic processes; for example, iron is necessary for respiration, photosynthesis, DNA repair and fundamental metabolic reactions (Guerinot and Yi 1994; Dunn et al. 2007). Moreover, iron homeostasis in living cells is crucial due to its highly reactive and toxic nature, producing ROS that initiate and mediate cell death (Dixon and Stockwell 2014). Therefore, organisms have evolved several strategies to maintain iron homeostasis such as iron transport, storage and involvement of regulatory proteins (Wang and Pantopoulos 2011). Iron bioavailability in most soils on earth is limited (Guerinot and Yi 1994). As a result, plants and microorganisms have evolved different strategies to favour the acquisition of iron. In plants, two strategies have been described: strategy I, used by non-graminaceous monocots, based on the acidification of the rhizosphere to increase iron solubility through proton secretion, trans-plasma membrane electron transfer, and transport; and strategy II, which relies on phytosiderophore secretion and is only present in graminaceous monocots; for example, maize (Staiger 2002). In contrast, microorganisms utilise three mechanisms to solubilise iron and incorporate it into the cell, including a) reduction of ferric ion (Fe^{3+}) to the ferrous ion (Fe^{2+}) form, b) acidification of the environment and c) excretion of soluble iron-chelating molecules (siderophores) (Philpott 2006).

Plants and root-associated microorganisms uptake iron mainly through the rhizosphere (Morrissey and Guerinot 2009), where its incorporation via rhizosphere associated microbes is essential, making iron acquisition more efficient to plants (Jin et al. 2014). Iron is a key element during plant-microbe interactions (Lemanceau et al. 2009) (Figure 4.1). *Trichoderma* stimulates iron uptake responses that readjust iron homeostasis in roots, enhancing lateral root development and root hair proliferation (Martínez-Medina et al. 2017). In the biotrophic fungus *U. maydis*, iron uptake via the ferroxidase/permease system is fundamental for pathogenic development (Eichhorn et al. 2006). In the phytopathogenic fungus *Cochliobolus heterostrophus* the production of siderophores is necessary for full virulence (Lee et al. 2005). Iron and chlorophyll content *in planta* was influenced by the presence of *Trichoderma asperellum* depending on the availability of iron in the media (de Santiago et al. 2009).

In the rhizosphere, iron competition is high, favouring those specialised microorganisms that have developed mechanisms to chelate and acquire iron by the production of high-affinity scavenging compounds such as siderophores (Jin et al. 2014). Siderophores are low molecular weight iron-chelating secondary metabolites, produced by many microorganisms and plants growing under limited iron conditions, that can remain intracellularly or be secreted into the surroundings (Ahmed and Holmström 2014). Siderophores synthesised by microbes have provided beneficial effects to

plants by direct competition with pathogenic microorganisms suppressing their growth, and through iron solubilisation (Leong 1986). Most fungi uptake iron by secreting siderophores into the soil to chelate or bind iron (Philpott 2006).The majority of microbial siderophores belong to the hydroxamate-, carboxylate- or catecholate-types (Saha et al. 2016). In general, fungi produce hydroxamate-type siderophores, in the genus *Trichoderma*, 18 different siderophores have been discovered in 10 different wild-type *Trichoderma* spp. (Lehner et al. 2013). The biocontrol *T. virens*, produce 13 siderophores, including dimerum acid, coprogren, fusigen, ferricrocin, fusarinine A, fusarinine B and des-diserylglycylferrirhodin (Lehner et al. 2013).

In *T. virens*, the non-ribosomal peptide synthase, TvTex10, is involved in intracellular siderophore(s) biosynthesis (ferricrocin). Interestingly, gene deletion of *TvTex10* was impaired in the activation of ISR and hyper-sensitivity to oxidative stress (Mukherjee et al. 2018). The siderophore harzianic acid (HA) produced by *T. harzianum* had a positive effect on seed germination, and shoot and root growth in tomato; in addition, iron content in these plants was increased when harzianic acid was supplemented under iron-deficient conditions (Vinale et al. 2013). Additionally, HA showed antifungal activity against three different plant pathogens (Vinale et al. 2009). Siderophores can act as elicitors to ISR in plants (Lemanceau et al. 2009). For example, the siderophore pseudobactin produced by the plant growth-promoting bacterium *Pseudomonas putida* elicits ISR in *Arabidopsis thaliana* (Meziane et al. 2005).

Iron directly or indirectly contributes to plant defence mechanisms depending on the modulation of iron supply during pathogen infection (Figure 4.1); for example, iron participates in the amplification of ROS production and can directly affect the metabolic activity of the plant (e.g. antimicrobial compounds) that require Fe-dependent enzymes for their synthesis (Aznar et al. 2015). In wheat, iron mediates the oxidative burst, the induction of PR proteins and the formation of localised cell wall appositions during the infection of *Blumeria graminis* f. sp. *tritici*, where PR genes were transcriptionally regulated under intracellular iron depletion (Liu et al. 2007). Iron redistribution and storage are defence mechanisms utilised by the host plant upon microbe colonisation; however, perturbation of plant iron homeostasis induced by pathogens is a common strategy to disturb host immunity (Verbon et al. 2017).

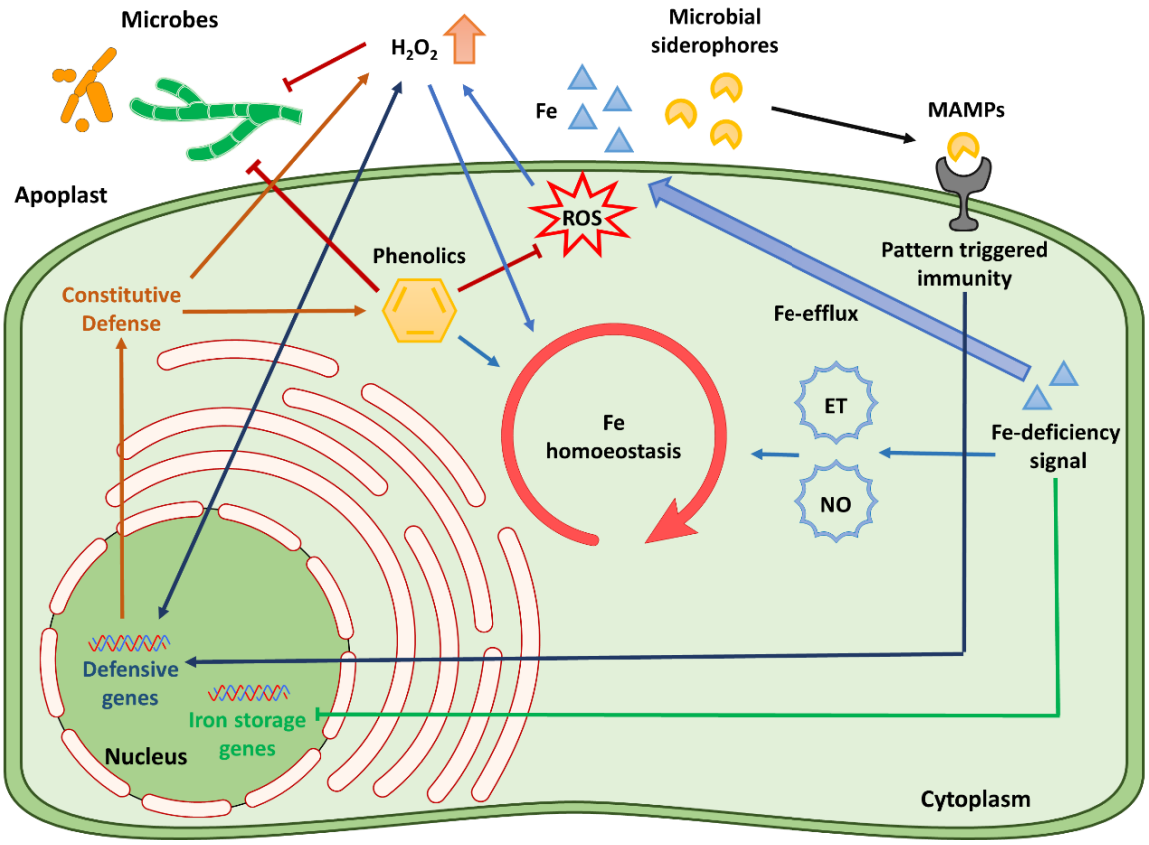

Figure 4.1 Iron homeostasis in plant-microbe interactions. Mobilisation and redistribution of iron in the plant cytoplasm and apoplast when encountering microbes. Secretion of microbial siderophores in the rhizosphere triggers an iron (Fe) deficiency signal and elicit pattern-triggered immunity via microbe-associated molecular patterns (MAMPs), which activate plant defence responses such as rective oxygen species (ROS) formation and accumulation of phenolic compounds. Iron efflux from the cytoplasm to the apoplast in colonised cells leads to an iron deficiency inside those cells, which triggers an oxidative burst in the apoplast caused by this accumulation of iron. In addition, phenolic compounds having antioxidant and antimicrobial properties contribute to the protection of the plant cell from ROS and pathogens. Ethylene (ET) and nitric oxide (NO) are involved in defence signalling that influences iron homoeostasis. Induction of defence-related genes and suppression of iron-storage-related genes are caused by extracellular hydrogen peroxide (H_2O_2) accumulation and iron deficiency. Figure modified from (Liu et al. 2007; Aznar et al. 2015).

The utilisation of iron for cellular processes involves fundamental redox reactions, where several 2-oxoglutarate/iron-dependent dioxygenases (2OG-Fe (II) dioxygenases) are active (Hausinger 2015; Islam et al. 2018). Different enzymes utilise Fe^{2+} as a cofactor to catalyse different reactions, including the 2OG-Fe (II) dioxygenases. The enzymatic activity of 2OG-Fe (II) dioxygenases (R + 2OG + O_2 → R-OH + succinate + CO_2) is regulated by the availability of O_2, energy metabolites (2-oxoglutarate/succinate) and Fe^{2+} (Salminen et al. 2015). The 2OG-Fe (II) dioxygenases have evolved and become specialised in several organisms and are adapted for synthesis and degradation of compounds present in specific niches (Hausinger 2015). Although the 2OG-Fe (II) dioxygenase superfamily has been characterised in animals, plants and bacteria, but their role in fungi is unexplored. The functional diversification of the 2OG-Fe (II) dioxygenase superfamily is vast. The

2OG-Fe (II) dioxygenases catalyse reactions on proteins involved in structural and oxygen sensing roles, and participate in different functional processes such as DNA repair and protein modifications, demethylation, lipid metabolism and in the synthesis of secondary metabolites such as flavonoids, gibberellin, alkaloids, phytosiderophores and antibiotics (Hausinger 2015). DMR6 from *A. thaliana* encodes a 2OG-Fe (II) dioxygenase (salicylic acid 5-hydroxylase) that is required for Arabidopsis susceptibility to *Hyaloperonospora parasitica* and negatively affects the expression of plant defence associated genes (van Damme et al. 2008). More recently, it has been suggested that salicylic acid 5-hydroxylase participates in the regulation of salicylic acid homoeostasis (Zhang et al. 2017).

The interaction between *Trichoderma* and its host plant during root colonisation is complex and involves the activation of several pathways. Using a transcriptome approach, the expression of numerous genes during the *T. virens*-maize relationship was studied by Lawry (2016). Genes including lytic enzymes, hydrophobins, putative-effector proteins and secondary metabolism-related were differentially expressed by *T. virens* during maize interaction. The protein ID 93146 from *T. virens* (https://genome.jgi.doe.gov/TriviGv29_8_2/), called here TVOX1 (from ***T**richoderma **v**irens* 2OG-Fe (II) di**ox**ygenase-**1**) belongs to the 2OG-Fe (II) dioxygenase family and has been shown that its encoding gene *tvox1* was part of the most highly up-regulated genes during the *T. virens*-maize interaction (Lawry 2016). However, its role during the interaction is unknown but likely involved in the production of *T. virens* secondary metabolites and iron regulation. This chapter aims to elucidate the function of *tvox1* on *T. virens* biology and when is interacting with its host plant.

4.2 Materials and methods

4.2.1 Selection of the candidate gene

A dual selection of putative encoding gene up-regulated during the *T. virens*-maize interaction was performed for identifying the candidate gene to be analysed. The first one corresponded to the expression values obtained from the transcriptome analysis of *T. virens* interacting or not with maize roots (Lawry 2016). The second criterion was the potential role of the gene in the plant-microbe interaction, using gene ontology prediction software (Blast2GO).

4.2.2 Validation of gene expression using quantitative real time (RT)-qPCR of up-regulated genes during the *Trichoderma virens*-maize interaction

4.2.2.1 RNA extraction for RT-qPCR analysis

Maize seeds were surface sterilised and inoculated with *T. virens* as described in sections 2.2.1 and 2.2.3. The plants were incubated under a cycle of 16 h light and 8 h dark at 25°C for 3, 5 and 7 d.p.i. For sampling, roots were soaked and washed gently with 4°C sterile nanopure water to eliminate

medium solution, and then a 2 cm section nearest to the seed was cut from the primary root. The 2 cm root sections were placed in 1.5 mL microcentrifuge tubes and immediately snap frozen in liquid nitrogen. RNA from root samples was extracted using the RNeasy Plant Mini Kit (Qiagen, Netherlands). RNA integrity was verified on denaturing 1% agarose gel prepared with 3-(morpholino) propane sulfonic acid (MOPS) buffer. For controls, *T. virens* samples were grown in Hoagland's agar medium cover with sterile cellophane to facilitate mycelium recovery; plates were incubated under the same grown conditions as the treatment. The experiment was performed using three biological replicates per treatment, each replicate consisted of three independent root samples.

4.2.2.2 Quantitative RT-qPCR of up-regulated genes

To validate the expression levels of the candidate gene (*tvox1*) previously reported by Lawry (2016), a RT-qPCR technique was used. During this analysis, a set of six additional *T. virens* genes that were up-regulated during its interaction with maize roots were used (Table 4.1). To quantify the relative expression of selected *T. virens* genes, SYBRGreen based RT-qPCR was done in a StepOne PlusTM (Applied Biosystems, USA). One microgram of total RNA isolated from roots inoculated or not with *T. virens* after different time points (3, 5 and 7 d.p.i) was reverse transcribed using a Blueprint cDNA kit (ClonTech, TakaRa, Japan). For each qRT-PCR reaction, 2 µL cDNA (10 ng of total RNA) was used as a template. Reactions were carried out following the master mix reported by Holyoake et al. (2008). This consist of a 16 µL solution containing: 0.44 µL PCR forward primer (200 nM), 0.44 µL PCR reverse primer (200 nM), 1.44 µL $MgSO_4$ (50 mM), 2.64 µL of 5X GC Rich buffer Fast Star, 1.28 µL dNTPs (2.5 mM each), 0.3 µL FastStart Taq DNA Polymerase (3U/mL) (Roche, Switzerland), 0.32 µL of 50X carboxy-X-rhodamine (ROX), 0.23 µL of 10X SYBRGreen (Invitrogen, USA), 1.6 µL of 10X PCR reaction buffer without $MgCl_2$ (from the Fast Star Kit, Roche, Switzerland) and 5.31 µL nanopure water. All qRT-PCR reactions were performed in triplicate (technical replicate).

The cycling conditions were 95°C for 5 min; followed by 40 cycles of 95°C for 15 s, 60°C for 1 min with data capture during the extension phase of each cycle. Specific primers for detection of up-regulated gene transcripts were designed using Primer3Plus software (https://primer3plus.com/) (Supplementary Table 6). The actin gene from *T. virens* was used as a reference gene, as previously reported by Djonović et al. (2007). To compare the relative abundance of gene expression, the transcripts levels were normalised against the expression levels of the actin gene. Then they were normalised against expression levels in axenic culture (PDA) versus root interaction conditions. Transcript levels were determined using the 2 ΔΔCT method described by Livak and Schmittgen (2001).

Table 4.1 List of up-regulated genes of *T. virens* during interaction with maize

Gene Id[1]	UniProt Id[2]	Hypothetical function
TV_51095	G9MX23_HYPVG	Endopolygalacturonase
TV_64881	G9NBW0_HYPVG	Aggrecan core protein
TV_66233	G9N8I2_HYPVG	MFS sugar transporter-like protein
TV_68245	G9N067_HYPVG	Hydrophobin
Tv_79197	G9MKB1_HYPVG	Small secreted cysteine-rich protein
Tv_93159	G9MW94_HYPVG	Small secreted cysteine-rich protein
Tv_93146	G9MW41_HYPVG	2OG-Fe (II) dioxygenase

1 Gene ID according to the *T. virens* JGI genome bank https://genome.jgi.doe.gov/TriviGv29_8_2/

2 Protein ID according to UniProt proteome bank https://www.uniprot.org/

4.2.3 Bioinformatic analysis of *Trichoderma virens tvox1* gene

Bioinformatic analysis of the selected gene was performed using different available software programs to analyse gene and protein sequences. DNA and protein sequences were obtained using the published genome of *T. virens* (http://genome.jgi.doe.gov/TriviGv29_8_2.html). Predictions of functional domains and motifs were achieved using the National Center for Biotechnology Information (NCBI) (http://www.ncbi.nlm.nih.gov/), UniProt database (https://www.uniprot.org) and The Eukaryotic Linear Motif resource (http://elm.eu.org/index.html). Protein features such as localisation and the presence of a signal peptide for secretion and transmembrane domains were predicted using WoLF PSORT (localisation) (https://www.genscript.com/wolf-psort.html), SignalP 4.1 server (signal peptide) (http://www.cbs.dtu.dk/services/SignalP/), and TMHMM Server v.2.0 (transmembrane domains) (http://www.cbs.dtu.dk/services/TMHMM/). Prediction of functional protein association networks were analysed using STRING v.10.5 (https://version-10-5.string-db.org/). Sequence alignment and phylogenetic trees were constructed with MEGA6: Molecular Evolutionary Genetics Analysis Version 6.0 (Tamura et al. 2013), and prediction of three-dimensional protein structure was conducted using Phyre2 software (http://www.sbg.bio.ic.ac.uk/~phyre2/).

4.2.4 Transformation of *Trichoderma virens*

4.2.4.1 Antibiotic sensitivity analysis

Antibiotic sensitivity of *T. virens* wild-type (WT) to hygromycin B and geneticin G418 was tested before used as positive selection markers for the screening of deletion (Δ*tvox*1) and complementing (C*tvox*1) mutants, respectively. Hygromycin resistance was tested on PDA plates amended with 0, 10, 20, 50, 75 and 100 µg/mL hygromycin B (AG Scientific, USA). Geneticin resistance was tested on Vogel's medium, complete media (CM) (mentioned in Appendix) and PDA plates containing 0, 50, 100, 250, 350, 500, 600 and 700 µg/mL geneticin G418 (Invitrogen, USA). The plates were inoculated centrally with 5 µL of conidia suspension containing $1x10^6$ conidia and

incubated at 25°C for 7 d under a light/dark cycle. The samples were observed using a stereo microscope (SZX12 Olympus, Japan) to confirm growth and germination inhibition. For each analysis, three replicates were used with the different antibiotic concentrations.

4.2.4.2 Design and construction of knockout (KO) construct

To delete *tvox1* in the *T. virens* genome, a *tvox1* KO-construct was created as follows: using the published genome of *T. virens* (http://genome.jgi.doe.gov/TriviGv29_8_2.html), primers were designed to amplify 1.2 kb of DNA up- and down-stream from the *tvox1* gene region to be deleted using gDNA from *T. virens* as a template, with the addition (on primers) of a *Sfi*I restriction site located on the 5'end of the left flank (LF) and 3'end of the right flank (RF). Flanking regions were ligated to the hygromycin B phosphotransferase gene (*hph*) from *E. coli* (conferring hygromycin B resistance, and called HygR) under control of the tryptophan gene promoter (*pTrpC*), for use as a selection marker in the following order: LF-HygR-RF (Figure 4.2).

To amplify *tvox*1 LF and RF the following PCR reaction and conditions were used. Each PCR reaction contained a total volume of 50 µL including: 1.25 U PrimeSTAR high fidelity polymerase (PrimeStar HS Premix, Takara, Japan), 2 X dNTP mixture (0.4 mM each nucleotide, 2 X PrimeStarBuffer (2 mM Mg^{2+}), 0.2 µM of each primer (Lf *tvox1*-F and Lf *tvox1 Sfi*I-R; Rf *tvox1*-R and Rf *tvox1 Sfi*I-F) and 3% dimethylsulfoxide (DMSO) and 200 ng gDNA (Supplementary Table 6). PCR reactions were carried out in an iCycler PCR machine (Biorad, USA) using the following parameters: 1 cycle of 1 min at 98°C; 35 cycles of 15 s at 98°C, 15 s at 62°C and 2 min at 72°C, followed by a final extension of 10 min at 72°C. Amplification of the *pTrpC*/*hph* fragment (1.4 kb) was carried out using a pair of primers (HygR *Sfi*I-F and HygR *Sfi*I-R) containing a *Sfi*I restriction site in the 5' and 3' regions, respectively (Supplementary Table 6). The vector pCR 2.1 TOPO containing a hygromycin B resistance marker was used as the template DNA (tDNA). tDNA was kindly provided by Dr Artemio Mendoza. Visualisation of PCR products was conducted by using 0.8% agarose TAE gel-electrophoresis. Expected PCR size fragments were purified using the Wizard SV Gel and PCR Clean-Up System (Promega, USA) using manufacturer's instructions. LF and RF PCR were digested with 10 U *Sfi*I (New England Biolabs, USA), at 50°C for 1.5 h. After digestion, the reactions were purified using the PCR Clean-UP System and quantified using a NanoDrop (NanoDrop Technologies Inc, USA). The digested and cleaned PCR products (LF and RF) were ligated with the *PtrpC*/*hph* fragment to create the *tvox1* KO-construct. The ligation reaction contained a total volume of 20 µL including 40 ng of each digested PCR product, 1 U T4 DNA ligase (Thermo Fisher Scientific, USA) and 10X T4 DNA ligase buffer (Thermo Fisher Scientific, USA). The ligation reaction was incubated at 4°C overnight.

The ligation product was used as tDNA to amplify the whole construct using nested primers (Lf nested *Hind*III-F and Rf nested *BamH*I-R), with the addition of a *BamH*I restriction site located on the 5'end of LF and *Hind*III on the 3'end of RF (Supplementary Table 6). The PCR conditions were

used as described above, except that 2 µL of ligation product was used as tDNA instead of gDNA. The PCR product (*tvox1* KO-construct) (3.6 kb) was inserted into a binary vector (pYT6) containing the left and right flanks required for *Agrobacterium*-mediated transformation (Figure 4.2). The pYT6 vector was kindly provided by Dr Johanna Steyaert. Amplification of the pYT6 backbone (Bb) (6.4 kb) was carried out using primers (Lf vector *Hind*III-F and Rf vector *BamH*I-R) containing *Hind*III and *BamH*I restriction sites that were specific to the left and right flanks, respectively (Supplementary Table 6). PCR reaction conditions were set up as previously described, using 100 ng of pYT6 as tDNA. Both PCR products were size fractionated and cleaned. The nested PCR product and pYT6 Bb were digested in separate reactions with *BamH*I and *Hind*III restriction enzymes in the following reaction, containing a final volume of 40 µL: 28 µL purified PCR product, 10 U *Hind*III (New England Biolabs, USA), 10 U *BamH*I (New England Biolabs, USA) and 1 X NEB CutSmart Buffer. The restriction reactions were incubated for 1.5 h at 37°C. Digested PCR products were cleaned, and their DNA concentration was determined as described in 3.2.11.1.1. Additionally, the digested *tvox1* KO-construct and pYT6 Bb were ligated using an insert to vector ratio 1:1 in a final volume of 20 µL containing: 80 ng KO*tvox1* construct, 80 ng pYT6 Bb, 1X T4 DNA ligation buffer and 1 U T4 DNA ligase. The ligation reaction was incubated at 4°C overnight.

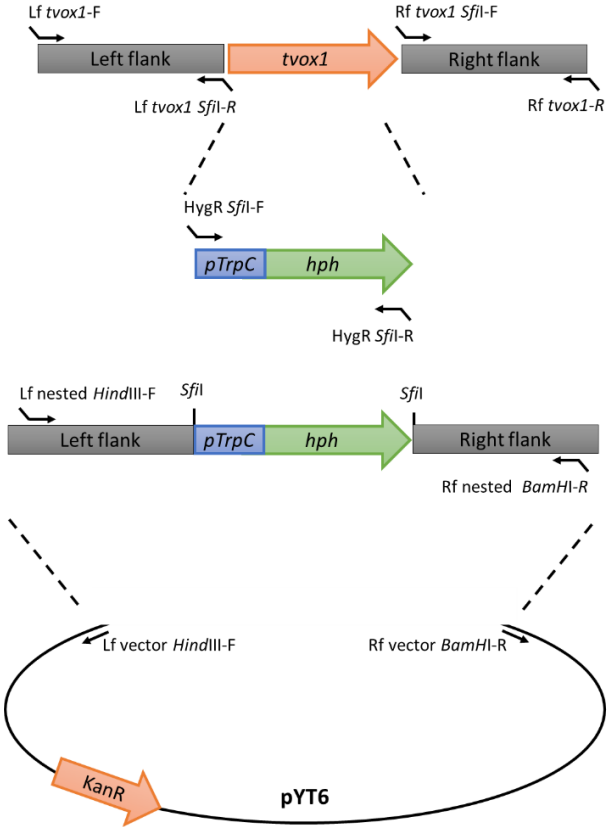

Figure 4.2 Overview of KO *tvox*1 construct design. Left and right flanks of *tvox1* were amplified and *Sfi*I restriction sites added to allow ligation with complementary restriction sites (*Sfi*I) contained in the *pTrpC/hph* fragment. Nested primers were used to amplify the whole KO *tvox1* construct with the addition of *Hind*III and *BamH*I into the left and right flanks, respectively. The Bb of the pYT6 vector was amplified with the addition of *Hind*III and *BamH*I restriction sites. Left and right flanks of the KO *tvox1* construct, and Bb of the pYT6 vector were digested using *Hind*III and *BamH*I to allow ligation between both fragments.

4.2.4.3 Subcloning of *tvox1* KO-vector (pΔ*tvox1*) in *Escherichia coli*

The resulting pΔ*tvox1* vector from the previous ligation was subcloned into *E. coli* TOPO F' chemically competent cells (Appendix). A total of 5 µL of pΔ*tvox1* was gently mixed with 40 µL of *E. coli* competent cells and subcloned as described in section 3.2.11.1.1. Plasmid DNA was isolated from the *E. coli* clones using the NucleoSpin Plasmid system (Macherey-Nagel, Germany) following the manufacturer's instructions. Plasmid concentration was determined on a NanoDrop machine. To verify the insertion of *tvox1* KO-construct into pYT6 Bb, the insert was digested using BamHI and *Hind*III restrictions enzymes. Six hundred nanograms of plasmid was digested as described in 3.2.11.1.1. Expected fragment sizes were (3.6 kb) for *tvox1* KO-construct and (6.4 kb) for pYT6 Bb. After validating fragment sizes, the plasmid was sequenced using the checkA and checkB primers (kindly provided by Dr. Johanna Steyaert) (Supplementary Table 6) to confirm the nature of the construct at the Bio-Protection Sequencing Facility, Lincoln University. The sequence integrity was analysed using Clone Manager Professional v. 8 (Sci-Ed Software, USA).

4.2.4.4 Subcloning of the *tvox1* KO-vector (pΔ*tvox1*) into *Agrobacterium tumefaciens*

Confirmed pΔ*tvox1* was subcloned into *A. tumefaciens* EHA105 electrocompetent cells (Appendix). Competent cells were placed on ice, and 10 ng of pΔ*tvox1* (dissolved in nanopure water) were added and gently mixed. The mixture was transferred to a pre-cooled electroporation cuvette. Electroporation was carried out using the ''Agr'' setting (cuvette 0.1 mm, 2.2 kV and single pulse) as per the manufacturer's instructions on a MicroPulser Electroporator (Bio-Rad, USA). The cells were immediately transferred to a 1.7 mL centrifuge tube using 1 mL of yeast mannitol (YM) broth and incubated for 3 h at 30°C, shaking at 250 rpm (Appendix). One aliquot (50 µL) of electroporated cells was plated on YM agar (YMA) plates amended with 25 µg/mL kanamycin and 25 µg/mL rifampicin (Sigma-Aldrich, USA) and incubated for 48 h at 30°C. Single colonies were picked off the plate with sterile tips and incubated in 4 mL LB medium containing 25 µg/mL kanamycin and 25 µg/mL rifampicin for 24 h at 28°C with continuous shaking at 250 rpm (Appendix). One millilitre aliquot of transformed cells was taken for plasmid isolation using the NucleoSpin Plasmid-*A. tumefaciens* protocol (Macherey-Nagel, Germany). Plasmid concentration was determined on a NanoDrop machine. To verify the insertion of pΔ*tvox1* into *A. tumefaciens* cells, the plasmid was digested using *BamH*I and *Hind*III restriction enzymes following the methodology described in 3.2.11.1.1.

4.2.4.5 *Agrobacterium*-mediated transformation

Agrobacterium-mediated transformation with modifications was performed according to the method reported by de Groot et al. (1998), with improvements as described in Zeilinger (2004). After vector verification, 0.1 mL of pre-cultured *A. tumefaciens* cells containing pΔ*tvox1* were inoculated into the MM supplemented with 25 µg/mL kanamycin and 25 µg/mL rifampicin and

incubated overnight at 28°C with shaking at 250 rpm (Appendix). The culture was centrifuged at 3,000 x g for 10 min at RT. *A. tumefaciens* cells were re-suspended in 50 mL IMAS broth to an optical density of OD_{660} = 0.15, and the culture was incubated for up to 4 h at 28°C with shaking at 200 rpm until OD_{660} of 0.3 was reached (Appendix).

T. virens protoplasts were created according to the method reported by Baek and Kenerley (1998) and improved by Lawry (2016). *T. virens* conidia from 7 d old colonies were incubated on PDA at 25°C with a 12 h day/night cycle. After 5 d, conidia were harvested by adding 5 mL nanopure water to the PDA plates and releasing the conidia from the cultures into suspension using a triangular spreader. Conidia were harvested and filtered through two layers of Miracloth (Millipore, USA), the conidia suspension were counted on a haemocytometer, and the concentration adjusted to $1x10^8$ conidia/mL. One hundred microliters of conidial suspension was inoculated and spread onto a large (150 mm x 150 mm) PDA plate covered with sterile cellophane. Plates were incubated for 18 h at 25°C with a 12 h day/night cycle. The cellophane with germinated conidia was removed from the PDA plate and transferred into a new large sterile plate. Then fifteen millilitres of sterile digestion solution (0.1 g/mL Glucanex (Novozymes, Denmark) in 0.7 M mannitol osmoticum) was added onto the top of the cellophane and then incubated for 3 h at 25°C with continuous shaking at 150 rpm. Protoplast formation was observed using a bright-field microscope (Leica, Germany). Protoplasts were recovered by filtration through a Swinnex filter holder (Millipore, USA) using two layers of 40 µm nylon mesh. The protoplast suspension was centrifuged at 4,000 x g for 10 min. The protoplast pellet was washed with 20 mL of 0.7 M mannitol osmoticum solution and centrifuged at 7,000 x g for 7 min and the supernatant was removed by inversion. The protoplast pellet was carefully resuspended in 500 µL of 0.7M mannitol osmoticum. Protoplasts contained in the suspension were counted on a haemocytometer, and their yield was calculated. Protoplasts were then maintained on ice until they were used.

Equal volumes containing 100 µL of each *A. tumefaciens* culture and *T. virens* protoplast suspension ($1x10^6$ protoplasts) were plated onto sterile cellophane placed on IMAS agar and incubated at 23°C for 48 h in complete darkness. The circular cellophane was cut into eight triangular size pieces and transferred to PDA plates supplemented with 100 µg/mL hygromycin B and 300 µg/mL timentin (GlaxoSmithKline, UK). Only one triangular piece was transferred to each PDA plate and was incubated at 25°C for 2 d in complete darkness.

4.2.4.6 Single colony purification

Conidia from *T. virens* Δ*tvox1* positive mutants were grown on PDA supplemented with 100 µg/mL hygromycin B and 300 µg/mL timentin for 5 d at 25°C under a 12 h day/night cycle to induce conidiation. To obtain monokaryotic transformants, aliquots of conidial suspensions ($1x10^3$ cells, 100 µL) were plated on PDA medium amended with 100 µg/mL hygromycin B and 300 µg/mL timentin and plates were incubated in darkness. After 18 h, colonies were observed using a stereo

microscope. A single colony was selected and inoculated to a new PDA with 100 µg/mL hygromycin B and 300 µg/mL timentin. Single spore purification was repeated ten times to ensure the isolation of monokaryotic strain. Positive *T. virens* deletion transformants derived from single spores purification were re-suspended in 25% glycerol and stored at -80°C before testing their stability.

4.2.4.7 Stability testing of deletion mutants

To confirm the stability of the mutation on *T. virens* transformants, all confirmed Δ*tvox1* mutants were sub-cultured (10 times) on PDA media without antibiotics and then transferred to PDA with 100 µg/mL hygromycin B and 300 µg/mL timentin, and growth compared. Stable mutants were selected for their confirmation by PCR and Southern blot.

4.2.5 Confirmation of homologous recombination of deletion transformants

4.2.5.1 DNA isolation from mycelia for PCR

Genomic DNA from *Trichoderma* conidia was isolated using the following protocol: *T. virens* conidia (concentration $1x10^5$) were grown in 3 mL of sterile PDB media for 24 h at 25°C with continuous shaking at 150 rpm. Mycelia were collected from the culture and transferred into 1.7 mL screw cap microcentrifuge tubes containing 0.25 mg of glass beads (BioSpec Products, USA), and then the samples were centrifuged for 1 min at 16,800 x g. To extract DNA, 400 µL of gDNA extraction buffer (50mM Tris, 50mM EDTA, 2% SDS, pH 8) and 400 µL of phenol:chloroform:isoamyl alcohol (25:24:1) were added and immediately snap frozen in liquid nitrogen. The samples were placed in the Fastprep24 (MP Biomedicals, USA) and agitated at 5.5 cycles for 30 s. After homogenisation, samples were placed on ice for 2 min and agitated again in the Fastprep using the same conditions. The lysate was centrifuged for 10 min at 16,800 x g at 4°C. The supernatant was recovered, and 1 mL of absolute ethanol (Lab Supply, New Zealand) was added, and then mixed by inversion. The samples were centrifuged for 10 min at 16,800 x g at 4°C. The DNA pellet was washed with 70% ethanol and centrifuged at RT for 5 min at 16,800 x g. Remaining ethanol was removed and air dried. The pellet was re-suspended in 50 µL ultrapure DNase/RNase distilled water (Invitrogen, USA) and incubated for 10 min at 37°C to allow resuspension.

4.2.5.2 Confirmation by PCR

Validation of the correct insertion of the *tvox1* KO-construct into the genome of Δ*tvox*1 mutants was performed by PCR amplification as follows: a) a fragment of *hph* ORF (0.4 kb) was amplified to confirm its insertion into the *T. virens* genome, b) a flanking region from outside of the deletion construct to the HygR cassette was amplified (1.4 kb) to confirm homologous recombination, and c) a fragment of *tvox*1 ORF (0.6 kb) was amplified to confirm its deletion from the *T. virens* genome (Figure 4.3).

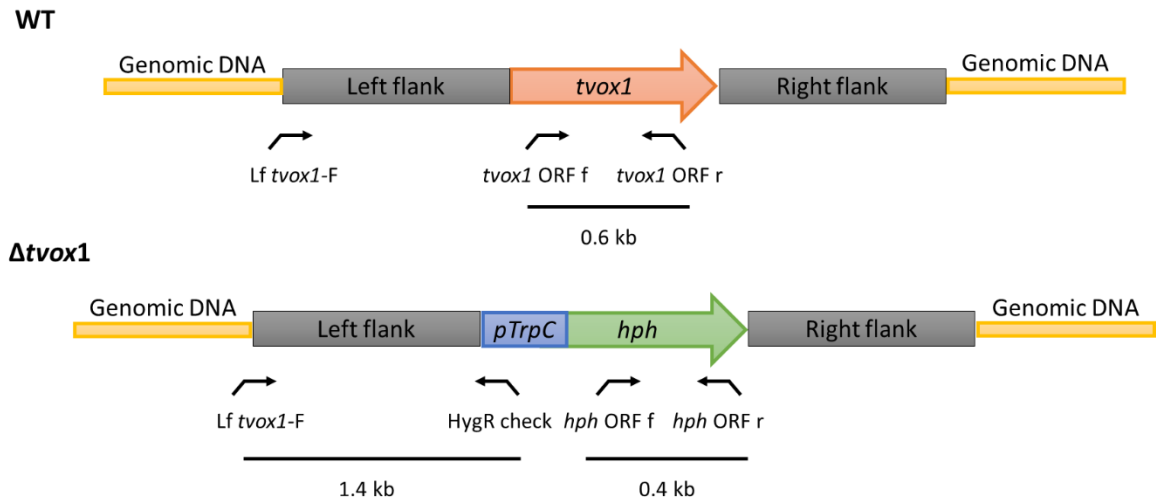

Figure 4.3 Localisation of primers for confirmation of homologous recombination by PCR. Set of primers used to corroborate deletion of the *tvox1* gene (*tvox1* ORF f and r), insertion of the HygR cassette (*hph* ORF f and r) and homologous recombination (Lf *tvox1*-F and HygR check).

The gDNA of selected transformants and WT (control) was extracted using standard phenol: chloroform methodology described in section 4.2.5.1. The isolated DNA was quantified using NanoDrop, and its quality was observed by 0.8% agarose TAE gel-electrophoresis. PCR products were amplified using the following cycling conditions in an iCycler PCR machine (Biorad, USA): 95°C for 5 min: followed by 35 cycles of 95°C for 30 s; 60°C for 30 s; 72°C for 45 s, and a final extension at 72°C for 10 min. For each PCR reaction, 1 µL gDNA (100 ng of total DNA) was used as the template. Reactions were carried out in a total volume of 25 µL containing: 0.5 µL (2.5 U) FastStart Taq DNA Polymerase (Roche, Switzerland), 2.5 µL Buffer with 20 mM $MgCl_2$, 1 µL dNTPs (2.5 mM each), 1 µL (0.2 µM) of each primer. The PCR products were size fractionated and visualised as previously described.

4.2.5.3 DNA isolation from mycelia for Southern blot

Isolation of *T. virens* DNA from mycelia was performed using the following methodology: in 100 mL sterile flasks, *T. virens* conidia ($1x10^6$) were grown in 30 mL of sterile PDB media for 36 h at 25°C with continuous shaking at 150 rpm. Mycelia were harvested on two layers of Miracloth and rinsed with sterile nanopure water. Collected mycelia were ground into a fine powder in liquid nitrogen to disrupt the cells. Mycelia powder (100 mg) was poured into a 2 mL screw-capped microcentrifuge tube and homogenised in 0.5 mL of lysis buffer (2% Triton X; 1% SDS; 100 mM NaCl; 10 mM Tris-HCl pH 8; 1 mM EDTA) and 0.5 mL phenol:chloroform:isoamyl alcohol (25:24:1). Samples were vortexed for 10 s and centrifuged at 14,500 x g for 10 min at 4°C. The supernatant was collected and transferred into a new 2 mL centrifuge tube, and then 2.5 volumes of absolute cold ethanol were added. The samples were mixed carefully to avoid damaging DNA and centrifuged at 14,500 x g for 5 min at 4°C. The supernatant was removed carefully without disturbing the DNA pellet and then centrifuged for 2 min. The remaining ethanol was removed with

a pipette, and the pellet was re-suspended in 30 µL ultrapure DNase/RNase distilled water and incubated for 24 h at 4°C. The DNA from the samples was quantified using a Qubit dsDNA HS assay kit (Thermo Fisher Scientific, USA).

4.2.5.4 Confirmation by Southern blot

A Southern blot strategy was designed to corroborate the *tvox1* ORF deletion and homologous insertion of one copy of the HygR cassette into the *T. virens* Δ*tvox1* genome. To confirm deletion of the *tvox1* gene the restriction map of DNA sequences (WT and Δ*tvox1*) was analysed for selection of one restriction enzyme (*Xba*I) that was present outside of the right flank and once in the *tvox1* ORF (Figure 4.4). To confirm homologous recombination, one restriction endonuclease (*Xba*I) was chosen which was located outside of both left and right flanks of *tvox1* and absent in the *pTrpC*/*hph* fragment (Figure 4.4).

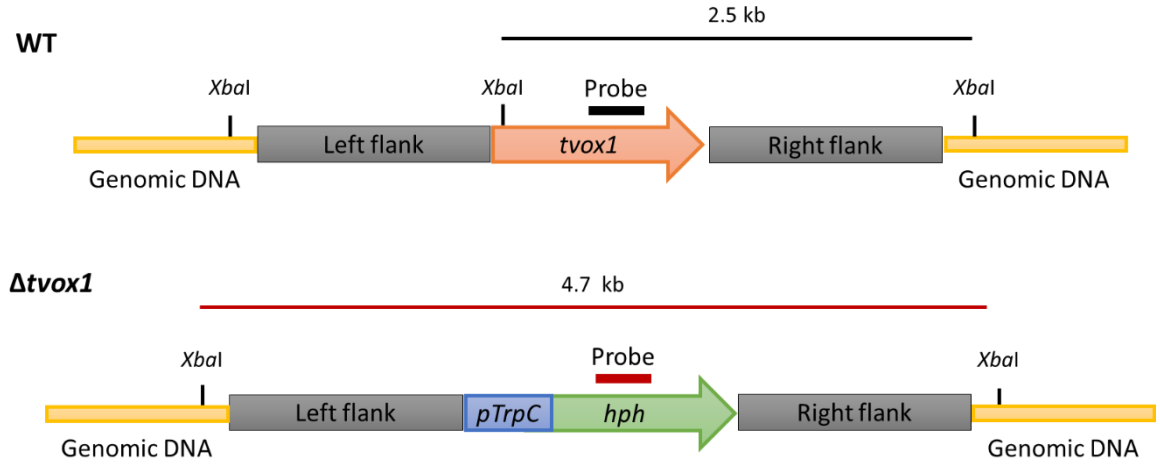

Figure 4.4 Restriction map of the Southern blot strategy used to verify deletion of the *tvox1* gene and homologous recombination of the HygR cassette in the *T. virens* genome. Scheme of Southern blot strategy to verify Δ*tvox1* construct homologous integration. For deletion confirmation, a fragment of *tvox1* ORF was used as a probe (black-thick line); a 2.5 kb fragment size was expected in the *T. virens* WT strain but not present in Δ*tvox1* mutants when DNA was digested with the *Xba*I restriction enzyme. For homologous integration of the HygR cassette, a fragment of *hph* ORF was used as a probe (red-thick line); a 4.7 kb fragment size was expected in Δ*tvox1* mutants but not present in the WT for homologous recombination when DNA was digested with *Xba*I.

Genomic DNA of WT and Δ*tvox1* mutants was isolated as described in section 4.2.8. To generate the probes to detect the *tvox1* gene and HygR cassette in Δ*tvox1* mutants, DNA of WT or vector pCR 2.1 TOPO containing the hygromycin B resistance marker were used, respectively. In the case of *tvox1* gene detection, a 638 bp region of the *tvox1* ORF using *tvox1* ORF-f and *tvox1* ORF-r was labelled utilising the DIG PCR Probe Synthesis Kit (Roche, Switzerland) according to the manufacturer's instructions. For the HygR cassette detection, a 466 bp region of the *hph* gene using *hph* ORF-f and *hph* ORF-r was labelled as described above (Supplementary Table 6). Probes were amplified using the following cycling conditions in an iCycler PCR machine (Biorad, USA): 95°C for 2

min: followed by 35 cycles of 95°C for 15 s; 60°C for 15 s; 72°C for 30 s, and a final extension at 72°C for 10 min. For each PCR reaction, 0.5 µL DNA (100 ng DNA of WT or vector pCR 2.1 TOPO containing the hygromycin B resistance marker) was used as the template. Reactions were carried out in a total volume of 25 µL containing: 1 µL (5 U) Mango Taq DNA Polymerase (Bioline, UK), 10 µL 5X Mango Taq Reaction Buffer, 3 µL 1X DIG mix (Roche, Switzerland) or 1 µL unlabelled dNTPs (2.5 mM each) for amplification of positive controls, 1 µL (0.2 µM) of each primer. The PCR products were size fractionated and visualised as previously described. Both DIG-labelled probes were cleaned using the Wizard SV Gel and PCR Clean-Up System (Promega, USA), and their concentration was calculated using the NanoDrop.

For digestion of gDNA from WT and deletion mutants, the following reactions were used: 10 µg of gDNA were digested with 30 U *Xba*I restriction enzyme, containing a final volume of 30 µL: 10 µg gDNA, 1.5 µL *Xba*I (30 U) (New England Biolabs, USA) and 3 µL of 1X NEW CutSmart Buffer (New England Biolabs, USA). The restriction reactions were incubated for 3 h at 37°C. Digested gDNA, was separated for 2:30 h at 80 V in 0.8 % agarose TAE gel-electrophoresis. Separated DNA was transferred to an Amersham Hybond-N^+ membrane (GE Healthcare, UK) overnight after denaturation by treatment for 30 min in a 0.5 M NaOH:1.5 M NaCl solution and neutralised with 0.5 M Tris-HCl pH 7.5: 1.5 M NaCl solution as described by Sambrook et al. (1989). After transfer, DNA was fixed by baking the membrane at 80°C for 2 h. Prehybridisation (30 min at 65°C) and hybridisation (overnight at 62°C) with DIG-labelled probes were performed by following DIG Luminescent Detection Kit instructions (Roche, Switzerland). The membrane placed between transparent plastic sheets for imaging the chemiluminescent substrate signal. The membrane in plastic sheets was placed in an X-ray film cassette and a sheet of CL-XPosure Film (Thermo Fisher Scientific, USA) placed on top. The cassette was closed, and the film exposed for 5 min. The film was developed manually using the Kodak GBX system (Kodak, USA).

4.2.6 Phenotypic characterisation of *Trichoderma virens* Δ*tvox1* transformants

Phenotypic characterisation was performed on three independent positive mutants. Five different criteria were used to evaluate phenotypical changes caused by the deletion of *tvox1* in *T. virens* genome: growth rate, conidiation, germination, endophytism and siderophore production.

4.2.6.1 Growth rate

The radial mycelial growth rates of *T. virens* WT and Δ*tvox1* strains were determined on PDA plates. *T. virens* conidia were incubated on PDA for 7 d at 25°C with a 12h day/night cycle, and conidia were harvested as described in section 3.2.3. The plates were inoculated centrally with a 5 µL conidia suspension containing $1x10^6$ conidia and were incubated in darkness at 25°C for 4 d. Radial growth was measured every 24 h in a dark room, the positions of the colony edges were recorded on the reverse of the plates. After data were collected, the margins for every day were measured,

and the radial growth rate (mm/d) was calculated using the following formula: [D3 growth – D2 growth = Linear growth per day]. The linear growth rate from the second day to the third day was used for this analysis since during that period; fungal growth was not limited by germination time (day one) or space (day four) when different strains were compared. The experiment was performed using ten replicates for each treatment and was repeated twice.

4.2.6.2 Conidial yield

The conidial yield of the *T. virens* WT and Δ*tvox*1 strains was determined on PDA plates. PDA plates were inoculated with a 100 µL conidial suspension containing $1x10^6$ conidia, which were spread across the surface of the plate. Plates were incubated at 25°C for 7 d with a 12h light/dark cycle. After 7 d, *T. virens* conidia were harvested adding 5 mL of sterile nanopure water and released from the culture into suspension using a triangular spreader. The conidial suspension was filtered through a double layer of sterile Miracloth to remove mycelial fragments, and the yield was determined using a haemocytometer. The results were expressed as conidia/plate. The experiment was done using the same number of replicates and repeats as in the growth rate experiment.

4.2.6.3 Germination

The germination of condia of *T. virens* WT and Δ*tvox1* strains was determined as follows. Conidia from *T. virens* were collected as previously described. The germination percentage was determined using a $5x10^5$ conidia suspension contained in 0.5 mL of sterile nanopure water. The conidia suspension was transferred into a 1.7 mL centrifuge tube with 0.5 mL of PDB. Samples were attached to the rotating wheel and incubated in a Stuart Hybridisation Oven S130H (Stuart, UK) for up to 18 h at 25°C with rotation at 7 rpm. After 18 h, samples were placed on ice and observed under the microscope. The conidia were assessed as germinated when the germ tube lengths exceeded the conidium diameter. Germination was recorded by randomly counting 100 conidia per sample. The results were expressed as a percentage. The experiment was done using the same number of replicates and repeats as in the growth rate and conidial yield experiments.

4.2.6.4 Endophytism

The endophytic association of *T. virens* WT and Δ*tvox*1 mutants with maize plants was assessed using the methodology described by Cripps-Guazzone et al. (2016); Mendoza-Mendoza et al. (2016). *T. virens* strains (WT and Δ*tvox1*) were propagated on PDA plates and incubated at 25°C for 7 d under a cycle of 12 h light/dark cycle to induce conidiation. Surface sterilised maize seeds were inoculated with *T. virens* conidial suspension ($1x10^6$) (see section 2.2.3). A maize seed was sown into a 50 mL falcon tube pre-filled with 45 mL of hydrated and sterile (gamma-radiated) 'John Innes' soil mix ('John Innes' composition: sieved and homogenised fresh soil mixed with Kiwi Peat and pumice at a ratio of 7:3:2- v/v/v, amended with 0.2 g L^{-1} blood and bone, 1.2 g L^{-1} superphosphate, 0.3 g L^{-1} potassium sulphate, 2 g L^{-1} Ag lime (calcium carbonate), 3.5 g L^{-1} dolomite lime (calcium

carbonate) at 2 cm depth using sterile tweezers. After planting the inoculated seeds with *T. virens* conidia, the tubes were moistened with 6 mL of sterile nanopure water. Plants were incubated in sterile cereal boxes for 7 d in a humidity controlled incubator at 25°C with 16 h light and 8 h dark cycle.

For endophytic determination, plant roots were excised and gently washed using sterile nanopure water to eliminate soil residues and dried briefly on sterile paper towels. Then, roots were soaked in a 5% NaOCl solution (active ingredient) for 5 min, and rinsed three times in sterile nanopure water for 2 min and subsequently dried using sterile paper towels. The plant primary root was cut into five equal pieces and placed on the surface of petri plates containing *Trichoderma* selective medium (TSM) (Appendix) (McLean et al. 2005). Plates were incubated at 20°C in the dark for 7 d, and the presence of *Trichoderma* mycelium growing on the plates was recorded. Colonisation percentage of endophytic *T. virens* was based on the number of colonised root pieces where one piece represents 20% of colonisation. Thus five pieces were equal to 100%. To verify the quality of the surface sterilisation procedure, the nanopure water used in the final rinse was plated from each treatment. Un-inoculated maize seedling samples were used as a control. A total of nine biological replicates per treatment were used for this experiment and it was reapeted twice.

4.2.6.5 Siderophore detection (semiquantitative)

To evaluate the presence and production of siderophores by *T. virens* strains, the chrome azurol S (CAS) assay was implemented (Schwyn and Neilands 1987) with modifications. This semiquantitative method is based on a change in colour of the dye from blue to orange or yellow in the presence of siderophores. The medium was prepared with 0.2 g yeast extract, 1.6 mM $MgSO_4.H_2O$, 2.28 mM K_2HPO_4 and 5.36 mM KCl. The pH of the media was adjusted to 5.5, and then 15 g L^{-1} of bacteriological agar was added. The medium was sterilised and cooled down to 50°C, then supplemented with sterile 20% glucose and one of two different nitrogen solutions (1 mM NH_4Cl or 1 mM KNO_3). The CAS solution was prepared by dissolving 60 mg of CAS (Fluka Chemicals, USA) in 50 mL of nanopure water, mixed with 2.7 mg of $FeCl_3$ dissolved in 9 mL of 10 mM HCl solution, then 73 mg of hexadecyltrimethylammonium (HDTMA) was dissolved in 40 mL and added. Both medium and CAS solution were mixed thoroughly, and poured into a petri dish. The CAS media was inoculated centrally with conidial suspension ($1x10^6$) and incubated for 72 h at 25°C in darkness. Diffusible secreted siderophores in the media were measured based on the formation of the halo (diameter) in respect to mycelial growth. The following responses were analysed: CAS reaction colour and halo formation as [(halo diameter-colony diameter) after 3 d.p.i. Ten biological replicates were used per treatment and the experiment was repeated twice.

4.2.7 Design and construction of complementation construct

To complement the *tvox1* in the *T. virens* deletion mutant genome, a *tvox1* complement (Comp) construct was created using Golden Gate methodology described in 3.2.11.1. Primers were designed using the published *T. virens* genome database to amplify approximately 1.5 kb native promoter and 0.5 kb terminator sequences from the *tvox1* gene region, using gDNA from *T. virens* as the template, with the addition of a *Bsa*I restriction site located on the 5' (LF) and 3' (RF) end flanks (Supplementary Table 6). The complementing region was fused to the neomycin phosphotransferase encoding gene (*nptII*) (conferring geneticin G418 resistance and termed GtR) under control of the tryptophan gene promoter (*pTrpC*) and tryptophan gene terminator (*tTrpC*), for use as a selection marker in the following order: Comp-GtR (Figure 4.5). To amplify the *tvox1* complementing region the PCR reaction conditions described in section 4.2.5.2 were used. Amplification of the *tvox1* complementing region and *pTrpC*/*nptII*/*tTrpC* fragment (1.8 kb) were carried out using a pair of primers (Lf Comp *Bsa*I-F and Rf Comp *Bsa*I-R; Lf nptII *Bsa*I-F and Rf *nptII* *Bsa*I-R) containing *BsaI* restriction sites in 5' and 3' regions, respectively (Supplementary Table 6). The pII99 (kindly provided by Dr B. Scott, Massey University) containing the geneticin resistance marker was used as tDNA. Visualisation of PCR products was conducted by using 0.8% agarose TAE gel-electrophoresis. Expected PCR size fragments were purified using the Wizard SV Gel and PCR Clean-Up System (Promega, USA). Restriction-ligation reaction and subcloning into *E. coli* competent cells were performed as mentioned in section 3.2.11.1.1. Positive colonies were analysed, and their plasmids were validated by restriction digestion and confirmed by sequencing.

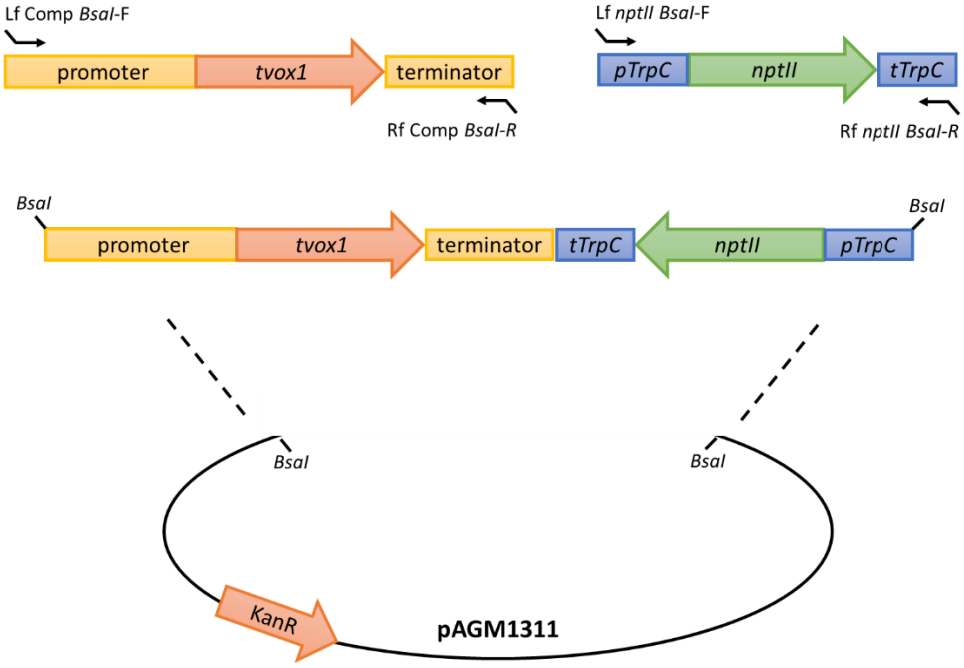

Figure 4.5 Overview of subcloning the complementation *tvox1* construct into the pAGM1311 vector. Amplification of the complementation fragment and GtR cassette with the addition of *Bsa*I into the left and right regions. Restriction and ligation reactions applying Golden Gate strategy to subclone C*tvox1* construct into a pAGM1311 vector.

4.2.8 Protoplast transformation and confirmation of complementation mutants

The strategy used for *T. virens* protoplast transformation is described in section 3.2.11.1.3. For transformation, ten micrograms of DNA containing the complement construct was linearised using *Xcm*I (New England Biolabs, USA) at 37°C for 2 h. The digested plasmid was purified and visualised as described in section 4.2.7 to verify its integrity. Positive transformants were recovered in Vogel´s medium containing 750 µg/mL geneticin G418 (Appendix).

Potential mutants grown on Vogel´s medium supplemented with 750 µg/mL geneticin G418 were recovered. Single colony mutants were firstly tested for their stability, then confirmed by PCR before being validated by Southern blot (see sections 4.2.5.2, 4.2.5.4 and 4.2.4.7). The DNA of selected mutants was isolated using standard methodologies explained in section 4.2.5.1 for PCR analysis and section 4.2.5.2 for Southern blot analysis. Validation of *tvox1* complementation and integration of GtR cassette were performed by PCR as follows: a) the GtR cassette was amplified to confirm its insertion into the *T. virens* Δ*tvox1* genome (Figure 4.6), and b) a fragment of *tvox1* ORF was amplified to confirm its complementation (Figure 4.6).

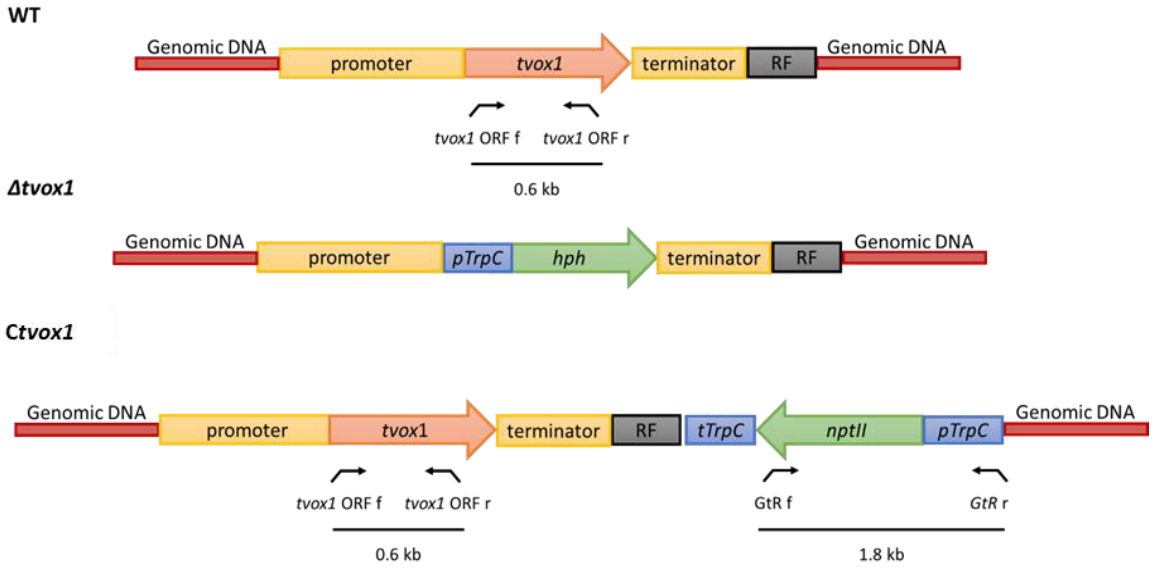

Figure 4.6 Localisation of primers for confirmation of insertion of the complementing construct by PCR. Sets of primers used to corroborate insertion of a *tvox1* gene (*tvox1* ORF f and r), and GtR cassette (GtR f and r).

Additionally, a Southern blot analysis was performed to corroborate the *tvox1* ORF complementation and insertion of the GtR cassette (Figure 4.7). DNA from WT and Δ*tvox1* strains was used as a positive and negative control, respectively. Ten micrograms of DNA were digested using a combination of two restriction enzymes (*Mlu*I and *Hind*III), and the *nptII* gene was used as a probe. The gDNA of the mutants and WT was digested, transferred and hybridised as mentioned in section 4.2.5.4. Once the integration of the resistant cassette and complementation of the gene was confirmed, conidia from positive complementing mutants were stored at -80°C.

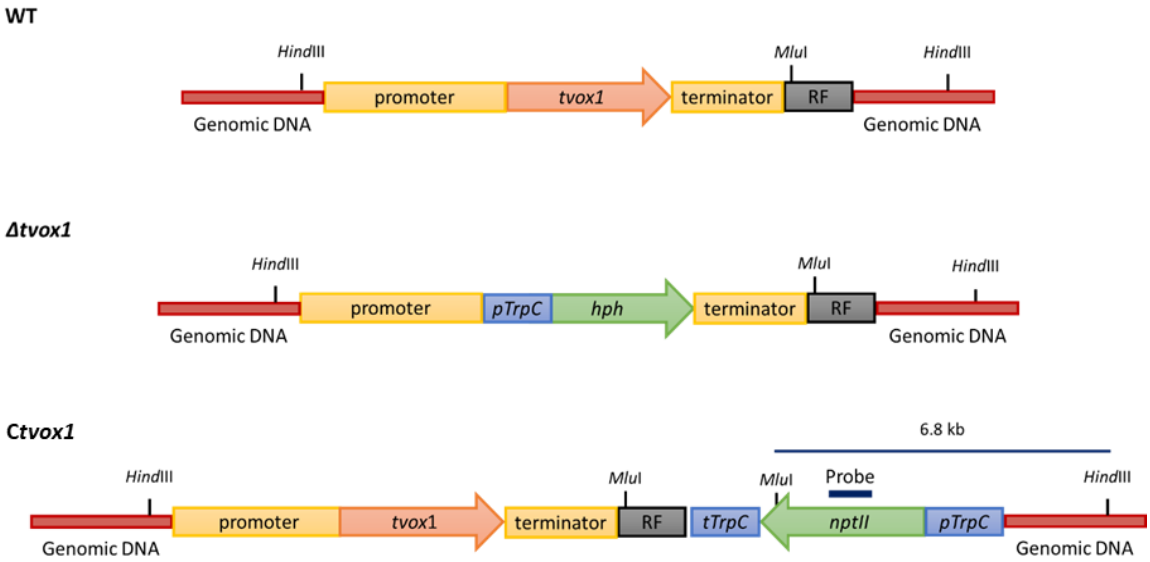

Figure 4.7 Restriction map of the Southern blot strategy used to verify complementation of the *tvox1* gene and integration of the GtR cassette in the *T. virens* genome. Southern blot strategy to verify C*tvox1* construct insertion. For complementation confirmation, a fragment of *nptII* ORF was used as a probe (blue thick line); a 6.8 kb fragment size was expected in *T. virens tvox1* complementation mutants for homologous integration but not present in WT or Δ*tvox1* strains when DNA was digested with a combination of restriction enzymes (*Mlu*I and *Hind*III).

4.2.9 Gene expression of *tvox1* in *Trichoderma virens* strains during their interaction with maize

To examine the expression levels of *tvox1* gene comparing WT to *tvox1* deletion (Δ*tvox1*) and complement (C*tvox1*) mutants, a RT-qPCR analysis was performed. For this experiment, *tvox1* was comparatively analysed in the in vivo *T. virens*-maize system under hydroponic and soil growth conditions. Maize seeds were inoculated and grown following the conditions described in section 2.2.3 for hydroponic and section 4.2.6.4 for soil growth conditions. Root samples were collected at 7 d.p.i. To quantify the relative expression of *tvox1* of *T. virens*, SYBRGreen based RT-qPCR was analysed in a StepOne PlusTM (Applied Biosystems, USA). One microgram of total RNA isolated from roots inoculated or not with *T. virens* and grown on axenic media (PDA) covered with sterile cellophane was reverse transcribed using iScript Reverse Transcription Supermix (Biorad, USA). Reverse transcription conditions were the following: priming at 25°C for 5 min, reverse transcription at 46°C for 20 min and inactivation at 95°C for 1 min. The real-time reactions were performed in a 10 µL reaction containing 2X SsoAdvanced universal SYBR Green Supermix (Biorad, USA) and 200 nM of each primer. Each reaction contained 50 ng of total RNA. Real-time qPCR cycling conditions, primer design and data analysis were performed as described in section 4.2.2.2. The transcripts leves were normalised against the expression of the reference gene. Then were normalised against expression levels in axenic conditions versus *T. virens*-root interaction conditions. Data were analysed using three biological replicates as described in section 4.2.2.2. The ß-tubulin gene from *T. virens* was used as an internal reference gene (Moran-Diez et al. 2009).

4.2.10 **Siderophore quantification**

To evaluate the secretion of siderophores, extracellular siderophores were quantified using the CAS liquid assay methodology (Schwyn and Neilands 1987; Payne 1994; Louden et al. 2011). Conidia of *T. virens* were inoculated in minimal liquid medium (MM) containing 2% glucose, 0.2 g yeast extract, KCl, $MgSO_4.7H_2O$, K_2HPO_4 (see section 4.2.6.5), using two different nitrogen sources (NH_4Cl and KNO_3) and five different $FeSO_4$ concentrations from 0 to 800 mg/L. The samples were incubated in 24-well culture plates (15.6 mm, Jet Biofil, China) at 25°C under shaking at 230 rpm for 96 h to induce siderophore production. The culture supernatants from each sample (*s*) were filtrated through 0.2 µm nylon filter (ReliaPrep, Ahlstrom-Mujnksjö, Promega, USA) to remove mycelial fragments. For siderophore quantification, 500 µL of culture filtrates were mixed with 500 µL of CAS solution containing 2 mM CAS stock solution, 1 mM Fe stock solution, piperazine (Sigma-Aldrich, USA) buffer (4.307 g piperazine/30 mL H_2O) and HDTMA (Sigma-Aldrich, USA) (0.0219 g HDTMA/50 mL H_2O). Then 10 µL of shuttle solution (0.2 M 5-Sulfosalicylic acid) were added in the reaction and incubated for 30 min. Reduction of blue colour by the presence of siderophores was measured absorbance (A) at 630 nm using a UV-Vis spectrophotometer (Genesys 10S, Thermo Fisher Scientific, USA). A reference (*r*) was prepared using MM+CAS+shuttle solution and the MM was used as a blank. Siderophore units were defined as [(A*r*-A*s*)/A*r*]*100 = % siderophore units.

4.2.11 **Intracellular iron content**

To analyse the acquisition of iron by *T. virens*, the intracellular iron concentration was measured using bathophenanthroline disulfonate (BPS) colorimetric assay methodology (Tamarit et al. 2006; Li et al. 2016a). Conidia were inoculated and incubated as described in the siderophore quantification assay with the difference being that six-well culture plates (34.8mm, Jet Biofil, China) were used. The mycelia were harvested by filtration, and then washed three times with nanopure water. The mycelial samples were freeze dried and ground until a fine powder was obtained. The ground mycelia was weighed and resuspended in 1 mL of 3 % nitric acid and boiled for 8 h using a thermoblock (Thermomixer R, Eppendorf, USA). The samples were centrifuged at 12,000 x g, and the supernatant was recovered. A total of 100 µL of supernatant was diluted 10-fold. The reaction was prepared by mixing 400 µL of supernatant diluent with 160 µL of ammonium acetate, and then incubating for 5 min at RT. The complex BPS-Fe was measured at 535 nm and nonspecific absorbance monitored at 680 nm was subtracted from 535 nm. A calibration curve of $FeSO_4$ (0.02-0.16 mM) was performed to quantify intracellular iron content, and the results were expressed as µmol g^{-1} dry weight.

4.2.12 **Oxidative stress sensitivity under different iron conditions**

To evaluate *T. virens* sensitivity to hydrogen peroxide under different treatments of iron as described by Li et al. (2016a) with modifications, the strains (WT, Δ*tvox1* and C*tvox1*) were grown on Vogel's medium without iron (Appendix) under different conditions. The iron-specific chelator BPS that blocks the reductive iron assimilation pathway was also used in this experiment. Conidia ($1x10^6$) was centrally inoculated, and radial growth was measured after 72 h at 25°C in darkness on Vogel's medium without iron (-Fe) or with 10 µM $FeSO_4$ (Fe) or 1.5 mM $FeSO_4$ (hFe), respectively, and with the addition of 0.25 mM BPS or/and 20 mM H_2O_2. The control was grown on Vogel's medium under the same conditions.

4.2.13 **Statistical analyses**

Statistical analyses were performed using the general ANOVA in the GenStat 18th package. Each value is the mean ± SD for three replicates (siderophore detection, siderophore quantification and intracellular iron content) or ten replicates (growth rate, conidial yield, germination and oxidative stress sensitivity) in each group, and $P<0.05$ was considered as significant. The least significant differences of means were determined as described in section 3.2.10.

4.3 Results

4.3.1 **Selection of candidate gene**

Based on a) the expression levels during the *T. virens*-maize interaction (Lawry 2016), and b) the potential role in iron regulation and synthesis of secondary metabolites that have been reported to be important during plant-microbe interactions (Lemanceau et al. 2009; Verbon et al. 2017; Mhlongo et al. 2018). The *T. virens* 2-oxoglutarate/Fe (II) dioxygenase gene (*tvox1*) was selected for further characterisation.

4.3.2 **Quantitative RT-qPCR of up-regulated genes**

To confirm the up-regulation of genes including *tvox1* during the *T. virens*-maize interaction at different time points. The results showed that changes in the expression levels of the *T. virens* genes were dependent on the presence of maize. The gene expression profiles showed that all seven genes were up-regulated during the different time points tested (Figure 4.8). However, gene SSCP2 (TV_93159) was down-regulated at 3 and 5 d.p.i, but was up-regulated at 7 d.p.i. This result validates the data obtained by Lawry (2016) demonstrating that these set of genes including *tvox1* are expressed during the *T. virens*-maize interaction at different time points.

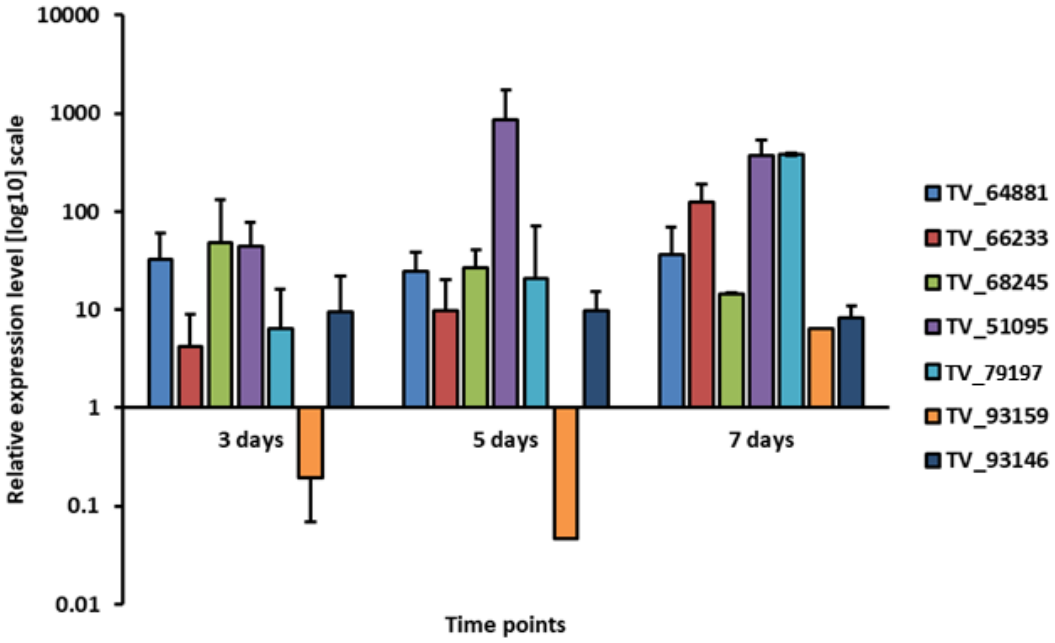

Figure 4.8 Confirmation of differential expression of up-regulated *T. virens* genes by RT-qPCR during the interaction with maize plants. The expression profiles of known *T. virens* genes were examined by RT-qPCR. For the control, actin gene was used as reference gene; all samples were adjusted to the level of expression compared with actin. Data were presented as mean ± SD of replicates.

4.3.3 Bioinformatic analysis of *tvox1* gene

Bioinformatic analysis was performed for TVOX1 using its amino acid sequence retrieved from the JGI genome databank. TVOX1 has a sequence of 357 amino acids in length, lacks a signal peptide and transmembrane domains, and belongs to the iron/ascorbate-dependent oxidoreductase family. Moreover, it contains two main domains including, a non-haem dioxygenase motif in the N-terminal region and a 2-oxoglutarate/Fe (II)-dependent dioxygenase domain located in position 171-289 (Figure 4.9 A). The secondary and tertiary structures of TVOX1 were predicted using Phyre2 software (Figure 4.9 A and B). The prediction showed that TVOX1 contains 31% alpha helix and 16% beta strand. TVOX1 is a metal ion binding protein with oxidoreductase activity that catalases the oxidation of an organic substrate using molecular oxygen, utilising ferrous iron as the active cofactor and 2-oxoglutarate as a co-substrate.

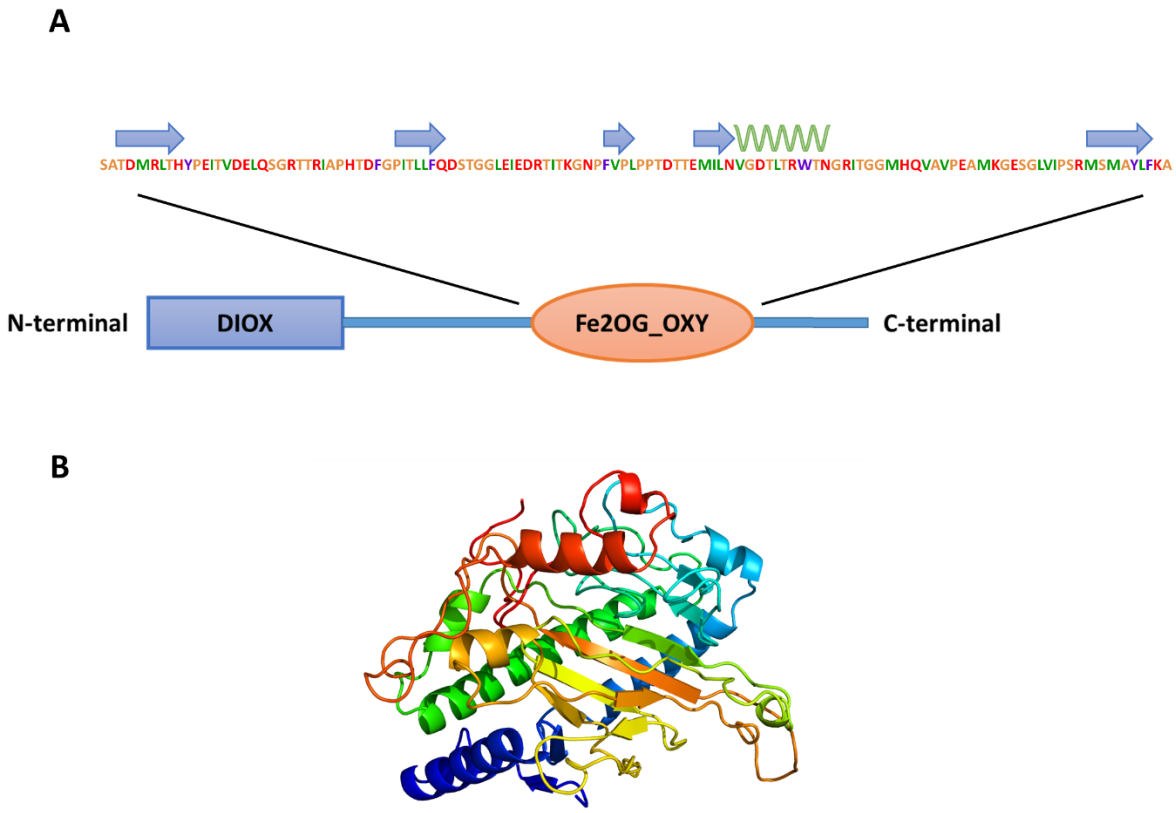

Figure 4.9 *T. virens* TVOX1 functional domains and tertiary structure. (A) Functional domains present in TVOX1 protein and secondary structure of the 2OG-Fe (II) dioxygenase domain. Arrows and helix indicate high confidence secondary structure regions of the Fe2OG_OXY domain predicted by Phyre2**. (B)** Prediction of tertiary structure for TVOX1 from *T. virens* by Phyre2**.**

Putative protein-protein interaction networks of *T. virens* TVOX1 were predicted using STRING software (Figure 4.10). The results showed that TVOX1 interacts with three non-ribosomal protein synthase (NRPs) proteins (TV_66940, TV_10003 and TV_69362), including Tex1, which participates in the synthesis of peptaibols (Viterbo et al. 2007); three 2OG-Fe (II) dioxygenases (TV_34790, TV_42714 and TV_217394); two NAD-dependent epimerase/dehydratase proteins (TV_24433 and TV_86039) and two hypothetical proteins (TV_ 68823 and TV_34270).

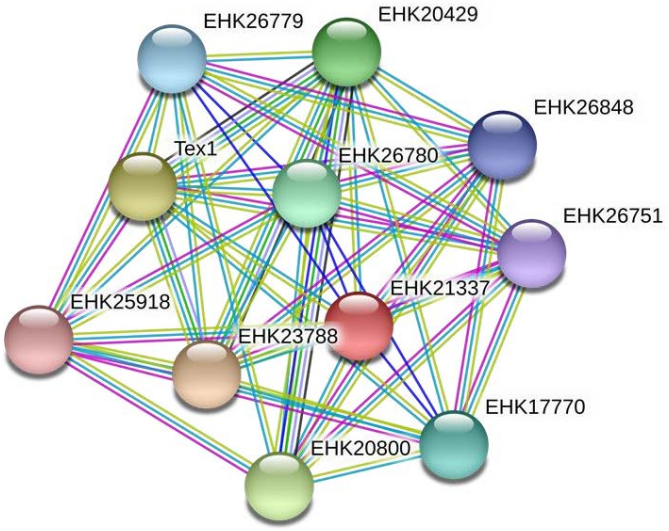

Figure 4.10 Prediction of protein interactions network of *T. virens* TVOX1. Prediction of protein-protein associations of 2OG-Fe (II) dioxygenase TVOX1 with other *T. virens* proteins using STRING software. Tex1 (TV_66940), non-ribosomal peptide synthase (NRPs) EHK23788 (TV_10003), EHK20800 (TV_69362) NRPs, EHK20429 (TV_ 68823) hypothetical protein, EHK26780 (TV_ 34790) 2OG-Fe (II) dioxygenase, EHK17770 (TV_42714) 2OG-Fe (II) dioxygenase, EHK26779 (TV_217394) 2OG-Fe (II) dioxygenase, EHK26848 (TV_24433) NAD-dependent epimerase/dehydratase protein, EHK26751 (TV_34270) Hypothetical protein, EHK25918 (TV_86039) NAD-dependent epimerase/dehydratase protein. Predicted interactions: blue lines, gene co-occurrence; dark-green lines, gene neighbourhood. Know interactions: pink lines, experimentally determined; light-blue lines, from curated databases. Other interactions: light-green lines, textmining; black lines, co-expression; purple lines, protein homology.

Based on the diversification of 2OG-Fe (II) dioxygenases and in the putative classification of TVOX1 as a gibberellin oxidase protein (BlastP results NCBI), a phylogenetic tree was constructed to compare the sequence of TVOX1 and its homologs in relation to characterised gibberellin oxidases that contain the 2OG-Fe (II) dioxygenase domain present in fungi and plants. The phylogenetic tree results show a clear diversification of 2OG-Fe (II) dioxygenases (DOX) between kingdoms (Figure 4.11). Also, it was observed that TVOX1 is separated from the characterised gibberellin oxidase from *Fusarium fujikorou* (Tudzynski 2005), suggesting that TVOX1 may not play a function as a gibberellin oxidase. Additional analysis was performed to compare the *F. fujikorou* gibberellin oxidase cluster with the *T. virens tvox1* putative cluster (Supplementary Figure 5). Based on the results, the cluster neighbourhood genes were absent in *T. virens*, confirming that TVOX1 may play an additional function related to secondary metabolism.

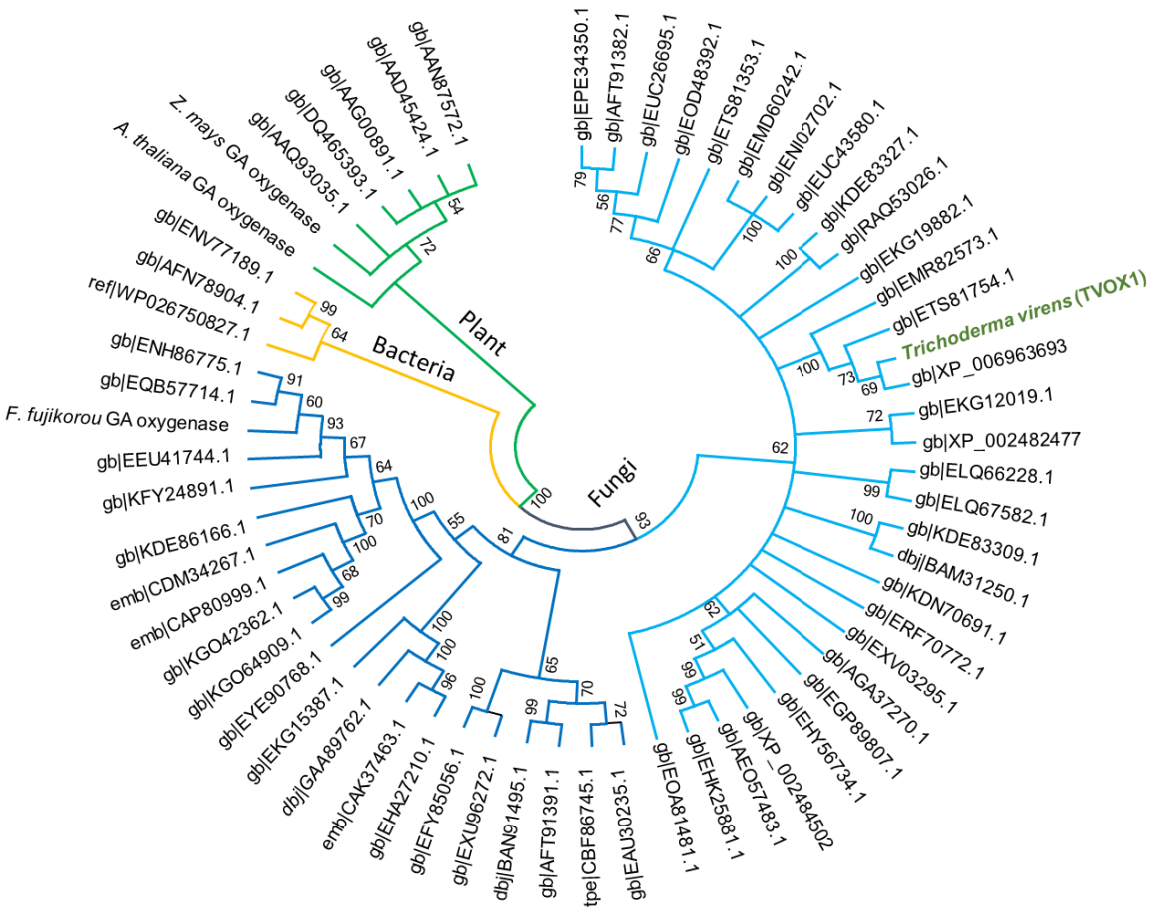

Figure 4.11 Phylogeny of TVOX1 2OG-Fe (II) dioxygenase homologs. Protein sequences retrieved from NCBI BLASTP search were analysed using MEGA6. A maximum-likehood phylogenetic tree was created with a bootstrap of 1000. Additional plant, fungi and bacteria protein sequences retrieved from the NCBI database were considered for this analysis. Abbreviations: gibberellin, GA. *T. virens* (TVOX1) is indicated in green letters.

A phylogenetic analysis was performed to compare the protein sequences of 2OG-Fe (II) dioxygenases from six *Trichoderma* spp. (*T. virens, T. harzianum, T. atroviride, T. asperellum, T. reesei, T. longibrachiatum*) (Figure 4.12). Putative 2OG-Fe (II) dioxygenases of *Trichoderma* spp. were classified into three different classes based on the classification proposed by Kawai et al. (2014) in plants: a) DOXA class for putative DNA repair proteins, b) DOXB class for putative prolyl 4-hydrolases and c) DOXC class for putative highly specialised metabolism proteins. As observed in Figure 4.12, the majority of 2OG-Fe (II) dioxygenases were classified into the DOXC class in which most of them were putatively annotated as genes involved in phytohormone, flavonoid and antibiotic biosynthesis. The analysis revealed that TVOX1 of *T. virens* belongs to the DOXC class 2OG-Fe (II) dioxygenases, and shares high homology to *T. reesei* 58580 and *T. longibrachiatum* 1459808 proteins (Figure 4.12).

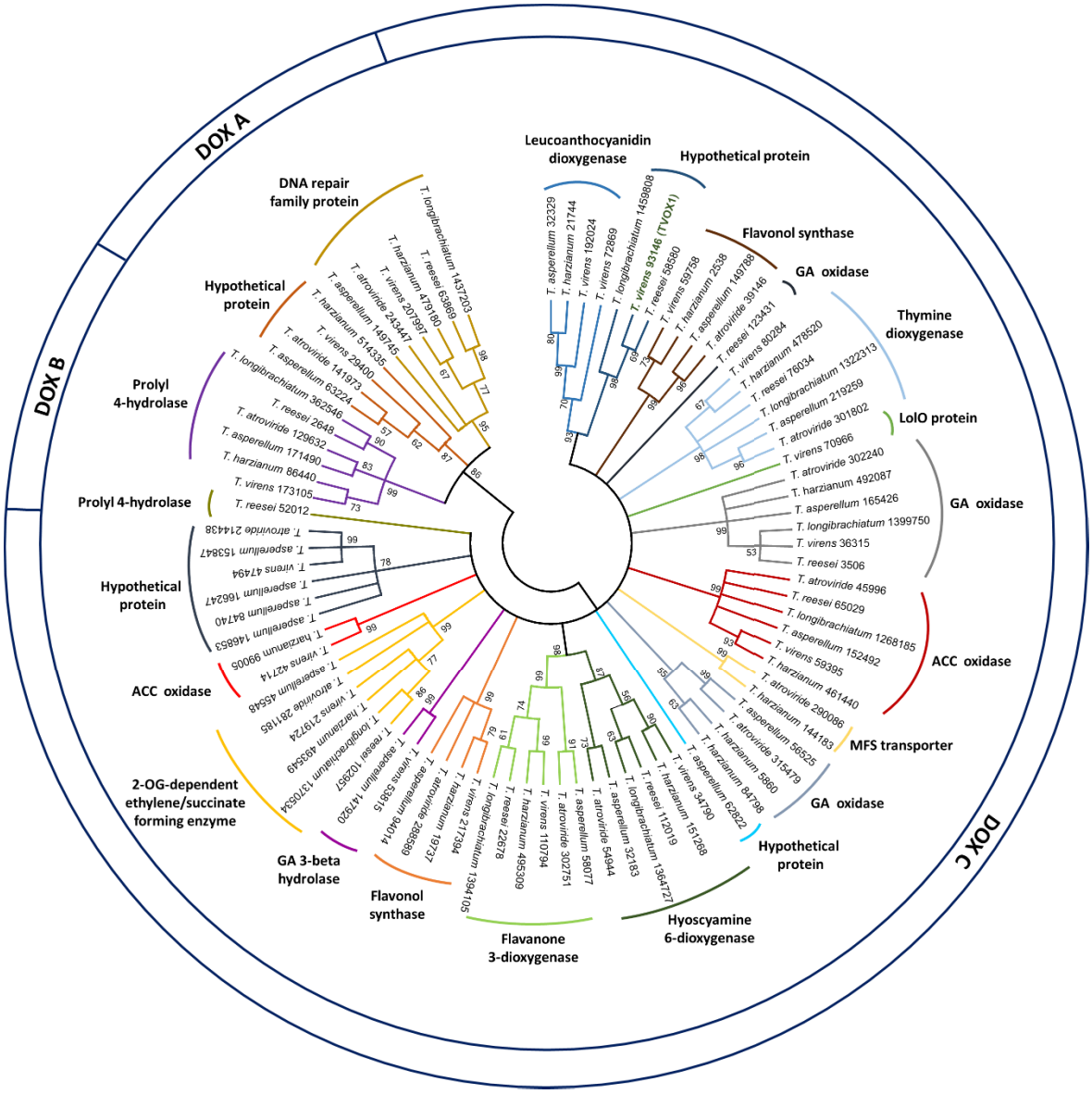

Figure 4.12 Phylogeny of 2OG-Fe (II) dioxygenase in *Trichoderma.* Protein sequences from six *Trichoderma* spp. were retrieved from the JGI database and were analysed using MEGA6. Multiple sequence alignment was performed by ClustalW, and a maximum-likehood phylogenetic tree was created with a bootstrap of 1,000. Abbreviations: gibberellin, GA; loline, Lol; 1-aminocyclopropane-1-carboxylate, ACC; major facilitator superfamily protein, MFS. *T. virens* (TVOX1) is indicated in green letters.

4.3.4 **Antibiotic sensitivity analysis**

Hygromycin sensitivity tested 7 d.p.i on germination and growth of *T. virens* WT growing on PDA plates containing 0 to 100 µg/mL hygromycin B concentration, showed that *T. virens* growth was reduced at 50 µg/mL concentration compared to 75-100 µg/mL, in which germination was completely inhibited (no geminated conidia or hyphae were detected) (Supplementary Figure 6). Geneticin resistance was analysed on the *T. virens* Δ*tvox1* mutant growing on three different media (PDA, CM and Vogel's medium) using seven antibiotic concentrations (0, 50, 100, 250, 350, 500, 600, 700 µg/mL geneticin G418). The PDA and CM plates with the highest concentration tested

(700 µg/mL) resulted in no growth inhibition in *T. virens Δtvox*1; however, in Vogel's medium plates at 700 µg/mL concentration stopped conidia germination after 7 d.p.i (Supplementary Figure 7).

4.3.5 Construction of *Trichoderma virens* deletion mutant gene (Δ*tvox1*)

Construction of KO *tvox1* vector and subcloning into *E. coli* and *A. tumefaciens* before *T. virens* transformation were created as shown in Supplementary Figure 8. Deletion of the *tvox1* gene in *T. virens* was performed by homologous recombination replacing the *tvox1* ORF with the HygR cassette. From a total of fifty stable transformants, sixteen were picked randomly and screened for their ability to grow continuously in 100 µg/mL hygromycin B. The genomic DNA of the transformants was extracted for validation of gene deletion and homologous recombination by PCR as described in section 4.2.5.1. The results confirmed that all screened mutants had the homologous insertion of pΔ*tvox1* (Figure 4.13 A). Therefore, the transformants were validated to have the replacement of the *tvox1* ORF with the HygR cassette (Figure 4.13 B and C).

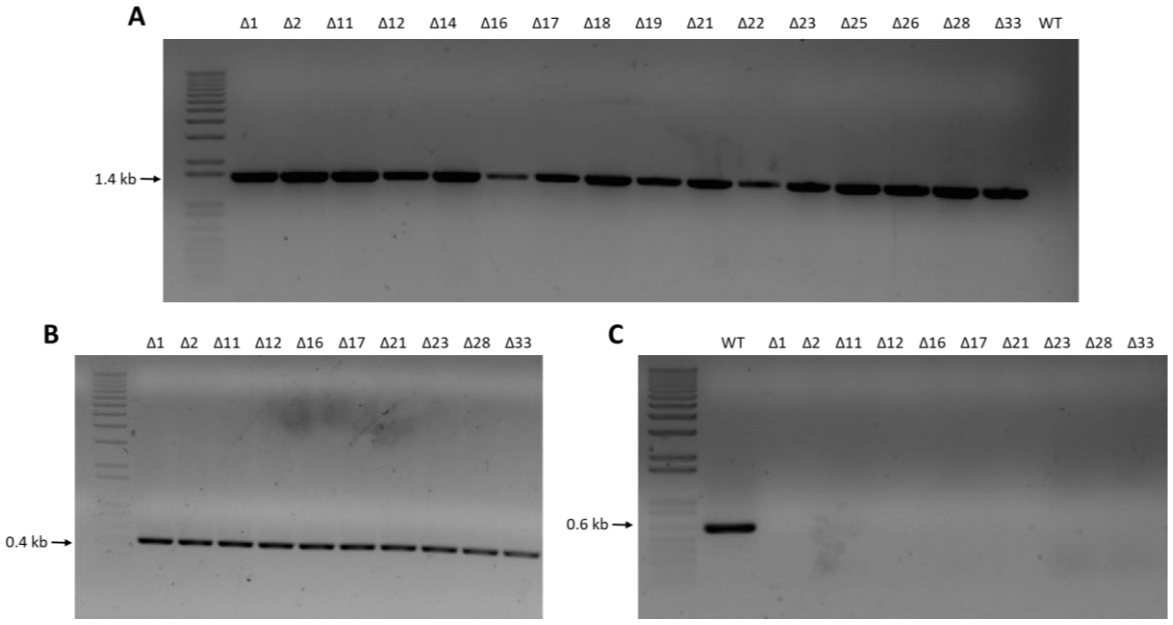

Figure 4.13 Confirmation of *tvox1* knockout by PCR. Verification of homologous integration by PCR of *T. virens* deletion mutants. **(A)** PCR product using primers (LF *tvox1*-F and HygR check) to identify homologous recombination (1.4 kb size product). **(B)** PCR product generated from primers (*hph* ORF f and r) that amplify a section of the *hph* ORF (0.4 kb size product). **(C)** PCR product generated from primers (*tvox1* ORF f and r) that amplify a section of the *tvox1* ORF (0.6 kb size product).

A southern analysis was performed on ten Δ*tvox1* transformants and WT strains to verify homologous recombination of HygR cassette in the *T. virens* genome (Figure 4.14). The DIG-labelled and un-labelled probes (*hph* and *tvox1*) were visualised on a gel-electrophoresis image to confirm their integrity (Supplementary Figure 9). The hybridisation results of the labelled *tvox1* probe showed a single band (2.5 kb fragment size) of *Xba*I digested gDNA of the WT, but was not present in the digested gDNA of the mutants (Figure 4.14 D). This result confirmed the deletion of the *tvox1* gene in the *T. virens* WT genome. In addition, the labelled *hph* probe used for homologous

recombination resulted in a single band for three of the mutants (12a, 16b and 33c) and two bands for the other seven. All ten mutants were positive for the 4.7 kb fragment associated with the homologous integration of HygR cassette in the WT genome (Figure 4.14 C). However, the rest of the mutants had an extra band of approximately 8 kb, suggesting ectopic integration of a second copy of the HygR cassette in the genome (Figure 4.14 C). Therefore, the three independent deletion mutants (Δ*tvox1*-12a, Δ*tvox1*-16b and Δ*tvox1*-33c) that had one copy of the HygR cassette and were positive for homologous recombination were selected for further characterisation.

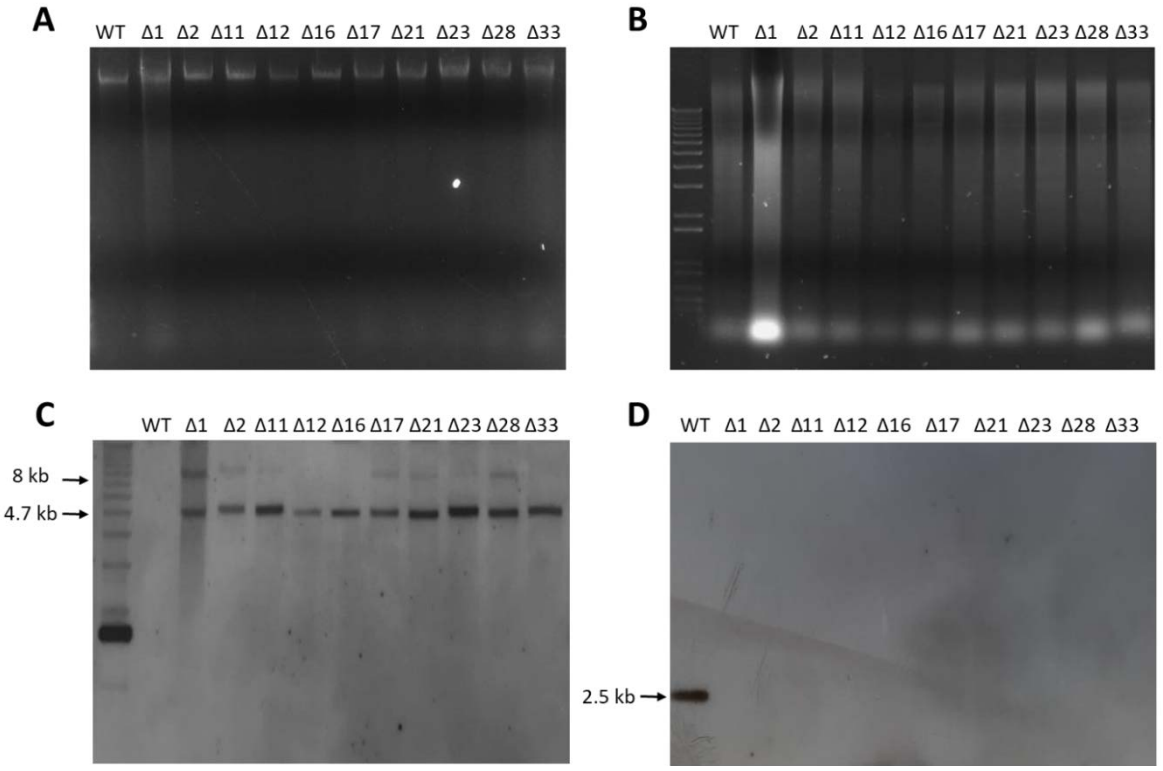

Figure 4.14 Confirmation of *tvox1* knockout by Southern blot. (A) DNA isolation of *T. virens* WT and Δ*tvox1*. **(B)** DNA of *T. virens* strains digested with *Xba*I. **(C)** Southern blot of WT and Δ*tvox1* mutants using *hph* ORF as a probe; a 4.7 kb fragment size is expected for homologous integration in *T. virens* mutants in the deletion event when digested with *Xba*I. **(D)** Southern blot of WT and Δ*tvox1* mutants using *tvox1* ORF as a probe; a 2.5 kb fragment size is expected in *T. virens* WT strain and an absence of a band in the deletion strains digested with *Xba*I.

4.3.6 Phenotypic characterisation of *tvox1* deletion mutants

4.3.6.1 Growth rate, conidiation and germination

General growth and morphology of three independent *T. virens* Δ*tvox1* mutants were compared to WT (Figure 4.15 A). The results showed that deletion mutants (Δ*tvox1*-12a, Δ*tvox1*-16b and Δ*tvox1*-33c) were significantly affected in growth rate, conidiation and germination (P<0.001). The growth rate of Δ*tvox1* mutants was significantly faster than the WT, but not among them (Figure 4.15 B). The conidiation and germination were also influenced in all mutants, being significantly higher rates

compared with the WT (Figure 4.15 C and D). The deletion of *tvox1* in the *T. virens* genome had an impact on the promotion of growth, conidiation and germination; however, the specific role of *tvox1* in all these aspects is currently unknown.

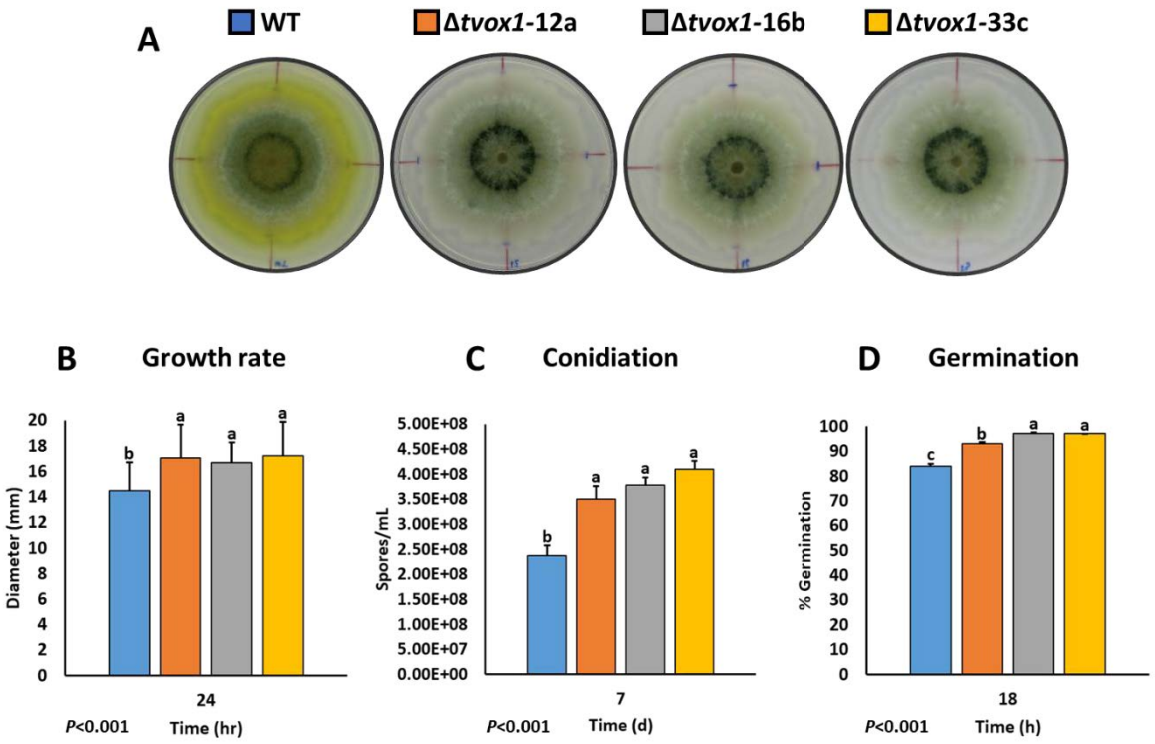

Figure 4.15 Phenotypic characterisation of deletion mutants (Δ*tvox1*) compared with the parental strain (WT). (A) Colony appearance growing on axenic media (PDA) under a light/dark cycle. **(B)** Average of growth rates, **(C)** conidiation, and **(D)** germination of WT and Δ*tvox1* mutants. Data were presented as mean ± SD of replicates. Statistical comparison between treatment groups were carried out using general ANOVA followed by Fisher's Unprotected LSD algorithm. Different letters indicate significance between treatments (P<0.05). All statistical analyses were performed using GenStat 18th software.

4.3.6.2 Endophytism analysis

The endophytic colonisation of deletion mutants was evaluated and compared with the WT to verify whether the Δ*tvox1* mutants were affected in their ability to colonise the root system and the stem of maize plants (Figure 4.16 A-C and Supplementary Figure 10). As shown in Figure 4.16 B and Supplementary Figure 10, *T. virens* WT and Δ*tvox1* mutants were able to internally colonise different sections of the primary root and the stem (first two centimetres) of maize plants after 7 d.p.i. The root colonisation results showed significant differences among strains (P<0.05). On average, the Δ*tvox1* mutants colonised 30% less than the WT (Figure 4.16 C). In the case of stem colonisation, no differences were observed. These results demonstrate an influence of *tvox1* on the root internal colonisation ability of *T. virens* under soil conditions.

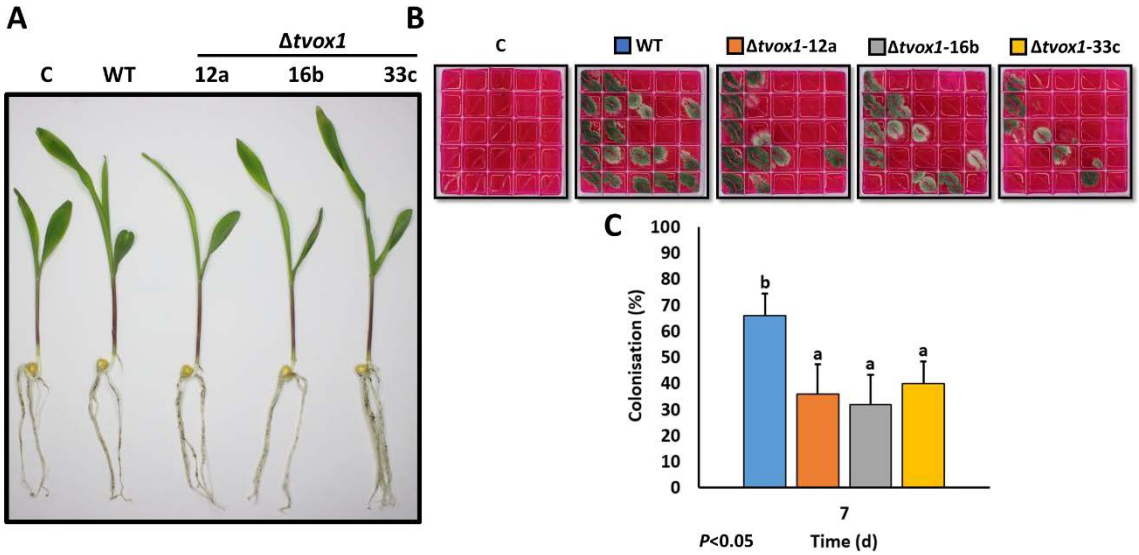

Figure 4.16 Endophytic analysis of *T. virens* (WT and Δ*tvox1*). The primary roots colonised by *T. virens* after 7 d.p.i were surface sterilised and five equal root fragments were placed on *Trichoderma* selective medium (TSM). **(A)** Maize plants appearance during interaction with *T. virens* under soil growth conditions (Random sampling). **(B)** Maize primary root fragments placed on TSM; *T. virens* growth was visualised on the media when roots were endophytically colonised. **(C)** Average of colonisation percentage of WT and Δ*tvox1* mutants. Data were presented as mean ± SD of replicates. Statistical comparison between treatment groups were carried out using general ANOVA followed by Fisher's Unprotected LSD algorithm. Different letters indicate significance between treatments (P<0.05). All statistical analyses were performed using GenStat 18th software.

4.3.6.3 Siderophore detection (semiquantitative)

A preliminary analysis of siderophore production by *T. virens* WT and deletion mutants was assessed to determine the effect of *tvox1* deletion on the biosynthesis of siderophores. In the CAS media supplemented with ammonium chloride (NH_4Cl) the colour change was from dark-blue to orange by the diffusion of secreted siderophore-type compounds. In contrast, in the CAS media supplemented with potassium nitrate (KNO_3) the colour change was different, from dark-blue to clear-blue (Figure 4.17 A). These responses were followed up to 7 d.p.i (Supplementary Figure 11). A comparison of the siderophore production by *T. virens* strains growing on CAS medium amended with two different nitrogen sources showed that in the presence of ammonium and nitrate, siderophore production was significantly reduced in *T. virens Δtovx1* mutants compared to the WT (Figure 4.17 B). These results suggest that siderophore production was affected by the deletion of the *tvox1* gene in the *T. virens* genome.

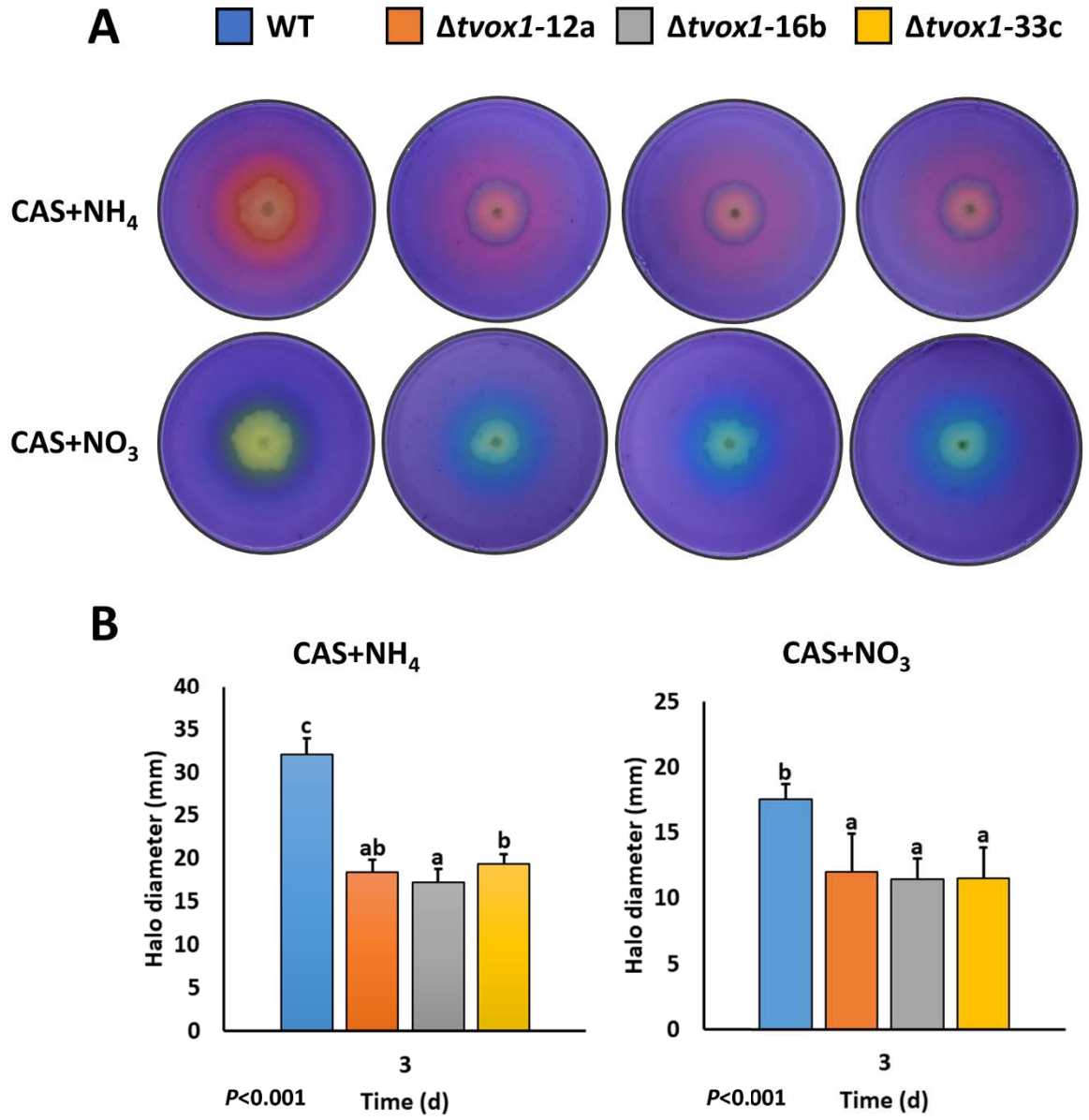

Figure 4.17 Siderophore activity of *T. virens* assessed on CAS-agar plates. (A) Detection of siderophore production by *T. virens* strains. Blue and orange haloes indicate the presence of siderophores. **(B)** Halo diameter of WT and Δ*tvox1* mutants. Data were presented as mean ± SD of replicates. Statistical comparison between treatment groups were carried out using general ANOVA followed by Fisher's Unprotected LSD algorithm. Different letters indicate significance between treatments (P<0.05). All statistical analyses were performed using GenStat 18th software.

After growth, conidiation, germination, endophytism, siderophore analysis (semiquantitative), one deletion mutant (Δ*tvox1*-16b) was selected to continue with the characterisation of the *tvox1* gene, because no significant differences within the independent transformants were observed.

4.3.7 Construction of *Trichoderma virens* complementation mutants (C*tvox1*)

Construction of complementation vector and sub cloning into *E. coli* before *T. virens* transformation were created as shown in Supplementary Figure 12. Complementation of the *tvox1* gene in *T. virens*

was performed by integration of the *tvox1* ORF, native promoter, native terminator and the GtR cassette. From fifty stable transformants able to grow continuously in 750 µg/mL geneticin (G418), ten were randomly selected to verify the integration of the GtR cassette. All the isolates were identified by PCR to be positive recombinants (Figure 4.18 A and B), showing the integration of *tvox1* ORF (0.6 kb) and insertion of the GtR cassette (1.8 kb). The results confirmed that all screened mutants had the insertion of the *tvox1* complementing construct (C*tvox1*). After PCR confirmation, Southern blot analysis was performed to corroborate insertion of the *tvox*1 complementing construct in the *T. virens* Δ*tvox1* genome.

The genomic DNA of ten C*tvox1* mutants, Δ*tvox1* and WT, was extracted to verify recombination of the GtR cassette in the *T. virens* genome. The DNA of the WT and Δ*tvox1* was used as a negative control for a *nptII* labelled probe. The DIG-labelled and un-labelled PCR products were visualised on a gel-electrophoresis image to confirm their integrity (Supplementary Figure 13). Digested gDNA of the mutants and WT (Figure 4.18 C) was transferred and hybridised as mentioned in section 4.2.5.4, using a labelled probe shown in Supplementary Figure 12. Similar shifts were observed in the digested DNA samples run in the electrophoresis gel compared to hybridisation bands (Figure 4.18 C and D), suggesting that DNA mobility through the gel was affected by other factors (e.g. proteins, carbohydrates and salt), indicating that height differences on the gel were translated to the Southern blot results. The hybridisation results of the labelled *nptII* probe, two bands (6.8 and 5.5 kb fragments size) were observed in nine of the mutants and one single band (6.8 kb fragment size) in mutant C*tvox1*-34a (Figure 4.18 D). All mutants were positive for the 6.8 kb band for homologous recombination. However, homologous recombination was discarded because all transformants were able to grow in PDA 100 µg/mL supplemented with hygromycin B. The WT and deletion mutant were all negative for any band. These results verify the insertion of the complementing cassette in all the mutants. The complementing mutant C*tvox1*-34a was selected for further characterisation.

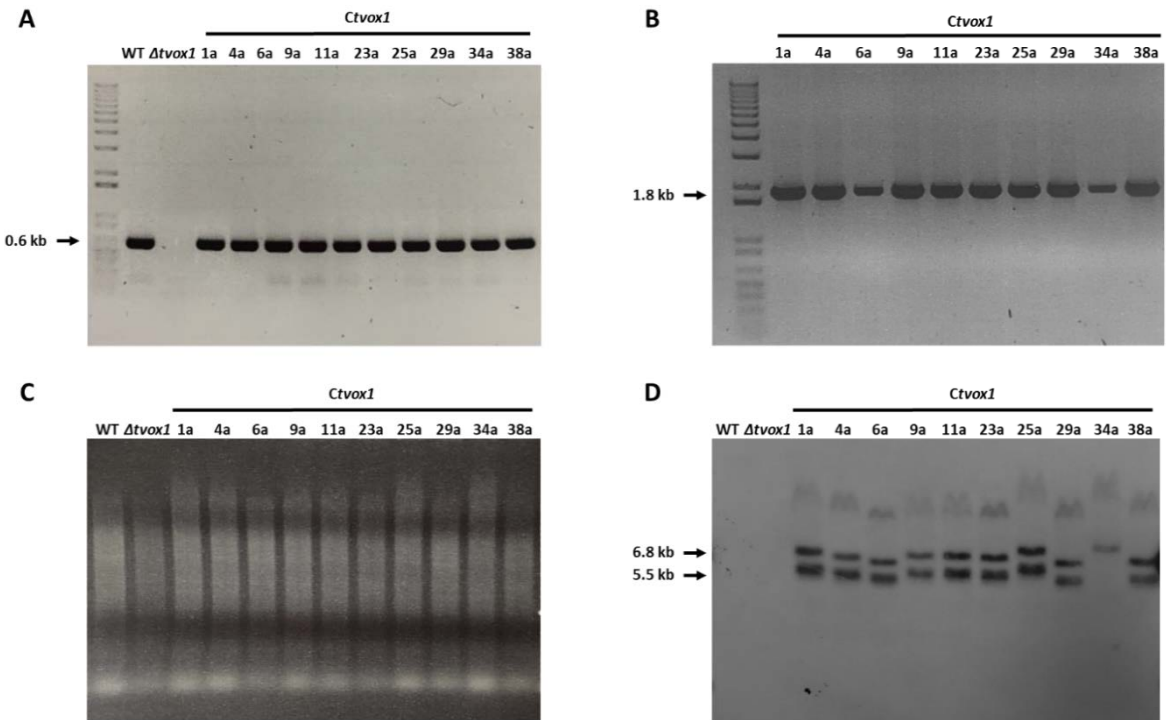

Figure 4.18 Confirmation of complementing mutants of the gene *tvox1* by PCR and Southern blot. **(A)** PCR product using primers (*tvox1* ORF f and r) to verify the insertion of *tvox1* ORF (0.6 kb size product). **(B)** PCR product generated from primers (GtR *f* and r) that amplify the GtR cassette (1.8 kb size product). **(C)** gDNA of *T. virens* strains digested with *Mlu*I and *Hind*III. **(D)** Southern blot of WT, *tvox1* deletion and complementing mutants using a fragment of *nptII* ORF as a probe; no fragments were expected in the WT, and deletion mutant and a 6.8 kb fragment size is expected for homologous recombination when digested with *Hind*III and *Mlu*I. However, in complementing mutants other fragment sizes were expected due to ectopic integrations of the GtR cassette in the *T. virens* genome.

4.3.8 Gene expression of *tvox1* gene during the *Trichoderma virens*-maize interaction

To evaluate the effect of the complementation mutant in the expression levels of *tvox1*, a quantitative RT-qPCR analysis was used. The results showed that the expression levels of *tvox1* gene in the *Ctvox1* mutant during the *T.* virens-maize interaction under hydroponic and soil growth conditions were higher than the WT, but not significant (P>0.05) (Figure 4.19). In addition, expression was not observed in deletion mutant (Δ*tvox1*) in any condition (data not shown).

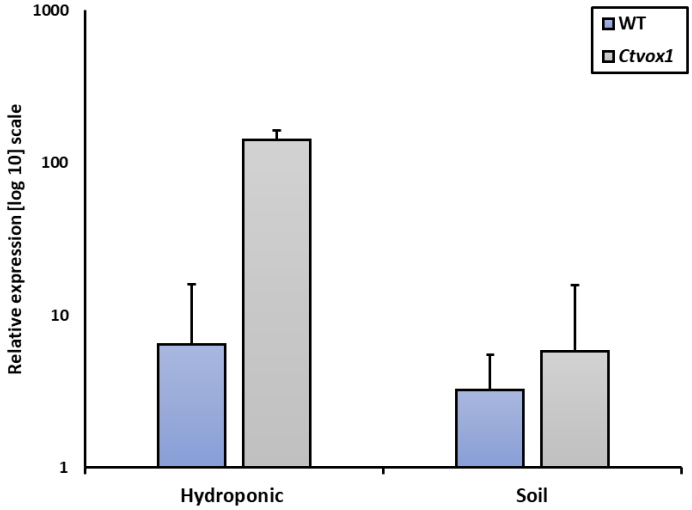

Figure 4.19 Relative expression levels of *tvox1* gene in *T. virens* strains (WT and C*tvox1*) during *T. virens*-maize interaction. The expression levels of *tvox1* were analysed by RT-qPCR during the *T. virens*-maize interaction under hydroponic and soil growth conditions. For the control, ß-tubulin gene was used as reference gene; all samples were adjusted to the level of expression compared with ß-tubulin. Data were presented as mean ± SD of replicates.

4.3.9 Siderophore production by *Trichoderma virens*

To understand the role of TVOX1 in the acquisition of iron, the extracellular siderophore in *T. virens* was measured using two nitrogen sources, and in the presence or absence of iron (Figure 4.20 A and B). During iron depletion conditions, siderophore production was detected in all the strains (WT, Δ*tvox1* and C*tvox1*) (Figure 4.20 C-F). Moreover, a progressive decrease of siderophores was observed when the iron concentration was increased. Negative values were taken as the absence of siderophore units in all cases; this change was because the darker-blue colour in some of the samples gave higher absorbance values compared to the reference (Figure 4.20 C and D). Contrasting siderophore production occurred when utilising different nitrogen sources; in ammonium conditions, no significant differences were observed among the three *T. virens* strains. However, siderophore secretion was significantly reduced in the presence of iron (Figure 4.20 E).

In contrast, under nitrate conditions, the siderophore production shifted in the presence of different concentrations of iron. The WT strain secreted siderophores from 0 to 600 mg/L $FeSO_4$ but was not observed at the highest concentration (800 mg/L $FeSO_4$) (Figure 4.20 F). The Δ*tvox1* and C*tvox1* strains showed a significantly larger percentage of siderophores when the iron was deficient (0-200 mg/L $FeSO_4$) compared to non-limiting iron conditions (400-800 mg/L $FeSO_4$) (Figure 4.20 F).

Interestingly, in the presence of nitrate a dramatic reduction in siderophore production was observed from 400 to 600 mg/L $FeSO_4$ in the WT, and from 200 to 400 mg/L $FeSO_4$ in the Δ*tvox1* and C*tvox1* strains (Figure 4.20 F), suggesting that the Δ*tvox1* strain has an alteration in iron

acquisition or/and regulation; in response, it produced larger amounts of siderophores when iron was limited in comparison with the parental strain. Also, the results showed that siderophore production in *T. virens* is influenced by nitrogen and, dependant on the nitrogen source used.

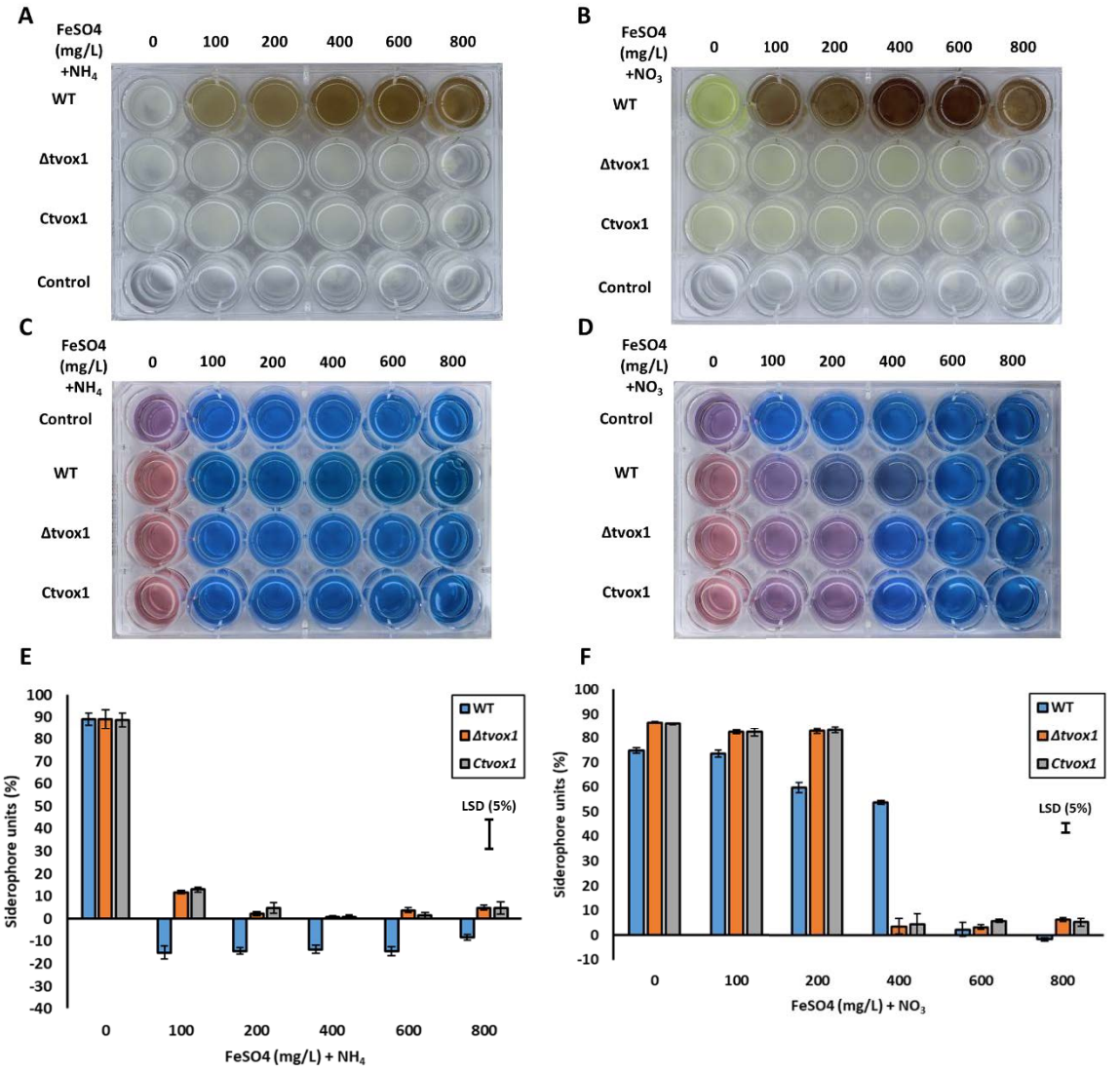

Figure 4.20 Quantitative analysis of extracellular siderophores synthesised by *T. virens* strains growing in two nitrogen sources and different concentrations of iron. *T. virens* growth in minimal medium supplemented with **(A)** NH_4 and **(B)** NO_3, plus different concentrations of $FeSO_4$. Visualisation of siderophore production (CAS reaction) in minimal media amended with **(C)** NH_4 and **(D)** NO_3 by *T. virens* WT, Δ*tvox1* and C*tvox1* strains; siderophores were quantified in the culture supernatant using the CAS liquid assay. Reduction of blue colour represents the presence of siderophores. Extracellular siderophore quantification of *T. virens* strains growing in **(E)** NH_4 and **(F)** NO_3 amended minimal media under different iron concentrations using CAS liquid methodology. Data were presented as mean ± SD of replicates. Statistical comparison between treatment groups were carried out using general ANOVA followed by Fisher's Unprotected LSD algorithm. Differences were considered significant at $P<0.05$. All statistical analyses were performed using GenStat 18th software.

In addition to siderophore secretion, in both nitrogen conditions, the accumulation of a brownish pigment was observed in the WT strain when the iron was supplied (Figure 4.20 A and B). However, in the Δ*tvox1* and C*tvox1* strains this phenotype was not observed. This result may suggest that this pigment (melanin-like) may protect the fungus against environmental stress; for example, ROS produced in the presence of iron which is an inducer of these toxic molecules.

4.3.10 **Iron storage in *Trichoderma virens***

To understand the role of TVOX1 in the incorporation of iron, and to evaluate the influence of siderophore production on iron acquisition and storage in the *T. virens* strains (WT, Δ*tvox1* and C*tvox1*) grown in different concentrations of iron and two nitrogen sources, intracellular iron in *T. virens* mycelia was measured (Figure 4.21 A-D). As observed during siderophore production analysis, the WT strain accumulated a melanin-like pigment in the presence of iron, but this phenotype was not present in the Δ*tvox1* and C*tvox1* strains (Figure 4.21 C and D). During fungal growth in the presence of ammonium, the intracellular iron significantly increased in the Δ*tvox1* and C*tvox1* strains in comparison with the WT. Comparison between Δ*tvox1* and C*tvox1* strains showed that iron content at 40O and 800 mg/L $FeSO_4$ conditions was significantly higher in the Δ*tvox1* than C*tvox1* strain, but not significant differences were detected at 600 mg/L (Figure 4.21 E). Significant shifts in intracellular iron were observed in the Δ*tvox1* mutant at higher concentrations of iron (Figure 4.21 E), whereas in the WT, iron storage gradually increased and then was stable.

In contrast, during fungal growth on nitrate, the intracellular iron in all strains progressively grew as the iron concentration was increased. However, at 600 mg/L $FeSO_4$ concentration, the iron levels were significantly higher in the WT than the Δ*tvox1* and C*tvox1* strains, and then significantly decreased at the highest concentration (800 mg/L $FeSO_4$) (Figure 4.21 F). The results showed that Δ*tvox1* has an alteration in iron storage in comparison with the WT and *Ctvox1* in the presence of higher concentrations of iron in both nitrogen sources. This phenotype was observed in ammonium condition. In addition, it was observed that nitrogen (nitrate and ammonium) influenced iron acquisition, suggesting that nitrogen may influence gene expression of iron storage-related genes.

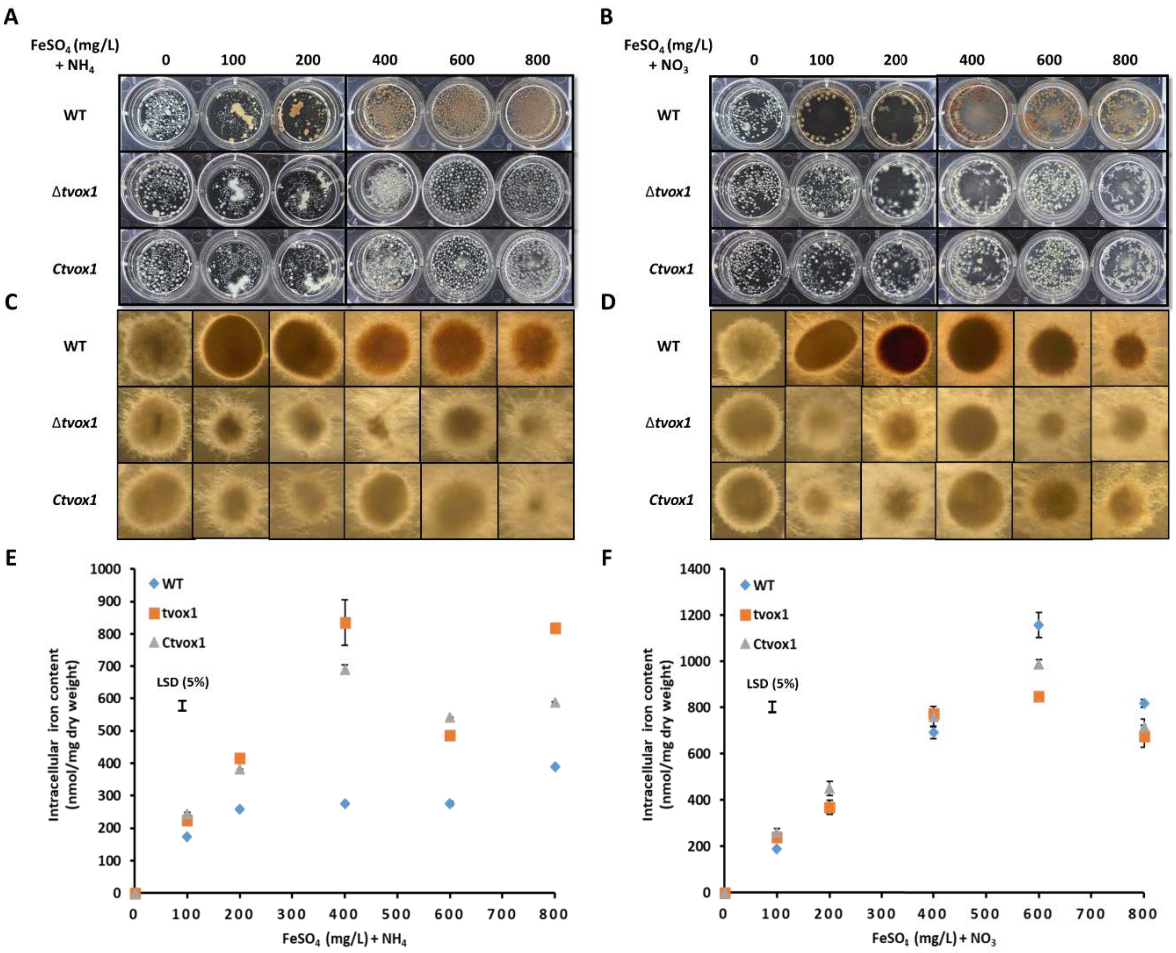

Figure 4.21 Quantitative analysis of intracellular iron and morphology of *T. virens* WT and mutants growing in two nitrogen sources. *T. virens* growth in minimal medium supplemented with **(A)** NH_4 and **(B)** NO_3, plus different concentrations of $FeSO_4$. Visualisation under stereoscopy of *T. virens* WT and mutants (Δ*tvox1* and C*tvox1*) morphology growing in **(C)** NH_4 and **(D)** NO_3 with different iron concentrations. Quantitative analysis of intracellular iron in *T. virens* mycelia under **(E)** NH_4 and **(F)** NO_3 growing conditions with the addition of different iron concentrations. Data were presented as mean ± SD of replicates. Statistical comparison between treatment groups were carried out using general ANOVA followed by Fisher's Unprotected LSD algorithm. Differences were considered significant at $P<0.05$. All statistical analyses were performed using GenStat 18th software.

4.3.11 *Trichoderma virens* sensitivity to iron and oxidative stress

To evaluate the sensitivity of WT and mutants to iron and iron-related stresses, the growth rates of deletion and complementing mutants were measured and compared to the WT. The growth rates of both mutants were significantly higher than the WT under these conditions: (-Fe, Fe, hFe, -Fe/BPS, Fe/BPS, hFe/BPS) (Figure 4.22). The growth rate in Δ*tvox1* and C*tvox1* was significantly reduced in the presence of high concentrations of iron (hFe); however, no limitation in growth was detected under low concentrations and without the addition of iron (Fe and -Fe) (Figure 4.22). Moreover, when strains were treated with the ferrous iron chelator BPS, mycelial growth was not

significantly affected (Figure 4.22). The susceptibility of *T. virens* to an oxidative stress molecule, hydrogen peroxide (H_2O_2), in the presence and absence of iron was also studied. Iron and ROS are closely related, the formation of ROS can be triggered by inadequate iron storage, and detoxifying enzymes such as peroxidases and catalases use iron as a cofactor. The results showed that Δ*tvox1* and C*tvox1* mutants were significantly more sensitive than the WT, showing a hypersensitivity to H_2O_2 in either the presence or absence of iron when compared to the control (Figure 4.22), suggesting that the oxidative-stress may be affected during the detoxification process by the inadequate utilisation of iron in both mutants. However, comparison between Δ*tvox1* and C*tvox1* mutants, showed that C*tvox1* mutant was more resistant to H_2O_2 than the Δ*tvox1* under iron-limited conditions, but under iron-sufficient conditions this phenotype was inverted.

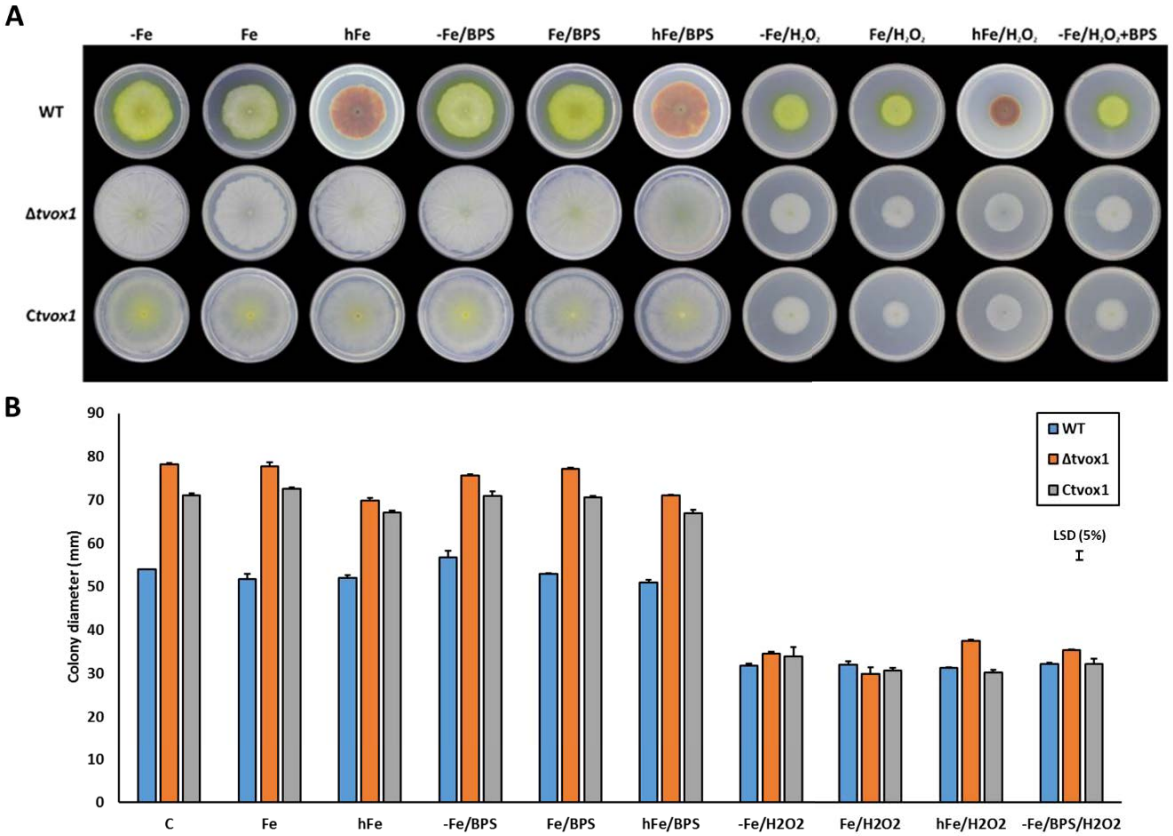

Figure 4.22 Resistance to iron limitation and oxidative stress by *T. virens*. *T. virens* WT, Δ*tvox1* and C*tvox1* conidia ($1x10^6$) were centrally inoculated on PDA without addition of iron (-Fe), containing 10 µM $FeSO_4$ (Fe), or 1.5 mM $FeSO_4$ (hFe), or 0.25 mM BPS, or 20 mM H_2O_2, respectively. **(A)** Colony appearance of *T. virens* strains. **(B)** Colony diameter of the WT and mutants. Data were presented as mean ± SD of replicates. Statistical comparison between treatment groups were carried out using general ANOVA followed by Fisher's Unprotected LSD algorithm. Differences were considered significant at $P<0.05$. All statistical analyses were performed using GenStat 18th software.

4.4 Discussion

4.4.1 *Trichoderma virens* 2OG-Fe (II) dioxygenase gene (*tvox1*)

In recent years, many studies have focused on the interaction of microbes with their host plant (Imam et al. 2016; Park et al. 2018; Schirawski and Perlin 2018). Transcriptome analysis using next-generation sequencing is one of the most widely used technologies to study the regulation of several genes during plant-microbe interactions (Dupont et al. 2015; Moran-Diez et al. 2015; Powell et al. 2017; De Palma et al. 2019). The selection of candidate genes is a common strategy utilised to understand their role during this multifactorial process; for example, four genes of *Magnaporthe oryzae* that encode for biotrophy-associated secreted (BAS 1-4) proteins were identified and are likely to function as putative effectors during fungal biotrophic invasion (Mosquera et al. 2009).

During plant-microbe interactions several genes are up- and down- regulated from both organisms. In this study, I selected a candidate gene (*tvox1*) based on the novel function of 2OG-Fe (II) dioxygenases in the secondary metabolism of fungi, and because that it was one of the most highly up-regulated genes of *T. virens* at 7 d.p.i during its interaction with maize (Lawry 2016). Moreover *tvox1* is up-regulated at different time points during the interaction with maize under hydroponic growth conditions (Figure 4.8), as previously found by Lawry (2016) in a soil-assay, suggesting that *tvox1* may play a role during the *T. virens* colonisation process.

Previous studies have demonstrated that misannotation (molecular function and enzyme superfamily) of proteins in public databases (GenBank, TrEMBL and KEGG) is common (Schnoes et al. 2009). Since putative annotation of TVOX1 as a gibberellin oxidase was based on similarity to uncharacterised protein matches using public database GenBank (NCBI BlastP), I decided to include other bioinformatic analysis to verify this. Based on the results from the phylogenetic and putative-cluster analysis performed on TVOX1 in comparison to the well-characterised gibberellin oxidase of the filamentous fungi *F. fujikuroi,* it was decided to maintain the annotation of TVOX1 as a 2OG-Fe (II) dioxygenase. In the analysis of the diversity of 2OG-Fe (II) dioxygenases in bacteria, Jia (2017) and her group identified that many 2OG-Fe (II) dioxygenases were misannotated or over-annotated.

The 2OG-Fe (II) dioxygenase superfamily is widely distributed among aerobic life forms in eukaryotes and prokaryotes (Islam et al. 2018). The 2OG-Fe (II) dioxygenases are considered the second largest enzyme family in the plant genome (Kawai et al. 2014), and in bacteria are widely present including in the *Proteobacteria, Actinobacteria, Bacteroidetes, Cyanobacteria* and *Firmicutes* (Jia et al. 2017). However, few studies have focused on the diversity and function of these enzymes in fungi. The *tvox1* gene (TV_93146) of *T. virens* coding for 2OG-Fe (II) dioxygenase contains a 1,074 bp ORF interrupted by two introns (74-bp and 62-bp) close to the 5´ end. The 2OG-Fe (II) dioxygenase superfamily is present in *Trichoderma* spp., including 18 members in the *T. virens*

genome, *T. asperellum* (19), *T. harzianum* (16), *T. atroviride* (14), *T. ressei* (11) and *T. longibrachiatum* (9) (Figure 4.12). TVOX1 has high homology to *T. ressei* (protein ID 58580) and *T. longibrachiatum* (protein ID 1459808). Both these enzymes belong to the 2OG-Fe (II) dioxygenase class (DOX C) and are part of the same phylogenetic clade (Figure 4.12). Interestingly, both these *Trichoderma* species have been reported as being plant symbionts (Onofre et al. 2014; Zhang et al. 2016a). The 2OG-Fe (II) dioxygenases are among the most biochemically flexible enzymes that participate in the metabolism of different secondary metabolites in plants and microbes; for example, gibberellins, ethylene, auxins, salicylic acid, alkaloids, coumarins, glucosinolates, flavonoids, siderophores and antibiotics (Farrow and Facchini 2014; Hausinger 2015; Wu et al. 2016; Islam et al. 2018).

4.4.2 *Trichoderma virens* Δ*tvox1* mutant is involved in growth, conidiation and germination

To study the function of the *tvox1* gene during the *T.* virens-maize interaction and its impact on the *T. virens* phenotype, the gene was deleted. The hypothesis for this mutational analysis was that if the *tvox1* gene has a role during the colonisation process, the disruption of this gene will cause a less efficient *T. virens* colonisation of maize roots. By using *Agrobacterium*-mediated transformation of *Trichoderma,* three independent-stable Δ*tvox1* mutants (12a, 16b and 33c) were generated and positively confirmed by homologous recombination. These results corroborated that the WT strain contains a single copy of *tvox1* gene in the *T. virens* genome which was replaced by the insertion of a single copy of a KO cassette in the three mutants that were selected for this study. Phenotypic characterisation of Δ*tvox1* mutants showed that they differed in growth, conidiation and gemination compared to the WT (Figure 4.15). Similar findings were reported by Mukherjee et al. (2018), in the study of a gene of *T. virens* involved in secondary metabolism, showing that the mutation of non-ribosomal peptide synthase TvTex10 that is implicated in the biosynthesis of an intracellular siderophore (ferricrocin) affected the growth and conidiation of *T. virens*. Secondary metabolism is associated with growth and developmental processes in filamentous fungi (Calvo et al. 2002). For example, the gene encoding *T. virens* Vel1 is a key regulator of biocontrol and participates secondary metabolism (antibiosis). Its deletion mutant also had altered growth and conidiation (Mukherjee and Kenerley 2010). The knockout of a terpene synthase (Vir4) in *T. virens* had a lower growth rate compared to the parental strain (Crutcher et al. 2013). All these findings suggest that secondary metabolism genes in *T. virens* have a direct impact on fungal growth and development. Nevertheless, new studies such as transcriptomics and metabolomics on these deletion mutants, including *tvox1*, are required to have a better understanding of how secondary metabolism gene clusters are regulated, and their influence on the metabolic flux of the fungus, having a direct impact on fungal growth and development.

4.4.3 *Trichoderma virens tvox1* is involved during colonisation of maize roots

The role of fungal 2OG-Fe (II) dioxygenases during plant-microbe interactions is largely unknown. Endophytic colonisation is a multifactorial process, where a vast array of molecules from both interacting partners take part. Therefore, there is an interest to understand the role of these molecules during the colonisation process. For example, in the present study, endophytic colonisation was evaluated on Δ*tvox1* mutants in a soil-assay after 7 d.p.i using a semiquantitative technique. Significant differences were observed in the efficiency to colonise maize roots. Deletion mutants were impaired in their ability to colonise roots in comparison to the WT (Figure 4.16). In *Trichoderma*, many studies have been focused on the interaction with its host plant. The deletion of hydrophobin-like elicitor, Sm1 in *T. virens*, that was expressed in the presence of the host plant, showed similar patterns of colonisation with respect to the WT (Djonović et al. 2007). The deletion of an ACC deaminase gene involved in plant growth-promotion in the rhizocompetent *T. asperellum* did not affect the ability to colonise canola seedlings (Viterbo et al. 2010). Also, the disruption of the *tvpg2* gene (endopolygalacturonase) in the *T. virens* genome did not affect the success of rhizosphere colonisation (Sarrocco et al. 2017).

In contrast, the *T. asperellum* hydrophobin gene, *TasHyd1*, was found to be essential for root attachment and colonisation of cucumber (Viterbo and Chet 2006), and recently, for the class II hydrophobin gene in *T. virens*, *tvhydii1*, its deletion mutant resulted in a reduction in colonisation of tomato roots (Guzman-Guzman et al. 2017). These results suggest that different genes participate during *Trichoderma*-plant interactions; however, some of them may play more important functions during fungal colonisation of host roots. Furthermore, the reason why Δ*tvox1* mutants were less effective in colonising the maize root system than the WT at this point is still unclear. Thus, further characterisation of the gene was performed.

4.4.4 *Trichoderma virens tvox1* role in siderophore production, iron uptake/storage, oxidative stress resistance and pigmentation

Based on the results obtained from the endophytic analysis the function of *tvox1* was evaluated, and in which biological process the fungi may be involved was investigated. Iron is indispensable for the correct function of 2OG-Fe (II) dioxygenases (Islam et al. 2018). Thus, iron uptake and storage from the environment into the cell is an essential task accomplished by the ferric iron-specific chelators referred to as siderophores. Additionally, it has been reported that 2OG-Fe (II) dioxygenases participate in the biosynthesis of siderophores (Nakanishi et al. 2000). For that reason, the impact of Δ*tvox1* mutants in siderophore production and intracellular iron content was investigated. By using the CAS-agar assay (semiquantitative), the siderophore production (halo) of *T. virens* WT and Δ*tvox1* was examined. Siderophore activity was detected in both WT and Δ*tvox1* mutants in the presence of two different nitrogen sources (ammonium and nitrate). When either ammonium or nitrate were supplemented in the media, there was a reduction in siderophore

production by the deletion mutants compared to the WT. This suggests that *tvox1* may have a role in the regulation of siderophores and be influenced by other metabolic factors such as nitrogen source availability. Several studies have demonstrated that nitrogen regulates secondary metabolism production in plants, fungi and bacteria (Kerry et al. 1988; Fritz et al. 2006; Liu et al. 2010). In cyanobacteria, siderophore production was directly influenced by the available nitrogen source (Kerry et al. 1988). In *Trichoderma,* low nitrogen levels favour the production of the volatile compound 6-pentyl-alpha-pyrone (Zeilinger and Schuhmacher 2013). Therefore, it cannot be discounted that the changes observed in the siderophore production in both media supplemented with different nitrogen sources may directly impact on siderophore activity in *T. virens*.

To continue with the characterisation of *tvox1,* a complemented *tvox1* mutant was generated. From ten confirmed complementing mutants (C*tvox1*), the transformant (34a) was selected because it had a single copy of the complementing cassette (Figure 4.18 D). To understand the influence of iron on siderophore production, iron uptake and storage in *T. virens* strains (WT, Δ*tvox1* and C*tvox1*), siderophore levels and intracellular iron content were analysed, using different concentrations of iron and nitrate or ammonium as nitrogen sources. Internal iron concentration regulates the expression of siderophore biosynthesis and iron uptake systems, where siderophores have a primary function for the transport of iron, but also serve as intracellular iron storage compounds (Renshaw et al. 2002). *T. virens* secretes 13 different siderophores (Lehner et al. 2013). In addition, the intracellular siderophore ferricrocin that participates in iron storage and oxidative stress protection in *Aspergillus fumigatus* (Wallner et al. 2009), in *T. virens* is involved in growth conidiation and induction of systemic resistance (Mukherjee et al. 2018). Interestingly, the prediction of protein-protein association of TVOX1 with other *T. virens* proteins revealed its possible interaction with three *T. virens* NRPs including Tex1 that participates in the synthesis of peptaibols. *Trichoderma* NRPs are responsible for the biosynthesis of peptaibiotics, epidithiodioxopiperazines, and siderophores (Zeilinger et al. 2016). Therefore, the putative interaction of TVOX1 with these proteins may be related with the production of siderophores in *T. virens*.

In all *T. virens* strains siderophore production was observed when the iron was depleted, confirming that siderophores being produced in response to iron-limited conditions and their biosynthesis controlled by iron availability (Neilands 1995). Interestingly, in ammonium supplementation, siderophore production in all the strains was drastically reduced in the presence of iron (Figure 4.20 E). However, in nitrate addition, different responses were observed; shifts in siderophore production were detected in Δ*tvox1* and C*tvox1* mutants when the iron was supplemented (Figure 4.20 F). This seemingly is the first report which links the deletion of fungal 2OG-Fe (II) dioxygenases with differences in siderophore production when compared to the parental strain. The *Δtvox1* and *Ctvox1* mutants both showed a different response in the production of siderophores in the presence of iron when compared to the WT, suggesting that an alteration to internal iron concentration may influence siderophore synthesis. It has been suggested that 2OG-Fe (II)

dioxygenases are involved in iron sensing which leads to a metabolic effect (Vigani et al. 2013). Therefore, one of the possible functions of *tvox1* may be related to iron sensing inside the cell influencing the biosynthesis of siderophores. Moreover, an increase in intracellular iron contents in the Δ*tvox1* and *Ctvox1* mutants in the presence of ammonium showed an over accumulation of iron in comparison to the WT. In contrast, the opposite phenotype was observed under nitrate conditions, where a reduction of the intracellular iron content was shown in the mutants. These findings suggest that nitrogen also alters physiological processes in *T. virens;* for example, iron acquisition and storage. Thus, given that one of the functional processes of 2OG-Fe (II) dioxygenases is that they can maintain iron homeostasis inside the cell (Kundu 2015), and based on the result presented it is hypothesised that *tvox1* may participate in the regulation of iron content in the cytoplasm of *T. virens* cells.

Furthermore, resistance to oxidative stress under different iron conditions was evaluated in all *T. virens* strains. ROS can be produced by the inadequate storage of iron inside cells, and one of the mechanisms to overcome ROS is by the expression of enzymes such as peroxidases and catalases that need iron as a cofactor that catalyse the decomposition of these toxic molecules (Dixon and Stockwell 2014). Production of ROS is one of the main defence mechanisms utilised by plants under microbe encounters (Qi et al. 2017). As shown in Figure 4.22, iron-sufficient conditions negatively impacted Δ*tvox1* mutant growth, but not significant differences were observed under other iron conditions. The Δ*tvox1* mutant grew faster than the WT as presented previously in the phenotypic analysis (Figure 4.15 and Figure 4.22), and the C*tvox1* mutant had an intermediate growth between the other two strains. In the presence of H_2O_2 but not in the presence of iron-chelator BPS, the growth of *T. virens* strains was significantly reduced. Interestingly, Δ*tvox1* and C*tvox1* mycelia showed higher hypersensitivity to H_2O_2 than the WT under iron-limited and -sufficient conditions (Figure 4.22). In the fungus *Nomuraea rileyi*, the deletion of a L-ornithine-N^5-monooxygenase (*NrSidA*) that is involved in the synthesis of siderophores resulted in reduced ROS detoxification under iron-limiting conditions (Li et al. 2016a). Brandon et al. (2015) proposed that iron regulation is essential for oxidative stress resistance in *Aspergillus fumigatus*. Thus, this suggests that the misregulation of iron homeostasis in the *tvox1* deletion mutant could have a direct effect on the resistance to oxidative stress molecules, leading to a reduction in growth in the presence of H_2O_2.

In this study, during the characterisation of *tvox1* under iron supplemented conditions, *T. virens* WT strain produced a melanin-like pigment (Figure 4.20, Figure 4.21 and Figure 4.22), but it was absent in the Δ*tvox1* and C*tvox1* mutants. Under stress conditions, fungi produce melanin (Philpott 2006). Fungal pigments protect fungi against different exogenous stresses; for example, ROS (Jacobson 2000). Melanin produced by fungi can bind to significant amounts of iron (Senesi et al. 1987), that may help to reduce the excess of iron in the environment that could lead to the formation of harmful radicals. In other fungal models, the alteration in iron uptake by the deletion of genes involved in siderophores biosynthesis leads to mutants defective in production of

pigmentation (Oide et al. 2006; Chen et al. 2013a; Li et al. 2016a). These findings suggest that *tvox1* may participate in the regulation of melanin-like pigments under different iron conditions.

Furthermore, based on the results obtained during the phenotypic characterisation of *tvox1* mutants, it was shown that the C*tvox1* did not recover the expected phenotype compared to the WT strain (siderophore and melanin-like pigment production). In addition, colony appearance of the C*tvox1* mutant growing on PDA media looked more similar to Δ*tvox1* than to the WT strain (Supplementary Figure 14). However, RT-qPCR results provided evidence that *tvox1* was expressed in the C*tvox1* (Figure 4.19), and showed partial responses in the intracellular iron storage and sensitivity to H_2O_2 under iron-limited conditons when compared to the WT and Δ*tvox1* mutant. Similar to our findings in relation to complementing *tvox1* mutant, partial complementation is not an isolated case in *T. virens*. Mukherjee and Kenerley (2010) and Crutcher et al. (2013) had demonstrated that the complementation mutants of two secondary metabolism-related genes (*vel1* and *vir4*) did not completely recover the phenotype of the WT strain. Secondary metabolism-related genes in filamentous fungi including *Trichoderma* usually form part of biosynthetic gene clusters (Zeilinger et al. 2016). In this study it has been proposed that *T. virens tvox1* regulates secondary metabolism and belongs to a putative-gene cluster (Supplementary Figure 5), where neighborhood genes such as methyl transferase (TV_51972) and major facilitator transporter (TV_78422) are likely elements of the putative biosynthetic *tvox1* cluster. Other studies have shown that the deletion of metabolism-related genes modify the expression levels of genes that belong to the same cluster (Yu and Keller 2005; Pachauri et al. 2018). Therefore, it will be interesting to analyse the expression levels of the genes that belong to the putative *tvox1* cluster in the the different *T. virens* strains (WT, Δ*tvox1* and C*tvox1*) and how this are regulated during the interaction with maize roots. However, it cannot be discarded pleiotropy in the knockout mutant or that other factors may be affecting complementation mutant such as epigenetic changes and/or mutations during transformation that may influence the phenotype of the fungus.

4.4.5 Putative role of *Trichoderma virens tvox1* gene during plant-microbe interaction

Evolution of mechanisms by plants and microbes based on acidification, chelation, and/or reduction processes for iron acquisition have led to the development of complex interactions; for example, mutualism and competition (Lemanceau et al. 2009). In the rhizosphere, competition for iron is highly demandant, favouring those microorganisms that have develop more effective high-affinity iron uptake strategies. During plant-microbe interactions, the capacity of both organisms to trigger changes in iron homeostasis directly impact host immunity. Plant iron-related defence strategies used against microbes involved a) iron-withholding or b) increase iron levels to trigger oxidative burst (Verbon et al. 2017). As a response, plant associated microbes secrete iron-scavenging siderophores that facilitate iron uptake and minimise iron-regulated host immune responses (Lemanceau et al. 2009). *Trichoderma* spp. secrete siderophores and modulate iron

homeostasis, which offers environmental advantages when interacting with plants (Lehner et al. 2013; Vinale et al. 2013; Mukherjee et al. 2018). In the present research, it was found that the *tvox1* deletion mutant showed a deficiency in siderophore production, iron regulation and oxidative stress resistance. Therefore, based on the importance of the interplay between iron homeostasis and host immunity responses, these findings suggest that the alteration in iron regulation processes of the *T. virens Δtvox1* mutant resulted in the deficiency in endophtysim. Iron incorporation is also essential for the maize pathogens such as *U. maydis* and *Cochliobolus heterostrophus* which highlights the relevance of iron-mediated mechanisms in plant-microbe interactions (Eichhorn et al. 2006; Oide et al. 2006). Even though iron is necessary for the establishment of plant-microbe interactions, it cannot be discarded that TVOX1 may participate in the synthesis of other secondary metabolites that may influence the capability of *T. virens* to endophytically colonise maize roots. Further analyses *in planta* are necessary to understand the role of *tvox1* during the *T. virens*-maize interaction.

4.5 Conclusions

This study elucidated the possible mechanisms of a 2OG-Fe (II) dioxygenases *tvox1* gene in iron regulation of *T. virens* physiology, and during the interaction with maize roots. In summary, *T. virens tvox1* indirectly or directly participates in siderophore production, iron uptake/storage, oxidative stress resistance, pigmentation and the colonisation processes. Further studies are required to understand the possible mechanisms in the regulation of iron by *T. virens tvox1* gene in the rhizosphere.

5 Untargeted metabolic fingerprinting of the *Trichoderma virens*-maize interaction: A closer insight of the metabolic role of 2OG-Fe (II) oxygenase (*tvox1*)

5.1 Introduction

The rhizosphere is an extensively complex ecosystem, where a vast array of organisms coexists. The communication between these organisms that inhabit the soil is regulated by the production of specialised metabolites. High-throughput omics technologies have been used for a better understanding of the facilitation, establishment, and maintenance of the complex interaction between *Trichoderma* and plants. Transcriptome analyses of the *Trichoderma*-plant interaction have been the preferred technique to study the gene expression of both plant and symbiont, which are differentially regulated upon root colonisation (Chacon et al. 2007; Moran-Diez et al. 2015; De Palma et al. 2019). Exploration of modulated proteins during *Trichoderma*-plant interactions has allowed the discovery of the proteomic interplay from both organisms (host plant and fungal symbiont), that influence the establishment of the interaction (Marra et al. 2006; Lamdan et al. 2015; Nogueira-Lopez et al. 2018). Contrary to transcriptomics, proteomics and metabolomics show the activity of the cell, providing a better understanding of interkingdom signalling of plant-specific responses to beneficial microorganisms.

Metabolomics allow the analysis of natural low molecular weight (< 1,000 Da) metabolites synthesised by a cell or tissue under specific conditions (Griffiths et al. 2007; Bundy et al. 2008; Wolfender et al. 2013). The metabolome comprises the complete set of metabolites synthesised by an organism or tissue, under certain conditions (Balmer et al. 2013). The plant kingdom is known to produce a varied diversity of metabolites estimated to be around 200,000 (Dixon and Strack 2003), although most of them remain unknown. The chemical diversity of plant metabolites (polarity, molecular weight and solubility) as well as the abundant differences among them, make the analysis of the chemical composition of plants (phytometabolome) more complex. Ideally, metabolomics tools would provide the capability to monitor, identify and quantify all metabolites present in a sample. However, the analytical methods currently available do not allow this. Plants produce a broad spectrum of metabolites that are either crucial to sustaining plant life (primary metabolites) or non-essential but required for survival in a given environment (specialised metabolites). Specialised metabolites play an important role in signaling and plant defence (Wink 2003).

The phytometabolome is very dynamic and responds to both environmental factors and microorganisms (Schweiger et al. 2014; Vaughan et al. 2018). Phytometabolome modulation can be studied throughout the use of targeted and untargeted metabolomics. Targeted metabolomics identifies and quantifies already known metabolites; in contrast, untargeted metabolic

fingerprinting allows the generation and comparison of metabolic phenotypes that change in a given biological system (Wolfender et al. 2013). Of all the 'omics' technologies, metabolomics offers the most functional information (Fiehn et al. 2000), which facilitates an overview of the chemical composition of the sample and enables monitoring metabolic shifts triggered by specific biotic or abiotic stimuli (Wolfender et al. 2013).

Metabolomics analyses provide large and complex datasets, and thus accurate data processing, statistical analysis and suitable data storage formats are fundamental (Allwood et al. 2008; Issaq et al. 2009). Moreover, the complexity regarding data analysis and interpretation obtained from metabolic fingerprinting is one of the main bottlenecks for the identification of metabolites. The main limitation for metabolite identification from plant samples is that most specialised metabolites tend to be species-specific and there is a lack of complete plant-metabolite databases. Despite these drawbacks metabolomic studies represent an important complement to the other "omics" technologies that are used in biological systems, and have yielded significant new biological knowledge (Wolfender et al. 2013). Nowadays, two main approaches are used for metabolic fingerprinting, Nuclear Magnetic Resonance (NMR) and MS-based metabolomics. NMR-based metabolomics facilitates the direct analysis of plant crude plant extracts (without chromatographic separation), providing quantitative information and structural composition of metabolites. However, the most significant limitation is its low sensitivity (Wolfender et al. 2013). On the other hand, MS-based metabolomics allows the sensitive detection of most plant metabolites (Hall 2006); MS can be performed by the direct injection of the samples into the mass spectrometer, or samples can be separated prior to injection by gas or liquid chromatography or capillary electrophoresis (GC-MS, LC-MS and CE-MS).

Recently, there has been an increased use of metabolomics to characterise plant responses to environmental conditions, and to unravel the mechanisms behind plant-plant, plant-herbivore and plant-microbe interactions (Bundy et al. 2008; Peters et al. 2018). Specifically, metabolomics has focused on studying the phytometabolome shifts triggered by environmental conditions (drought, salt tolerance) and plant pathogens (herbivores, nematodes or fungi) (Peters et al. 2018). The use of metabolomic approaches to unravel plant-symbiont interactions has just started to emerge.

Beneficial interactions between plants and arbuscular mycorrhizal fungi (AMF) are the most well characterised using metabolic approaches. Overall targeted metabolomics of AMF-plant interactions have revealed modulation of the core primary metabolism and differences in the secondary or specialised metabolites content (phenolic compounds, phenolic acids, iridoid glycosides, alkaloids) to understand systemic plant responses mediated by AMF colonisation (Subramanian and Charest 1995; Ceccarelli et al. 2010; Andrade et al. 2013; Wu et al. 2013; Schweiger and Muller 2015). However, it was not until the report from Schweiger et al. (2014) that a comprehensive metabolic approach combining a targeted metabolite profiling (carbohydrate, organic acids, sugars, alcohols and amino acids) with untargeted metabolic fingerprinting, was

implemented to achieve a better understanding of how core phytometabolome shifts occurred due to beneficial microorganisms in a species-specific manner. The effect of AMF on the maize leaf metabolome has been explored in the last decade; for instance, Sheng et al. (2011) evaluated shifts in leaf primary metabolism induced by AMF colonisation under salt stress, showing it was differentially modulated during the maize roots-AMF interaction.

Trichoderma spp. root colonisation has a direct impact on phytohormone content, soluble sugars, amino acids, phenolic compounds, citric cycle intermediates and polyamines (Yedidia et al. 2003; Brotman et al. 2012; Vinci et al. 2018). Under *in vitro* conditions, Mazzei et al. (2016) evaluated the effect of two specialised metabolites synthesised by *Trichoderma* (6-pentyl-α-pyrone (6PP) and harzianic acid isolated from *T. atroviride* and *T. harzianum*, respectively) on the metabolome modulation of tomato leaves by Proton HRMAS NMR spectroscopy. Overall, the metabolic profile of tomato leaves treated with 6PP and harzianic acid revealed that phytometabolome modulation was dose-dependent, showing significant differences in amino acids, sugars, and GABA. Additionally, the phytometabolome modulation of maize leaves following *T. harzianum* root colonisation in soil, comparing different phosphate fertilisers was examined by Vinci et al. (2018). They showed that primary maize leaf metabolism, total phosphorus (P) and nitrogen (N) content, were not only modulated by the *T. harzianum*-maize roots interaction, but also by the type of phosphate fertilizers applied. Remarkably, the combination of both organic phosphate-fertilisers and *T. harzianum* significantly increased P, N and chlorophyll content in comparison to non-inoculated plants. Metabolomic analyses carried out in the last few years have increased the knowledge of the phytometabolome modulation by *Trichoderma* root colonisation, but the metabolic events activated in plants in response to *Trichoderma* colonisation are mostly unknown.

During endophytic interactions, the disruption or alteration of essential encoding genes that are up-regulated during the symbiotic relationship may lead to a potent immunological plant response against the foreign coloniser. Previous results demonstrated that *T. virens* 2OG-Fe (II)-dependent oxygenase encoding the gene *tvox1* participate in *Trichoderma* secondary metabolism and indicated that the deletion of this gene affects the capability of *T. virens* to colonise maize roots under soil conditions. Therefore, non-targeted metabolomics was applied to investigate the metabolic responses of the host to *Trichoderma* colonisation. The use of non-targeted metabolomics allows the detection of a broad range of primary and secondary metabolites in a single experiment to aid an understanding of the endophytic interaction with the host plant (Schweiger et al. 2014). The aim of this chapter is a) elucidate the metabolic responses during the *T. virens*-maize interaction by comparing two *T. virens* genotypes (WT and Δ*tvxo1*), and b) how the absence of *tvox1* gene affects the intra- and extracellular metabolome in *T. virens*.

5.2 Material and methods

5.2.1 *Trichoderma virens* endophytism under hydroponic growth conditions

To test the endophytic colonisation of the *T. virens* WT and the *tvox1* deletion mutant, the methodology described in section 4.2.6.4 was used with modifications. Endophytism was assessed under hydroponic growth conditions. Maize sterile seedlings were grown in sterile 50 mL falcon tubes containing 45 mL of Hoagland´s solution supplemented with filtered sterilised 0.5% sucrose (Sigma-Aldrich, USA) and placed inside sterile cereal boxes. Plants were incubated for 60 h following conditions described in section 2.2.3 and using a randomised complete block design. Endophytism was recorded by *T. virens* presence/absence after 5 d.p.i (25°C in darkness), where each root piece colonised was considered as a 20% of colonisation. A total of nine biological replicates were used for this experiment and it was repeated twice.

5.2.2 Sample collection for metabolic fingerprinting analysis

5.2.2.1 Root tissue

Maize seeds (inbred line 34H31) were surfaced sterilised and inoculated with *T. virens* (WT and Δ*tvox1*) conidia suspension ($1x10^6$/seed) describe in sections 2.2.1 and 2.2.3. Un-inoculated (control) and inoculated seeds were placed on sterile-damp germination paper and incubated in sterile cereal boxes for 60 h using a humidity controlled incubator at 25°C with 16 h light/8 h dark cycle and a relative humidity of 80%. Seedlings were transferred to sterile 50 mL falcon tubes containing 45 mL of sterile Hoagland´s solution supplemented with 0.5% sucrose and placed inside sterile cereal boxes. Seedlings were incubated for another 60 h under the same conditions, using a randomised complete block design. Roots were excised and immediately frozen in liquid nitrogen to quench their metabolism. Plant material was stored at -80°C until all plants were sampled. Root samples were freeze-dried (Thermo Savant Micro Modulyo-115, Thermo Fisher Scientific, USA), and then ground until a fine powder was obtained (1600 Mini6, SPEX SamplePrep, USA) at 1,000 rpm.

5.2.2.2 Mycelia and supernatant

Conidia of *T. virens* (WT and Δ*tvox1*) were harvested from 7 d old PDA plates using 5 mL of sterile nanopure water and filtered through two layers of sterile Miracloth. *Trichoderma* conidia ($1x10^6$) were inoculated into 100 mL sterile flasks previously washed with 0.6 M HCl and sterile nanopure water. Sterile flasks were filled with 50 mL of Hoagland´s solution basal salt no. 2 supplemented with 0.5% sucrose. Flasks were incubated using a randomised complete block design at 25°C at constant shaking (150 rpm) (Orbital Mixer Incubator, Australia). After 72 h, fungal cultures were filtered with two layers of sterile Miracloth to separate the mycelia from the supernatant. Mycelia fragments were snap frozen with liquid nitrogen and stored at -80°C. The secreted fraction was filtered through a 0.2 µL membrane, and samples were stored at -80°C. Mycelia and supernatants

were freeze-dried. Fungal tissue was ground until a fine powder was obtained as described in previous section. Un-inoculated sterile culture media was used as a control.

5.2.3 Sample preparation for metabolic fingerprinting analysis

For metabolic fingerprinting, 4 and 6 mg (±0.1 mg) of dried-ground roots and mycelia material were used, respectively. For the fungal secreted fraction analysis, all freeze dried material generated from the 50 mL cultures was used. Root, mycelia and supernatant material were extracted threefold on ice using 130 µL, 50 µL and 200 µL of 90% cold methanol (LC-MS grade) (Sigma-Aldrich, USA), respectively. The extraction solution was supplemented with 0.5 mg/100 mL of hydrocortisone (> 98%, Sigma-Aldrich, USA) as an internal standard (pH 7). Samples were homogenised by vortexing for 5 s, followed by a second vortex round of 5 min. Samples were centrifuged for 10 min at 13,200 x g at 4°C. After each extraction phase, the supernatant was transferred to new 2 mL microcentrifuge tubes (Eppendorf, Germany). The total volume of supernatant recovered (250-300 µL) was filtered into an autosampler vial with a glass insert using a 0.2 µm filter (Phenomenex, USA). Vial caps were used to seal the vials using an 11 mm crimper, for subsequent metabolic fingerprinting analysis.

5.2.4 UHPLC-DAD-ESI$^-$-QTOF-MS/MS samples measurement

The metabolic fingerprinting analysis was done via ultra-high performance liquid chromatography connected to diode array detection and quadrupole time of flight mass spectrometry (UHPLC-DAD-ESI$^-$-QTOF-MS/MS; UHPLC: Dionex UltiMate 3,000, Thermo Fisher Scientific, USA; QTOF: Compact, Bruker Daltonics, Germany). The Compass 1.9 software (Otof control 4.0 and Hystar 3.2, Bruker Daltonics) was employed to perform the analysis. The sample tray was maintained at 5°C, injection volumes were 3 µL for roots and supernatant samples and 4 µL for mycelia samples. After injection, compounds were separated at 45°C on a Kinetex XB-C18 column (1.7 µm, 150 x 2.1 mm, with a pre-column, Phenomenex, USA). Separation was performed using a multi-step gradient from eluent A [0.1% formic acid (eluent additive for LC-MS, > 98%, Sigma-Aldrich, USA) in Millipore-H_2O] to eluent B [0.1% formic acid in acetonitrile (LC-MS grade, Fisher Scientific, UK)] using a flow rate of 0.5 mL min^{-1}: 2% B to 30% B within 20 min, followed by 30% B to 75% B within 9 min, continuing with column washing and re-equilibration. DAD spectra (210-400 nm) were recorded, as were line spectra (50-1,500 *m/z*) in MS and MS/MS modes using negative electrospray ionisation (ESI) at 8 Hz. The parameters were: end plate offset: 500 V, capillary voltage: 3,000 V, nebulizer (N_2) pressure: 3 bar, dry gas (N_2) flow and temperature: 12 L min^{-1} at 275°C, quadrupole ion energy: 4 eV, low mass: 90 *m/z*, collision energy: 7 eV, transfer time: 100 µs, pre-pulse storage: 5 µs. Auto MS/MS was carried out using N_2 as the collision gas, and the following settings were applied: 50-1,500 *m/z*, precursor ions: 3, absolute threshold: 1,980 counts, no charge state restrictions, active precursor exclusion after 2 spectra, precursor reconsideration after 0.2 min, in case the current intensity was at least 3X higher than the one which preceded it, and smart exclusion with a threshold of 3

(current/previous intensity). Isolation width and collision energies were from 8 Da and 25 eV, respectively. A sodium formate based calibration solution was injected into the ESI sprayer prior to each sample to perform mass axis recalibration.

5.2.5 Data analysis

The picking of molecular features and spectral background subtraction were performed using the Find Molecular Features (FMF) algorithm in Compass DataAnalysis 4.4 (Bruker Daltonics, Germany). The FMF parameters were: signal-to-noise ratio of three, correlation coefficient threshold of 0.75, minimum compound length of 25 (roots) or 30 (mycelia and supernatant); and smoothing width of seven for all samples. The ion types permitted for bucket generation were the following: $[M-H]^-$, $[M-H2O-H]^-$, $[M+HCOOH-H]^-$, $[M+CH3COOH-H]^-$, $[M+Cl]^-$, $[2M-H]^-$, $[2M+HCOOH-H]^-$, $[2M+CH3COOH-H]^-$ and $[3M-H]^-$. Compounds were aligned across samples with Compass ProfileAnalysis 2.3 (Bruker, Daltonics, Germany) using the *m/z* with the highest intensity as the bucketing basis for every compound. Advanced bucketing was performed, allowing deviations of 0.1 min (retention time) and 5 mDa *(m/z)*, respectively. Data were normalised to the intensities of the hydrocortisone adduct $[M+HCOOH-H]^-$ ion. Additionally, compounds were maintained according to two different criteria: 1) if the compound mean intensity in at least one treatment group was more than 50X higher than the mean in the blanks, and 2) if the compound occurred in at least half of the replicates of at least one group. Data were normalised to dry weights of the samples (except for the supernatant samples). Zero values were substituted by small random numbers (10-13-10-12) with R software 3.4.1 version (https://www.r-project.org/). Principal component analysis was performed after auto-scaling (i.e., mean-centering and scaling to unit variance) using R software. For selected pairwise group comparisons, those compounds which occurred in at least half of the samples of at least one treatment group were retained. For supernatant samples, those compounds that were present in the control groups were left out. Volcano plots were created in Matlab (Mathworks Inc., USA) based on fold changes of compounds (i.e., mean intensities in the treatment group divided by mean intensities in the control group), and P-values resultant from Mann-Whitney U-tests were calculated in Matlab. Venn diagrams were generated in R software using the gplots package.

5.2.6 Compound identification

For compound identification, the metabolic features for which intensities were modulated ($P<0.05$ in Mann Whitney U-test: fold change < 0.5 or > 2) by *T. virens* colonisation were chosen. In addition, the targeted maize-defence related metabolite (DIMBOA-glu) was also selected for identification by measuring the commercial standard using methodology described in section 5.2.4. The selection of modulated metabolic features was based on the Venn diagram data generated, by choosing those which represented general and specific responses to each genotype. Compound identification was performed using Compass Data Analysis 4.4, using the base peak chromatogram

of the replicate with the highest peak intensity for each metabolic feature of interest. For the determination of the sum formula the following parameters were considered: a) ion types permitted $[M-H]^-$, $[M-H2O-H]^-$, $[M+HCOOH-H]^-$, $[M+CH3COOH-H]^-$, $[M+Cl]^-$, $[2M-H]^-$, $[2M+HCOOH-H]^-$, $[2M+CH3COOH-H]^-$ and $[3M-H]^-$, b) enable tolerance (2 mDa), and c) ion charge (-1). Two metabolic databases were used, including, PubChem (Bolton et al. 2008) and Chemspider (Pence and Williams 2010) that have robust and extensive datasets of compound name and exact mass of organic molecules from plant and fungi. Levels of compound identification were determined as described by Longnecker et al. (2015). The putative classification of the metabolic features of interest into chemical classes was done by combining the sum formulas previously determined, and the chemical structures obtained from the databases, according to Irchhaiya et al. (2014) and Kabera (2014).

5.3 Results

5.3.1 Endophytism of *Trichoderma virens* under hydroponic growth conditions

Colonisation of maize plants was tested to assess the ability of *T. virens* WT and Δ*tvox1* strains to endophytically colonise maize roots under hydroponic growing conditions. The results showed that maize growth was inhibited by the presence of *T. virens* strains when compared with the control plants (Figure 5.1 A). In addition, *T. virens* WT and Δ*tvox1* were able to internally colonise maize primary roots after 5 d.p.i (Figure 5.1 B). However, no significant differences in root colonisation were observed between strains (P>0.05) (Figure 5.1 C).

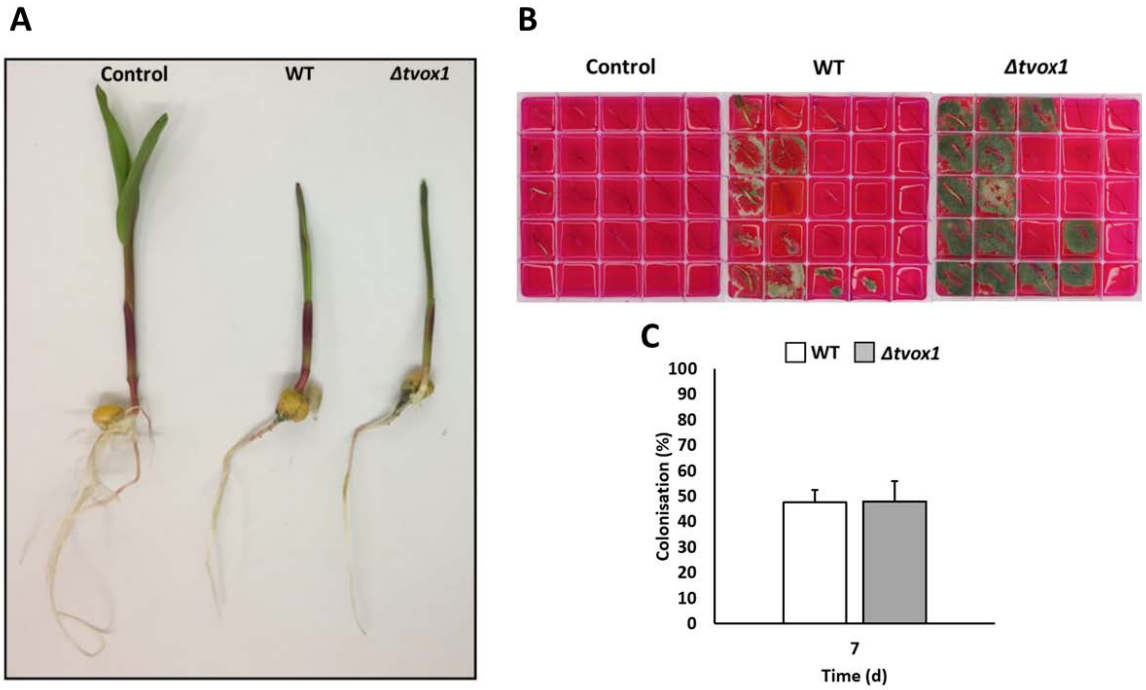

Figure 5.1 Endophytic colonisation of maize seedlings grown in an hydroponic system by *T. virens* WT and Δ*tvox1* strains. (A) Un-inoculated and inoculated (WT and Δ*tvox*1) maize plants with *T. virens* growing under hydroponic growth conditions. **(B)** Surface sterilised primary root sections placed on *Trichoderma* selective medium (TSM) to observe *T. virens* endophytic colonisation. **(C)** Percentage of root fragments colonised by *T. virens* strains under hydroponic growth conditions. Data were presented as mean ± SD of replicates. Statistical comparison between treatment groups were carried out using general ANOVA followed by Fisher's Unprotected LSD algorithm. All statistical analyses were performed using GenStat 18th software.

5.3.2 Metabolic fingerprinting of *Trichoderma virens*-maize interaction

To study *Trichoderma*-maize interaction, the untargeted metabolic fingerprinting approach (via UHPLC-DAD-ESI$^-$-QTOF-MS/MS) of methanolic root, mycelia and supernatant extracts was performed. Overall, the results revealed changes in the root metabolome (local response) comparing two different *T. virens* genotypes (WT and Δ*tvox1*) when interacting with their host plant. Furthermore, modifications in mycelia and supernatant metabolomes of the *T. virens* deletion mutant (Δ*tvox1*) were identified in comparison with the parental strain (WT).

5.3.2.1 *Trichoderma virens* colonisation triggers local response in maize roots

The untargeted metabolic fingerprinting of root extracts allowed the detection of a total of 487 different metabolic features during the interaction of maize roots with *T. virens*, including, 256 features present in the control plants. In contrast, in treated plants (WT and Δ*tvox1*) 377 and 379 features were detected, respectively. Based on retention times and peak areas, a data matrix was built to compare treatments groups by principal component analysis (PCA). The total variance explained by axes 1 and 2 showed 37% variability among treatments, where a prominent distribution of metabolic phenotypes between inoculated and un-inoculated roots was observed

(Figure 5.2). Interestingly, the metabolome during *T. virens*-maize roots interaction was separately clustered for each *T. virens* genotype, shown by axis 2 (Figure 5.2).

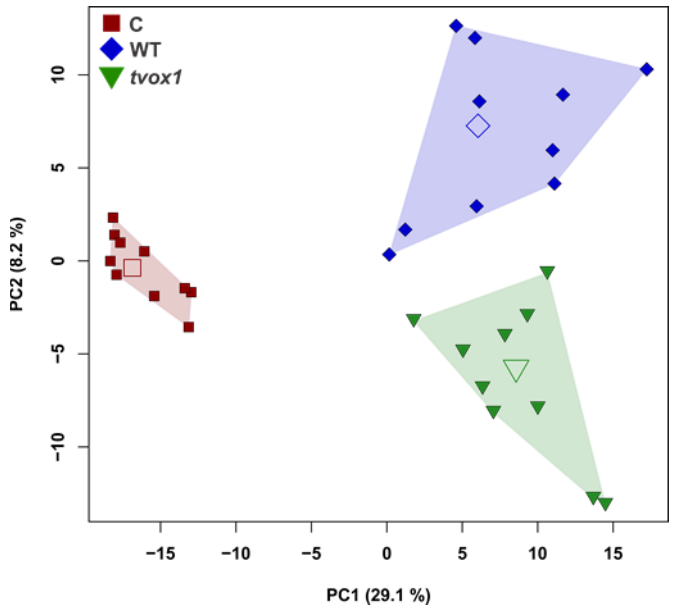

Figure 5.2 *Trichoderma virens* modulates maize roots metabolome. Metabolic pattern of maize roots inoculated with *T. virens* (WT and Δ*tvox1*) and un-inoculated roots (C) by principal component analysis (PCA). Total variance explained by the first two PCs in brackets. Median scores shown as larger symbols for each treatment. Groups surrounded by convex hulls. *n* = 10 biological replicates.

To underline the influence of *T. virens* colonisation in maize root metabolome, and to highlight the modulated metabolic features induced by the different *T. virens* genotypes in comparison with un-inoculated plants, two thresholds (Mann-Whitney U-test, $P<0.05$ and fold change of < 0.5 or > 2 for decreased or increased metabolites, respectively) were implemented. The results showed that the colonisation of the two genotypes of *T. virens* in maize roots, induced a similar responsiveness (percentage of modulated compared to all features) (WT: 12% and Δ*tvox1*: 11%) of decreased plant metabolic features (Figure 5.3 A). Additionally, a high responsiveness was observed in increased metabolic features (WT: 46% and Δ*tvox1*: 42%) which is given by both plant and fungal features, showing that the responsiveness to the WT was higher in relation with the other genotypes (Figure 5.3 A). Overall, these results underline differences in the proportions of metabolic features being decreased or increased during the interaction, showing that a strong modulation of the maize root metabolome occurs in the presence of *T. virens*. An overlapping response of decreased and increased modulated metabolic features comparing all genotypes showed a general response of maize roots to *T. virens* colonisation. Specific responses to each *T. virens* genotype were also detected (Figure 5.3 B). From the total of decrease features, the general response of maize roots to *T. virens* colonisation was represented by 38 (58%) metabolic features. Specific responses of maize roots to each genotype showed that the highest specificity was found in the roots treated with the Δ*tvox1* (17%), followed by the WT (25%) (Figure 5.3 C). Moreover, it was found that the general response of increased metabolic features is explained by 145 (60%) different metabolic

features, which belong to both organisms; whereas specific responses showed higher values of specificity in the WT than Δ*tvox1* (WT: 57 (24%) and Δ*tvox1*: 38 (16%)) (Figure 5.3 D).

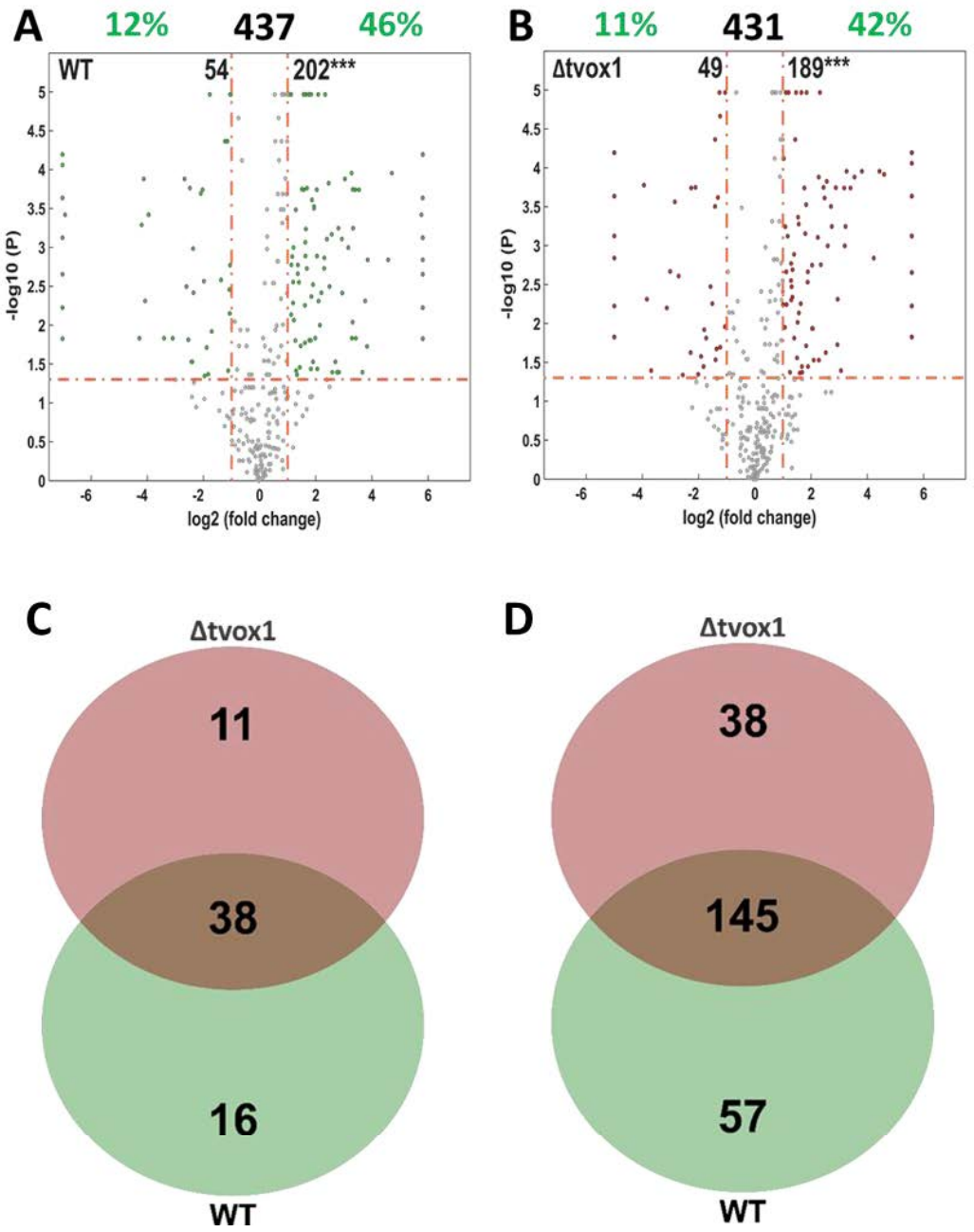

Figure 5.3 Maize root metabolome is modulated by *T. virens* in a genotype-dependent manner. Metabolic features modulated by *T. virens* **(A)** WT and **(B)** Δ*tvox1* shown as a coloured circle outside the cut off-lines in volcano plots. Features in the left parts of the plots had lower intensities in *T. virens*-inoculated compared to uninoculated plants, whereas those in the right part had higher intensities. Green numbers represent the metabolic responsiveness (percentage of modulated compared to all features) to each *T. virens* genotype. Bold numbers (top center) represent the total number of metabolic features found for each treatment comparison. The feature numbers of decreased versus increased features were compared (χ2-tests; ****P*<0.001). Features modulated **(C)** left: decreased and **(D)** right: increased by the genotypes or specifically by one *T. virens* genotype, presented as Venn-diagrams**.**

In general, these results revealed that metabolic shifts occur when *T. virens* is present in the root system of maize, showing that the metabolome of maize roots was strongly modulated by the colonisation of *T. virens*, with a total of 65 and 240 metabolic features being decreased/increased based on the thresholds selected for the analysis. More importantly, the results showed that the maize root metabolome modulation is *T. virens* genotype-dependent. Furthermore, this is the first report that shows that single knockout mutants on the *T. virens* genome have a direct impact on the metabolome of the symbiotic interaction of *Trichoderma*-maize.

5.3.2.2 Identification of modulated metabolites during *Trichoderma virens*-maize interaction

All the modulated metabolic features detected during the *T. virens*-maize interaction, involving the general and specific responses for the two genotypes (WT and Δ*tvox1*), were selected for identification. A total of 35 increased metabolites were putatively identified; for example, 13 nitrogen-containing secondary metabolites, 11 phenolic compounds, two organic acids, three sugars and six unknown (Table 5.1). Additionally, 15 decreased metabolites were identified, including, seven nitrogen-containing secondary metabolites, five phenolic compounds, and three unknowns (Table 5.2). The majority of the identified metabolites correspond to the general response to *T. virens* colonisation (non-genotype dependent).

5.3.3 Metabolic shifts in *Trichoderma virens* deletion (Δ*tvox1*) genotype

The metabolic fingerprinting of mycelia and supernatant extracts from *T. virens* genotypes (WT and Δ*tvox1*) permitted the detection of 483 and 1,799 metabolic features, respectively. The comparison of the mycelia metabolome showed that the two genotypes shared 242 (50%) metabolic features; while, the supernatant metabolome only shared 379 (21%) features (Figure 5.4 A and B). Interestingly, specific metabolic features were detected for the two genotypes in both assays, which highlighted the effect of the deletion mutant in the *T. virens* metabolic network (Figure 5.4 A and B). The PCA analysis from the mycelia data, highlights that the metabolome of the two genotypes was separately distributed (Figure 5.4 C). The total variance explained by axes 1 and 2 in the mycelia samples was equal to 41%. The distribution of the samples was not influenced by the fungal biomass of each genotype (t test, t=-0343, df=16, *P*=0.7357). In addition, the total variance explained by both axes on the PCA on supernatant samples was higher (54%), than for the mycelia (31%) (Figure 5.4 C and D). The supernatant data also showed a separate distribution of the two genotypes with overlapping caused by independent biological replicates (Figure 5.4 D).

Table 5.1 Putative identification of increased metabolic features modulated during the *T. virens*-maize interaction.

Putative compound Id	Molecular formula	RT (min)	Precursor ion (*m/z*)	Pseudomolecular ion	Chemical group	Treatment
•(E)-3-[3,5-dimethyl-4-(pyridin-4-yl methoxy) phenyl] prop-2-enoic acid*[2]	$C_{17}H_{17}NO_3$	14.94	282.1137	$[M-H]^-$	NSM	WT, Δ*tvox1*
•N-(4-ethoxyphenyl)-2-methyl-2,3-dihydro-1,4-benzodioxine-3-carboxamide[2]	$C_{18}H_{19}NO_4$	15.93	312.1242	$[M-H]^-$	NSM	WT, Δ*tvox1*
•Unknown*[3]	$C_{22}H_{31}NO_{15}$	10.26	594.1678	$[M+HCOOH-H]^-$	NSM	WT, Δ*tvox1*
•Unknown*[3]	$C_{23}H_{27}N_5O_{11}$	10.74	594.1675	$[M+HCOOH-H]^-$	NSM	WT, Δ*tvox1*
•Unknown*[3]	$C_{27}H_{28}N_4O_7$	13.24	565.1925	$[M+HCOOH-H]^-$	NSM	WT, Δ*tvox1*
•Unknown*[3]	$C_{22}H_{26}N_4O_4$	14.98	455.1925	$[M+HCOOH-H]^-$	NSM	WT, Δ*tvox1*
•Unknown*[3]	$C_{19}H_{18}N_8O_2$	2.90	435.1507	$[M+HCOOH-H]^-$	NSM	WT, Δ*tvox1*
•Unknown*[3]	$C_{36}H_{36}N_2O_8$	23.06	623.2397	$[M-H]^-$	NSM	WT, Δ*tvox1*
•2-(6-Benzoyl-1H-benzimidazol-2-yl)-N-4-[5-(3,4,5-trimethoxyphenyl)-1,2-oxazol-3-yl] phenyl benzamide*[2]	$C_{39}H_{30}N_4O_6$	26.76	649.2077	$[M-H]^-$	NSM	WT, Δ*tvox1*
•4-[2-(2-Oxo-3,4-dihydro-1(2H)-quinolinyl) ethyl] morpholin-4-ium 2,4,6-trinitrophenolate*[2]	$C_{21}H_{23}N_5O_9$	5.08	534.1464	$[M+HCOOH-H]^-$	NSM	WT, Δ*tvox1*
•Unknown*[3]	$C_{17}H_{18}N_6O_8$	10.57	479.1156	$[M+HCOOH-H]^-$	NSM	WT
•Unknown*[3]	$C_{22}H_{28}N_4O_5$	11.63	473.2019	$[M-H]^-$	NSM	Δ*tvox1*
•Unknown*[3]	$C_{22}H_{29}KN_2O$	25.20	375.1844	$[M-H]^-$	NSM	Δ*tvox1*

•2-oxoglutarate*[2]	$C_5H_6O_5$	1.03	191.0198	$[M+HCOOH-H]^-$	Organic acid	WT, Δ*tvox1*
•Unknown*[3]	$C_6H_6O_6$	1.54	173.0092	$[M-H]^-$	Organic acid	WT
•5,5'-Methylenedisalicylic acid*[2]	$C_{15}H_{12}O_6$	12.56	287.0561	$[M-H]^-$	Phenolic	WT, Δ*tvox1*
•Dimethyl (2R)-2-[(2-acetyloxy-5-methoxycarbonylphenyl) methoxy] butanedioate*[2]	$C_{16}H_{18}O_7$	6.51	367.1034	$[M+HCOOH-H]^-$	Phenolic	WT, Δ*tvox1*
•Naringenin*[2]	$C_{15}H_{12}O_5$	18.21	271.0614	$[M-H]^-$	Phenolic	WT, Δ*tvox1*
•Phenacyl 2-hydroxy-5-methoxybenzoate*[2]	$C_{16}H_{14}O_5$	13.59	285.0768	$[M-H]^-$	Phenolic	WT, Δ*tvox1*
•Unknown*[3]	$C_{15}H_{14}O_9$	9.18	337.0566	$[M-H]^-$	Phenolic	WT, Δ*tvox1*
•Unknown*[3]	$C_{31}H_{36}O_8S$	11.63	613.2141	$[M+HCOOH-H]^-$	Phenolic	WT, Δ*tvox1*
•Unknown*[3]	$C_{32}H_{38}O_{17}$	13.69	693.2035	$[M-H]^-$	Phenolic	WT, Δ*tvox1*
•Unknown*[3]	$C_{15}H_{12}O_6$	19.19	269.0457	$[M+H2O-H]^-$	Phenolic	WT, Δ*tvox1*
•5-[(2S,3R,4S,5S,6R)-3,4,5-trihydroxy-6-(hydroxymethyl) oxan-2-yl] oxy-3H-1,3-benzoxazol-2-one*[2]	$C_{32}H_{48}O_{15}$	19.73	671.2923	$[M-H]^-$	Phenolic	WT, Δ*tvox1*
•Unknown*[3]	$C_{38}H_{44}O_{20}$	21.98	819.2354	$[M-H]^-$	Phenolic	WT, Δ*tvox1*
•Unknown*[3]	$C_{23}H_{24}O_9$	22.21	443.1346	$[M-H]^-$	Phenolic	WT, Δ*tvox1*
•Lactulose*[2]	$C_{12}H_{22}O_{11}$	0.72	683.2253	$[2M-H]^-$	Sugar	WT, Δ*tvox1*
•Unknown*[3]	$C_5H_{10}O_5$	0.70	195.051	$[M+HCOOH-H]^-$	Sugar	WT, Δ*tvox1*
•Unknown*[3]	$C_6H_{14}O_6$	0.68	181.0715	$[M-H]^-$	Sugar	WT, Δ*tvox1*
•Unknown*[4]	$C_4H_8O_4$	0.70	165.0405	$[M+HCOOH-H]^-$	Unknown	WT, Δ*tvox1*
•Unknown*[4]	$C_{18}H_{39}NO_3$	24.90	362.2911	$[M+HCOOH-H]^-$	Unknown	WT, Δ*tvox1*

•Unknown*[4]	$C_{19}H_{32}O_3S$	25.79	385.2053	$[M+HCOOH-H]^-$	Unknown	WT, Δ*tvox1*
•Unknown*[4]	$C_{18}H_{30}O_3$	26.94	293.212	$[M-H]^-$	Unknown	WT, Δ*tvox1*
•Unknown*[4]	$C_5H_4O_3$	2.69	111.0086	$[M-H]^-$	Unknown	WT
•Unknown*[4]	$C_{21}H_{32}O_9$	10.79	473.2027	$[M-H]^-$	Unknown	Δ*tvox1*

Identification was based on MS/MS spectra using SmartFormula algorithm and PubChem database: https://pubchem.ncbi.nlm.nih.gov/. Chemical group classification as described by Kabera (2014); Irchhaiya et al. (2014). *Level of identification as described by Longnecker et al. (2015) Abbreviation: NSM, nitrogen containing secondary metabolite.

Table 5.2 Putative identification of decreased metabolic features modulated during the *T. virens*-maize interaction.

Putative compound Id	Molecular formula	RT (min)	Precursor ion (*m/z*)	Pseudomolecular ion	Chemical group	Treatment
•4-vinylaniline*[2]	C_8H_9N	2.00	164.072	$[M+HCOOH-H]^-$	NSM	WT, Δ*tvox1*
•Unknown*[3]	$C_9H_{11}NO_3$	1.06	180.067	$[M-H]^-$	NSM	WT, Δ*tvox1*
•Unknown*[3]	$C_{20}H_{21}NO_{12}$	15.56	466.1	$[M-H]^-$	NSM	WT, Δ*tvox1*
•Unknown*[3]	$C_{24}H_{29}N_4O_5$	21.13	453.213	$[M-H]^-$	NSM	WT, Δ*tvox1*
•Unknown*[3]	$C_{22}H_{26}N_4O_5$	7.76	471.187	$[M+HCOOH-H]^-$	NSM	WT
•Unknown*[3]	C_4H_5NO	1.07	128.035	$[M+HCOOH-H]^-$	NSM	Δ*tvox1*
•Unknown*[3]	$C_{28}H_{36}N_4O_4$	6.51	491.266	$[M-H]^-$	NSM	Δ*tvox1*
•2-(alpha-L-rhamnopyranosyloxy)-4-methyl-5-hydroxybenzeneacetic acid ethyl ester*[2]	$C_{17}H_{24}O_8$	9.84	401.146	$[M+HCOOH-H]^-$	Phenolic	WT, Δ*tvox1*
•Erigeroside*[2]	$C_{11}H_{14}O_8$	2.50	319.067	$[M+HCOOH-H]^-$	Phenolic	WT, Δ*tvox1*
•Unknown*[3]	$C_{14}H_{17}O_9$	4.27	329.088	$[M-H]^-$	Phenolic	WT, Δ*tvox1*
•Unknown*[3]	$C_{13}H_{16}O_7$	6.28	329.088	$[M+HCOOH-H]^-$	Phenolic	WT, Δ*tvox1*
•Unknown*[3]	$C_{25}H_{30}O_{16}$	9.03	631.152	$[M+HCOOH-H]^-$	Phenolic	WT, Δ*tvox1*
•Unknown*[3]	$C_5H_4O_3$	2.49	111.009	$[M-H]^-$	Unknown	WT, Δ*tvox1*
•Unknown*[4]	$C_4H_8O_4$	0.68	119.035	$[M-H]^-$	Unknown	WT, Δ*tvox1*
•Unknown*[4]	$C_{16}H_{22}O_9$	12.62	357.119	$[M-H]^-$	Unknown	WT, Δ*tvox1*

Identification was based on MS/MS spectra using SmartFormula algorithm and PubChem database: https://pubchem.ncbi.nlm.nih.gov/. Chemical group classification as described by Kabera (2014); and Irchhaiya et al. (2014).*level of identification as described by Longnecker et al. (2015). Abbreviation: NSM, nitrogen containing secondary metabolite.

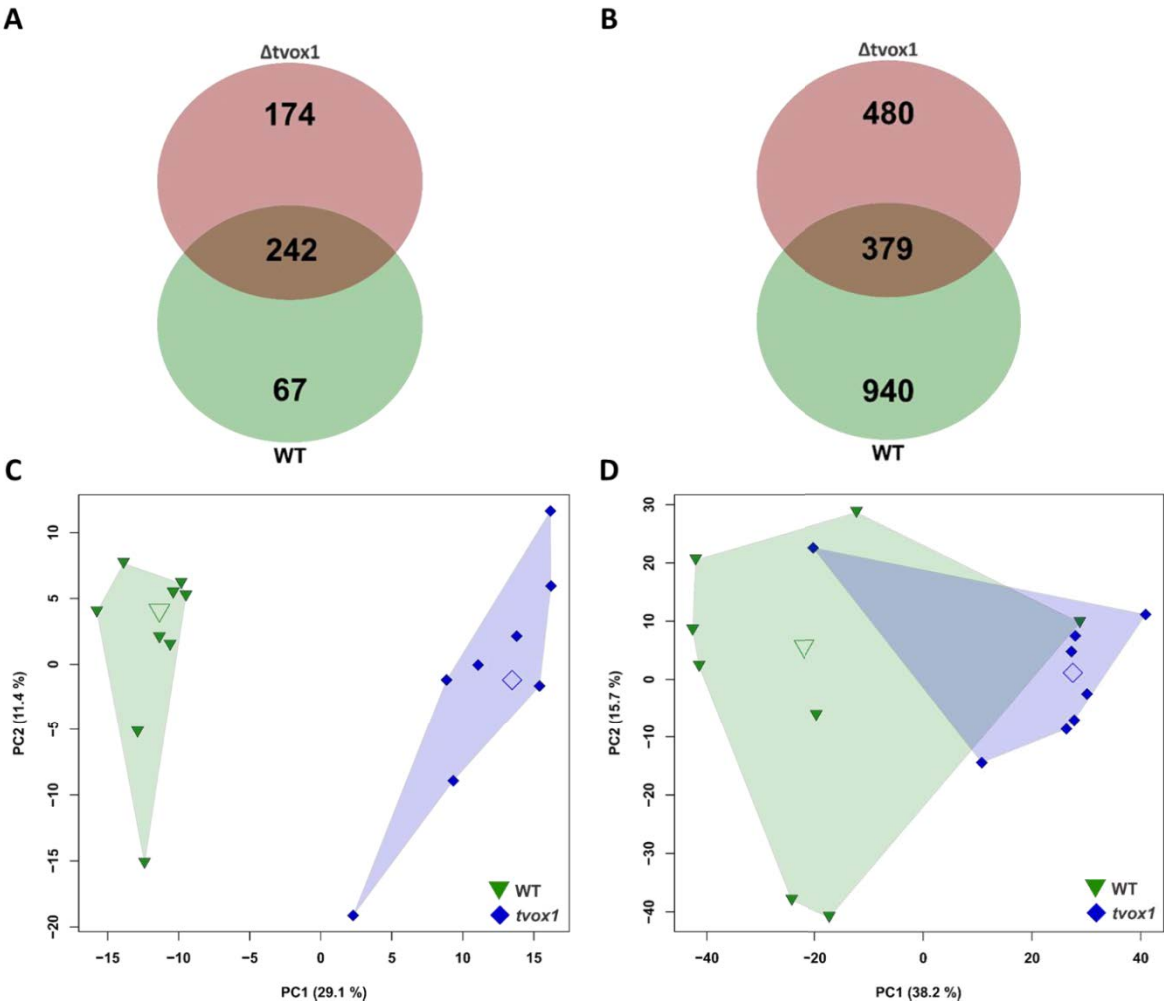

Figure 5.4 Metabolic fingerprinting of *T. virens* (WT and Δ*tvox1*) mycelia and supernatant. Number of metabolites overlapping in a comparison of all genotypes represented in Venn diagrams. **(A)** and **(B)** represent the metabolites found in mycelia and supernatant samples, respectively. Metabolic pattern of **(C)** mycelia and **(D)** supernatant from *T. virens* genotypes as principal component analysis (PCA) with scores (black axis); the total variance percent explained by the PCs in brackets, and the median scores as larger symbols for each group. *n* = 9 biological replicates for mycelia and *n* = 8 biological replicates for supernatant.

The same thresholds described for the root samples analysis were used to highlight those metabolites whose concentrations significant differed between mycelia and supernatant samples of *T. virens* genotype (Δ*tvox1*) in comparison with the parental strain (WT) (Figure 5.5). The analysis of the mycelia (Figure 5.5 A), showed a significant 39% increase in the number of metabolic features present in the genotype Δ*tvox1* compared with the WT. However, no significant differences (10%) were identified in the decreased metabolites (Figure 5.5 A). The volcano plots of the supernatants (Figure 5.5 B), showed significant differences in the decreased metabolic features (40%), but no differences were identified in the increased features (13%) of the Δ*tvox1* genotype (Figure 5.5 B).

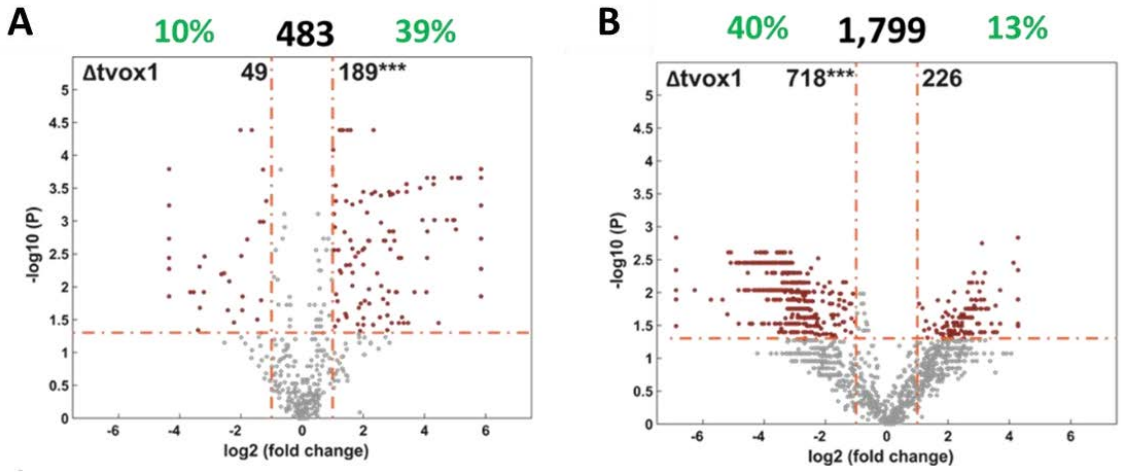

Figure 5.5 Modulated metabolites of *T. virens* deletion genotype (Δ*tvox1*). (A) Mycelia, and **(B)** supernatant in comparison with the WT genotype (parental strain), growing in culture media and represented in volcano plots. Modulated metabolites as coloured symbols outside the cut-off lines in volcano plots. Green numbers represent the responsiveness percentage of modulated metabolites for each genotype tested. Bold numbers (top-centre) represent the total number of metabolites identified for each treatment. The numbers of decreased versus increased features were compared (χ2-tests; ****P*<0.001).

In general, these results highlight differences in the proportions of metabolites being decreased or increased between *T. virens* genotypes, showing modification of the *T. virens* metabolome is influenced by the deletion of the gene involved in *T. virens* metabolism. Overall, these results highlight the influence of the deletion knockout of the specialised metabolism related gene on the *T. virens* metabolic network.

5.4 Discussion

Plants respond to biotic and abiotic stresses by modifying their chemical composition, employing chemical defence mechanisms through metabolic adaptations (Balmer et al. 2013; Vaughan et al. 2018). In the rhizosphere, plant roots communicate with microbes through chemical signals by releasing different primary and secondary metabolites that lead to the establishment of beneficial or detrimental interactions (Balmer et al. 2013; Mhlongo et al. 2018). In addition, plant beneficial microbes secrete molecules that are advantageous to the plant; however, plant pathogens influence the host metabolism to favour plant infection by manipulating host defence mechanisms and facilitating enhanced nutritional conditions (Balmer et al. 2013; Mhlongo et al. 2018). Metabolic technologies including metabolic fingerprinting and profiling are efficient strategies to explore plant microbe interactions by allowing the detection, identification and quantification of the metabolic composition of an organism or tissue (Kopka et al. 2004; Hall 2006; Allwood et al. 2008). In this study, through the use of an untargeted metabolic analysis during the *Trichoderma*-maize root interaction, it was found that the metabolome of the host roots was strongly modified during the interaction independently of the *T. virens* genotype. A large number of metabolic features were shown to be increased or decreased as part of the metabolic response between both

organisms, including metabolic features involved in plant defence pathways. In addition, this work demonstrates the impact on the *T. virens* metabolome by the deletion of a gene (*tvox1*) that participates in secondary metabolism.

5.4.1 *Trichoderma virens* endophytism under hydroponic growth conditions

An aseptic method was employed to study the interaction between *T. virens*-maize. An hydroponic culture system has been widely utilised for the analysis of *Trichoderma* as a plant symbiont through the use of transcriptomics, proteomics and metabolomics technologies (Brotman et al. 2012; Lamdan et al. 2015; Moran-Diez et al. 2015). The endophytic analysis of *T. virens* genotypes showed that inoculated plants had a growth reduction compared to the un-inoculated plants (Figure 5.1). These findings were previously discussed in section 2.3.1. This phenotype matches with other studies in *Trichoderma*, suggesting that competition for nutrient uptake between *Trichoderma* and its host has a negative effect on plant growth (Li et al. 2015; Vinci et al. 2018). Both *T. virens* genotypes were able to colonise the primary root, but no differences were noticed in the colonisation percentage between them, showing that Δ*tvox1* was not affected in endophytic colonisation under hydroponic growth conditions, but does have different behaviour when colonisation was tested in soil (see section 4.3.6.2), suggesting that the interaction of *T. virens* and maize may be influenced by environmental factors such as media composition.

5.4.2 *Trichoderma virens* triggers local response in maize

The process of initiating and developing the plant-microbe relationship consists of several metabolic changes. In the presence of *T. virens*, the maize metabolome shifted strongly, showing a specific response to each *T. virens* genotype as shown in the PCA (Figure 5.2). For exploration of metabolomics data, PCA has been a useful technique to explore variation between samples during studies of plant-microbe interactions (Balmer et al. 2013; Schweiger et al. 2014; Mazzei and Piccolo 2017). Maize roots not only interact with fungi, but also with rhizobacteria. The study of Planchamp et al. (2014) revealed that *P. putida* modulates the maize metabolome upon colonisation at different time points. The results revealed that the local and systemic responses differed, demonstrating pronounced changes in the local tissue (roots), those responses diminishing overtime. In addition, PCA of maize roots and leaves from the metabolic fingerprinting demonstrated a separation between treated and untreated roots at 3 d.p.i, but no significant changes were detected at later stages of the *P. putida*-maize interaction. In the present study, the PCA results demonstrate that *T. virens* genotypes were able to modulate the maize root phytometabolome at 5 d.p.i, revealing a strong response of maize roots to *T. virens* colonisation. Interestingly, comparison between *T. virens* genotypes interacting with maize roots showed a genotype dependent metabolic response. These findings reveal that the deletion of *tvox1* gene modifies the metabolic responses of the host plant to *T. virens,* suggesting a different outcome in the metabolic network during the interaction.

In addition, differences were discovered in the phytometabolome between un-inoculated and maize plants inoculated with each *T. virens* genotype tested (WT and Δ*tvox1*). This study focused on those metabolic features that were specifically modulated upon colonisation of the different *T. virens* genotypes. The number of modulated metabolic features with lower and higher intensities were similar between genotypes, but the total number of modulated features was higher in response to the WT (Figure 5.3 A and B). This analysis demonstrates for the first time that maize root response to *T. virens* colonisation is genotype dependent, and more importantly it is the first report which shows that a single deletion mutant on the plant symbiont (implicated in fungal secondary metabolism), shifts the general metabolic response of the *T. virens*-maize interaction. Moreover, the general response of maize roots upon colonisation (Figure 5.3 C and D), suggests that this set of metabolic features may regulate the symbiosis between *T. virens* and maize.

5.4.3 Metabolites involved in *Trichoderma virens*-maize interaction

5.4.3.1 Benzoxazinoids

Upon microbial colonisation, plants actively respond by secreting a vast array of secondary metabolites. Plant immunity is multilayered and comprises pre-formed, constitutive and inducible defence mechanisms (Pieterse et al. 2009). In maize, benzoxacinoids (BXs) constitute the most important group of defence-related secondary metabolites (Ahmad et al. 2011; Neal et al. 2012; Robert et al. 2012; Betsiashvili et al. 2015). Dual functions of BXs have been described in plants, acting as defence-related compounds (allelochemicals), but also as chemoattractants; for example, facilitating root colonisation of the rhizobacteria *P. putida* (Neal et al. 2012). BXs accumulate as glucosides inside plant tissue, serving as a defensive reserve. DIMBOA is the major BX in maize, and its accumulation in plant tissue is mainly associated as a response against pathogens and herbivores (Niemeyer 2009). In addition, beneficial microbes including arbuscular mycorrhiza have been linked with the modulation of BXs; for example, it was found that *Glomus mosseae* triggered an increase of DIMBOA in the maize root system (Song et al. 2011). Therefore, the accumulation of DIMBOA-glucoside (DIMBOA-Glu) as a priming response upon *T. virens* colonisation was evaluated. After 5 d.p.i, it was determined that DIMBOA-Glu is not being accumulated as a response of maize roots to any *T. virens* genotype tested (Figure 5.6). Concentration of BXs in root tissue is not equal to its concentration in root exudates (Niemeyer 2009), thus further exploration of BXs levels in maize roots exudates during *T. virens* interaction could be considered for further studies. Furthermore, a filamentous fungus, Fusarium verticillioides, is capable of detoxifying BXs (Glenn et al. 2003), suggesting that *T. virens* may use this strategy to detoxify BXs in maize roots during the colonisation process.

5.4.3.2 Flavonoids

Flavonoids are well known plant secondary metabolites which display diverse biological activities (Mierziak et al. 2014), acting as signaling molecules during plant-microbe interactions (Harborne

and Williams 2000; Treutter 2005; Gould and Lister 2006; Cheynier et al. 2013). Flavonoids have been associated as facilitators of symbiotic interactions, particularly in the facilitation of root colonisation by beneficial bacteria. In addition, shifts of flavonoid levels have also been detected during plant-mycorrhiza interactions, as a consequence of modifications to the expression levels of genes involved in phenylpropanoid biosynthesis. Furthermore, some flavonoids (quercetin, quercetin galactoside and kaempferol) stimulate hyphae growth and spore germination in mycorrhiza (Tsai and Phillips 1991; Poulin et al. 1997).

Within the flavonoids, naringenin, is an inhibitor of the activity of 4-coumarate: CoA ligase, a key enzyme of the phenylpropanoid pathway. Its accumulation can suppress the growth and diminish lignin content in graminaceus plants, including maize (Deng et al. 2004). Interestingly the metabolic fingerprints of both *T. virens* genotypes (WT and Δ*tvox1*) showed an accumulation of naringenin content in inoculated plants (Figure 5.6), implying that the reduction of lignin content may be a key factor in the success of *T. virens* to internally colonise the maize root system. Furthermore, naringenin has been shown to reduce *A. thaliana* roots (Brown et al. 2001). The accumulation of naringenin in maize roots triggered by *T. virens* colonisation possibly explains the growth reduction of treated roots as shown in Figure 5.1.

5.4.3.3 2-oxoglutarate

Organic acids are associated with different processes in the rhizosphere such as nutrient acquisition and microbe attraction (Jones 1998). Plant symbionts mediate the accumulation of organic acids in their host plant; for example, mycorrhizal fungi increased the accumulation of organic acids in leaves that help in the mitigation of deleterious effects of salt stress in maize plants Sheng et al. (2011). *Trichoderma* colonisation has also been associated with the modulation of the tricarboxylic acid cycle intermediates, including 2-oxoglutarate (Brotman et al. 2012). 2-oxoglutarate levels were modulated during the *T. virens*-maize interaction (Figure 5.6), showing increased levels in the presence of *Trichoderma* when compared to un-inoculated roots. 2-oxoglutarate is an important substrate for different enzymes; for example, the 2OG-Fe (II)-dependent oxygenases, which are considered sensors of energy metabolism, redox activity and iron homeostasis (Salminen et al. 2015). The 2OG-Fe (II)-dependent oxygenases regulate 2-oxoglutarate levels inside the cell, and participate in the metabolism of several plant defence associated metabolites, including flavonoids, auxins, ethylene, gibberellin, alkaloids, glucosinolates, BXs, coumarins and siderophores (Farrow and Facchini 2014; Islam et al. 2018). The 2OG-Fe (II)-dependent oxygenases are present in the *Trichoderma* genome; however, their role hasn't been characterised. Recently, the mechanisms employed by *Trichoderma* as a versatile plant symbiont were reviewed by Guzman-Guzman et al. (2019), suggesting that the fungus, during the relationship with its host, produces secondary metabolites such as phytohormones that mediate the beneficial interaction, and that enzymes such as 2OG-Fe (II)-dependent oxygenases participate in their synthesis. Overall, these results suggest that *T. virens* genes that belong to the 2OG-Fe (II)-dependent oxygenase superfamily use 2-

oxoglutarate as a substrate for example, *tvox1*, may participate in the production of secondary metabolites that are required for the interaction with maize plants. However, no significant differences were observed in the levels of 2-oxoglutarate between the WT and deletion mutant (Δ*tvox1*) (Figure 5.6). An analysis of 2-oxoglutarate levels at different time points during *T. virens*-maize interaction, comparing the WT and the deletion mutant may provide a better understanding of the role of fungal 2OG-Fe (II)-dependent oxygenases during symbiosis.

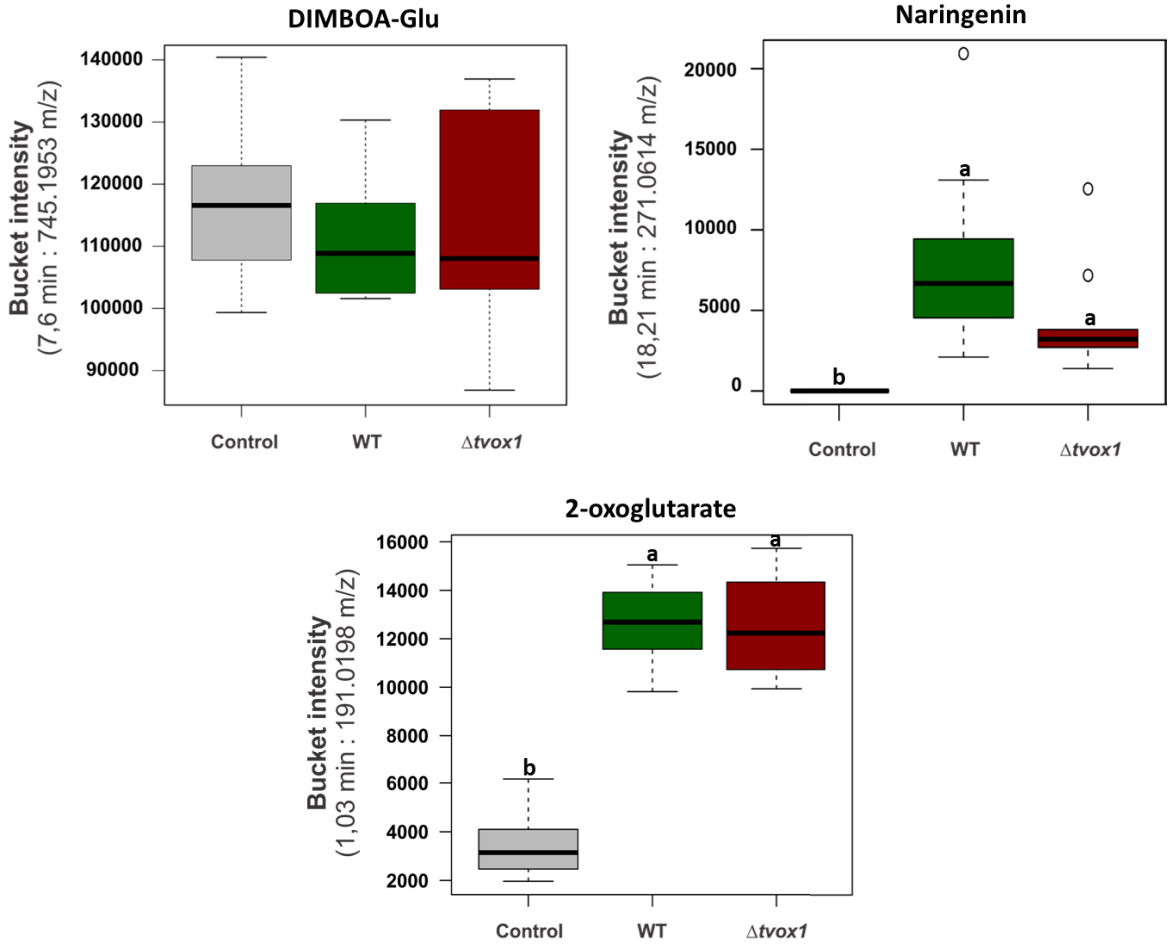

Figure 5.6 Bucket intensity of identified metabolites during *T. virens*-maize interaction. Intensities of metabolites identified in uninoculated and inoculated maize roots as Box-Whisker plots showing the median (horizontal line), the interquartile range (box) and the whiskers (extending to the 5 and 95% percentile, respectively). Different letters indicate significance between treatments (P<0.05).

5.4.4 2OG-Fe (II) oxygenase deletion mutant (*tvox1*) alters the *Trichoderma virens* metabolome

Untargeted fingerprinting analysis was performed to study the metabolome differences of two *T. virens* genotypes (WT and Δ*tvox1*). The results revealed that deletion of 2OG-Fe (II) oxygenase (*tvox1*) in the *T. virens* genome drastically modifies the fungal metabolome. The 2OG-Fe (II)-dependent oxygenases are complex enzymes present in all organisms. These enzymes have only

been widely studied in humans, plants and bacteria (Hausinger 2015; Islam et al. 2018). In contrast to cytochrome P450 (monooxygenases), the 2OG-Fe (II)-dependent oxygenases modify hydrophilic substrates and act in subcellular regions (Kawai et al. 2014). The role of these enzymes in fungal secondary metabolism has not been explored so far. By using an untargeted metabolic fingerprinting approach, the present study demonstrates that the deletion of the *tvox1* gene, impacted strongly on *T. virens* core metabolism, suggesting the importance of 2OG-Fe (II)-dependent oxygenases in the regulation of both internal (inside the cell and attached to the cell wall) and secreted metabolites. This is the first attempt to characterise the effect of a single deletion mutant in a fungal metabolome by using untargeted metabolic fingerprinting technology. *Trichoderma* spp. produce a large number of secondary metabolites such as peptabiotics, siderophores, epipolythiodioxopiperazines, polyketides, terpenes, pyrones and isocyane metabolites (Zeilinger et al. 2016). Previous studies in *T. virens* have shown that the knockout of genes involved in secondary metabolism affect the production of specific metabolites; for example, sesquiterpenes and peptaibols (Viterbo et al. 2007; Crutcher et al. 2013). Interestingly, using *E. coli* as a study model, Fuhrer et al. (2017) and colleagues revealed that the deletion of > 3,800 unique gene knockouts, perturbed regular cell metabolic fluxes, which correlates with the present findings regarding the impact of single deletion mutants on microbial metabolism.

5.5 Conclusions

Overall, this study demonstrates that untargeted metabolic fingerprinting is a useful tool which allows the detection of hundreds of metabolites in a single sample, and that an accurate data processing and management protocol allows the detection of even small shifts in the metabolome, providing a good insight of how symbiotic interactions between plants and microorganisms are being regulated. This study elucidates the metabolic changes during the *T. virens*-maize relationship. By comparing two *T. virens* genotypes a general and specific metabolic response was demonstrated when *Trichoderma* was interacting with its host plant. Moreover, this work showed that the deletion of single gene involved in fungal secondary metabolism shifted the metabolic flux in *T. virens.*

6 General discussion

This research aimed to investigate the consequences of maize root colonisation by *Trichoderma virens* WT strain Gv 29.8 to endophytically colonise maize (*Zea mays*) roots under a hydroponic growing system. Subsequently, the interaction of *T. virens* with maize was studied using genetics, proteomics and metabolomics approaches to uncover the molecular mechanisms that the fungus utilises to communicate with its host plant. Despite the fact that *T. virens* is widely used as a biocontrol agent and plant symbiont, there are many unanswered questions in relation to the molecular processes that occur during the colonisation of plant tissues. This work provides a closer insight into the establishment of *T. virens* as a plant endophyte and generates new knowledge of the strategies that *T. virens* employs to interact with maize roots.

6.1 *Trichoderma virens* as an endophyte model

Several microorganisms inhabit the rhizosphere, and among them *Trichoderma* spp. have the ability to interact with plants symbiotically. Although *T. virens* is considered a facultative-plant symbiont, its transition from saprophyte to mutualistic endophyte has not been deeply studied. This transition has been characterised in the root-endophytic fungi such as *Piromosfora indica* and *Phomobis liquidambari* that have a biphasic lifestyle (saprophytism-endophytism) (Zuccaro et al. 2011; Zhou et al. 2018). During the encounter process with its host plant, *T. virens* activates different molecular mechanisms to actively become endophytic and survive inside the host tissues (Moran-Diez et al. 2015; Lawry 2016). *T. virens* colonises root surfaces extensively and utilises specialised structures to penetrate and endophytically colonise the plant (Lawry 2016).

In this study, maize was used as a model plant based on its commercial importance worldwide, and it was found that *T. virens* was capable of colonising maize root inter- and intracellular spaces by the formation of haustorium- and appressorium-like structures. The formation of these specialised structures has high relevance because they function as feeding and delivery structures where a wide range of molecules are transported. These molecules become necessary for the establishment of the interaction. *T. virens* widely colonised the epidemical and cortical sections of the root system. To accomplish this process, the secretion of cell wall degrading enzymes, effector proteins, secondary metabolites, and the activation of sugar transporters are indispensable (Vargas et al. 2011; Lawry 2016; Nogueira-Lopez et al. 2018). Based on the microscopic observations during the *T. virens* colonisation, it was shown that several hyphae colonise a single root cell. This suggest that the fungus could kill the host cell as a strategy of colonisation as reported in *P. indica* (Deshmukh et al. 2006), or that there is a formation of specialised hyphae creating an interface between the fungal and host cell plasma membrane without disrupting host cell integrity (Lo Presti and Kahmann 2017).

Therefore, further analysis of host cell viability during the *T. virens* colonisation process is necessary to understand its endophytic behaviour. Moreover, *T. virens* has been reported as an avirulent plant endophyte, but under hydroponic growing conditions an interesting phenotype was observed. In the presence of *T. virens,* the development of the root system was negatively affected, thereby having an impact on maize growth. However, this phenotype was not present under soil growth conditions, suggesting that environmental cues during the *T. virens*-maize interaction may influence the behaviour of the endophyte to the host plant by inducing metabolism, cellular organisation, protein secretion and gene expression changes as reviewed by van der Does and Rep (2017) in other plant-fungal models. Even though the findings obtained from the *T. virens*-maize interaction under hydroponic growth conditions through proteomics and metabolomics tools provided interesting evidence on the mechanisms used by *T. virens* to successfully colonise maize roots, the next step will be the developing of an accurate methodology of samples collection to study the *T. virens*-maize interaction in the soil.

Plant-microbe interactions on fungal models have focused primarily on the study of hemibiotrophic, obligate-biotrophic plant pathogens, and obligate-beneficial fungi such as mycorrhiza. Regularly the deletion of candidate genes expressed during the infection and/or colonisation phase cause a reduction in colonisation and/or pathogenesis. However, an understanding of regulated genes during the plant-microbe interaction, regularly requires their functional analysis to unravel the specific mechanisms utilised by the fungi in the manipulation of plant defence processes, allowing a better understanding of the interaction with their host plant. However, the nature of *T. virens* as a facultative-plant symbiont, and the lack of detailed information of the full mechanisms to become an endophyte, make its study challenging.

Most of the studies of the functional role of different *T. virens* genes have focused on the impact on plant growth promotion, induction of systemic resistance and mycoparasitism. In recent years, several studies on *T. virens* have used ´omics´ to study the interaction with its host plant (Lamdan et al. 2015; Moran-Diez et al. 2015; Lawry 2016; Nogueira-Lopez et al. 2018). Gene disruption during the interaction in *Trichoderma* studies have aimed at the impact on colonisation, but few have investigated the specific role of these genes during the interaction and the strategies that *Trichoderma* employs to overcome plant immune responses. Furthermore, apart from the lack of information of *T. virens* biology as an endophyte, its genetic manipulation has been a continuing limitation.

6.2 Genetic transformation of *Trichoderma virens*

T. virens is a challenging fungal model for genetic manipulation because of the low frequency of homologous integration events which is required for the generation of gene knockout strains. The percentage of homology recombination in *Trichoderma* spp. is approximately 2% (Mach and Zeilinger 1998). In the present study, by using the conventional protoplast transformation

described by Baek and Kenerley (1998), low rates of homologous recombination were detected (< 5%). In addition, those transformants that were confirmed to have the gene replacement also contained ectopic integrations of the resistance cassette, showing different phenotypes (colony appearance) of a single deletion gene (Supplementary Figure 15). As a result, a new strategy was implemented to overcome this issue, which consisted in the use of *Agrobacterium*-mediated transformation and allowed a higher rate of homologous recombination (> 60%) as previously reported by Zeilinger (2004). However, the presence of heterokaryon cells having both the insert and native gene has been another recurrent problem during *T. virens* transformation, which has been reported in other studies using the same strain (Crutcher et al. 2013; Crutcher et al. 2015). In addition, another disadvantage to study gene functionality in *T. virens* as a model system, is the selection of a second resistance cassette for gene complementation because *T. virens* is resistant to a wide range of antibiotics (data not shown), and this issue has been addressed by other members of *Trichoderma's* scientific community (Pachauri et al. 2018). Therefore, the implementation of new technologies; for example, the CRISP-Cas9 system (Nødvig et al. 2015), for the genetic engineering of *T. virens* are required for an efficient study of gene functionality during plant-microbe interactions. Furthermore, improvements in the construction of specific vectors for localisation, overexpression and complementation of candidate genes by using Golden Gate technology as reported in this work will provide an efficient method to elucidate gene functionality during the *Trichoderma*-plant interaction.

6.3 Intermolecular responses during the *Trichoderma virens*-maize relationship

Plant-microbe interactions are complex and dynamic biological processes, where several mechanisms are activated to allow the communication of both organisms. The establishment of *T. virens* as a maize endophyte combines the synthesis and secretion of a wide range of proteins and metabolites as part of the crosstalk between microbe and host as shown in Chapters 3, 4 and 5. Based on the evidence generated through this study several mechanisms are proposed as the molecular interplay between *T. virens* and maize: a) glycosyl hydrolases and lignification, b) ROS homeostasis, and C) iron and secondary metabolism (Figure 6.1).

6.3.1 Glycosyl hydrolases and lignification

Endophytic colonisation of maize roots by *T. virens* is supported by the secretion of GHs that degrade plant cell wall components. These enzymes were identified in the apoplastic secretome of *T. virens*. Fortification of the plant cell wall by the accumulation of polymers such as lignin form part of the first line of plant defence against successful microbe penetration (Vance et al. 1980; Bhuiyan et al. 2009). However, it was found that during the maize root colonisation process, *T. virens* overcomes cell wall reinforcement by diminishing lignin biosynthesis through two possible mechanisms: a) by reducing peroxidase activity, which mediates the formation of lignin (Ros

Barcelo 1997; Almagro et al. 2009) and b) by inducing the accumulation of the flavonoid naringenin, which inhibits a key component of the phenylpropanoid metabolism pathway (Deng et al. 2004). Altogether, these results showed different strategies utilised by *T. virens* to overcome the physical barrier of the host plant, resulting in a successful colonisation of epidermal and cortical root sections of the maize root system. In order to investigate how lignification of maize roots occurs upon *T. virens* colonisation, further microscopic analyses using specific dies for lignin visualisation will be necessary to increase the understanding of this mechanism.

6.3.2 Reactive oxygen species homoeostasis

Production of ROS is one of the earliest responses of plant cells to the perception of MAMPs (Van Camp et al. 1998; O'Brien et al. 2012). ROS act as signal molecules that trigger plant immune responses and their homeostasis regulation is crucial to maintain symbiotic relationships (Jwa and Hwang 2017). Plant-associated microorganisms have evolved sophisticated mechanisms that target ROS-generation pathways to suppress ROS production, thus facilitating colonisation (Nath et al. 2016; Jwa and Hwang 2017). During the *T. virens*-maize interaction, redox activity in the apoplast was modified as follows: a) the expression of detoxification enzymes that protect the fungi from ROS such as superoxide dismutase [Cu-Zn] and catalase-peroxidase, b) the secretion of thioredoxin-like proteins that are considered as putative effectors, and participate in ROS scavenging in the apoplast and c) the inhibition of expression of specific maize peroxidases. Overall, ROS homoeostasis may be considered as a fundamental strategy implemented by *T. virens* to manipulate plant immune responses and generate a suitable environment for the interaction. Generation of knockout mutants to investigate the specific functions of *T. virens* genes that participate in the regulation of ROS will provide a better understanding of their role during the interaction.

6.3.3 Iron and secondary metabolism

Iron plays an important role as a cofactor in many metabolic processes and acts as a regulator of plant-microbe interactions. Plants are capable of increasing iron levels to cause oxidative burst and withhold iron as defence mechanisms against microorganisms (Verbon et al. 2017). Microorganisms can synthesise siderophores that enhance iron uptake and diminish iron-regulated host immune responses (Lemanceau et al. 2009). Other secondary metabolites are also key elements that modulate and facilitate plant-microbe interactions, including *Trichoderma* derived secondary metabolites (Pusztahelyi et al. 2015; Zeilinger et al. 2016). Moreover, shifts in primary metabolites such as amino acids, sugars and organic acids are modulated by microorganisms *in planta* (Sheng et al. 2011*;* Brotman et al., 2012). Within organic acids, 2-oxoglutarate is a key signal molecule for the coordination of carbon and nitrogen metabolic pathways (Huergo and Dixon 2015). 2-oxoglutarate is the co-substrate of 2OG-Fe (II) dioxygenases that participate in the biosynthesis of several plant and microbe secondary metabolites, and are regulators of redox

activity and iron homeostasis (Hausinger 2015; Salminen et al. 2015; Islam et al. 2018). In the *T. virens*-maize interaction the protein TVOX1 that belongs to the 2OG-Fe (II) dioxygenases participates in the regulation of iron and fungal colonisation. Furthermore, levels of 2-oxoglutarate were increased during the interaction, suggesting that maize and *T. virens* 2OG-Fe (II) dioxygenases utilise it as a co-substrate for the synthesis of secondary metabolites that may regulate the symbiotic relationship.

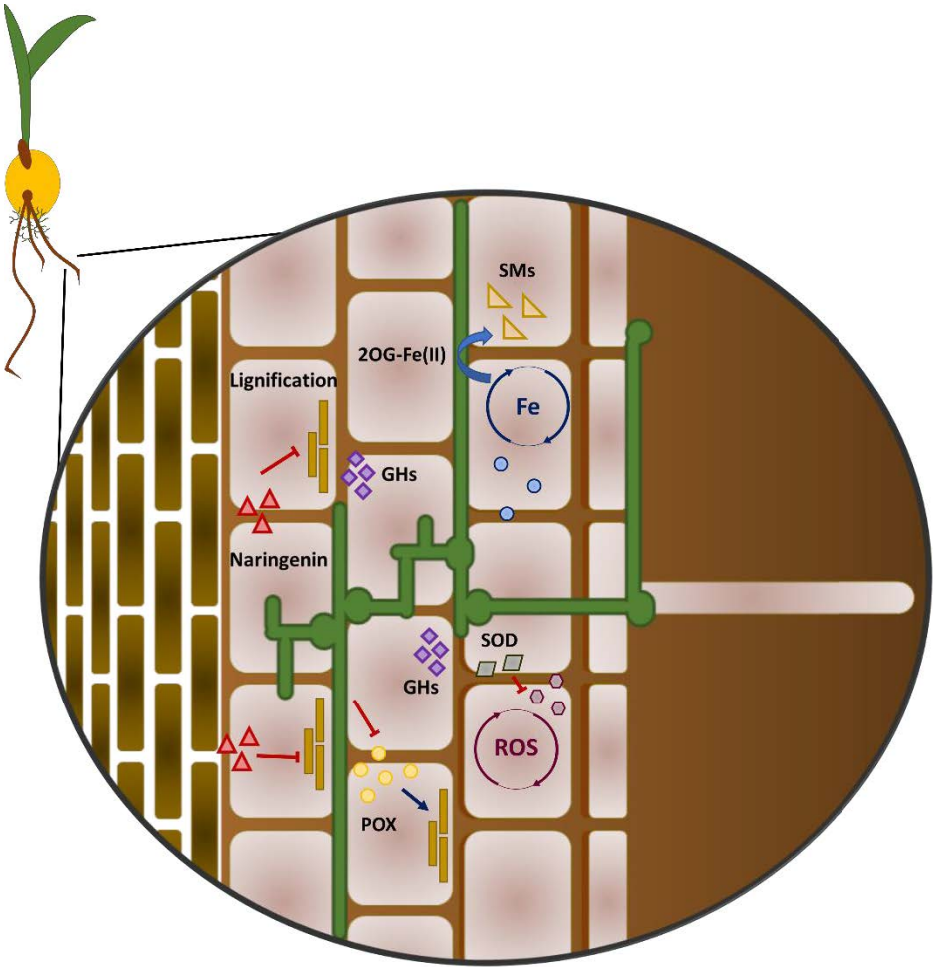

Figure 6.1 Intermolecular responses during *T. virens*-maize interaction. The establishment of *T. virens* as a maize endophyte combines the synthesis and secretion of a wide range of proteins and metabolites as part of the crosstalk between microbe and host. Several mechanisms are proposed as the molecular interplay between *T. virens* and maize including secretion of glycosyl hydrolases, lignification, ROS homeostasis, iron regulation and production of secondary metabolites. Abbreviations: GHS, glycosyl hydrolases; Fe, iron; POX, peroxidases; ROS, reactive oxygen species; SOD, superoxide dismutase; SMs, secondary metabolites; 2OG-Fe(II), 2-oxoglutarate/Fe (II)-dependent dioxygenase.

6.4 Future perspectives

- Improvement of methods for genetic manipulation of *T. virens* using new technologies; for example, the CRISP-Cas9 system, to overcome difficulties such as low recombination rates, ectopic integration and open reading frame persistence of the native gene.

- Selection of candidate genes based on proteomic findings for the generation of deletion mutants of *T. virens*; for example, genes related to ROS regulation.

- Generation of vectors for localisation, overexpression and complementation of candidate genes using Golden Gate cloning system for the study of *T. virens* biology as an endophyte.

- Continue with the analysis of the *tvox1* gene during the *Trichoderma*-maize interaction, to understand the function in iron homeostasis and production of secondary metabolites *in planta*, in order to get a better insight into the role of this gene during the interaction.

- Microscopic visualisation of WT and Δ*tvox1* strains to observe possible differences in colonisation pattern, ROS production, lignin and callose deposition.

- Targeted metabolomics of maize-roots interactions comparing *tvox1* with its parental strain to detect shifts in sugar content, amino acids and organic acids which will complement the findings of the untargeted metabolic fingerprinting which mostly uncover secondary metabolites.

- Confirmation of putative identified metabolites from the metabolic fingerprinting analysis of *T. virens*-maize roots interaction by the analysis of commercial standards.

- Use of alternative analytic techniques such as Nuclear magnetic resonance (NMR) to elucidate the structures of modulated metabolic features during the *T. virens*-maize roots interaction, looking for the specific modulated features with the lowest and highest intensities from the plants treated with *Δtvox1* to increase the understanding of fungal 2OG-Fe (II) dioxygenases during the symbiotic interaction.

6.5 Conclusion

Overall this research has unraveled the mechanisms used by *T. virens* to successfully colonise maize roots. These were identified by the combination of different approaches including microscopy, functional genomics, proteomics and metabolomics. During the *T. virens*-maize interaction it was shown that *T. virens* modifies the host plant secretome and metabolism. The results demonstrate the importance of iron homeostasis and the modulation of reactive oxygen species and secondary metabolism for *T. virens* colonisation of maize roots colonisation. This study generated knowledge for a better understanding of *Trichoderma* as an endophyte.

7 Appendix

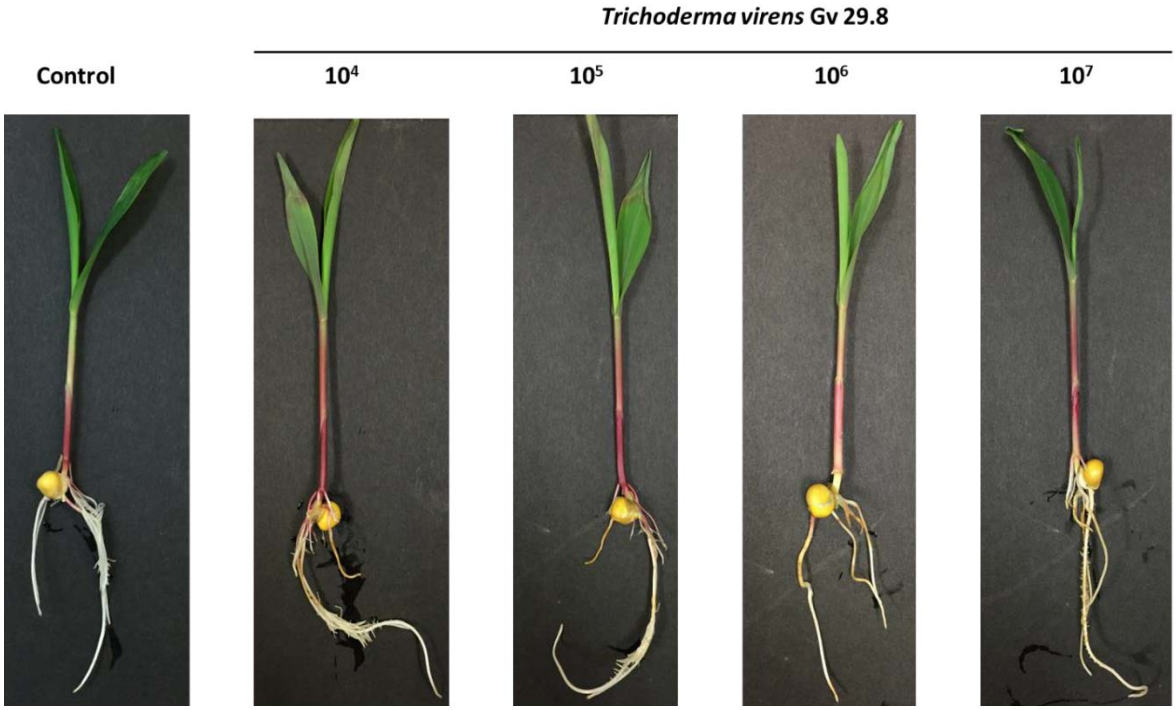

Supplementary Figure 1. Observations of phenotypic changes in the maize root system inoculated with different concentrations of *T. virens* conidia. Maize roots showed brownish pigmentation on the root surface independently to different concentrations of inoculum (*T. virens*), starting from 10^4 to 10^7 conidia, after 7 d.p.i.

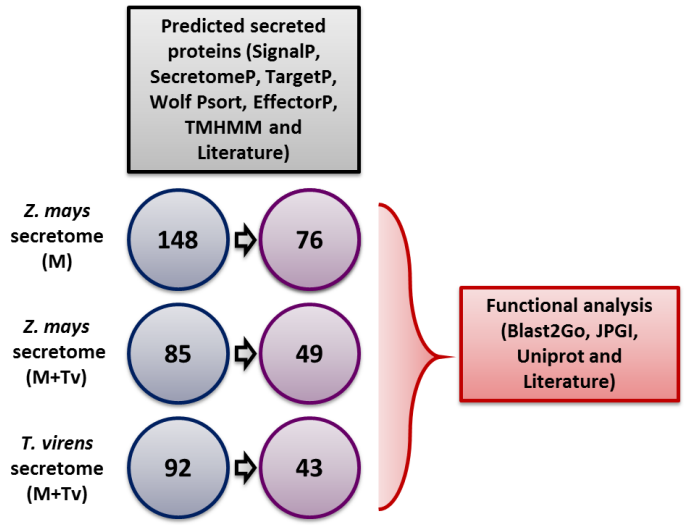

Supplementary Figure 2. Diagrammatic outline of the process used to detect and analyse putative proteins secreted by *T. virens* and maize during 5 d.p.i. The secretome was obtained after isolation of apoplastic proteins during the T. virens-maize interaction. The secretome was examined with different prediction software to detect secretion status (SignalP, SecretomeP, TargetP, WoLF PSORT, EffectorP, TMHMM and literature review). The predicted secreted proteins were then analysed for likely function based on their ontology, homology, and domains (Blas2GO, JPGI, Uniprot and literature review).

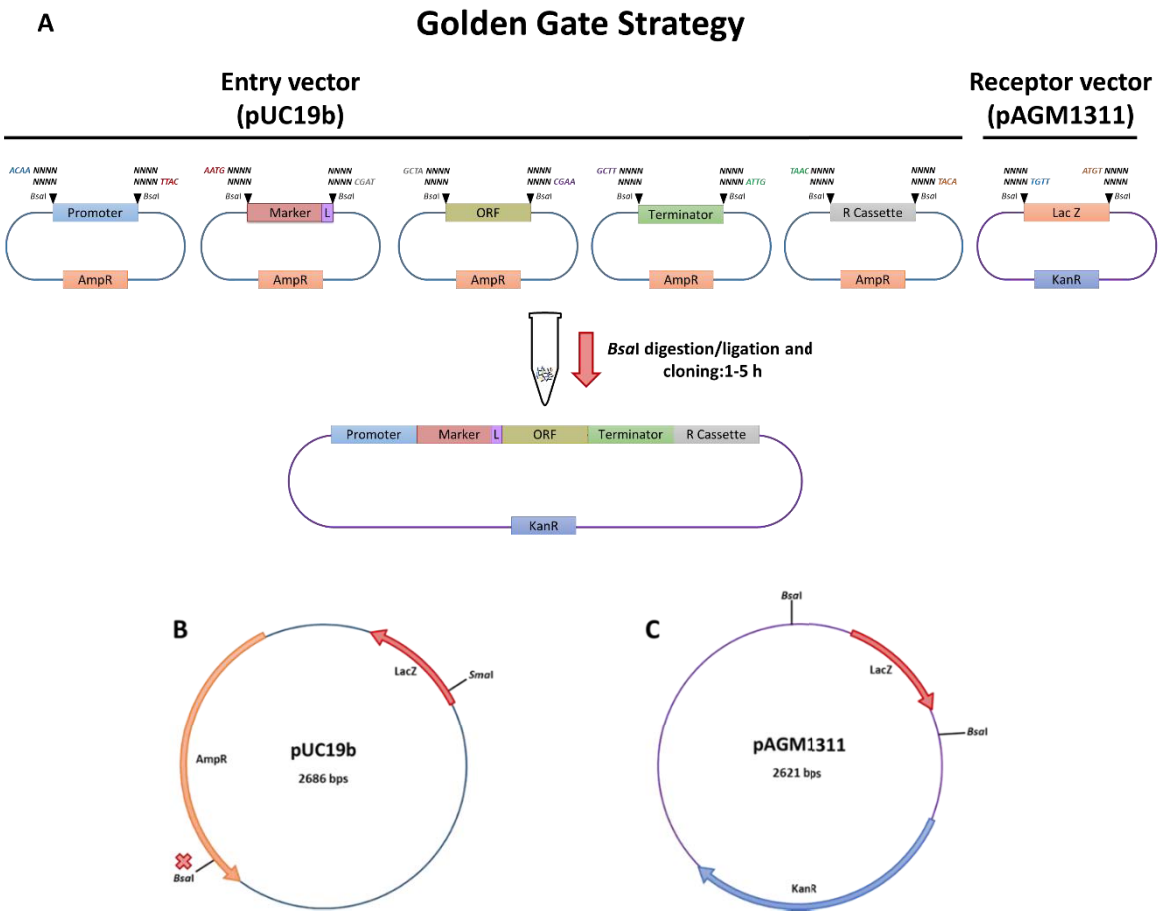

Supplementary Figure 3. Golden Gate strategy. Vectors theoretically created to accomplish genomic modification in *T. virens* (e.g. protein localisation) using type II restriction enzymes (*Bsa*I). **(A)** Molecules of interest subcloned into entry vector (pUC19b) and receptor vector (pAGM1311) were mixed in one tube *Bsa*I digestion-ligation reaction to create a new construct containing promoter-ORF-fluorescent marker-terminator and resistance cassette and subcloned into pAGM1311. **(B)** Backbone of entry vector and **(C)** receptor vector.

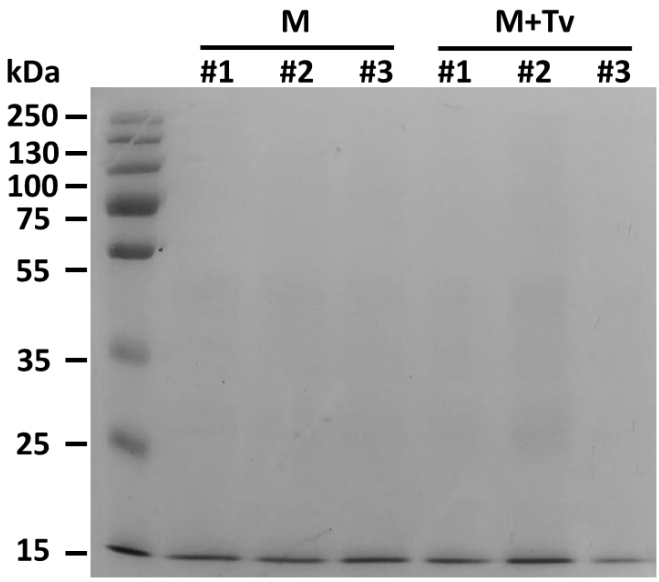

Supplementary Figure 4. Electrophoretic profile (1D-SDS-PAGE) of protein extracts of apoplastic fluid from maize primary roots isolated by the sorption method. Three biological replicates of apoplastic proteins fractions from maize roots un-inoculated (M) and inoculated (M+Tv) with *T. virens* were separated by 1D-SDS-PAGE. No visible protein fractions were observed in the samples.

Supplementary Table 1 Analysis of apoplastic fluid and apoplastic proteins obtained from un-inoculated and maize roots using the centrifugation-infiltration method

Sample	FW (g)	V (µL)	TPC (µg.mL^{-1})	TPA (µg)
Un-inoculated sample 1	1.3864	750	1450	40.6
Un-inoculated sample 2	1.3494	800	1990	55.72
Un-inoculated sample 3	1.4073	700	721	20.19
T. virens inoculated sample 1	0.8408	380	612	17.14
T. virens inoculated sample 2	0.9561	400	866	24.25
T. virens inoculated sample 3	0.868	350	579	16.21

Root fresh weight (FW), volume (V), total protein concentration (TPC) and total protein amount (TPA) of apoplastic fluid obtained from three biological replicates (20 plants each replica) for each condition, un-inoculated and inoculated maize roots.

Supplementary Table 2 Malate dehydrogenase activity assay

Treatments	MDH Activity (apoplast/total, %)	Total protein (µg/mg FW)	Apoplast protein µg/mg
Un-inoculated	1.19 ± 0.07	1.986 ± 0.011	0.019 ± 0.004
Inoculated	1.44 ± 0.03	1.98 ± 0.02	0.015 ± 0.002

Data are represented by the means of the values of three biological replicates ± SD. Malate dehydrogenase activity was calculated by the decrease in absorbance at 340nm/min (mg protein/g FW). Abbreviations: MDH, malate dehydrogenase; FW, fresh weight of the maize primary root.

Supplementary Table 3 Summary of the apoplastic proteins secreted by *Z. mays* and *T. virens* at 5 d.p.i

Uniprot ID*	Protein ID*	Protein annotation	Organism	Section	Mass (kDA)	Condition
G9MSH9_HYPVG	TV_29366	β-xylosidase	*T. virens*	2	75-120 kDa	Inoculated
C0P5Y3_MAIZE	GRMZM2G149751	Methionine synthase	*Z. mays*	2	75-120 kDa	Inoculated
A0A1D6MWU7_MAIZE	GRMZM2G340251	Heat shock protein 70	*Z. mays*	2	75-120 kDa	Inoculated
C0PHR4_MAIZE	GRMZM2G015295	Adenosy homocysteine	*Z. mays*	3	50-75 kDa	Inoculated
B6SSX0_MAIZE	GRMZM2G175499	Pectinesterase	*Z. mays*	4	30-50 kDa	Inoculated
A0A1D6LS36_MAIZE	GRMZM2G171078	Peroxidase	*Z. mays*	4	30-50 kDa	Uninoculated
A0A1D6PD14_MAIZE	GRMZM2G150356	Ascorbate peroxidase (APx1)	*Z. mays*	5	15-30 kDa	Uninoculated
A0A1D6K5Y8_MAIZE	GRMZM2G304442	Pathogenesis-related protein 1 (PR-1)	*Z. mays*	5	15-30 kDa	Uninoculated
A0A1D6ERY2_MAIZE	AC233861.1	Protein kinase	*Z. mays*	3	50-75 kDa	Uninoculated/inoculated
A0A0B4J327_MAIZE	GRMZM2G053206	Aspartic-type endopeptidase	*Z. mays*	4	30-50 kDa	Uninoculated/inoculated
B4FRS8_MAIZE	GRMZM2G122018	Germin-like protein	*Z. mays*	5	15-30 kDa	Uninoculated/inoculated
B6SH12_MAIZE	GRMZM2G117989	Barwin-like protein (Win1)	*Z. mays*	5	15-30 kDa	Uninoculated/inoculated
PER66_MAIZE	GRMZM2G133475	Peroxidase 66	*Z. mays*	5	15-30 kDa	Uninoculated/inoculated

Supplementary Table 4 Summary of the apoplastic proteins secreted by *Z. mays* after 5 d.p.i (un-inoculated)

Uniprot ID[a]	Protein annotation[b]	SignalP[c]	TMHMM[d]	SecretomeP[e]	WoLF-PSORT/ Target P [f,h]
B6U284_MAIZE	14-3-3-like protein	N	N	N	Cytoplasm
B8A306_MAIZE	2,3-bisphosphoglycerate- phosphoglycerate mutase	N	N	Y	Cytoplasm
B4FSW0_MAIZE	40S ribisomal protein S10-1	N	N	Y	Cytoplasm
B4G286_MAIZE	40S ribosomal protein S18	N	N	Y	Cytoplasm
B6SHZ1_MAIZE	40S ribosomal protein S5	N	N	Y	Cytoplasm
RS8_MAIZE	40S ribosomal protein S8	Y	N	N	Extracellular
B4FFB8_MAIZE	5a2 protein (al-9)	Y	N	N	Extracellular
A0A1D6N1Z8_MAIZE	6-phosphogluconate dehydrogenase	Y	N	N	Extracellular
C0PHR4_MAIZE	Adenosylhomocysteinase	N	N	N	Cytoplasm
A0A1D6KJM7_MAIZE	AIR12 protein	Y	Y	N	Extracellular
B4G231_MAIZE	Alpha-amylase	Y	N	N	Vacuole
B4FYM6_MAIZE	Alpha-amylase	N	Y	Y	Peroxisome
B4G1X1_MAIZE	Alpha-galactosidase	Y	Y	N	Extracellular
A0A1D6L3U6_MAIZE	Aluminum induced protein with YGL and LRDR motifs	N	N	Y	Cytoplasm
B6TM55_MAIZE	APx1-Cytosolic ascorbate peroxidase	N	N	Y	Cytoplasm
B6U9S6_MAIZE	APx1-Cytosolic ascorbate peroxidase (Pod1)	N	N	Y	Cytoplasm
A0A1D6F8J3_MAIZE	Aspartic-type endopeptidase	Y	N	N	Extracellular
A0A1D6MRM3_MAIZE	ATP-citrate synthase beta chain protein 2	N	N	Y	Cytoplasm
Q9SYS1_MAIZE	Beta-amylase (Amy2)	N	N	Y	Extracellular
Q94KS7_MAIZE	Beta-expansin 7 precursor	N	N	Y	Extracellular
B8A0V4_MAIZE	Beta-galactosidase	Y	Y	N	Vacuole
B6UHQ8_MAIZE	Blue copper protein	Y	N	N	Extracellular
C0HII8_MAIZE	Bowman-Birk type trypsin inhibitor	N	N	Y	Extracellular
B4FPL1_MAIZE	Bowman-Birk wound-induced proteinase inhibitor (Wip1)	Y	N	N	Extracellular
Q7FU57_MAIZE	Bowman-Birk wound-induced proteinase inhibitor (Wip1)	Y	Y	N	Extracellular
B4FBW7_MAIZE	Calmodulin	N	N	Y	Cytoplasm
CALR_MAIZE	Calreticulin	Y	Y	N	Extracellular

C0P451_MAIZE	Chitinase B1	Y	N	N	Extracellular
B4FTS6_MAIZE	Endochitinase A	Y	N	N	Extracellular
B4FMR3_MAIZE	Expansin-like protein B4	Y	N	N	Extracellular
K7VT58_MAIZE	Fasciclin-like arabinogalactan protein 7	Y	N	N	Extracellular
B4FAG0_MAIZE	GDP-mannose 4,6 dehydratase	N	N	N	Cytoplasm
A0A1D6GWL6_MAIZE	GDSL esterase/lipase	Y	Y	N	Extracellular
A0A1D6HV20_MAIZE	Glucose/Sorbosone dehydrogenase (HIPL1)	Y	N	N	Extracellular
B4FSR6_MAIZE	Glutathione S-transferase	N	N	Y	Extracellular
GSTF4_MAIZE	Glutathione S-transferase (Gst4)	N	N	N	Extracellular
B6TL20_MAIZE	Glutathione S-transferase (Gstu6)	Y	N	N	Extracellular
C0PGU8_MAIZE	Glycerophosphodiester phosphodiesterase (GDPDL3)	Y	N	N	Vacuole
B4FAW5_MAIZE	Glycide hydrolase family 17 protein	Y	N	N	Extracellular
B4F8M8_MAIZE	Glycide hydrolase family 3 protein (exg1)	Y	N	N	Extracellular
A0A1D6KE29_MAIZE	Heat shock 70 protein	N	N	N	Cytoplasm
B7ZZ42_MAIZE	Heat shock 70 protein	N	N	N	Cytoplasm
K7W288_MAIZE	KDEL-tailed cysteine endopeptidase CEP1	Y	N	N	Extracellular
C0PBS1_MAIZE	Lipase	Y	Y	N	Vacuole
C0P5Y3_MAIZE	Methionine synthase	N	N	N	Cytoplasm
B4FWD0_MAIZE	NADPH dehydrogenase (quinone) FQR1	N	N	N	Extracellular
A0A1D6F224_MAIZE	Non-specific lipid transfer protein-like	Y	N	N	Extracellular
B4FPA4_MAIZE	Non-specific lipid transfer protein-like (xylogen protein)	Y	Y	N	Extracellular
A0A1D6N932_MAIZE	Osmotin-like protein OSM34	Y	N	N	Extracellular
Q29SB6_MAIZE	Pathogenesis-related protein 10 (PR-10)	N	N	N	Cytoplasm
B4FZZ2_MAIZE	Peptidyl-prolyl cis-trans isomerase (cyclophilin)	N	N	N	Cytoplasm
A0A1D6H658_MAIZE	Peroxidase (Per52)	Y	N	N	Extracellular
A0A1D6KAW3_MAIZE	Peroxidase (Per54)	Y	Y	N	Extracellular
A0A1D6LYW3_MAIZE	Peroxidase (Per5)	Y	N	N	Extracellular
A0A1D6IMZ9_MAIZE	Peroxidase (Per3)	Y	N	N	Extracellular
A0A1D6IKV8_MAIZE	Peroxidase (Per2-like)	Y	N	N	Extracellular
B4FG39_MAIZE	Peroxidase (Per12)	Y	Y	N	Extracellular

B4FYH1_MAIZE	Peroxidase (Per64)	Y	N	N	Extracellular
C0P2D4_MAIZE	Peroxidase (Per17)	Y	N	N	Extracellular
A0A1D6QGI0_MAIZE	Peroxidase (Per67)	Y	Y	N	Extracellular
A0A1D6F4C8_MAIZE	Peroxidase (Per66)	Y	N	N	Extracellular
PER70_MAIZE	Peroxidase (Per70)	Y	Y	N	Extracellular
A0A1D6K431_MAIZE	Peroxidase (Per2)	Y	Y	N	Extracellular
B4FN24_MAIZE	Peroxiredoxin-2B	N	N	Y	Cytoplasm
PROF5_MAIZE	Profilin-5	N	N	Y	Cytoplasm
Q5EUE1_MAIZE	Protein disulfide-isomerase (Pdil1-1)	Y	N	N	Extracellular
K7V329_MAIZE	Putative O-Glycosyl hydrolase superfamily protein	Y	N	N	Peroxisome
B8A1R0_MAIZE	Putative O-Glycosyl hydrolase (beta-D-xylosidase 5)	Y	Y	N	Extracellular
B6SHR9_MAIZE	PVR3-like protein	Y	Y	N	Extracellular
A0A1D6IKH3_MAIZE	Ribonuclease 1	Y	N	N	Extracellular
B4FBD6_MAIZE	Ribonuclease 1	Y	Y	N	Extracellular
B6SNA6_MAIZE	Subtilisin-chymotrypsin inhibitor CI-1B	N	N	Y	Cytoplasm
SODC5_MAIZE	Superoxide dismutase [Cu-Zn]	N	N	Y	Cytoplasm
B6SHW5_MAIZE	Thioredoxin H-type (Trxh1)	N	N	Y	Cytoplasm
B6SK03_MAIZE	Ubiquitin-conjugating enzyme (Spm2)	N	N	Y	Peroxisome

Abbreviations: a www.uniprot.org/uniprot/; b Blast2GO https://www.blast2go.com/; c http://www.cbs.dtu.dk/services/SignalP; d http://www.cbs.dtu.dk/services/TMHMM; e http://www.cbs.dtu.dk/services/SecretomeP; f http://www.genscript.com/wolf-psort.html; h hhttp://www.cbs.dtu.dk/services/TargetP; Y, yes; N, no.

Supplementary Table 5. The sequence of primers used in chapter 3

Primer Id	Sequence
pAGM check-F	5'-TGC CAC CTG ACG TCT AAG-3'
pAGM check-R	5'-GAG CGC CCA ATA CGC AAA C-3'
M13-F	5'-GGAAACAGCTATGACCATG-3'
M13-R	5'-GTA AAA ACG CGG CCA GTG-3'
mCherry ORF-f	5'-ATG GTC AGC AAG GGC GAA GAA-3'
mCherry ORF-r	5'-TTA CTT GTA GAG TTC GTC-3'
gpdh1 Fw BsaI	5'-GGT CTC TAC AAA ATT CCC GTT CCT GGA AG-3'
gpdh1 Rw BsaI	5'-GGT CTC ACA TTG TAG CTG ATT TGT-3'
HygR Fw BsaI	5'-GGT CTC TTA ACC CGT TAA CGG AAC CCG GTC GG-3'
HygR Rw BsaI	5'-GGT CTC AAC ATT GAT ATT GAA GGA GCA TTT TTG-3'
mCherry Rw BsaI	5'-GGT CTC TAA GCT TAC TTG TAG AGT TCG TC-3'
T-nos Fw BsaI	5'-GGT CTC TGC TTG GCG CGC CGG CCG CCC GGC-3'
T-nos Rw BsaI	5'-GGT CTC CGT TAA ATT CTC ATG TTT GAC AGC-3'
GliI Loc Fw BsaI	5'-GGT CTC CCG GCG GCC TCC GCC CGC GTT TGC AC-3'
GliI Loc Rw BsaI	5'-GGT CTC TAA TGC CCA ACG ACG CAG CCA AGT CC-3'
Sm1 Loc Fw BsaI	5'-GGT CTC CCG GCG AGT CCG CAG TTC TTA ACA GGA A-3'
Sm1 Loc Rw BsaI	5'-GGT CTC TAA TGC AAC TGT CCA ACA TCT TCA CTC TC-3'
Linker-mCherry Fw BsaI	5'-GGT CTC AGC CGG ATC TGC TGG TTC TGC TGC TGG TTC TGG TGA ATT CAT GGT CAG CAA GGG CGA AGA A-3'

Underlined are additional sequences to introduce restriction sites.

Supplementary Table 6. The sequence of primers used in chapter 4

Primer Id	Sequence
Lf *tvox1*-F	5'-TCC GTG TAT GCG TAT AGG-3'
Lf *tvox1 Sfi*I-R	5'-TTT GGC CAT CTA GGC CGA CTG CCA TCT TGA TGA C-3'
Rf *tvox1*-R	5'-GTT CGA TCT ACC AGA CGG TTT G-3'
Rf *tvox1 Sfi*I-F	5'-AAA GGC CTG AGT GGC CCC CAT GCC TAA CTT TAG GTC TC-3'
Lf nested *Hind*III-F	5'-AGG TCA AGC TTC CAA TCA GCC TTC ATA AGG TAG C-3'
Rf nested *BamH*I-R	5'-GTA ATG GAT CCA ATG GGA TCT ACC AGA CGG TTT G-3'
Lf vector *Hind*III-F	5'-AGG TCA AGC TTC CAA TCC GCA ATG TGT TAT TAA GTT GTC-3'
Rf vector *BamH*I-R	5'-GTA ATG GAT CCA ATG GGT CAT CTA TGT TAC TAG ATC GGG-3'
tvox1 ORF f	5'-AGC ATT TCG ATC AGG GTC CTA-3'
tvox1 ORF r	5'-AAA CTC AAG AGC GGT GAT GTC-3'
tvox1 qPCR f	5'-CAG ACC TAT GCG TGG CTA CA-3'
tvox1 qPCR r	5'-GAG TCT GTG GGC CAT TTG TT-3'
TV_93159 qPCR f	5'-CAA TTG TGT TTG GTC AACG-3'

TV_93159 qPCR r	5'-AGT CGC TTC CCA CAC CAT AG-3'
TV_51095 qPCR f	5'-TGC TGG AGA TAG TGC AGG TG-3'
TV_51095 qPCR r	5'-GAT GTT CGT GCC AGA GTT GA-3'
TV_64881 qPCR f	5'-GGT TAC ACT CCT CAC ATT TAC GC-3'
TV_64881 qPCR r	5'-GCT TAT CAC GCT TGG CAT C-3'
TV_66233 qPCR f	5'-TGC CAT TGA AGC AGA GAA TG-3'
TV_66233 qPCR r	5'-TGT TGC AGA GGA AGA CAT CG-3'
TV_68245 qPCR F	5'-TGT TTG TTG CAG TGG CCT TA-3'
TV_68245 qPCR r	5'-GCG TTC GAG TCA CAG CAG TA-3'
TV_79197 qPCR F	5'-CCA ACG TCA ACA ACA AAC TGG
TV_79197 qPCR r	5'-TGT TGC AGC AAA CAA TGA CA
HygR check	5'-CAG AAA CTT CTC GAC AGA CG-3'
hph ORF f	5'-CGT TGC AAG ACC TGC CTG AA-3'
hph ORF r	5'-GGA TGC CTC CGC TCG AAG TA-3'
Lf Comp *Bsa*I-F	5'-GGT CTC TAC AAG TCC AAG TAT AGT AGA GCA CTT-3'
Rf Comp *Bsa*I-R	5'-GGT CTC CGT TAT TCC GTG GTT CCG AGG GCT TGG-3'
Actin-F	5'-TAG AAG GTG TGG TGC CAG ATC TT-3'
Actin-R	5'-GTA TCA TGA TCG GTA TGG GTC AGA A-3'
nptII probe-F	5'-AAT ATC ACG GGT AGC CAA CG-3'
nptII probe-R	5'-TGA ATG AAC TGC AGG ACG AG-3'
Lf *nptII Bsa*I-F	5'-GGT CTC TTA ACC TCG ACT CTA GAG GAT CCT CT-3'
Rf *nptII Bsa*I-R	5'-GGT CTC AAC ATC GTC GTC CAG GCG GTG AGC AC-3'
B-tubulin-F	5'-TCC TTG TAC ACT AGC G-3'
B-tubulin-R	5'-ATC GTT CAT GTT GGA CTC AGC C-3'
pAGM check-F	5'-TGC CAC CTG ACG TCT AAG-3'
pAGM check-R	5'-GAG CGC CCA ATA CGC AAA C-3'
pYT6 check-F	5'-AAC GCT TCT GTC ATC GTT ACA-3'
pYT6 check-R	5'-TTA GGA CTT GTG CGA CAT GT-3'
M13-F	5'-GGAAACAGCTATGACCATG-3'
M13-R	5'-GTA AAA ACG CGG CCA GTG-3'

Underlined are additional sequences to introduce restriction sites.

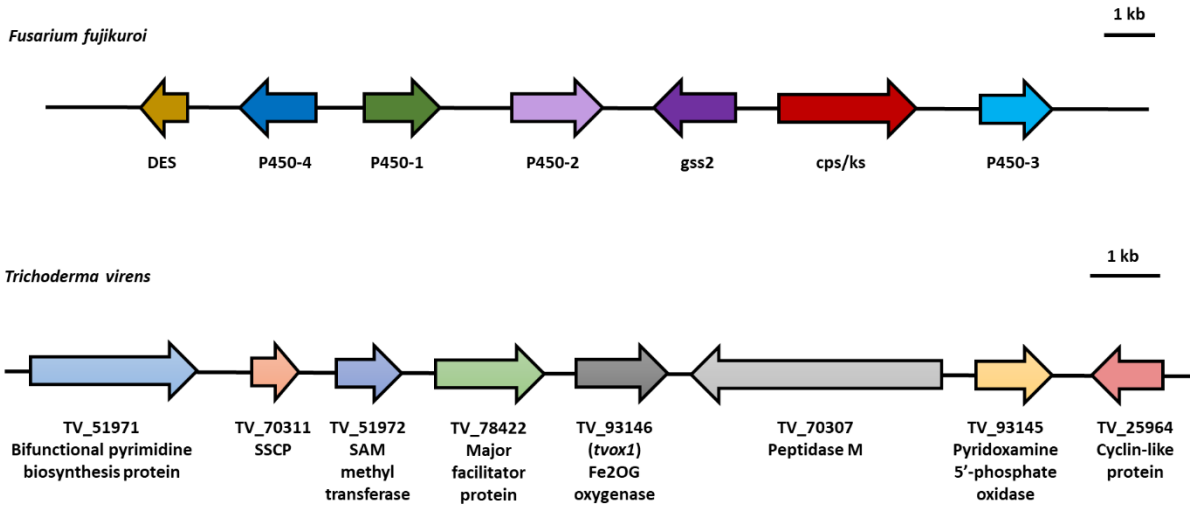

Supplementary Figure 5. Comparison between the gibberellin gene cluster in *F. fujikuroi* and the *tvox1* putative cluster in *T. virens*. Abbreviations: GA_4 1,2-desaturase; des. *ent*-kaurene oxidase (P450 monooxygenase; P450-4. Multifunctional cytochrome P450 (GA_{14}-synthase); P450-1. GA 20-oxidase; P450-2. GA-specific GGDP-synthase; gss2. Bifunctional *ent*-copalyl-*ent*-kaurene synthase; cps/ks. 13-hydroxylase; P450-3.

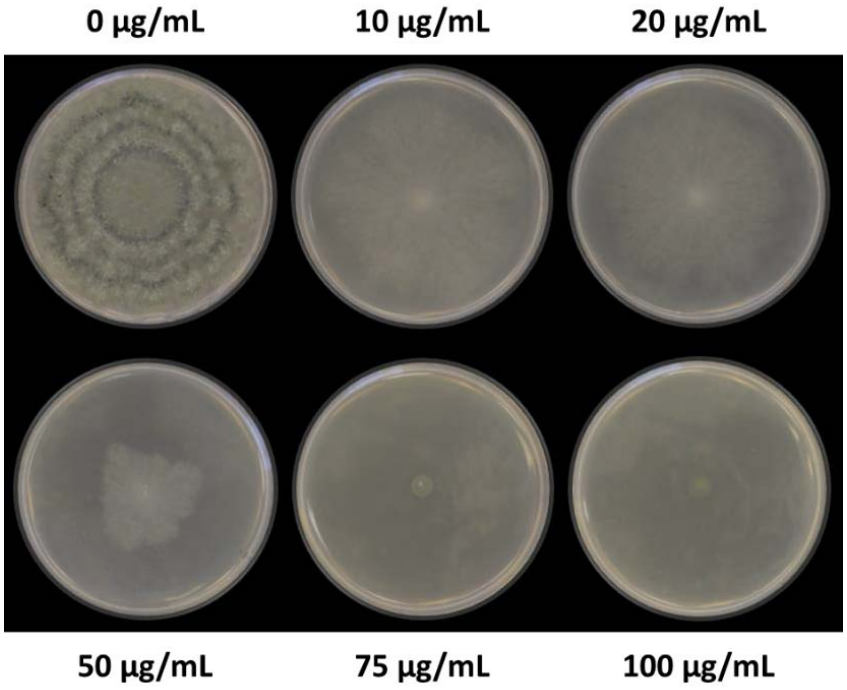

Supplementary Figure 6. Antibiotic resistance of *T. virens* to hygromycin B. Germination, mycelial growth and conidiation of *T. virens* were inhibited at 75 µg/mL hygromycin B.

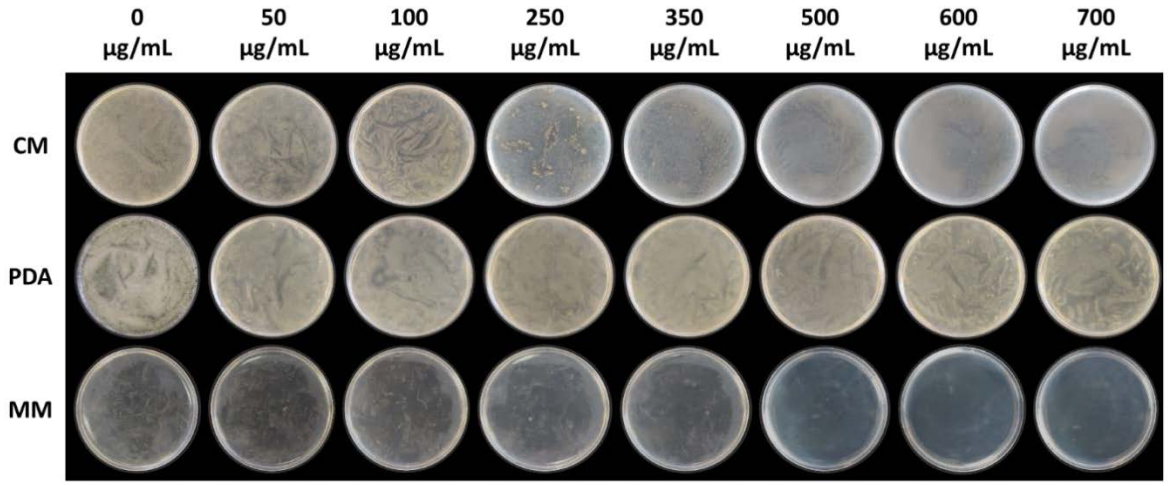

Supplementary Figure 7. Antibiotic resistance of *T. virens* geneticin G418. Germination, mycelial growth and conidiation of *T. virens* were inhibited at 700 µg/mL geneticin G418 on minimal medium (MM). Mycelial growth of *T. virens* was not inhibited at any of the concentrations tested on potato dextrose agar (PDA) and complete media (CM).

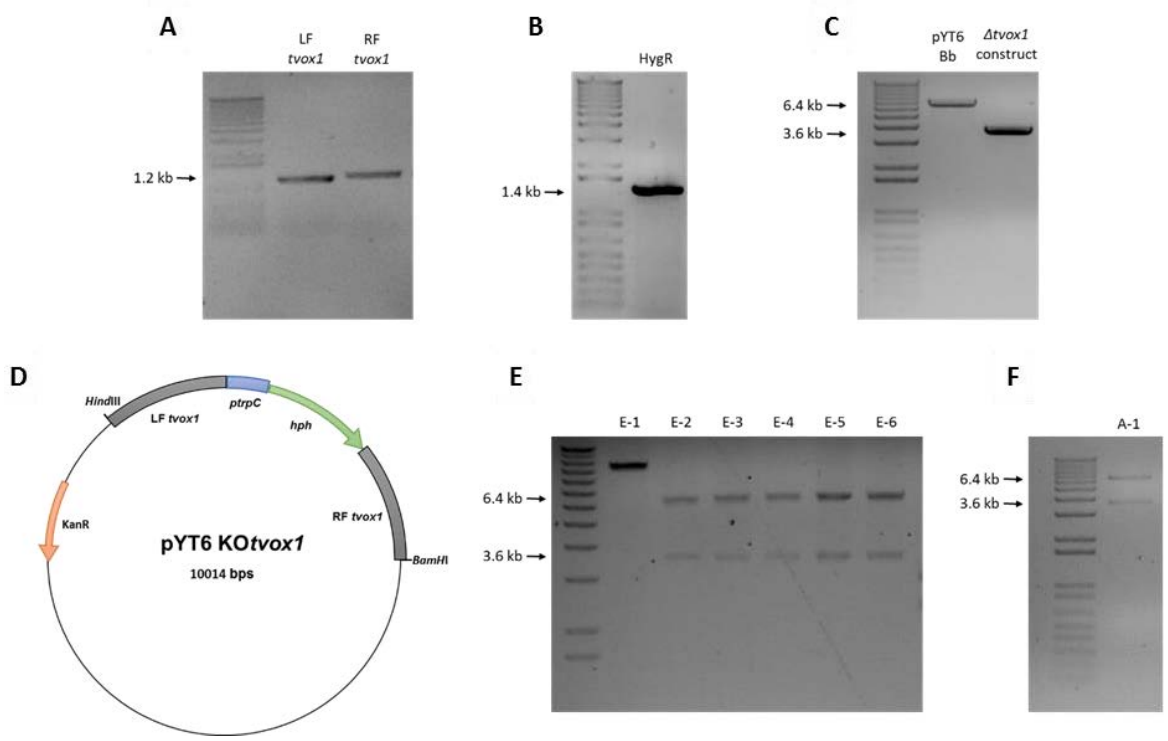

Supplementary Figure 8. Construction of the gene knockout construct. (A) PCR products of left and right flanks of the *tvox1* gene (1.2 kb size product). **(B)** PCR product of HygR cassette (1.4 kb size product). **(C)** PCR products of the deletion construct using nested primers and the pYT6 back bone containing *Hind*III and *BamH*I restriction sites. **(D)** Scheme of the vector containing deletion construct. **(E)** Restriction verification of plasmid of *E. coli* colonies containing deletion construct digested with *Hind*III and *BamH*I (3.6 and 6.4 kb size products); colonies (E-2 to E-6) contained desirable size plasmid. **(F)** Restriction verification of plasmid of *A. tumefaciens* colony containing deletion construct digested with *Hind*III and *BamH*I (3.6 and 6.4 kb size products); colony (A-1) contained the desired size plasmid.

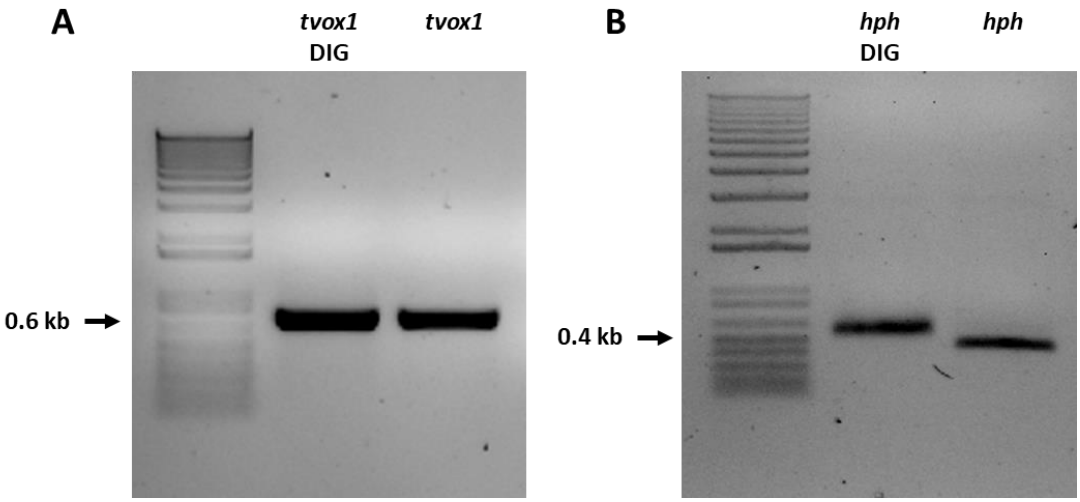

Supplementary Figure 9. Amplification of the probes for confirmation of *tvox1* deletion by Southern blot. (A) DIG-labelled probe of *tvox1* fragment and **(B)** DIG-labelled probe of *hph* fragment.

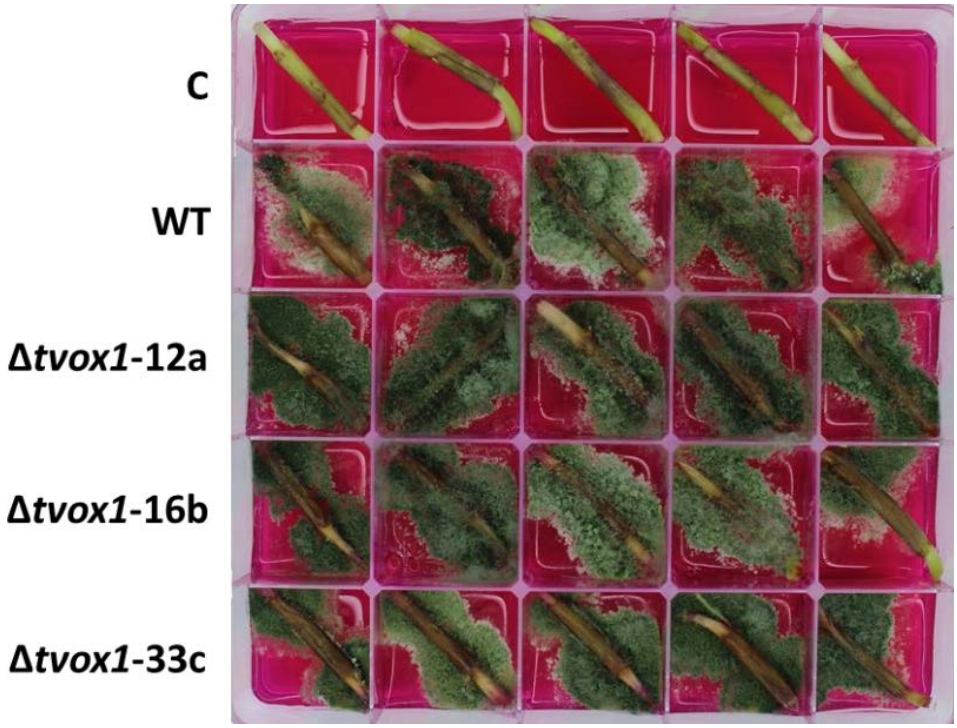

Supplementary Figure 10. Endophytism of *T. virens* WT and Δ*tvox1* mutants in the first 2 cm of maize stem. Endophytic colonisation of *T. virens* in maize stem. Maize stem fragments placed on *Trichoderma* selective media (TSM). Abbreviations: C, control.

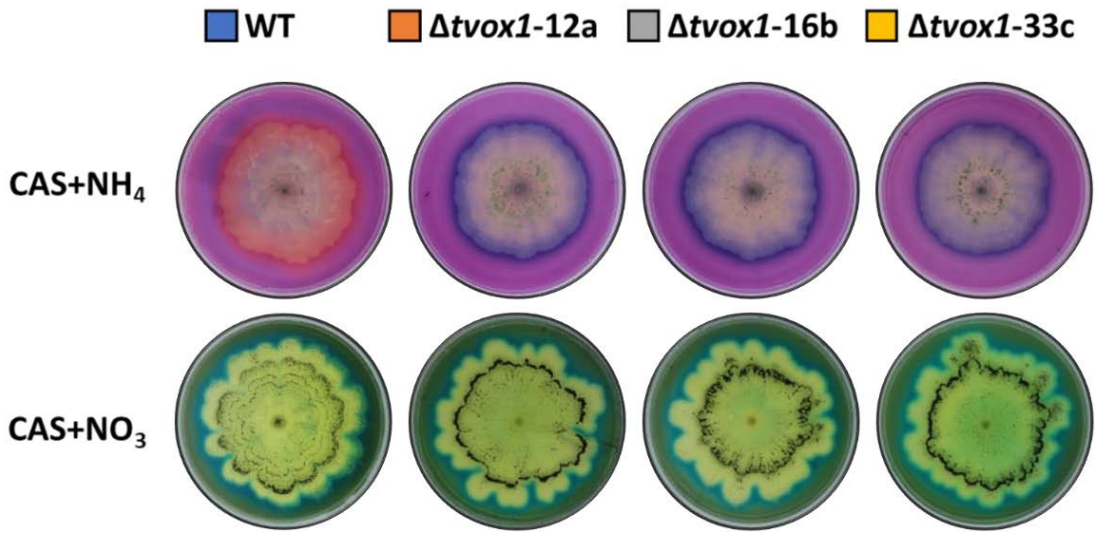

Supplementary Figure 11. Growth of *T. virens* WT and Δ*tvox1* mutants on CAS-agar plates. *T. virens* mycelial growth on CAS-agar plates after 7 d.p.i at 25°C.

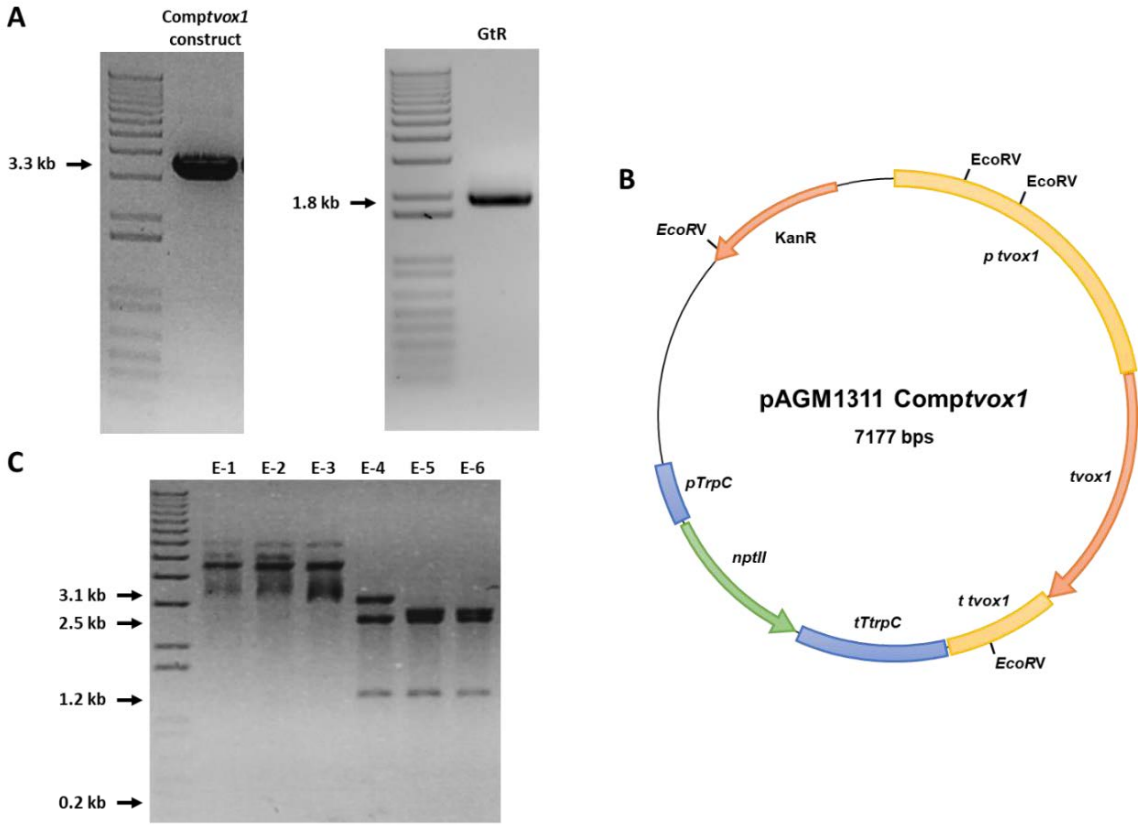

Supplementary Figure 12. Construction of gene complementation construct. (A) PCR product of complementing construct of *tvox1* (3.3 kb size product) and GtR cassette (1.8 kb size product) containing *Bsa*I restriction sites. **(B)** Scheme of the vector containing complementation construct. **(C)** Restriction verification of plasmid of *E. coli* colonies containing complementing construct digested with *EcoR*V (3.1, 2.5, 1.2 and 0.2 kb sizes products); colony (E-4) contained desirable size plasmid.

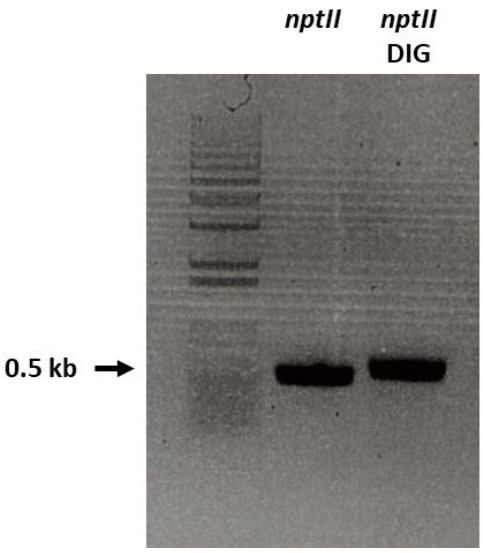

Supplementary Figure 13. Amplification of probe for confirmation of *tvox1* complementation by Southern blot. Control and DIG-labelled probe of *nptII* fragment.

Supplementary Figure 14. Colony appearance of *T. virens* WT, Δ*tvox1* and C*tvox1*. Radial growth and conidiation pattern of *T. virens* WT, Δ*tvox1* and C*tvox1* strains after incubation on potato dextrose agar (PDA) for 7 d with dark/light cycle at 25°C.

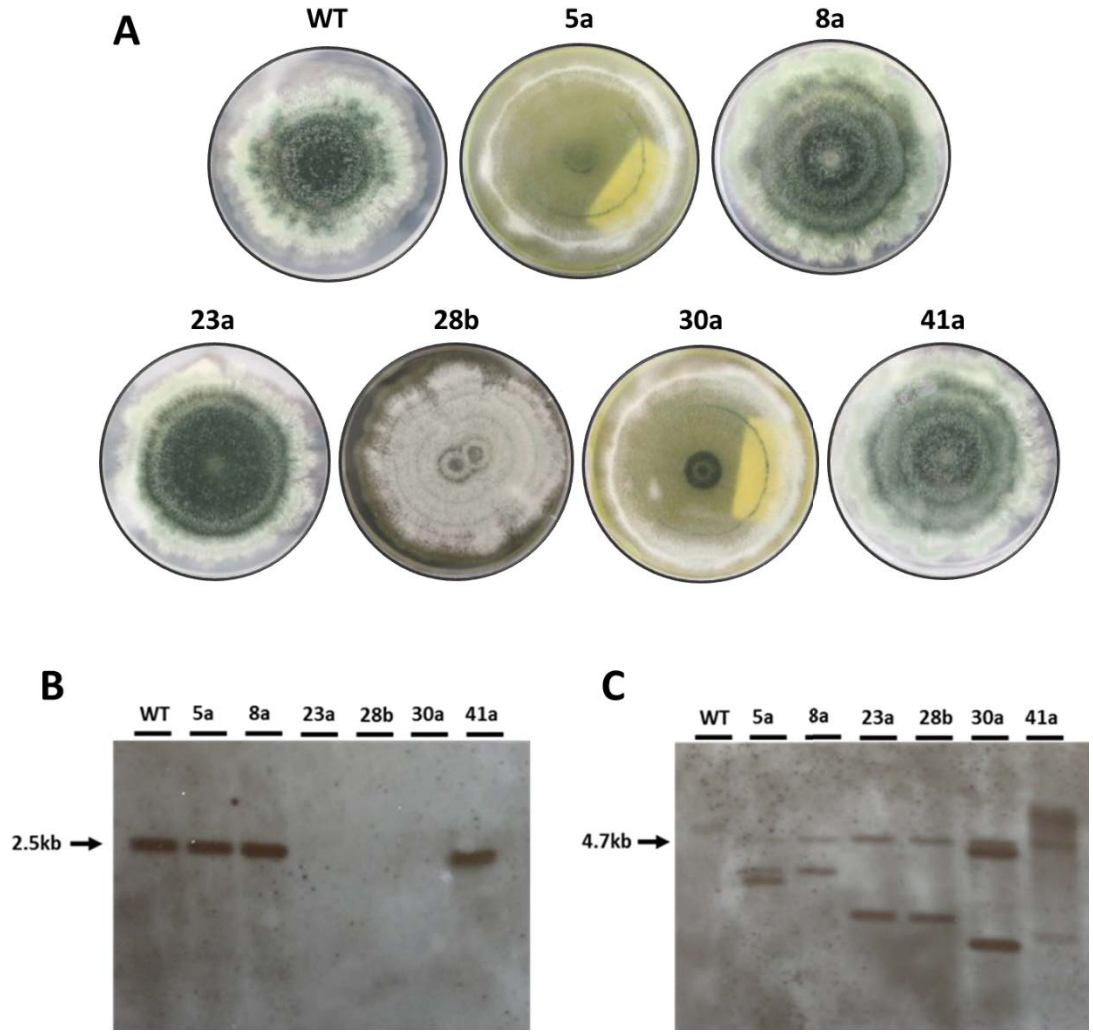

Supplementary Figure 15. Colony appearance and Southern blot analysis of *tvox1* deletion mutants showing ectopic integrations. (A) Colony appearance of *T. virens* WT and Δ*tvox1* mutants. **(B)** Southern blot of native gene (expected fragment of 2.5 kb) and **(C)** Southern blot of resistance cassette integration (expected fragment of 4.7 kb for homologus integration), other fragment sizes represent ectopic integrations in *T. virens* genome.

Preparation of *Escherichia coli* competent cells

A single colony of *E. coli* TOPO F' cells was inoculated to 50 mL of super optimal broth (SOB) and grown overnight at 37°C with shaking at 225 rpm. Four milliliters were inoculated into 400 mL SOB medium in a 1 L conical flask and incubated at 37°C with shaking at 225 rpm to an optical density OD_{560} of 0.5. The culture was aliquoted into eight 45 mL falcon tubes and chilled on ice for 10 min. The cells were centrifuged at 3,000 x g for 7 min at 4°C, the supernatant was removed, and the cells were gently re-suspended in 10 mL of ice cold $CaCl_2$ solution (60 mM $CaCl_2$, 15% glycerol and 10 mM HEPES, pH 7). The cells were centrifuged at 2,500 x g for 5 min at 4°C, the supernatant was removed, and the cells were gently re-suspended in 2 mL of ice cold $CaCl_2$ solution. The cells were stored in 50 µL aliquots at -80°C until required.

Preparation of *Agrobacterium tumefaciens* competent cells

A single colony of *A. tumefaciens* EHA105 was inoculated to 30 mL of Luria broth (LB) amended with 25 µg/mL rifampicin and grown overnight at 30°C with shaking at 250 rpm. Five milliliters were inoculated into 2 x 500 mL Yeast Mannitol (YM) broth in 1 L conical flasks and incubated overnight at 30°C with shaking at 300 rpm. The culture was aliquoted into ten 45 mL falcon tubes and chilled on ice for 10 min. The cells were centrifuged at 3,000 x g for 10 min at 4°C and the cell pellet re-suspended by vortexing in 40 mL ice-cold 10% glycerol. Cells were centrifuged as described above and gently re-suspended in 500 µL ice-cold 10% glycerol and combined in one tube. Cells were pelleted once more as previously described and the pellet was re-suspended in 500 µL ice-cold 1 M sorbitol. Aliquots of 40 µL were transferred on ice to 1.5 mL centrifuge tubes and stored at -80°C until required.

Preparation of media and solutions

All media were sterilised by autoclaving (121°C, 15 min) and made up to 1 L unless otherwise specified. Culture media containing thermally unstable components were sterilised by filtration (0.22 µm) and poured into previously autoclaved containers.

Luria Bertani Agar (LBA)

- 10 g/L Tryptone
- 5 g/L Yeast extract
- 10 g/L NaCl
- 15 g/L Bacteriological agar

Luria Bertani Broth (LBB)

- 10 g/L Tryptone
- 5 g/L Yeast extract
- 10 g/L NaCl

Potato Dextrose Agar (PDA)

- 4 g/L Potato starch infusion
- 20 g/L Dextrose
- 15 g/L Bacteriological agar

Complete Media (CM)

- 25 g/L Glucose
- 5 g/L Malt extract
- 15 g/L Bacteriological agar

Potato Dextrose Broth (PDB)

- 4 g/L Potato starch infusion
- 20 g/L Dextrose
- 15 g/L Bacteriological agar

Kanamycin Stock (25 mg/mL)

- 125 mg Kanamycin sulphate (Sigma-Aldrich, USA)
- 5 mL H_2O

The solution was filter sterilised and 500 µL aliquots stored at -20°C.

Rifampicin Stock (25 mg/mL)

- 125 mg Rifampicin (Sigma-Aldrich, USA)
- 5 mL DMSO (Sigma-Aldrich, USA)

The solution was filter sterilised and 500 µL aliquots stored at -20°C.

Timentin Stock (100 mg/mL)

- 500 mg Timentin (GlaxoSmithKline Plc, UK)
- 5 mL H_2O

The solution was filter sterilised and 500 µL aliquots stored at -20°C.

Hygromycin Stock (100 mg/mL)

- 500 mg Hygromycin (AG Scientific, USA)
- 5 mL H_2O

The solution was filter sterilised and 500 µL aliquots stored at -20°C.

Vogel´s Minimal Media (VMM)

- 20 mL Vogel´s salts
- 15 g/L Sucrose

Vogel´s salts (20 mL)

- 150 g/L Sodium citrate
- 250 g/L KH_2PO_4
- 100 g/L NH_4NO_3
- 10 g/L $MgSO_4.7H_2O$
- 5 g/L $CaCl_2.2H_2O$
- 5 mL Trace elements
- 2.5 mL Biotin solution

Trace elements (100 mL)

- 5 g Citric acid
- 5 g $ZnSO_4.7H_2O$
- 1 g $Fe(NH_4)_2 (SO_4)_2.6H_2O$
- 0.25 g $CuSO_4.5H_2O$
- 0.05 g $MnSO_4.H_2O$
- 0.05 g H_3BO_4
- 0.05 g $Na_2MoO_4.2H_2O$

Biotin solution (50 mL)

- 5 mg Biotin

***Trichoderma* selective media (TSM)**

- 20 g/L Bacteriological agar
- 3 g/L Glucose
- 1 g/L Ammonium nitrate
- 0.9 g/L $K_2HPO_4.3H_2O$
- 0.2 g/L $MgSO_4.7H_2O$
- 0.15 g/L KCl
- 0.2 g/L Terrachlor 75 WP
- 0.15 g/L Rose bengal
- 1 mL Chloramphenicol (2.5 mg/mL stock)
- 1 mL Metal salt solution

Metal Salt Solution

- 1 g/L $FeSO_4.7H_2O$
- 0.65 g/L $MnSO_4.4H_2O$
- 0.9 g/L $ZnSO_4.7H_2O$

Minimal Media Broth (10 mL)

- Solution 1: 100 µL 10 M K_2HPO_4 + 10 M KH_2PO_4
- Solution 2: 200 µL 100 mM $MgSO_4$ + 125 mM NaCl
- Solution 3: 10 µL 700 mM $CaCl_2$
- Solution 4: 100 µL 1 M D-glucose
- Solution 5: 100 µL 0.9 mM $FeSO_4$
- Solution 6: 25 µL 400 mM $(NH_4)_2SO_4$

IMAS Broth (50 mL)

- Solution 1: 500 µL
- Solution 2: 1 mL
- Solution 3: 50 µL
- Solution 4: 500 µL
- Solution 5: 500 µL
- Solution 6: 125 µL
- 2 mL 1 M MES buffer
- 500 µL 50% glycerol
- 100 µL Acetosyringone

IMAS Agar

- Solution 1: 10 mL/L
- Solution 2: 20 mL/L
- Solution 3: 1 mL/L
- Solution 4: 10 mL/L
- Solution 5: 10 mL/L
- Solution 6: 2.5 mL/L
- 40 mL/L 1 M MES buffer
- 10 mL/L 50% glycerol
- 2 mL/L Acetosyringone

MES buffer

- 1 M MES. H_2O pH 5.3
  (Adjusted with NaOH)

Acetosyringone

- 0.2 mM diluted with ethanol (Freshly made).

Lignocellulose Agar (LCA) Minimal Media: Stock Solutions (500 mL)

- Solution A 50X: 5 g $MgSO_4.7H_2O$
- Solution B 50X: 22.5 g K_2HPO_4
- Solution C 50X: 5 g KCl

Lignocellulose Agar (LCA) Minimal Media pH 5.5

- Solution A: 20 mL/L
- Solution B: 20 mL/L
- Solution C: 20 mL/L
- 0.2 g Yeast extract
- 750 mL/L Nanopure water

The pH was adjusted to 5.5 with 50% HCl.

Salts solution was filled up to 870 mL with Nanopure water and the total content was split in half in separate bottles and label as CAS-NH_4 and CAS-NO_3.

- Bacto Agar 7.5 g for each bottle.

Media was autoclaved and cooled to 50°C.

- 5 mL 1M NH_4Cl to CAS-NH_4
- 5 mL 1M KNO_3 to CAS-NO_3
- 10 mL 20% filtered sterilised glucose to CAS-NH_4 and to CAS-NO_3 solutions.

References

Agrawal, G.K., Jwa, N.S., Lebrun, M.H., Job, D. and Rakwal, R. (2010) Plant secretome: unlocking secrets of the secreted proteins. *Proteomics* **10**, 799-827.

Ahmad, S., Veyrat, N., Gordon-Weeks, R., Zhang, Y., Martin, J., Smart, L., Glauser, G., Erb, M., Flors, V., Frey, M. and Ton, J. (2011) Benzoxazinoid metabolites regulate innate immunity against aphids and fungi in maize. *Plant Physiology* **157**, 317-327.

Ahmed, E. and Holmström, S.J.M. (2014) Siderophores in environmental research: roles and applications. *Microbial Biotechnology* **7**, 196-208.

Akum, F.N., Steinbrenner, J., Biedenkopf, D., Imani, J. and Kogel, K.-H. (2015) The *Piriformospora indica* effector PIIN_08944 promotes the mutualistic Sebacinalean symbiosis. *Frontiers in Plant Science* **6**.

Alexandersson, E., Ali, A., Resjo, S. and Andreasson, E. (2013) Plant secretome proteomics. *Frontiers in Plant Science* **4**, 9.

Almagro, L., Gomez Ros, L.V., Belchi-Navarro, S., Bru, R., Ros Barcelo, A. and Pedreno, M.A. (2009) Class III peroxidases in plant defence reactions. *Journal of Experimental Botany* **60**, 377-390.

Alonso-Ramirez, A., Poveda, J., Martin, I., Hermosa, R., Monte, E. and Nicolas, C. (2014) Salicylic acid prevents *Trichoderma harzianum* from entering the vascular system of roots. *Molecular Plant Pathology* **15**, 823-831.

Alqueres, S., Meneses, C., Rouws, L., Rothballer, M., Baldani, I., Schmid, M. and Hartmann, A. (2013) The bacterial superoxide dismutase and glutathione reductase are crucial for endophytic colonization of rice roots by *Gluconacetobacter diazotrophicus* PAL5. *Molecular Plant-Microbe Interactions* **26**, 937-945.

Allen, M.F., Allen, E.B. and Friese, C.F. (1989) Responses of the non-mycotrophic plant *Salsola kali* to invasion by vesicular-arbuscular mycorrhizal fungi. *New Phytologist* **111**, 45-49.

Allwood, J.W., Ellis, D.I. and Goodacre, R. (2008) Metabolomic technologies and their application to the study of plants and plant-host interactions. *Physiologia Plantarum* **132**, 117-135.

Andrade, S.A.L., Malik, S., Sawaya, A.C.H.F., Bottcher, A. and Mazzafera, P. (2013) Association with arbuscular mycorrhizal fungi influences alkaloid synthesis and accumulation in *Catharanthus roseus* and *Nicotiana tabacum* plants. *Acta Physiologiae Plantarum* **35**, 867-880.

Appels, F.V.W., Dijksterhuis, J., Lukasiewicz, C.E., Jansen, K.M.B., Wösten, H.A.B. and Krijgsheld, P. (2018) Hydrophobin gene deletion and environmental growth conditions impact mechanical properties of mycelium by affecting the density of the material. *Scientific Reports* **8**, 4703.

Arner, E.S. and Holmgren, A. (2000) Physiological functions of thioredoxin and thioredoxin reductase. *European Journal of Biochemistry* **267**, 6102-6109.

Aznar, A., Chen, N.W.G., Thomine, S. and Dellagi, A. (2015) Immunity to plant pathogens and iron homeostasis. *Plant Science* **240**, 90-97.

Backman, P.A. and Sikora, R.A. (2008) Endophytes: An emerging tool for biological control. *Biological Control* **46**, 1-3.

Baek, J.M. and Kenerley, C.M. (1998) The arg2 gene of *Trichoderma virens*: cloning and development of a homologous transformation system. *Fungal Genetics and Biology* **23**, 34-44.

Bailey, B.A., Bae, H., Strem, M.D., Roberts, D.P., Thomas, S.E., Crozier, J., Samuels, G.J., Choi, I.Y. and Holmes, K.A. (2006) Fungal and plant gene expression during the colonization of cacao seedlings by endophytic isolates of four *Trichoderma* species. *Planta* **224**, 1449-1464.

Bailey, B.A., Strem, M.D. and Wood, D. (2009) *Trichoderma* species form endophytic associations within *Theobroma cacao* trichomes. *Mycological Research* **113**, 1365-1376.

Bais, H.P., Weir, T.L., Perry, L.G., Gilroy, S. and Vivanco, J.M. (2006) The role of root exudates in rhizosphere interactions with plants and other organisms. *Annual Review of Plant Biology* **57**, 233-266.

Bakker, P.A.H.M., Doornbos, R.F., Zamioudis, C., Berendsen, R.L. and Pieterse, C.M.J. (2013) Induced systemic resistance and the rhizospherre micriobiome. *The Plant Pathology Journal* **29**, 136-143.

Balmer, D., Flors, V., Glauser, G. and Mauch-Mani, B. (2013) Metabolomics of cereals under biotic stress: current knowledge and techniques. *Frontiers in Plant Science* **4**, 82.

Beckman, C.H. (2000) Phenolic-storing cells: keys to programmed cell death and periderm formation in wilt disease resistance and in general defence responses in plants? *Physiological and Molecular Plant Pathology* **57**, 101-110.

Bendtsen, J.D., Jensen, L.J., Blom, N., Von Heijne, G. and Brunak, S. (2004a) Feature-based prediction of non-classical and leaderless protein secretion. *Protein Engineering, Design and Selection* **17**, 349-356.

Bendtsen, J.D., Nielsen, H., von Heijne, G. and Brunak, S. (2004b) Improved prediction of signal peptides: SignalP 3.0. *Journal of Molecular Biology* **340**, 783-795.

Bensadoun, A. and Weinstein, D. (1976) Assay of proteins in the presence of interfering materials. *Analytical Biochemistry* **70**, 241-250.

Berendsen, R.L., Pieterse, C.M. and Bakker, P.A. (2012) The rhizosphere microbiome and plant health. *Trends in Plant Science* **17**, 478-486.

Berens, M.L., Berry, H.M., Mine, A., Argueso, C.T. and Tsuda, K. (2017) Evolution of hormone signaling networks in plant defense. *Annual Review of Phytopathology* **55**, 401-425.

Betsiashvili, M., Ahern, K.R. and Jander, G. (2015) Additive effects of two quantitative trait loci that confer *Rhopalosiphum maidis* (corn leaf aphid) resistance in maize inbred line Mo17. *Journal of Experimental Botany* **66**, 571-578.

Bhadauria, V. and Peng, Y.L. (2010) Optimization of a protein extraction technique for fungal proteomics. *Indian Journal of Microbiology* **50**, 127-131.

Bhuiyan, N.H., Selvaraj, G., Wei, Y. and King, J. (2009) Role of lignification in plant defense. *Plant Signaling and Behavior* **4**, 158-159.

Biely, P. (1985) Microbial xylanolytic systems. *Trends in Biotechnology* **3**, 286-290.

Bittel, P. and Robatzek, S. (2007) Microbe-associated molecular patterns (MAMPs) probe plant immunity. *Current Opinion in Plant Biology* **10**, 335-341.

Blilou, I., Bueno, P., Ocampo, J.A. and García-Garrido, J.M. (2000) Induction of catalase and ascorbate peroxidase activities in tobacco roots inoculated with the arbuscular mycorrhizal *Glomus mosseae*. *Mycological Research* **104**, 722-725.

Bolte, S., Talbot, C., Boutte, Y., Catrice, O., Read, N.D. and Satiat-Jeunemaitre, B. (2004) FM-dyes as experimental probes for dissecting vesicle trafficking in living plant cells. *Journal of Microscopy* **214**, 159-173.

Bolton, E.E., Wang, Y., Thiessen, P.A. and Bryant, S.H. (2008) PubChem: integrated platform of small molecules and biological activities. *Annual Reports in Computational Chemistry* eds. Wheeler, R.A. and Spellmeyer, D.C. pp.217-241: Elsevier.

Boller, T. and Felix, G. (2009) A renaissance of elicitors: perception of microbe-associated molecular patterns and danger signals by pattern-recognition receptors. *Annual Review of Plant Biology* **60**, 379-406.

Brader, G., Compant, S., Vescio, K., Mitter, B., Trognitz, F., Ma, L.-J. and Sessitsch, A. (2017) Ecology and genomic insights into plant-pathogenic and plant-nonpathogenic endophytes. *Annual Review of Phytopathology* **55**, 61-83.

Brandon, M., Howard, B., Lawrence, C. and Laubenbacher, R. (2015) Iron acquisition and oxidative stress response in *Aspergillus fumigatus*. *BMC Systems Biology* **9**, 19-19.

Broekgaarden, C., Caarls, L., Vos, I.A., Pieterse, C.M.J. and Van Wees, S.C.M. (2015) Ethylene: traffic controller on hormonal crossroads to defense. *Plant Physiology* **169**, 2371-2379.

Brotman, Y., Kapuganti, J.G. and Viterbo, A. (2010) *Trichoderma*. *Current Biology* **20**, R390-391.

Brotman, Y., Lisec, J., Meret, M., Chet, I., Willmitzer, L. and Viterbo, A. (2012) Transcript and metabolite analysis of the *Trichoderma*-induced systemic resistance response to *Pseudomonas syringae* in *Arabidopsis thaliana*. *Microbiology* **158**, 139-146.

Brown, D.E., Rashotte, A.M., Murphy, A.S., Normanly, J., Tague, B.W., Peer, W.A., Taiz, L. and Muday, G.K. (2001) Flavonoids act as negative regulators of auxin transport in vivo in Arabidopsis. *Plant Physiology* **126**, 524-535.

Bundy, J.G., Davey, M.P. and Viant, M.R. (2008) Environmental metabolomics: a critical review and future perspectives. *Metabolomics* **5**, 3-21.

Busby, P.E., Ridout, M. and Newcombe, G. (2016) Fungal endophytes: modifiers of plant disease. *Plant Molecular Biology* **90**, 645-655.

Calvo, A.M., Wilson, R.A., Bok, J.W. and Keller, N.P. (2002) Relationship between secondary metabolism and fungal development. *Microbiology and Molecular Biology Reviews* **66**, 447-459.

Casarrubia, S., Daghino, S., Kohler, A., Morin, E., Khouja, H.-R., Daguerre, Y., Veneault-Fourrey, C., Martin, F.M., Perotto, S. and Martino, E. (2018) The hydrophobin-like OmSSP1 may be an effector in the ericoid mycorrhizal symbiosis. *Frontiers in Plant Science* **9**.

Castro-Sowinski, S., Matan, O., Bonafede, P. and Okon, Y. (2007) A thioredoxin of *Sinorhizobium meliloti* CE52G is required for melanin production and symbiotic nitrogen fixation. *Molecular Plant-Microbe Interactions* **20**, 986-993.

Ceccarelli, N., Curadi, M., Martelloni, L., Sbrana, C., Picciarelli, P. and Giovannetti, M. (2010) Mycorrhizal colonization impacts on phenolic content and antioxidant properties of artichoke leaves and flower heads two years after field transplant. *Plant and Soil* **335**, 311-323.

Clark, K., Franco, J.Y., Schwizer, S., Pang, Z., Hawara, E., Liebrand, T.W.H., Pagliaccia, D., Zeng, L., Gurung, F.B., Wang, P., Shi, J., Wang, Y., Ancona, V., van der Hoorn, R.A.L., Wang, N., Coaker, G. and Ma, W. (2018) An effector from the Huanglongbing-associated pathogen targets citrus proteases. *Nature Communications* **9**, 1718.

Conesa, A., Gotz, S., Garcia-Gomez, J.M., Terol, J., Talon, M. and Robles, M. (2005) Blast2GO: a universal tool for annotation, visualization and analysis in functional genomics research. *Bioinformatics* **21**, 3674-3676.

Cook, D.E., Mesarich, C.H. and Thomma, B.P.H.J. (2015) Understanding plant immunity as a surveillance system to detect invasion. *Annual Review of Phytopathology* **53**, 541-563.

Costa, T.R.D., Felisberto-Rodrigues, C., Meir, A., Prevost, M.S., Redzej, A., Trokter, M. and Waksman, G. (2015) Secretion systems in Gram-negative bacteria: structural and mechanistic insights. *Nature Reviews Microbiology* **13**, 343.

Coulthurst, S.J. (2013) The Type VI secretion system - a widespread and versatile cell targeting system. *Research in Microbiology* **164**, 640-654.

Cripps-Guazzone, N., Jones, E., Condron, L.M., McLean, K.L., Stewart, A. and Ridgway, H. (2016) Rhizosphere and endophytic colonisation of ryegrass and sweet corn roots by the isolate *Trichoderma atroviride* LU132 at different soil pHs. *New Zealand Plant Protection* **69**, 78-85.

Crutcher, F.K., Moran-Diez, M.E., Ding, S., Liu, J., Horwitz, B.A., Mukherjee, P.K. and Kenerley, C.M. (2015) A paralog of the proteinaceous elicitor SM1 is involved in colonization of maize roots by *Trichoderma virens*. *Fungal Biology* **119**, 476-486.

Crutcher, F.K., Parich, A., Schuhmacher, R., Mukherjee, P.K., Zeilinger, S. and Kenerley, C.M. (2013) A putative terpene cyclase, vir4, is responsible for the biosynthesis of volatile terpene compounds in the biocontrol fungus *Trichoderma virens*. *Fungal Genetics and Biology* **56**, 67-77.

Cui, H., Tsuda, K. and Parker, J.E. (2015) Effector-triggered immunity: from pathogen perception to robust defense. *Annual Review of Plant Biology* **66**, 487-511.

Cui, S., Guo, X., Chang, F., Cui, Y., Ma, L., Sun, Y. and Sun, D. (2005) Apoplastic calmodulin receptor-like binding proteins in suspension-cultured cells of *Arabidopsis thaliana*. *The Journal of Biological Chemistry* **280**, 31420-31427.

Chacon, M.R., Rodriguez-Galan, O., Benitez, T., Sousa, S., Rey, M., Llobell, A. and Delgado-Jarana, J. (2007) Microscopic and transcriptome analyses of early colonization of tomato roots by *Trichoderma harzianum*. *International Microbiology* **10**, 19-27.

Chen, L.H., Lin, C.H. and Chung, K.R. (2013a) A nonribosomal peptide synthetase mediates siderophore production and virulence in the citrus fungal pathogen *Alternaria alternata*. *Molecular Plant Pathology* **14**, 497-505.

Chen, X., Zaro, J.L. and Shen, W.C. (2013b) Fusion protein linkers: property, design and functionality. *Advanced Drug Delivery Reviews* **65**, 1357-1369.

Chen, Y., Zhu, J., Ying, S.H. and Feng, M.G. (2014) The GPI-anchored protein Ecm33 is vital for conidiation, cell wall integrity, and multi-stress tolerance of two filamentous entomopathogens but not for virulence. *Applied Microbiology and Biotechnology* **98**, 5517-5529.

Cheynier, V., Comte, G., Davies, K.M., Lattanzio, V. and Martens, S. (2013) Plant phenolics: recent advances on their biosynthesis, genetics, and ecophysiology. *Plant Physiology and Biochemistry* **72**, 1-20.

Choi, D.S., Hwang, I.S. and Hwang, B.K. (2012) Requirement of the cytosolic interaction between pathogenesis-related protein 10 and leucine-rich repeat protein 1 for cell death and defense signaling in pepper. *The Plant Cell* **24**, 1675-1690.

Choi, J., Park, J., Kim, D., Jung, K., Kang, S. and Lee, Y.H. (2010) Fungal secretome database: integrated platform for annotation of fungal secretomes. *BMC Genomics* **11**, 105.

Choy, C.H., Han, B.K. and Botelho, R.J. (2017) Phosphoinositide diversity, distribution, and effector function: stepping out of the box. *BioEssays* **39**.

Chu, J., Li, W.-F., Cheng, W., Lu, M., Zhou, K.-H., Zhu, H.-Q., Li, F.-G. and Zhou, C.-Z. (2015) Comparative analyses of secreted proteins from the phytopathogenic fungus *Verticillium dahliae* in response to nitrogen starvation. *Biochimica et Biophysica Acta* **1854**, 437-448.

Dannel, F., Pfeffer, H. and Marschner, H. (1995) Isolation of apoplasmic fluid from sunflower leaves and its use for studies on influence of nitrogen supply on apoplasmic pH. *Journal of Plant Physiology* **146**, 273-278.

de Groot, M.J., Bundock, P., Hooykaas, P.J. and Beijersbergen, A.G. (1998) *Agrobacterium tumefaciens*-mediated transformation of filamentous fungi. *Nature Biotechnology* **16**, 839-842.

de Jonge, R., van Esse, H.P., Kombrink, A., Shinya, T., Desaki, Y., Bours, R., van der Krol, S., Shibuya, N., Joosten, M.H. and Thomma, B.P. (2010) Conserved fungal LysM effector Ecp6 prevents chitin-triggered immunity in plants. *Science* **329**, 953-955.

De Palma, M., Salzano, M., Villano, C., Aversano, R., Lorito, M., Ruocco, M., Docimo, T., Piccinelli, A.L., D'Agostino, N. and Tucci, M. (2019) Transcriptome reprogramming, epigenetic modifications and alternative splicing orchestrate the tomato root response to the beneficial fungus *Trichoderma harzianum*. *Horticulture Research* **6**, 5.

de Santiago, A., Quintero, J.M., Avilés, M. and Delgado, A. (2009) Effect of *Trichoderma asperellum* strain T34 on iron nutrition in white lupin. *Soil Biology and Biochemistry* **41**, 2453-2459.

De Wit, P.J., Mehrabi, R., Van den Burg, H.A. and Stergiopoulos, I. (2009) Fungal effector proteins: past, present and future. *Molecular Plant Pathology* **10**, 735-747.

Degani, O., Lev, S. and Ronen, M. (2013) Hydrophobin gene expression in the maize pathogen *Cochliobolus heterostrophus*. *Physiological and Molecular Plant Pathology* **83**, 25-34.

Delaunois, B., Jeandet, P., Clement, C., Baillieul, F., Dorey, S. and Cordelier, S. (2014) Uncovering plant-pathogen crosstalk through apoplastic proteomic studies. *Frontiers in Plant Science* **5**, 249.

Deng, F.A.N., Aoki, M. and Yogo, Y. (2004) Effect of naringenin on the growth and lignin biosynthesis of gramineous plants. *Weed Biology and Management* **4**, 49-55.

Deng, Y., Wang, J., Tung, J., Liu, D., Zhou, Y., He, S., Du, Y., Baker, B. and Li, F. (2018) A role for small RNA in regulating innate immunity during plant growth. *PLOS Pathogens* **14**, e1006756.

Deshmukh, S., Hückelhoven, R., Schäfer, P., Imani, J., Sharma, M., Weiss, M., Waller, F. and Kogel, K.-H. (2006) The root endophytic fungus *Piriformospora indica* requires host cell death for proliferation during mutualistic symbiosis with barley. *Proceedings of the National Academy of Sciences of the United States of America* **103**, 18450-18457.

Ding, Y., Wang, J., Wang, J., Stierhof, Y.D., Robinson, D.G. and Jiang, L. (2012) Unconventional protein secretion. *Trends in Plant Science* **17**, 606-615.

Dixon, R.A. and Strack, D. (2003) Phytochemistry meets genome analysis, and beyond. *Phytochemistry* **62**, 815-816.

Dixon, S.J. and Stockwell, B.R. (2014) The role of iron and reactive oxygen species in cell death. *Nature Chemical Biology* **10**, 9-17.

Djamei, A., Schipper, K., Rabe, F., Ghosh, A., Vincon, V., Kahnt, J., Osorio, S., Tohge, T., Fernie, A.R., Feussner, I., Feussner, K., Meinicke, P., Stierhof, Y.D., Schwarz, H., Macek, B., Mann, M. and Kahmann, R. (2011) Metabolic priming by a secreted fungal effector. *Nature* **478**, 395-398.

Djonovic, S., Pozo, M.J., Dangott, L.J., Howell, C.R. and Kenerley, C.M. (2006) Sm1, a proteinaceous elicitor secreted by the biocontrol fungus *Trichoderma virens* induces plant defense responses and systemic resistance. *Molecular Plant-Microbe Interactions* **19**, 838-853.

Djonović, S., Vargas, W.A., Kolomiets, M.V., Horndeski, M., Wiest, A. and Kenerley, C.M. (2007) A proteinaceous elicitor Sm1 from the beneficial fungus *Trichoderma virens* is required for induced systemic resistance in maize. *Plant Physiology* **145**, 875-889.

Doehlemann, G. and Hemetsberger, C. (2013) Apoplastic immunity and its suppression by filamentous plant pathogens. *New Phytologist* **198**, 1001-1016.

Doehlemann, G., Requena, N., Schaefer, P., Brunner, F., O'Connell, R. and Parker, J.E. (2014) Reprogramming of plant cells by filamentous plant-colonizing microbes. *New Phytologist* **204**, 803-814.

Dragisic Maksimovic, J., Maksimovic, V., Zivanovic, B., Hadzi-Taskovic Sukalovic, V. and Vuletic, M. (2008) Peroxidase activity and phenolic compounds content in maize root and leaf apoplast, and their association with growth. *Plant Science* **175**, 656-662.

Dragisic Maksimovic, J., Zivanovic, B.D., Maksimovic, V.M., Mojovic, M.D., Nikolic, M.T. and Vucinic, Z.B. (2014) Filter strip as a method of choice for apoplastic fluid extraction from maize roots. *Plant Science* **223**, 49-58.

Druzhinina, I.S., Seidl-Seiboth, V., Herrera-Estrella, A., Horwitz, B.A., Kenerley, C.M., Monte, E., Mukherjee, P.K., Zeilinger, S., Grigoriev, I.V. and Kubicek, C.P. (2011) *Trichoderma*: the genomics of opportunistic success. *Nature Reviews Microbiology* **9**, 749-759.

Druzhinina, I.S., Shelest, E. and Kubicek, C.P. (2012) Novel traits of *Trichoderma* predicted through the analysis of its secretome. *FEMS Microbiology Letters* **337**, 1-9.

Dubey, M.K., Jensen, D.F. and Karlsson, M. (2014) Hydrophobins are required for conidial hydrophobicity and plant root colonization in the fungal biocontrol agent *Clonostachys rosea*. *BMC Microbiology* **14**, 18.

Dunn, L.L., Rahmanto, Y.S. and Richardson, D.R. (2007) Iron uptake and metabolism in the new millennium. *Trends in Cell Biology* **17**, 93-100.

Dupont, P.-Y., Eaton, C.J., Wargent, J.J., Fechtner, S., Solomon, P., Schmid, J., Day, R.C., Scott, B. and Cox, M.P. (2015) Fungal endophyte infection of ryegrass reprograms host metabolism and alters development. *New Phytologist* **208**, 1227-1240.

Egamberdieva, D., Wirth, S.J., Alqarawi, A.A., Abd_Allah, E.F. and Hashem, A. (2017) Phytohormones and beneficial microbes: essential components for plants to balance stress and fitness. *Frontiers in Microbiology* **8**, 2104.

Eichhorn, H., Lessing, F., Winterberg, B., Schirawski, J., Kämper, J., Müller, P. and Kahmann, R. (2006) A ferroxidation/permeation iron uptake system is required for virulence in *Ustilago maydis*. *The Plant Cell* **18**, 3332.

Emanuelsson, O., Brunak, S., von Heijne, G. and Nielsen, H. (2007) Locating proteins in the cell using TargetP, SignalP and related tools. *Nature Protocols* **2**, 953-971.

Emanuelsson, O., Nielsen, H., Brunak, S. and von Heijne, G. (2000) Predicting subcellular localization of proteins based on their N-terminal amino acid sequence. *Journal of Molecular Biology* **300**, 1005-1016.

Engler, C., Gruetzner, R., Kandzia, R. and Marillonnet, S. (2009) Golden Gate shuffling: a one-pot DNA shuffling method based on type IIs restriction enzymes. *PLOS One* **4**, e5553.

Engler, C., Kandzia, R. and Marillonnet, S. (2008) A one pot, one step, precision cloning method with high throughput capability. *PLOS One* **3**, e3647.

Faeth, S.H. (2002) Are endophytic fungi defensive plant mutualists? *Oikos* **98**, 25-36.

Farrow, S.C. and Facchini, P.J. (2014) Functional diversity of 2-oxoglutarate/Fe(II)-dependent dioxygenases in plant metabolism. *Frontiers in Plant Science* **5**, 524.

Fatima, U. and Senthil-Kumar, M. (2015) Plant and pathogen nutrient acquisition strategies. *Frontiers in Plant Science* **6**, 750.

Fernandez, J. and Wilson, R.A. (2014) Characterizing roles for the glutathione reductase, thioredoxin reductase and thioredoxin peroxidase-encoding genes of *Magnaporthe oryzae* during rice blast disease. *PLOS One* **9**, e87300.

Fernandez, M.B., Pagano, M.R., Daleo, G.R. and Guevara, M.G. (2012) Hydrophobic proteins secreted into the apoplast may contribute to resistance against *Phytophthora infestans* in potato. *Plant Physiology and Biochemistry* **60**, 59-66.

Fiehn, O., Kopka, J., Dormann, P., Altmann, T., Trethewey, R.N. and Willmitzer, L. (2000) Metabolite profiling for plant functional genomics. *Nature Biotechnology* **18**, 1157-1161.

Figueroa, M., Manning, V.A., Pandelova, I. and Ciuffetti, L.M. (2015) Persistence of the host-selective toxin Ptr ToxB in the apoplast. *Molecular Plant-Microbe Interactions* **28**, 1082-1090.

Floerl, S., Majcherczyk, A., Possienke, M., Feussner, K., Tappe, H., Gatz, C., Feussner, I., Kues, U. and Polle, A. (2012) *Verticillium longisporum* infection affects the leaf apoplastic proteome, metabolome, and cell wall properties in *Arabidopsis thaliana*. *PLOS One* **7**, e31435.

Fraymouth, J. (1956) Haustoria of the Peronosporales. *Transactions of the British Mycological Society* **39**, 79-107.

Friesen, T.L., Faris, J.D., Solomon, P.S. and Oliver, R.P. (2008) Host-specific toxins: Effectors of necrotrophic pathogenicity. *Cellular Microbiology* **10**, 1421-1428.

Fritz, C., Palacios-Rojas, N., Feil, R. and Stitt, M. (2006) Regulation of secondary metabolism by the carbon-nitrogen status in tobacco: nitrate inhibits large sectors of phenylpropanoid metabolism. *The Plant Journal* **46**, 533-548.

Fuhrer, T., Zampieri, M., Sevin, D.C., Sauer, U. and Zamboni, N. (2017) Genomewide landscape of gene-metabolome associations in *Escherichia coli*. *Molecular Systems Biology* **13**, 907.

Gaderer, R., Lamdan, N.L., Frischmann, A., Sulyok, M., Krska, R., Horwitz, B.A. and Seidl-Seiboth, V. (2015) Sm2, a paralog of the *Trichoderma* cerato-platanin elicitor Sm1, is also highly important for plant protection conferred by the fungal-root interaction of *Trichoderma* with maize. *BMC Microbiology* **15**, 2.

Gafur, A., Schutzendubel, A. and Polle, A. (2007) Peroxidase activity in poplar inoculated with compatible and incompetent isolates of *Paxillus involutus*. *HAYATI Journal of Biosciences* **14**, 49-53.

Giardina, B.J. and Chiang, H.-L. (2013) Fructose-1,6-bisphosphatase, malate dehydrogenase, isocitrate lyase, phosphoenolpyruvate carboxykinase, glyceraldehyde-3-phosphate dehydrogenase, and cyclophilin A are secreted in *Saccharomyces cerevisiae* grown in low glucose. *Communicative and Integrative Biology* **6**, e27216.

Gibeaux, R., Politi, A.Z., Philippsen, P., Nédélec, F. and Mogilner, A. (2017) Mechanism of nuclear movements in a multinucleated cell. *Molecular Biology of the Cell* **28**, 645-660.

Gimenez-Ibanez, S., Boter, M., Fernandez-Barbero, G., Chini, A., Rathjen, J.P. and Solano, R. (2014) The bacterial effector HopX1 targets JAZ transcriptional repressors to activate jasmonate signaling and promote infection in Arabidopsis. *PLOS Biology* **12**, e1001792.

Giraldo, M.C., Dagdas, Y.F., Gupta, Y.K., Mentlak, T.A., Yi, M., Martinez-Rocha, A.L., Saitoh, H., Terauchi, R., Talbot, N.J. and Valent, B. (2013) Two distinct secretion systems facilitate tissue invasion by the rice blast fungus *Magnaporthe oryzae*. *Nature Communications* **4**, 1996.

Girard, V., Dieryckx, C., Job, C. and Job, D. (2013) Secretomes: the fungal strike force. *Proteomics* **13**, 597-608.

Glenn, A.E., Meredith, F.I., Morrison, W.H., 3rd and Bacon, C.W. (2003) Identification of intermediate and branch metabolites resulting from biotransformation of 2-benzoxazolinone by *Fusarium verticillioides*. *Applied and Environmental Microbiology* **69**, 3165-3169.

Gohre, V. and Robatzek, S. (2008) Breaking the barriers: microbial effector molecules subvert plant immunity. *Annual Review of Phytopathology* **46**, 189-215.

Gong, X., Hurtado, O., Wang, B., Wu, C., Yi, M., Giraldo, M., Valent, B., Goodin, M. and Farman, M. (2014) pFPL vectors for high-throughput protein localization in fungi: detecting cytoplasmic accumulation of putative effector proteins. *Molecular Plant-Microbe Interactions* **28**, 107-121.

González-Fernández, R., Prats, E. and Jorrín-Novo, J.V. (2010) Proteomics of plant pathogenic fungi. *Journal of Biomedicine and Biotechnology* **2010**, 36.

Gould, K.S. and Lister, C. (2006) Flavonoid functions in plants. In *flavonoids: chemistry, biochemistry and applications* eds. Andersen, Ø.M. and Markham, K.R. pp.397-441. Boca Raton, FL: CRC Press.

Griffiths, W.J., Karu, K., Hornshaw, M., Woffendin, G. and Wang, Y. (2007) Metabolomics and metabolite profiling: past heroes and future developments. *European Journal of Mass Spectrometry* **13**, 45-50.

Guerinot, M.L. and Yi, Y. (1994) Iron: Nutritious, noxious, and not readily available. *Plant Physiology* **104**, 815-820.

Gupta, R., Lee, S.E., Agrawal, G.K., Rakwal, R., Park, S., Wang, Y. and Kim, S.T. (2015) Understanding the plant-pathogen interactions in the context of proteomics-generated apoplastic proteins inventory. *Frontiers in Plant Science* **6**, 352.

Guyon, K., Balagué, C., Roby, D. and Raffaele, S. (2014) Secretome analysis reveals effector candidates associated with broad host range necrotrophy in the fungal plant pathogen *Sclerotinia sclerotiorum*. *BMC Genomics* **15**, 336.

Guzman-Guzman, P., Aleman-Duarte, M.I., Delaye, L., Herrera-Estrella, A. and Olmedo-Monfil, V. (2017) Identification of effector-like proteins in *Trichoderma* spp. and role of a hydrophobin in the plant-fungus interaction and mycoparasitism. *BMC Genetics* **18**, 16.

Guzman-Guzman, P., Porras-Troncoso, M.D., Olmedo-Monfil, V. and Herrera-Estrella, A. (2019) *Trichoderma* species: versatile plant symbionts. *Phytopathology* **109**, 6-16.

Hajirezaei, M.R., Takahata, Y., Trethewey, R.N., Willmitzer, L. and Sonnewald, U. (2000) Impact of elevated cytosolic and apoplastic invertase activity on carbon metabolism during potato tuber development. *Journal Experimental Botany* **51**, 439-445.

Hall, R.D. (2006) Plant metabolomics: from holistic hope, to hype, to hot topic. *New Phytologist* **169**, 453-468.

Ham, H., Sreelatha, A. and Orth, K. (2011) Manipulation of host membranes by bacterial effectors. *Nature Reviews Microbiology* **9**, 635-646.

Harborne, J.B. and Williams, C.A. (2000) Advances in flavonoid research since 1992. *Phytochemistry* **55**, 481-504.

Hardoim, P.R., van Overbeek, L.S., Berg, G., Pirttila, A.M., Compant, S., Campisano, A., Doring, M. and Sessitsch, A. (2015) The hidden world within plants: ecological and evolutionary considerations for defining functioning of microbial endophytes. *Microbiology and Molecular Biology Reviews* **79**, 293-320.

Harman, G.E. (2006) Overview of mechanisms and uses of *Trichoderma* spp. *Phytopathology* **96**, 190-194.

Harman, G.E., Howell, C.R., Viterbo, A., Chet, I. and Lorito, M. (2004) *Trichoderma* species-opportunistic, avirulent plant symbionts. *Nature Reviews Microbiology* **2**, 43-56.

Hausinger, R.P. (2015) Biochemical diversity of 2-oxoglutarate-dependent oxygenases. In *2-oxoglutarate-dependent oxygenases*. pp.1-58: The Royal Society of Chemistry.

Heller, J. and Tudzynski, P. (2011) Reactive oxygen species in phytopathogenic fungi: signaling, development, and disease. *Annual Reviews of Phytopathology* **49**, 369-390.

Hermosa, R., Rubio, M.B., Cardoza, R.E., Nicolas, C., Monte, E. and Gutierrez, S. (2013) The contribution of *Trichoderma* to balancing the costs of plant growth and defense. *International Microbiology* **16**, 69-80.

Hiraga, S., Sasaki, K., Ito, H., Ohashi, Y. and Matsui, H. (2001) A large family of class III plant peroxidases. *Plant and Cell Physiology* **42**, 462-468.

Hoagland, D.R. and Arnon, D.I. (1950) The water-culture method for growing plants without soil. *California Agricultural Experiment Station* **347**, 1-32.

Holyoake, A., O'Sullivan, P., Pollock, R., Best, T., Watanabe, J., Kajita, Y., Matsui, Y., Ito, M., Nishiyama, H., Kerr, N., da Silva Tatley, F., Cambridge, L., Toro, T., Ogawa, O. and Guilford, P. (2008) Development of a multiplex RNA urine test for the detection and stratification of transitional cell carcinoma of the bladder. *Clinical Cancer Research* **14**, 742-749.

Horton, P., Park, K.J., Obayashi, T., Fujita, N., Harada, H., Adams-Collier, C.J. and Nakai, K. (2007) WoLF PSORT: protein localization predictor. *Nucleic Acids Research* **35**, W585-587.

Hoson, T. (1998) Apoplast as the site of response to environmental signals. *Journal of Plant Research* **111**, 167-177.

Houston, K., Tucker, M.R., Chowdhury, J., Shirley, N. and Little, A. (2016) The plant cell wall: a complex and dynamic structure as revealed by the responses of genes under stress conditions. *Frontiers in Plant Science* **7**, 984.

Huang, J., Yang, M., Lu, L. and Zhang, X. (2016) Diverse functions of small RNAs in different plant–pathogen communications. *Frontiers in Microbiology* **7**, 1552.

Huergo, L.F. and Dixon, R. (2015) The Emergence of 2-oxoglutarate as a master regulator metabolite. *Microbiology and Molecular Biology Reviews* **79**, 419-435.

Husted, S. and Schjoerring, J.K. (1995) Apoplastic pH and ammonium concentration in leaves of *Brassica napus* L. *Plant Physiology* **109**, 1453-1460.

Ibrahim, Z.A., Armour, C.L., Phipps, S. and Sukkar, M.B. (2013) RAGE and TLRs: relatives, friends or neighbours? *Molecular Immunology* **56**, 739-744.

Imam, J., Singh, P.K. and Shukla, P. (2016) Plant microbe interactions in post genomic era: perspectives and applications. *Frontiers in Microbiology* **7**, 1488-1488.

Incarbone, M. and Dunoyer, P. (2013) RNA silencing and its suppression: novel insights from in planta analyses. *Trends in Plant Science* **18**, 382-392.

Irchhaiya, R., Kumar, A., Yadav, A., Gupta, N., Kumar, S., Gupta, N., Kumar, S., Yadav, V., Prakash, A. and Gurjar, H. (2014) Metabolites in plants and its classification. *World Journal of Pharmacy and Pharmaceutical Sciences* **4**.

Islam, M.S., Leissing, T.M., Chowdhury, R., Hopkinson, R.J. and Schofield, C.J. (2018) 2-oxoglutarate-dependent oxygenases. *Annual Review of Biochemistry* **87**, 585-620.

Issaq, H.J., Van, Q.N., Waybright, T.J., Muschik, G.M. and Veenstra, T.D. (2009) Analytical and statistical approaches to metabolomics research. *Journal of Separation Science* **32**, 2183-2199.

Jacobson, E.S. (2000) Pathogenic roles for fungal melanins. *Clinical Microbiology Reviews* **13**, 708-717.

Jashni, M.K., Mehrabi, R., Collemare, J., Mesarich, C.H. and de Wit, P.J. (2015) The battle in the apoplast: further insights into the roles of proteases and their inhibitors in plant-pathogen interactions. *Frontiers in Plant Science* **6**, 584.

Jayaraman, D., Forshey, K.L., Grimsrud, P.A. and Ane, J.M. (2012) Leveraging proteomics to understand plant-microbe interactions. *Frontiers in Plant Science* **3**, 44.

Jenkinson, C.B., Jones, K., Zhu, J., Dorhmi, S. and Khang, C.H. (2017) The appressorium of the rice blast fungus *Magnaporthe oryzae* remains mitotically active during post-penetration hyphal growth. *Fungal Genetics and Biology* **98**, 35-38.

Jha, G., Rajeshwari, R. and Sonti, R.V. (2005) Bacterial type two secretion system secreted proteins: double-edged swords for plant pathogens. *Molecular Plant-Microbe Interactions* **18**, 891-898.

Jia, B., Jia, X., Kim, K.H. and Jeon, C.O. (2017) Integrative view of 2-oxoglutarate/Fe(II)-dependent oxygenase diversity and functions in bacteria. *Biochimica et Biophysica Acta General Subjects* **1861**, 323-334.

Jin, C.W., Ye, Y.Q. and Zheng, S.J. (2014) An underground tale: contribution of microbial activity to plant iron acquisition via ecological processes. *Annals of Botany* **113**, 7-18.

Jones, D.L. (1998) Organic acids in the rhizosphere – a critical review. *Plant and Soil* **205**, 25-44.

Jones, J.D. and Dangl, J.L. (2006) The plant immune system. *Nature* **444**, 323-329.

Jwa, N.S. and Hwang, B.K. (2017) Convergent evolution of pathogen effectors toward reactive oxygen species signaling networks in plants. *Frontiers in Plant Science* **8**, 1687.

Kabera, J. (2014) Plant secondary metabolites: biosynthesis, classification, function and pharmacological classification, function and pharmacological properties. *Journal of Pharmacy and Pharmacology* **2**, 377-392.

Kaffarnik, F.A., Jones, A.M., Rathjen, J.P. and Peck, S.C. (2009) Effector proteins of the bacterial pathogen *Pseudomonas syringae* alter the extracellular proteome of the host plant, *Arabidopsis thaliana*. *Molecular and Cellular Proteomics* **8**, 145-156.

Kale, S.D. (2012) Oomycete and fungal effector entry, a microbial trojan horse. *New Phytology* **193**, 874-881.

Kale, S.D., Gu, B., Capelluto, D.G.S., Dou, D., Feldman, E., Rumore, A., Arredondo, F.D., Hanlon, R., Fudal, I., Rouxel, T., Lawrence, C.B., Shan, W. and Tyler, B.M. (2010) External lipid PI3P mediates entry of eukaryotic pathogen effectors into plant and animal host cells. *Cell* **142**, 284-295.

Kamoun, S. (2009) The secretome of plant-associated fungi and oomycetes. In *Plant Relationships* ed. Deising, H. pp.173-180: Springer Berlin Heidelberg.

Karnovsky, M. (1965) A formaldehyde-glutaraldehyde fixative of high osmolality for use in electron microscopy. *The Journal of Cell Biology* **27**, 137.

Katiyar-Agarwal, S., Morgan, R., Dahlbeck, D., Borsani, O., Villegas, A., Jr., Zhu, J.K., Staskawicz, B.J. and Jin, H. (2006) A pathogen-inducible endogenous siRNA in plant immunity. *Proceedings of the National Academy of Science of the United States of America* **103**, 18002-18007.

Kawai, Y., Ono, E. and Mizutani, M. (2014) Evolution and diversity of the 2-oxoglutarate-dependent dioxygenase superfamily in plants. *The Plant Journal* **78**, 328-343.

Kawalleck, P., Plesch, G., Hahlbrock, K. and Somssich, I.E. (1992) Induction by fungal elicitor of S-adenosyl-L-methionine synthetase and S-adenosyl-L-homocysteine hydrolase mRNAs in cultured cells and leaves of *Petroselinum crispum*. *Proccedings of the National Academy of Sciences of the United States of America* **89**, 4713-4717.

Kazan, K. and Lyons, R. (2014) Intervention of phytohormone pathways by pathogen effectors. *The Plant Cell* **26**, 2285-2309.

Kerry, A., Laudenbach, D.E. and Trick, C.G. (1988) Influence of iron limitation and nitrogen source on growth and siderophore production by Cyanobacteria. *Journal of Phycology* **24**, 566-571.

Kim, J.Y., Wu, J., Kwon, S.J., Oh, H., Lee, S.E., Kim, S.G., Wang, Y., Agrawal, G.K., Rakwal, R., Kang, K.Y., Ahn, I.P., Kim, B.G. and Kim, S.T. (2014) Proteomics of rice and *Cochliobolus miyabeanus* fungal interaction: insight into proteins at intracellular and extracellular spaces. *Proteomics* **14**, 2307-2318.

Kim, K.-T., Jeon, J., Choi, J., Cheong, K., Song, H., Choi, G., Kang, S. and Lee, Y.-H. (2016) Kingdom-wide analysis of fungal small secreted proteins (SSPs) reveals their potential role in host association. *Frontiers in Plant Science* **7**.

Kim, S.G., Wang, Y., Lee, K.H., Park, Z.Y., Park, J., Wu, J., Kwon, S.J., Lee, Y.H., Agrawal, G.K., Rakwal, R., Kim, S.T. and Kang, K.Y. (2013) In-depth insight into in vivo apoplastic secretome of rice-*Magnaporthe oryzae* interaction. *Journal of Proteomics* **78**, 58-71.

Kim, S.T., Kang, Y.H., Wang, Y., Wu, J., Park, Z.Y., Rakwal, R., Agrawal, G.K., Lee, S.Y. and Kang, K.Y. (2009) Secretome analysis of differentially induced proteins in rice suspension-cultured cells triggered by rice blast fungus and elicitor. *Proteomics* **9**, 1302-1313.

Kloppholz, S., Kuhn, H. and Requena, N. (2011) A secreted fungal effector of *Glomus intraradices* promotes symbiotic biotrophy. *Current Biology : CB* **21**, 1204-1209.

Koeck, M., Hardham, A.R. and Dodds, P.N. (2011) The role of effectors of biotrophic and hemibiotrophic fungi in infection. *Cellular Microbiology* **13**, 1849-1857.

Kopka, J., Fernie, A., Weckwerth, W., Gibon, Y. and Stitt, M. (2004) Metabolite profiling in plant biology: platforms and destinations. *Genome Biology* **5**, 109.

Kubicek, C.P., Baker, S., Gamauf, C., Kenerley, C.M. and Druzhinina, I.S. (2008) Purifying selection and birth-and-death evolution in the class II hydrophobin gene families of the ascomycete *Trichoderma*/*Hypocrea*. *BMC Evolutionary Biology* **8**, 4.

Kubicek, C.P., Starr, T.L. and Glass, N.L. (2014) Plant cell wall-degrading enzymes and their secretion in plant-pathogenic fungi. *Annual Review of Phytopathology* **52**, 427-451.

Kundu, S. (2015) Co-operative intermolecular kinetics of 2-oxoglutarate dependent dioxygenases may be essential for system-level regulation of plant cell physiology. *Frontiers in Plant Science* **6**.

Kunkel, B.N. and Brooks, D.M. (2002) Cross talk between signaling pathways in pathogen defense. *Current Opinion in Plant Biology* **5**, 325-331.

Kwon, C., Bednarek, P. and Schulze-Lefert, P. (2008) Secretory pathways in plant immune responses. *Plant Physiology* **147**, 1575-1583.

Lamdan, N.L., Shalaby, S., Ziv, T., Kenerley, C.M. and Horwitz, B.A. (2015) Secretome of *Trichoderma* interacting with maize roots: role in induced systemic resistance. *Molecular and Cellular Proteomics* **14**, 1054-1063.

Lanver, D., Berndt, P., Tollot, M., Naik, V., Vranes, M., Warmann, T., Munch, K., Rossel, N. and Kahmann, R. (2014) Plant surface cues prime *Ustilago maydis* for biotrophic development. *PLOS Pathogens* **10**, e1004272.

Lanver, D., Tollot, M., Schweizer, G., Lo Presti, L., Reissmann, S., Ma, L.S., Schuster, M., Tanaka, S., Liang, L., Ludwig, N. and Kahmann, R. (2017) *Ustilago maydis* effectors and their impact on virulence. *Nature Reviews Microbiology* **15**, 409-421.

Lawry, R. (2016) Cross-communication between *Trichoderma* and plants during root cololnisation. In *Bio-Protection Centre*: Lincoln University.

Lee, B.N., Kroken, S., Chou, D.Y., Robbertse, B., Yoder, O.C. and Turgeon, B.G. (2005) Functional analysis of all nonribosomal peptide synthetases in *Cochliobolus heterostrophus* reveals a factor, NPS6, involved in virulence and resistance to oxidative stress. *Eukaryotic Cell* **4**, 545-555.

Lehner, S.M., Atanasova, L., Neumann, N.K., Krska, R., Lemmens, M., Druzhinina, I.S. and Schuhmacher, R. (2013) Isotope-assisted screening for iron-containing metabolites reveals a high degree of diversity among known and unknown siderophores produced by *Trichoderma spp*. *Applied Environmental Microbiology* **79**, 18-31.

Lemanceau, P., Expert, D., Gaymard, F., Bakker, P.A.H.M. and Briat, J.F. (2009) Role of iron in plant–microbe interactions. In *Advances in Botanical Research*. pp.491-549: Academic Press.

Leong, J. (1986) Siderophores: their biochemistry and possible role in the biocontrol of plant pathogens. *Annual Review of Phytopathology* **24**, 187-209.

Li, R.X., Cai, F., Pang, G., Shen, Q.R., Li, R. and Chen, W. (2015) Solubilisation of phosphate and micronutrients by *Trichoderma harzianum* and its relationship with the promotion of tomato plant growth. *PLOS One* **10**, e0130081.

Li, Y., Wang, Z., Liu, X., Song, Z., Li, R., Shao, C. and Yin, Y. (2016a) Siderophore biosynthesis but not reductive iron assimilation is essential for the dimorphic fungus *Nomuraea rileyi* conidiation, dimorphism transition, resistance to oxidative stress, pigmented microsclerotium formation, and virulence. *Frontiers in Microbiology* **7**, 931.

Li, Y.B., Han, L.B., Wang, H.Y., Zhang, J., Sun, S.T., Feng, D.Q., Yang, C.L., Sun, Y.D., Zhong, N.Q. and Xia, G.X. (2016b) The thioredoxin GbNRX1 plays a crucial role in homeostasis of apoplastic reactive oxygen species in response to *Verticillium dahliae* infection in cotton. *Plant Physiology* **170**, 2392-2406.

Liao, C., Hochholdinger, F. and Li, C. (2012) Comparative analyses of three legume species reveals conserved and unique root extracellular proteins. *Proteomics* **12**, 3219-3228.

Linder, M.B., Szilvay, G.R., Nakari-Setala, T. and Penttila, M.E. (2005) Hydrophobins: the protein-amphiphiles of filamentous fungi. *FEMS Microbiology Reviews* **29**, 877-896.

Lionetti, V., Raiola, A., Camardella, L., Giovane, A., Obel, N., Pauly, M., Favaron, F., Cervone, F. and Bellincampi, D. (2007) Overexpression of pectin methylesterase inhibitors in Arabidopsis restricts fungal infection by *Botrytis cinerea*. *Plant Physiology* **143**, 1871-1880.

Liu, G., Greenshields, D.L., Sammynaiken, R., Hirji, R.N., Selvaraj, G. and Wei, Y. (2007) Targeted alterations in iron homeostasis underlie plant defense responses. *Journal of Cell Science* **120**, 596-605.

Liu, T., Song, T., Zhang, X., Yuan, H., Su, L., Li, W., Xu, J., Liu, S., Chen, L., Chen, T., Zhang, M., Gu, L., Zhang, B. and Dou, D. (2014) Unconventionally secreted effectors of two filamentous pathogens target plant salicylate biosynthesis. *Nature Communications* **5**, 4686.

Liu, W., Zhu, D.-W., Liu, D.-H., Geng, M.-J., Zhou, W.-B., Mi, W.-J., Yang, T.-W. and Hamilton, D. (2010) Influence of nitrogen on the primary and secondary metabolism and synthesis of flavonoids in *Chrysanthemum morifolium* ramat. *Journal of Plant Nutrition* **33**, 240-254.

Livak, K.J. and Schmittgen, T.D. (2001) Analysis of relative gene expression data using real-time quantitative PCR and the $2^{-\Delta\Delta C_T}$ method. *Methods* **25**, 402-408.

Lo Presti, L. and Kahmann, R. (2017) How filamentous plant pathogen effectors are translocated to host cells. *Current Opinion in Plant Biology* **38**, 19-24.

Lo Presti, L., Lanver, D., Schweizer, G., Tanaka, S., Liang, L., Tollot, M., Zuccaro, A., Reissmann, S. and Kahmann, R. (2015) Fungal effectors and plant susceptibility. *Annual Review of Plant Biology* **66**, 513-545.

Longnecker, K., Futrelle, J., Coburn, E., Kido Soule, M.C. and Kujawinski, E.B. (2015) Environmental metabolomics: databases and tools for data analysis. *Marine Chemistry* **177**, 366-373.

Lopez-Villar, E., Monteoliva, L., Larsen, M.R., Sachon, E., Shabaz, M., Pardo, M., Pla, J., Gil, C., Roepstorff, P. and Nombela, C. (2006) Genetic and proteomic evidences support the localization of yeast enolase in the cell surface. *Proteomics* **6 Suppl 1**, S107-118.

Lorito, M., Woo, S.L., Harman, G.E. and Monte, E. (2010) Translational research on *Trichoderma:* from 'omics to the field. *Annual Review of Phytopathology* **48**, 395-417.

Louden, B.C., Haarmann, D. and Lynne, A.M. (2011) Use of blue agar CAS assay for siderophore detection. *Journal of Microbiology and Biology Education* **12**, 51-53.

Lozano-Duran, R. and Robatzek, S. (2015) 14-3-3 proteins in plant-pathogen interactions. *Molecular Plant-Microbe Interactions* **28**, 511-518.

Luo, Y., Yuan, Z., Luo, G. and Zhao, F. (2008) Expression of secreted His-tagged S-adenosylmethionine synthetase in the methylotrophic yeast *Pichia pastoris* and its characterization, one-step purification, and immobilization. *Biotechnology Progress* **24**, 214-220.

Lloubes, R., Bernadac, A., Houot, L. and Pommier, S. (2013) Non classical secretion systems. *Research in Microbiology* **164**, 655-663.

Ma, W., Muthreich, N., Liao, C., Franz-Wachtel, M., Schutz, W., Zhang, F., Hochholdinger, F. and Li, C. (2010) The mucilage proteome of maize (*Zea mays* L.) primary roots. *Journal of Proteome Research* **9**, 2968-2976.

Mach, R.L. and Zeilinger, S. (1998) Genetic transformation of *Trichoderma* and *Gliocladium*

In *Trichoderma and Gliocladium: basic biology, taxonomy and genetics* eds. Kubicek, C.P. and Harman, G.E. pp.226-241. London: Taylor and Francis.

Maimbo, M., Ohnishi, K., Hikichi, Y., Yoshioka, H. and Kiba, A. (2007) Induction of a small heat shock protein and its functional roles in *Nicotiana* plants in the defense response against *Ralstonia solanacearum*. *Plant Physiology* **145**, 1588-1599.

Marra, R., Ambrosino, P., Carbone, V., Vinale, F., Woo, S.L., Ruocco, M., Ciliento, R., Lanzuise, S., Ferraioli, S., Soriente, I., Gigante, S., Turra, D., Fogliano, V., Scala, F. and Lorito, M. (2006) Study of the three-way interaction between *Trichoderma atroviride,* plant and fungal pathogens by using a proteomic approach. *Current Genetics* **50**, 307-321.

Marschall, R. and Tudzynski, P. (2016) Reactive oxygen species in development and infection processes. *Seminars in Cell Developmental Biology* **57**, 138-146.

Martínez-Medina, A., Van Wees, S.C.M. and Pieterse, C.M.J. (2017) Airborne signals from *Trichoderma* fungi stimulate iron uptake responses in roots resulting in priming of jasmonic acid-dependent defences in shoots of *Arabidopsis thaliana* and *Solanum lycopersicum*. *Plant, Cell and Environment* **40**, 2691-2705.

Mazzei, P. and Piccolo, A. (2017) HRMAS NMR spectroscopy applications in agriculture. *Chemical and Biological Technologies in Agriculture* **4**, 11.

Mazzei, P., Vinale, F., Woo, S.L., Pascale, A., Lorito, M. and Piccolo, A. (2016) Metabolomics by proton high-resolution magic-angle-spinning nuclear magnetic resonance of tomato plants treated with two secondary metabolites isolated from *Trichoderma*. *Journal of Agricultural and Food Chemistry* **64**, 3538-3545.

McCotter, S.W., Horianopoulos, L.C. and Kronstad, J.W. (2016) Regulation of the fungal secretome. *Current Genetics* **62**, 533-545.

McLean, K.L., Swaminathan, J., Frampton, C.M., Hunt, J.S., Ridgway, H.J. and Stewart, A. (2005) Effect of formulation on the rhizosphere competence and biocontrol ability of *Trichoderma atroviride* C52. *Plant Pathology* **54**, 212-218.

Medina, M.L. and Francisco, W.A. (2008) Isolation and enrichment of secreted proteins from filamentous fungi. In *2D PAGE: Sample Preparation and Fractionation* ed. Posch, A. pp.275-285. Totowa, NJ: Humana Press.

Mehdy, M.C. (1994) Active oxygen species in plant defense against pathogens. *Plant Physiology* **105**, 467-472.

Meinken, J., Asch, K.D., Neizer-Ashun, A.K., Guang-Hwa, C., Cooper, J.R.C. and Xiang, J.M. (2014) FunSecKB2: a fungal protein subcellular location knowledgebase. *Computational Molecular Biology* **4**.

Mendgen, K. and Deising, H. (1993) Infection structures of fungal plant pathogens – a cytological and physiological evaluation. *New Phytologist* **124**, 193-213.

Mendoza-Mendoza, A., Clouston, A., Li, J.H., Nieto-Jacobo, M.F., Cummings, N., Steyaert, J. and Hill, R. (2016) Isolation and mass production of *Trichoderma*. *Methods in Molecular Biology* **1477**, 13-20.

Mendoza-Mendoza, A., Zaid, R., Lawry, R., Hermosa, R., Monte, E., Horwitz, B.A. and Mukherjee, P.K. (2018) Molecular dialogues between *Trichoderma* and roots: role of the fungal secretome. *Fungal Biology Reviews* **32**, 62-85.

Meng, X. and Zhang, S. (2013) MAPK cascades in plant disease resistance signaling. *Annual Review of Phytopathology* **51**, 245-266.

Meziane, H., Van Der Sluis, I., Van Loon, L.C., HöFte, M. and Bakker, P.A.H.M. (2005) Determinants of *Pseudomonas putida* WCS358 involved in inducing systemic resistance in plants. *Molecular Plant Pathology* **6**, 177-185.

Mhlongo, M.I., Piater, L.A., Madala, N.E., Labuschagne, N. and Dubery, I.A. (2018) The chemistry of plant–microbe interactions in the rhizosphere and the potential for metabolomics to reveal signaling related to defense priming and induced systemic resistance. *Frontiers in Plant Science* **9**.

Mierziak, J., Kostyn, K. and Kulma, A. (2014) Flavonoids as important molecules of plant interactions with the environment. *Molecules* **19**, 16240-16265.

Miller, R.N.G., Costa Alves, G.S. and Van Sluys, M.-A. (2017) Plant immunity: unravelling the complexity of plant responses to biotic stresses. *Annals of Botany* **119**, 681-687.

Min, X.J., Lum, G., Meinken, J., Orr, J. and Frazier, S. (2014) PlantSecKB: the plant secretome and subcellular proteome knowledge base. *Computational Molecular Biology* **4**, 1-17.

Minic, Z. (2008) Physiological roles of plant glycoside hydrolases. *Planta* **227**, 723-740.

Mitsumasu, K., Seto, Y. and Yoshida, S. (2015) Apoplastic interactions between plants and plant root intruders. *Frontiers in Plant Science* **6**, 617.

Mochizuki, S., Saitoh, K.-i., Minami, E. and Nishizawa, Y. (2011) Localization of probe-accessible chitin and characterization of genes encoding chitin-binding domains during rice–*Magnaporthe oryzae* interactions. *Journal General Plant Pathology* **77**, 163-173.

Moonjely, S., Keyhani, N.O. and Bidochka, M.J. (2018) Hydrophobins contribute to root colonization and stress responses in the rhizosphere-competent insect pathogenic fungus *Beauveria bassiana*. *Microbiology* **164**, 517-528.

Moran-Diez, E., Hermosa, R., Ambrosino, P., Cardoza, R.E., Gutierrez, S., Lorito, M. and Monte, E. (2009) The ThPG1 endopolygalacturonase is required for the *Trichoderma harzianum*-plant beneficial interaction. *Molecular Plant-Microbe Interactions* **22**, 1021-1031.

Moran-Diez, M.E., Trushina, N., Lamdan, N.L., Rosenfelder, L., Mukherjee, P.K., Kenerley, C.M. and Horwitz, B.A. (2015) Host-specific transcriptomic pattern of *Trichoderma virens* during interaction with maize or tomato roots. *BMC Genomics* **16**, 8.

Morgan, W. and Kamoun, S. (2007) RXLR effectors of plant pathogenic oomycetes. *Current Opinion in Microbiology* **10**, 332-338.

Morrissey, J. and Guerinot, M.L. (2009) Iron uptake and transport in plants: the good, the bad, and the ionome. *Chemical Reviews* **109**, 4553-4567.

Mosquera, G., Giraldo, M.C., Khang, C.H., Coughlan, S. and Valent, B. (2009) Interaction transcriptome analysis identifies *Magnaporthe oryzae* BAS1-4 as biotrophy-associated secreted proteins in rice blast disease. *The Plant Cell* **21**, 1273.

Mueller, A.N., Ziemann, S., Treitschke, S., Assmann, D. and Doehlemann, G. (2013) Compatibility in the *Ustilago maydis*-maize interaction requires inhibition of host cysteine proteases by the fungal effector Pit2. *PLOS Pathogens* **9**, e1003177.

Mukaihara, T., Hatanaka, T., Nakano, M. and Oda, K. (2016) *Ralstonia solanacearum* type III effector RipAY is a glutathione-degrading enzyme that is activated by plant cytosolic thioredoxins and suppresses plant immunity. *MBio* **7**.

Mukherjee, P.K., Horwitz, B.A., Herrera-Estrella, A., Schmoll, M. and Kenerley, C.M. (2013) *Trichoderma* research in the genome era. *Annual Review of Phytopathology* **51**, 105-129.

Mukherjee, P.K., Horwitz, B.A. and Kenerley, C.M. (2012) Secondary metabolism in *Trichoderma*-a genomic perspective. *Microbiology* **158**, 35-45.

Mukherjee, P.K., Hurley, J.F., Taylor, J.T., Puckhaber, L., Lehner, S., Druzhinina, I., Schumacher, R. and Kenerley, C.M. (2018) Ferricrocin, the intracellular siderophore of *Trichoderma virens*, is involved in growth, conidiation, gliotoxin biosynthesis and induction of systemic resistance in maize. *Biochemical and Biophysical Research Communications* **505**, 606-611.

Mukherjee, P.K. and Kenerley, C.M. (2010) Regulation of morphogenesis and biocontrol properties in *Trichoderma virens* by a VELVET protein, Vel1. *Applied and Environmental Microbiology* **76**, 2345.

Musilova, L., Ridl, J., Polivkova, M., Macek, T. and Uhlik, O. (2016) Effects of secondary plant metabolites on microbial populations: changes in community structure and metabolic activity in contaminated environments. *International Journal of Molecular Sciences* **17**, 1205.

Nakanishi, H., Yamaguchi, H., Sasakuma, T., Nishizawa, N.K. and Mori, S. (2000) Two dioxygenase genes, Ids3 and Ids2, from *Hordeum vulgare* are involved in the biosynthesis of mugineic acid family phytosiderophores. *Plant Molecular Biolology* **44**, 199-207.

Nanda, A.K., Andrio, E., Marino, D., Pauly, N. and Dunand, C. (2010) Reactive oxygen species during plant-microorganism early interactions. *Journal of Integrative Plant Biology* **52**, 195-204.

Nath, M., Bhatt, D., Prasad, R., Gill, S.S., Anjum, N.A. and Tuteja, N. (2016) Reactive oxygen species generation-scavenging and signaling during plant-arbuscular mycorrhizal and *Piriformospora indica* interaction under stress condition. *Frontiers in Plant Science* **7**, 1574.

Neal, A.L., Ahmad, S., Gordon-Weeks, R. and Ton, J. (2012) Benzoxazinoids in root exudates of maize attract *Pseudomonas putida* to the rhizosphere. *PLOS One* **7**, e35498.

Neilands, J.B. (1995) Siderophores: structure and function of microbial iron transport compounds. *The Journal of Biological Chemistry* **270**, 26723-26726.

Newman, M.-A., Sundelin, T., Nielsen, J.T. and Erbs, G. (2013) MAMP (microbe-associated molecular pattern) triggered immunity in plants. *Frontiers in Plant Science* **4**, 139.

Niemeyer, H.M. (2009) Hydroxamic acids derived from 2-hydroxy-2H-1,4-benzoxazin-3(4H)-one: key defense chemicals of cereals. *Journal of Agricultural Food Chemistry* **57**, 1677-1696.

Nieto-Jacobo, M.F., Steyaert, J.M., Salazar-Badillo, F.B., Nguyen, D.V., Rostás, M., Braithwaite, M., De Souza, J.T., Jimenez-Bremont, J.F., Ohkura, M., Stewart, A. and Mendoza-Mendoza, A. (2017) Environmental growth conditions of *Trichoderma* spp. affects indole acetic acid derivatives, volatile organic compounds, and plant growth promotion. *Frontiers in Plant Science* **8**, 102.

Nobori, T., Mine, A. and Tsuda, K. (2018) Molecular networks in plant-pathogen holobiont. *FEBS Letters* **592**, 1937-1953.

Nødvig, C.S., Nielsen, J.B., Kogle, M.E. and Mortensen, U.H. (2015) A CRISPR-Cas9 system for genetic engineering of filamentous fungi. *PLOS One* **10**, e0133085.

Nogueira-Lopez, G., Greenwood, D.R., Middleditch, M., Winefield, C., Eaton, C., Steyaert, J.M. and Mendoza-Mendoza, A. (2018) The apoplastic secretome of *Trichoderma virens* during interaction with maize roots shows an inhibition of plant defence and scavenging oxidative stress secreted proteins. *Frontiers in Plant Science* **9**.

Nummi, M., Niku-Paavola, M.L., Lappalainen, A., Enari, T.M. and Raunio, V. (1983) Cellobiohydrolase from *Trichoderma reesei*. *Biochemical Journal* **215**, 677-683.

O'Brien, J.A., Daudi, A., Finch, P., Butt, V.S., Whitelegge, J.P., Souda, P., Ausubel, F.M. and Bolwell, G.P. (2012) A peroxidase-dependent apoplastic oxidative burst in cultured Arabidopsis cells functions in MAMP-elicited defense. *Plant Physiology* **158**, 2013-2027.

Oide, S., Moeder, W., Krasnoff, S., Gibson, D., Haas, H., Yoshioka, K. and Turgeon, B.G. (2006) NPS6, encoding a nonribosomal peptide synthetase involved in siderophore-mediated iron metabolism, is a conserved virulence determinant of plant pathogenic ascomycetes. *The Plant Cell* **18**, 2836-2853.

Onofre, S.B., Bonfante, T., Santos, Z.p.M.Q.d., Moura, M.C.d. and Cardoso, A.F. (2014) Cellulase production by endophytic strains of *Trichoderma reesei* from *Baccharis dracunculifolia* D. C. (Asteraceae). *Advances in Microbiology* **4**, 275-283.

Pachauri, S., Chatterjee, S., Kumar, V. and Mukherjee, P.K. (2018) A dedicated glyceraldehyde-3-phosphate dehydrogenase is involved in the biosynthesis of volatile sesquiterpenes in *Trichoderma virens*-evidence for the role of a fungal GAPDH in secondary metabolism. *Current Genetics* **65**, 243-252.

Palaniyandi, U., Anandaraj, M. and Benjamin, S. (2017) Endophytic interactions of *Trichoderma harzianum* in a tropical perennial rhizo-ecosystem. *Research Journal of Biotechnology* **12**, 3.

Park, C.J. and Seo, Y.S. (2015) Heat shock proteins: a review of the molecular chaperones for plant immunity. *The Plant Pathology Journal* **31**, 323-333.

Park, E., Nedo, A., Caplan, J.L. and Dinesh-Kumar, S.P. (2018) Plant–microbe interactions: organelles and the cytoskeleton in action. *New Phytologist* **217**, 1012-1028.

Payne, S.M. (1994) Detection, isolation, and characterization of siderophores. *Methods in Enzymology* **235**, 329-344.

Pedras, M.S. and Ahiahonu, P.W. (2005) Metabolism and detoxification of phytoalexins and analogs by phytopathogenic fungi. *Phytochemistry* **66**, 391-411.

Pence, H.E. and Williams, A. (2010) ChemSpider: an online chemical information resource. *Journal of Chemical Education* **87**, 1123-1124.

Peters, K., Worrich, A., Weinhold, A., Alka, O., Balcke, G., Birkemeyer, C., Bruelheide, H., Calf, O.W., Dietz, S., Dührkop, K., Gaquerel, E., Heinig, U., Kücklich, M., Macel, M., Müller, C., Pöschl, Y., Pohnert, G., Ristok, C., Rodriguez, V. and Dam, N. (2018) Current challenges in plant eco-metabolomics. *International Journal of Molecular Sciences* **19**, 1385.

Petersen, T.N., Brunak, S., von Heijne, G. and Nielsen, H. (2011) SignalP 4.0: discriminating signal peptides from transmembrane regions. *Nature Methods* **8**, 785-786.

Philpott, C.C. (2006) Iron uptake in fungi: a system for every source. *Biochimica et Biophysica Acta* **1763**, 636-645.

Pieterse, C.M., Leon-Reyes, A., Van der Ent, S. and Van Wees, S.C. (2009) Networking by small-molecule hormones in plant immunity. *Nature Chemical Biology* **5**, 308-316.

Pieterse, C.M., Zamioudis, C., Berendsen, R.L., Weller, D.M., Van Wees, S.C. and Bakker, P.A. (2014) Induced systemic resistance by beneficial microbes. *Annual Review of Phytopathology* **52**, 347-375.

Planchamp, C., Glauser, G. and Mauch-Mani, B. (2014) Root inoculation with *Pseudomonas putida* KT2440 induces transcriptional and metabolic changes and systemic resistance in maize plants. *Frontiers in Plant Science* **5**, 719.

Plett, J.M., Daguerre, Y., Wittulsky, S., Vayssières, A., Deveau, A., Melton, S.J., Kohler, A., Morrell-Falvey, J.L., Brun, A., Veneault-Fourrey, C. and Martin, F. (2014) Effector MiSSP7 of the mutualistic fungus *Laccaria bicolor* stabilizes the Populus JAZ6 protein and represses jasmonic acid (JA) responsive

genes. *Proceedings of the National Academy of Sciences of the United States of America* **111**, 8299-8304.
Plett, J.M., Kemppainen, M., Kale, S.D., Kohler, A., Legue, V., Brun, A., Tyler, B.M., Pardo, A.G. and Martin, F. (2011) A secreted effector protein of *Laccaria bicolor* is required for symbiosis development. *Current Biology* **21**, 1197-1203.
Plett, J.M. and Martin, F. (2011) Mutualistic effectors: architects of symbiosis. In *Effectors in plant–microbe interactions*. pp.295-326: Wiley-Blackwell.
Porter, B.W., Yuen, C.Y.L. and Christopher, D.A. (2015) Dual protein trafficking to secretory and non-secretory cell compartments: clear or double vision? *Plant Science* **234**, 174-179.
Postel, S. and Kemmerling, B. (2009) Plant systems for recognition of pathogen-associated molecular patterns. *Seminars in Cell and Developmental Biology* **20**, 1025-1031.
Poulin, M.-J., Simard, J., Catford, J.-G., Librie, F. and Piché, Y. (1997) Response of symbiotic endomycorrhizal fungi to estrogens and antiestrogens. *Molecular Plant-Microbe Interactions* **10**, 481-487.
Powell, J.J., Carere, J., Sablok, G., Fitzgerald, T.L., Stiller, J., Colgrave, M.L., Gardiner, D.M., Manners, J.M., Vogel, J.P., Henry, R.J. and Kazan, K. (2017) Transcriptome analysis of *Brachypodium* during fungal pathogen infection reveals both shared and distinct defense responses with wheat. *Scientific Reports* **7**, 17212.
Pusztahelyi, T., Holb, I.J. and Pócsi, I. (2015) Secondary metabolites in fungus-plant interactions. *Frontiers in Plant Science* **6**, 573.
Qi, J., Wang, J., Gong, Z. and Zhou, J.-M. (2017) Apoplastic ROS signaling in plant immunity. *Current Opinion in Plant Biology* **38**, 92-100.
Rabouille, C. (2017) Pathways of unconventional protein secretion. *Trends in Cell Biology* **27**, 230-240.
Rafiqi, M., Ellis, J.G., Ludowici, V.A., Hardham, A.R. and Dodds, P.N. (2012) Challenges and progress towards understanding the role of effectors in plant–fungal interactions. *Current Opinion in Plant Biology* **15**, 477-482.
Ranwala, A.P., Suematsu, C. and Masuda, H. (1992) The role of β-galactosidases in the modification of cell wall components during muskmelon fruit ripening. *Plant Physiology* **100**, 1318-1325.
Reichling, J. (2010) Plant–microbe interactions and secondary metabolites with antibacterial, antifungal and antiviral properties. *Annual Plant Reviews*. pp.214-347.
Renshaw, J.C., Robson, G.D., Trinci, A.P.J., Wiebe, M.G., Livens, F.R., Collison, D. and Taylor, R.J. (2002) Fungal siderophores: structures, functions and applications. *Mycological Research* **106**, 1123-1142.
Ridout, C.J., Skamnioti, P., Porritt, O., Sacristan, S., Jones, J.D. and Brown, J.K. (2006) Multiple avirulence paralogues in cereal powdery mildew fungi may contribute to parasite fitness and defeat of plant resistance. *The Plant Cell* **18**, 2402-2414.
Robert, C.A.M., Veyrat, N., Glauser, G., Marti, G., Doyen, G.R., Villard, N., Gaillard, M.D.P., Köllner, T.G., Giron, D., Body, M., Babst, B.A., Ferrieri, R.A., Turlings, T.C.J. and Erb, M. (2012) A specialist root herbivore exploits defensive metabolites to locate nutritious tissues. *Ecology Letters* **15**, 55-64.
Robinson, D.G., Ding, Y. and Jiang, L. (2016) Unconventional protein secretion in plants: a critical assessment. *Protoplasma* **253**, 31-43.
Rodriguez, R.J., White, J.F., Jr., Arnold, A.E. and Redman, R.S. (2009) Fungal endophytes: diversity and functional roles. *New Phytologist* **182**, 314-330.
Romão-Dumaresq, A.S., Dourado, M.N., Fávaro, L.C.d.L., Mendes, R., Ferreira, A. and Araújo, W.L. (2016) Diversity of cultivated fungi associated with conventional and transgenic sugarcane and the interaction between endophytic *Trichoderma virens* and the host plant. *PLOS One* **11**, e0158974.
Ron, M. and Avni, A. (2004) The receptor for the fungal elicitor ethylene-inducing xylanase is a member of a resistance-like gene family in tomato. *The Plant Cell* **16**, 1604-1615.
Ros Barcelo, A. (1997) Lignification in plant cell walls. *International Review of Cytology* **176**, 87-132.
Rotblat, B., Enshell-Seijffers, D., Gershoni, J.M., Schuster, S. and Avni, A. (2002) Identification of an essential component of the elicitation active site of the EIX protein elicitor. *Plant Jounal* **32**, 1049-1055.

Ruocco, M., Lanzuise, S., Lombardi, N., Woo, S.L., Vinale, F., Marra, R., Varlese, R., Manganiello, G., Pascale, A., Scala, V., Turra, D., Scala, F. and Lorito, M. (2015) Multiple roles and effects of a novel *Trichoderma* hydrophobin. *Molecular Plant-Microbe Interactions : MPMI* **28**, 167-179.

Rutter, B.D. and Innes, R.W. (2017) Extracellular vesicles isolated from the leaf apoplast carry stress-response proteins. *Plant Physiology* **173**, 728-741.

Saha, M., Sarkar, S., Sarkar, B., Sharma, B.K., Bhattacharjee, S. and Tribedi, P. (2016) Microbial siderophores and their potential applications: a review. *Environmental Science and Pollution Research* **23**, 3984-3999.

Salminen, A., Kauppinen, A. and Kaarniranta, K. (2015) 2-oxoglutarate-dependent dioxygenases are sensors of energy metabolism, oxygen availability, and iron homeostasis: potential role in the regulation of aging process. *Cellular and Molecular Life Sciences* **72**, 3897-3914.

Saloheimo, M. and Pakula, T.M. (2012) The cargo and the transport system: secreted proteins and protein secretion in *Trichoderma reesei* (*Hypocrea jecorina*). *Microbiology* **158**, 46-57.

Salomon, D., Guo, Y., Kinch, L.N., Grishin, N.V., Gardner, K.H. and Orth, K. (2013) Effectors of animal and plant pathogens use a common domain to bind host phosphoinositides. *Nature Communications* **4**, 2973.

Sambrook, J., Fristsch, E.F. and Maniatis, T. (1989) *Molecular cloning: a laboratory manual*. Second edition. Cold Spring Harbor, N.Y. Cold Spring Harbor Laboratory Press.

Santoyo, G., Moreno-Hagelsieb, G., del Carmen Orozco-Mosqueda, M. and Glick, B.R. (2016) Plant growth-promoting bacterial endophytes. *Microbiological Research* **183**, 92-99.

Saravanakumar, K., Fan, L., Fu, K., Yu, C., Wang, M., Xia, H., Sun, J., Li, Y. and Chen, J. (2016) Cellulase from *Trichoderma harzianum* interacts with roots and triggers induced systemic resistance to foliar disease in maize. *Scientific Reports* **6**, 35543.

Sarrocco, S., Matarese, F., Baroncelli, R., Vannacci, G., Seidl-Seiboth, V., Kubicek, C.P. and Vergara, M. (2017) The constitutive endopolygalacturonase TvPG2 regulates the induction of plant systemic resistance by *Trichoderma virens*. *Phytopathology* **107**, 537-544.

Sattelmacher, B. (2001) The apoplast and its significance for plant mineral nutrition. *New Phytologist* **149**, 167-192.

Schirawski, J. and Perlin, M.H. (2018) Plant-microbe interaction 2017-the good, the bad and the diverse. *International Journal of Molecular Sciences* **19**, 1374.

Schmidt, F. and Volker, U. (2011) Proteome analysis of host-pathogen interactions: investigation of pathogen responses to the host cell environment. *Proteomics* **11**, 3203-3211.

Schmoll, M., Dattenböck, C., Carreras-Villaseñor, N., Mendoza-Mendoza, A., Tisch, D., Alemán, M.I., Baker, S.E., Brown, C., Cervantes-Badillo, M.G., Cetz-Chel, J., Cristobal-Mondragon, G.R., Delaye, L., Esquivel-Naranjo, E.U., Frischmann, A., Gallardo-Negrete, J.d.J., García-Esquivel, M., Gomez-Rodriguez, E.Y., Greenwood, D.R., Hernández-Oñate, M., Kruszewska, J.S., Lawry, R., Mora-Montes, H.M., Muñoz-Centeno, T., Nieto-Jacobo, M.F., Nogueira Lopez, G., Olmedo-Monfil, V., Osorio-Concepcion, M., Piłsyk, S., Pomraning, K.R., Rodriguez-Iglesias, A., Rosales-Saavedra, M.T., Sánchez-Arreguín, J.A., Seidl-Seiboth, V., Stewart, A., Uresti-Rivera, E.E., Wang, C.-L., Wang, T.-F., Zeilinger, S., Casas-Flores, S. and Herrera-Estrella, A. (2016) The genomes of three uneven siblings: footprints of the lifestyles of three *Trichoderma* species. *Microbiology and Molecular Biology Reviews* **80**, 205-327.

Schnoes, A.M., Brown, S.D., Dodevski, I. and Babbitt, P.C. (2009) Annotation error in public databases: misannotation of molecular function in enzyme superfamilies. *PLOS Computational Biology* **5**, e1000605.

Schornack, S., Huitema, E., Cano, L.M., Bozkurt, T.O., Oliva, R., Van Damme, M., Schwizer, S., Raffaele, S., Chaparro-Garcia, A., Farrer, R., Segretin, M.E., Bos, J., Haas, B.J., Zody, M.C., Nusbaum, C., Win, J., Thines, M. and Kamoun, S. (2009) Ten things to know about oomycete effectors. *Molecular Plant Pathology* **10**, 795-803.

Schulz, B. and Boyle, C. (2006) What are Endophytes? In *Microbial Root Endophytes* eds. Schulz, B.E., Boyle, C.C. and Sieber, T. pp.1-13: Springer Berlin Heidelberg.

Schulz, M., Filary, B., Kuhn, S., Colby, T., Harzen, A., Schmidt, J., Sicker, D., Hennig, L., Hofmann, D., Disko, U. and Anders, N. (2016) Benzoxazolinone detoxification by N-glucosylation: the multi-compartment-network of *Zea mays L*. *Plant Signaling and Behavior* **11**, e1119962.

Schweiger, R., Baier, M.C., Persicke, M. and Muller, C. (2014) High specificity in plant leaf metabolic responses to arbuscular mycorrhiza. *Nature Communications* **5**, 3886.

Schweiger, R. and Muller, C. (2015) Leaf metabolome in arbuscular mycorrhizal symbiosis. *Current Opinion in Plant Biology* **26**, 120-126.

Schwyn, B. and Neilands, J.B. (1987) Universal chemical assay for the detection and determination of siderophores. *Analytical biochemistry* **160**, 47-56.

Senesi, N., Sposito, G. and Martin, J.P. (1987) Copper (II) and iron (III) complexation by humic acid-like polymers (melanins) from soil fungi. *Science of The Total Environment* **62**, 241-252.

Sheng, M., Tang, M., Zhang, F. and Huang, Y. (2011) Influence of arbuscular mycorrhiza on organic solutes in maize leaves under salt stress. *Mycorrhiza* **21**, 423-430.

Shenton, M.R., Berberich, T., Kamo, M., Yamashita, T., Taira, H. and Terauchi, R. (2012) Use of intercellular washing fluid to investigate the secreted proteome of the rice-*Magnaporthe* interaction. *Journal of Plant Research* **125**, 311-316.

Shi, L.-n., Li, F.-q., Huang, M., Lu, J.-f., Kong, X.-x., Wang, S.-q. and Shao, H.-f. (2012) Immunoproteomics based identification of thioredoxin reductase GliT and novel *Aspergillus fumigatus* antigens for serologic diagnosis of invasive aspergillosis. *BMC Microbiology* **12**, 1-9.

Shi, X., Long, Y., He, F., Zhang, C., Wang, R., Zhang, T., Wu, W., Hao, Z., Wang, Y., Wang, G.-L. and Ning, Y. (2018) The fungal pathogen *Magnaporthe oryzae* suppresses innate immunity by modulating a host potassium channel. *PLOS Pathogens* **14**, e1006878.

Shigenaga, A.M. and Argueso, C.T. (2016) No hormone to rule them all: Interactions of plant hormones during the responses of plants to pathogens. *Seminars in Cell & Developmental Biology* **56**, 174-189.

Shoresh, M. and Harman, G.E. (2008) The relationship between increased growth and resistance induced in plants by root colonizing microbes. *Plant Signaling and Behavior* **3**, 737-739.

Shoresh, M., Harman, G.E. and Mastouri, F. (2010) Induced systemic resistance and plant responses to fungal biocontrol agents. *Annual Review of Phytopathology* **48**, 21-43.

Sofo, A., Scopa, A., Manfra, M., De Nisco, M., Tenore, G., Troisi, J., Di Fiori, R. and Novellino, E. (2011) *Trichoderma harzianum* strain T-22 induces changes in phytohormone levels in cherry rootstocks (*Prunus cerasus* × *P. canescens*). *Plant Growth Regulation* **65**, 421-425.

Sonah, H., Deshmukh, R.K. and Bélanger, R.R. (2016) Computational prediction of effector proteins in fungi: opportunities and challenges. *Frontiers in Plant Science* **7**, 126.

Song, J., Win, J., Tian, M., Schornack, S., Kaschani, F., Ilyas, M., van der Hoorn, R.A.L. and Kamoun, S. (2009) Apoplastic effectors secreted by two unrelated eukaryotic plant pathogens target the tomato defense protease Rcr3. *Proceedings of the National Academy of Sciences of the United States of America* **106**, 1654-1659.

Song, Y.Y., Cao, M., Xie, L.J., Liang, X.T., Zeng, R.S., Su, Y.J., Huang, J.H., Wang, R.L. and Luo, S.M. (2011) Induction of DIMBOA accumulation and systemic defense responses as a mechanism of enhanced resistance of mycorrhizal corn (*Zea mays* L.) to sheath blight. *Mycorrhiza* **21**, 721-731.

Spaepen, S. and Vanderleyden, J. (2011) Auxin and plant-microbe interactions. *Cold Spring Harbor Perspectives in Biology* **3**.

Sperschneider, J., Gardiner, D.M., Dodds, P.N., Tini, F., Covarelli, L., Singh, K.B., Manners, J.M. and Taylor, J.M. (2016) EffectorP: predicting fungal effector proteins from secretomes using machine learning. *New Phytologist* **210**, 743-761.

Staiger, D. (2002) Chemical strategies for iron acquisition in plants. *Angewandte Chemie* **41**, 2259-2264.

Stock, J., Sarkari, P., Kreibich, S., Brefort, T., Feldbrugge, M. and Schipper, K. (2012) Applying unconventional secretion of the endochitinase Cts1 to export heterologous proteins in *Ustilago maydis*. *Journal of Biotechnology* **161**, 80-91.

Stotz, H.U., Mitrousia, G.K., de Wit, P.J. and Fitt, B.D. (2014) Effector-triggered defence against apoplastic fungal pathogens. *Trends in Plant Science* **19**, 491-500.

Subramanian, K.S. and Charest, C. (1995) Influence of arbuscular mycorrhizae on the metabolism of maize under drought stress. *Mycorrhiza* **5**, 273-278.

Sundstrom, P. and Aliaga, G.R. (1994) A subset of proteins found in culture supernatants of *Candida albicans* includes the abundant, immunodominant, glycolytic enzyme enolase. *The Journal of Infectious Diseases* **169**, 452-456.

Sutton, J.C., Sopher, C.R., Owen-Going, T.N., Liu, W., Grodzinski, B., Hall, J.C. and Benchimol, R.L. (2006) Etiology and epidemiology of *Pythium* root rot in hydroponic crops: current knowledge and perspectives. *Summa Phytopathologica* **32**, 307-321.

Tadych, M. and White, J.F. (2009) Endophytic microbes. In *Encyclopedia of Microbiology*. pp.431-442.

Takeda, N., Handa, Y., Tsuzuki, S., Kojima, M., Sakakibara, H. and Kawaguchi, M. (2015) Gibberellin regulates infection and colonization of host roots by arbuscular mycorrhizal fungi. *Plant Signaling and Behavior* **10**, e1028706.

Tamarit, J., Irazusta, V., Moreno-Cermeno, A. and Ros, J. (2006) Colorimetric assay for the quantitation of iron in yeast. *Analytical Biochemistry* **351**, 149-151.

Tamura, K., Stecher, G., Peterson, D., Filipski, A. and Kumar, S. (2013) MEGA6: molecular evolutionary genetics analysis version 6.0. *Molecular Biology and Evolution* **30**, 2725-2729.

Tanabe, S., Ishii-Minami, N., Saitoh, K., Otake, Y., Kaku, H., Shibuya, N., Nishizawa, Y. and Minami, E. (2011) The role of catalase-peroxidase secreted by *Magnaporthe oryzae* during early infection of rice cells. *Molecular Plant-Microbe Interactions* **24**, 163-171.

Tanaka, A., Christensen, M.J., Takemoto, D., Park, P. and Scott, B. (2006) Reactive oxygen species play a role in regulating a fungus–perennial ryegrass mutualistic interaction. *The Plant Cell* **18**, 1052-1066.

Tang, D., Wang, G. and Zhou, J.-M. (2017) Receptor kinases in plant-pathogen interactions: more than pattern recognition. *The Plant Cell* **29**, 618-637.

Tanveer, T., Shaheen, K., Parveen, S., Kazi, A.G. and Ahmad, P. (2014) Plant secretomics: identification, isolation, and biological significance under environmental stress. *Plant Signaling and Behavior* **9**, e29426.

Thomma, B.P., Nurnberger, T. and Joosten, M.H. (2011) Of PAMPs and effectors: the blurred PTI-ETI dichotomy. *The Plant Cell* **23**, 4-15.

Tiwari, P., Misra, B.N. and Sangwan, N.S. (2013) Beta-glucosidases from the fungus trichoderma: an efficient cellulase machinery in biotechnological applications. *BioMed Research International* **2013**, 10.

Toruño, T.Y., Stergiopoulos, I. and Coaker, G. (2016) Plant-pathogen effectors: cellular probes interfering with plant defenses in spatial and temporal manners. *Annual Review of Phytopathology* **54**, 419-441.

Treutter, D. (2005) Significance of flavonoids in plant resistance and enhancement of their biosynthesis. *Plant Biology* **7**, 581-591.

Tsai, S.M. and Phillips, D.A. (1991) Flavonoids released naturally from alfalfa promote development of symbiotic glomus spores in vitro. *Applied and Environmental Microbiology* **57**, 1485-1488.

Tudzynski, B. (2005) Gibberellin biosynthesis in fungi: genes, enzymes, evolution, and impact on biotechnology. *Applied Microbiology and Biotechnology* **66**, 597-611.

Urbanek, H., Kuzniak-Gebarowska, E. and Herka, K. (1991) Elicitation of defence responses in bean leaves by *Botrytis cinerea* polygalacturonase. *Acta Physiologiae Plantarum* **13**, 43-50.

Van Camp, W., Van Montagu, M. and Inzé, D. (1998) H_2O_2 and NO: redox signals in disease resistance. *Trends in Plant Science* **3**, 330-334.

van Damme, M., Huibers, R.P., Elberse, J. and Van den Ackerveken, G. (2008) Arabidopsis DMR6 encodes a putative 2OG-Fe(II) oxygenase that is defense-associated but required for susceptibility to downy mildew. *The Plant Journal* **54**, 785-793.

van der Does, H.C. and Rep, M. (2017) Adaptation to the host environment by plant-pathogenic fungi. *Annual Review Phytopathology* **55**, 427-450.

van Loon, L.C., Rep, M. and Pieterse, C.M. (2006) Significance of inducible defense-related proteins in infected plants. *Annual Review of Phytopathology* **44**, 135-162.

Vance, C.P., Kirk, T.K. and Sherwood, R.T. (1980) Lignification as a mechanism of disease resistance. *Annual Review of Phytopathology* **18**, 259-288.

Vargas, W.A., Crutcher, F.K. and Kenerley, C.M. (2011) Functional characterization of a plant-like sucrose transporter from the beneficial fungus *Trichoderma virens*. Regulation of the symbiotic association with plants by sucrose metabolism inside the fungal cells. *New Phytologist* **189**, 777-789.

Vargas, W.A., Djonovic, S., Sukno, S.A. and Kenerley, C.M. (2008) Dimerization controls the activity of fungal elicitors that trigger systemic resistance in plants. *The Journal of Biological Chemistry* **283**, 19804-19815.

Vargas, W.A., Mandawe, J.C. and Kenerley, C.M. (2009) Plant-derived sucrose is a key element in the symbiotic association between *Trichoderma virens* and maize plants. *Plant Physiology* **151**, 792-808.

Vargas, W.A., Mukherjee, P.K., Laughlin, D., Wiest, A., Moran-Diez, M.E. and Kenerley, C.M. (2014) Role of gliotoxin in the symbiotic and pathogenic interactions of *Trichoderma virens*. *Microbiology* **160**, 2319-2330.

Vaughan, M.M., Block, A., Christensen, S.A., Allen, L.H. and Schmelz, E.A. (2018) The effects of climate change associated abiotic stresses on maize phytochemical defenses. *Phytochemistry Reviews* **17**, 37-49.

Venkateshwaran, M., Volkening, J.D., Sussman, M.R. and Ane, J.M. (2013) Symbiosis and the social network of higher plants. *Current Opinion in Plant Biology* **16**, 118-127.

Verbon, E.H., Trapet, P.L., Stringlis, I.A., Kruijs, S., Bakker, P.A.H.M. and Pieterse, C.M.J. (2017) Iron and immunity. *Annual Review of Phytopathology* **55**, 355-375.

Viefhues, A., Heller, J., Temme, N. and Tudzynski, P. (2014) Redox systems in *Botrytis cinerea*: impact on development and virulence. *Molecular Plant-Microbe Interactions* **27**, 858-874.

Vierheilig, H., Alt, M., Lange, J., Gut-Rella, M., Wiemken, A. and Boller, T. (1995) Colonization of transgenic tobacco constitutively expressing pathogenesis-related proteins by the vesicular-arbuscular mycorrhizal fungus *Glomus mosseae*. *Applied and Environmental Microbiology* **61**, 3031-3034.

Vigani, G., Morandini, P. and Murgia, I. (2013) Searching iron sensors in plants by exploring the link among 2-OG-dependent dioxygenases, the iron deficiency response and metabolic adjustments occurring under iron deficiency. *Frontiers in Plant Science* **4**, 169.

Vinale, F., Flematti, G., Sivasithamparam, K., Lorito, M., Marra, R., Skelton, B.W. and Ghisalberti, E.L. (2009) Harzianic acid, an antifungal and plant growth promoting metabolite from *Trichoderma harzianum*. *Journal of Natural Products* **72**, 2032-2035.

Vinale, F., Nigro, M., Sivasithamparam, K., Flematti, G., Ghisalberti, E.L., Ruocco, M., Varlese, R., Marra, R., Lanzuise, S., Eid, A., Woo, S.L. and Lorito, M. (2013) Harzianic acid: a novel siderophore from Trichoderma harzianum. *FEMS Microbiology Letters* **347**, 123-129.

Vinale, F., Sivasithamparam, K., Ghisalberti, E.L., Marra, R., Barbetti, M.J., Li, H., Woo, S.L. and Lorito, M. (2008a) A novel role for *Trichoderma* secondary metabolites in the interactions with plants. *Physiological and Molecular Plant Pathology* **72**, 80-86.

Vinale, F., Sivasithamparam, K., Ghisalberti, E.L., Marra, R., Woo, S.L. and Lorito, M. (2008b) *Trichoderma*–plant–pathogen interactions. *Soil Biology and Biochemistry* **40**, 1-10.

Vinci, G., Cozzolino, V., Mazzei, P., Monda, H., Spaccini, R. and Piccolo, A. (2018) An alternative to mineral phosphorus fertilizers: The combined effects of *Trichoderma harzianum* and compost on *Zea mays*, as revealed by 1H NMR and GC-MS metabolomics. *PlOS One* **13**, e0209664.

Vitale, A. and Denecke, J. (1999) The endoplasmic reticulum-gateway of the secretory pathway. *The Plant Cell* **11**, 615-628.

Viterbo, A. and Chet, I. (2006) TasHyd1, a new hydrophobin gene from the biocontrol agent *Trichoderma asperellum,* is involved in plant root colonization. *Molecular Plant Pathology* **7**, 249-258.

Viterbo, A., Landau, U., Kim, S., Chernin, L. and Chet, I. (2010) Characterization of ACC deaminase from the biocontrol and plant growth-promoting agent *Trichoderma asperellum* T203. *FEMS Microbiology Letters* **305**, 42-48.

Viterbo, A., Wiest, A., Brotman, Y., Chet, I. and Kenerley, C. (2007) The 18mer peptaibols from *Trichoderma virens* elicit plant defence responses. *Molecular Plant Pathology* **8**, 737-746.

Waldo, G.S., Standish, B.M., Berendzen, J. and Terwilliger, T.C. (1999) Rapid protein-folding assay using green fluorescent protein. *Nature Biotechnology* **17**, 691-695.

Wallner, A., Blatzer, M., Schrettl, M., Sarg, B., Lindner, H. and Haas, H. (2009) Ferricrocin, a siderophore involved in intra- and transcellular iron distribution in *Aspergillus fumigatus*. *Applied and Environmental Microbiology* **75**, 4194-4196.

Wang, J. and Pantopoulos, K. (2011) Regulation of cellular iron metabolism. *Biochemical Journal* **434**, 365-381.

Wang, S., Boevink, P.C., Welsh, L., Zhang, R., Whisson, S.C. and Birch, P.R.J. (2017) Delivery of cytoplasmic and apoplastic effectors from *Phytophthora infestans* haustoria by distinct secretion pathways. *New Phytologist* **216**, 205-215.

Wang, X., Chung, K.P., Lin, W. and Jiang, L. (2018) Protein secretion in plants: conventional and unconventional pathways and new techniques. *Journal of Experimental Botany* **69**, 21-37.

Weber, E., Engler, C., Gruetzner, R., Werner, S. and Marillonnet, S. (2011) A modular cloning system for standardized assembly of multigene constructs. *PlOS One* **6**, e16765.

Weber, S.S., Parente, A.F.A., Borges, C.L., Parente, J.A., Bailão, A.M. and de Almeida Soares, C.M. (2012) Analysis of the secretomes of *Paracoccidioides* mycelia and yeast cells. *PLOS One* **7**, e52470.

Wink, M. (2003) Evolution of secondary metabolites from an ecological and molecular phylogenetic perspective. *Phytochemistry* **64**, 3-19.

Witzel, K., Shahzad, M., Matros, A., Mock, H.P. and Muhling, K.H. (2011) Comparative evaluation of extraction methods for apoplastic proteins from maize leaves. *Plant Methods* **7**, 48.

Wolfender, J.L., Rudaz, S., Choi, Y.H. and Kim, H.K. (2013) Plant metabolomics: from holistic data to relevant biomarkers. *Current Medicinal Chemistry* **20**, 1056-1090.

Wu, L.-F., Meng, S. and Tang, G.-L. (2016) Ferrous iron and α-ketoglutarate-dependent dioxygenases in the biosynthesis of microbial natural products. *Biochimica et Biophysica Acta* **1864**, 453-470.

Wu, Q.-S., Zou, Y.-N., Huang, Y.-M., Li, Y. and He, X.-H. (2013) Arbuscular mycorrhizal fungi induce sucrose cleavage for carbon supply of arbuscular mycorrhizas in citrus genotypes. *Scientia Horticulturae* **160**, 320-325.

Wu, X., Xiong, E., Wang, W., Scali, M. and Cresti, M. (2014) Universal sample preparation method integrating trichloroacetic acid/acetone precipitation with phenol extraction for crop proteomic analysis. *Nature Protocols* **9**, 362-374.

Wu, Y., Li, J., Yang, H. and Shin, H.-J. (2017) Fungal and mushroom hydrophobins: a review. *Journal of Mushroom* **15**, 1-7.

Xu, J., Zhou, L., Venturi, V., He, Y.-W., Kojima, M., Sakakibari, H., Höfte, M. and De Vleesschauwer, D. (2015) Phytohormone-mediated interkingdom signaling shapes the outcome of rice-*Xanthomonas oryzae* pv. *oryzae* interactions. *BMC Plant Biology* **15**, 1-16.

Xu, X., He, Q., Chen, C. and Zhang, C. (2016) Differential communications between fungi and host plants revealed by secretome analysis of phylogenetically related endophytic and pathogenic fungi. *PLOS One* **11**, e0163368.

Yadav, N., Khurana, S.M.P. and Yadav, D.K. (2015) Plant secretomics: unique initiatives. In *PlantOmics: The Omics of Plant Science* eds. Barh, D., Khan, M.S. and Davies, E. pp.357-384. New Delhi: Springer India.

Yajima, W., Liang, Y. and Kav, N.N. (2009) Gene disruption of an arabinofuranosidase/beta-xylosidase precursor decreases *Sclerotinia sclerotiorum* virulence on canola tissue. *Molecular Plant-Microbe Interactions* **22**, 783-789.

Yang, F., Li, W., Derbyshire, M., Larsen, M.R., Rudd, J.J. and Palmisano, G. (2015) Unraveling incompatibility between wheat and the fungal pathogen *Zymoseptoria tritici* through apoplastic proteomics. *BMC Genomics* **16**, 362.

Ye, J., Guo, Y., Zhang, D., Zhang, N., Wang, C. and Xu, M. (2013) Cytological and molecular characterization of quantitative trait locus qRfg1, which confers resistance to gibberella stalk rot in maize. *Molecular Plant-Microbe Interactions* **26**, 1417-1428.

Yedidia, I., Benhamou, N., Kapulnik, Y. and Chet, I. (2000) Induction and accumulation of PR proteins activity during early stages of root colonization by the mycoparasite *Trichoderma harzianum* strain T-203. *Plant Phisiology and Biochemistry* **38**, 863-873.

Yedidia, I., Shoresh, M., Kerem, Z., Benhamou, N., Kapulnik, Y. and Chet, I. (2003) Concomitant induction of systemic resistance to *Pseudomonas syringae* pv. *lachrymans* in cucumber by *Trichoderma asperellum* (T-203) and accumulation of phytoalexins. *Applied and Environmental Microbiology* **69**, 7343-7353.

Yedidia, I.I., Benhamou, N. and Chet, I.I. (1999) Induction of defense responses in cucumber plants (*Cucumis sativus* L.) by the biocontrol agent *Trichoderma harzianum*. *Applied and Environmental Microbiology* **65**, 1061-1070.

Yu, J.H. and Keller, N. (2005) Regulation of secondary metabolism in filamentous fungi. *Annual Review Phytopathology* **43**, 437-458.

Zamioudis, C. and Pieterse, C.M. (2012) Modulation of host immunity by beneficial microbes. *Molecular Plant-Microbe Interactions* **25**, 139-150.

Zeilinger, S. (2004) Gene disruption in *Trichoderma atroviride* via *Agrobacterium*-mediated transformation. *Current Genetics* **45**, 54-60.

Zeilinger, S., Gruber, S., Bansal, R. and Mukherjee, P.K. (2016) Secondary metabolism in *Trichoderma*–chemistry meets genomics. *Fungal Biology Reviews* **30**, 74-90.

Zeilinger, S. and Schuhmacher, R. (2013) Volatile organic metabolites of *Trichoderma* spp: bioynthesis, biology and analytics. In *Trichoderma: Biology and Applications*. pp.110-127.

Zeng, T., Holmer, R., Hontelez, J., Te Lintel-Hekkert, B., Marufu, L., de Zeeuw, T., Wu, F., Schijlen, E., Bisseling, T. and Limpens, E. (2018) Host- and stage-dependent secretome of the arbuscular mycorrhizal fungus *Rhizophagus irregularis*. *The Plant Journal : for Cell and Molecular Biology* **94**, 411-425.

Zhang, N., Zhang, S., Borchert, S., Richardson, K. and Schmid, J. (2011) High levels of a fungal superoxide dismutase and increased concentration of a PR-10 plant protein in associations between the endophytic fungus *Neotyphodium lolii* and ryegrass. *Molecular Plant-Microbe Interactions* **24**, 984-992.

Zhang, S., Gan, Y. and Xu, B. (2016a) Application of plant-growth-promoting fungi *Trichoderma longibrachiatum* T6 enhances tolerance of wheat to salt stress through improvement of antioxidative defense system and gene expression. *Frontiers in Plant Science* **7**, 1405.

Zhang, S. and Xu, J.R. (2014) Effectors and effector delivery in *Magnaporthe oryzae*. *PLOS Pathogens* **10**, e1003826.

Zhang, Y., Zhao, L., Zhao, J., Li, Y., Wang, J., Guo, R., Gan, S., Liu, C.-J. and Zhang, K. (2017) S5H/DMR6 encodes a salicylic scid 5-hydroxylase that fine-tunes salicylic acid homeostasis. *Plant Physiology* **175**, 1082.

Zhang, Z., Chao, M., Wang, S., Bu, J., Tang, J., Li, F., Wang, Q. and Zhang, B. (2016b) Proteome quantification of cotton xylem sap suggests the mechanisms of potassium-deficiency-induced changes in plant resistance to environmental stresses. *Scientific Reports* **6**, 21060.

Zhou, J., Li, X., Huang, P.-W. and Dai, C.-C. (2018) Endophytism or saprophytism: decoding the lifestyle transition of the generalist fungus *Phomopsis liquidambari*. *Microbiological Research* **206**, 99-112.

Zuccaro, A., Lahrmann, U., Güldener, U., Langen, G., Pfiffi, S., Biedenkopf, D., Wong, P., Samans, B., Grimm, C., Basiewicz, M., Murat, C., Martin, F. and Kogel, K.-H. (2011) Endophytic life strategies decoded by genome and transcriptome analyses of the mutualistic root symbiont *Piriformospora indica*. *PLOS Pathogens* **7**, e1002290.